2020-01-15

# The Snakeskin-Mesh Complex of Smooth Septate Junction Restricts Yorkie to Regulate Intestinal Homeostasis in Drosophila

Hsi-Ju Chen
*University of Massachusetts Medical School*

# The Snakeskin-Mesh Complex of Smooth Septate Junction Restricts Yorkie to Regulate Intestinal Homeostasis in *Drosophila*

A Dissertation Presented

by

Hsi-Ju Chen

Submitted to the Faculty of the
University of Massachusetts Graduate School of Biomedical Sciences, Worcester
In partial fulfilment of the requirement for the requirements
for the Degree of Doctor of Philosophy

November 19, 2019

# TABLE OF CONTENTS

# FIGURE LIST

# ABSTRACT

The work presented in this thesis provides insights into the *Drosophila* smooth septate junction complex Ssk-Mesh that regulates ISC proliferation and tissue homeostasis in addition to the well-known barrier function in the epithelial integrity. With CRISPR-generated tag knockin alleles of Ssk and Mesh, I characterized the intracellular expression pattern of Ssk and Mesh. Ssk and Mesh had low but detectable expression in punctate format in the cytoplasm of enteroblasts (EBs). The protein expression profile of Ssk and Mesh correlated with their ability to regulate the ISC proliferation even though the septate junctions in EBs had not fully formed. Along with further differentiation into mature enterocytes (ECs), Ssk and Mesh gradually localized to the epithelial apical domain, where they coordinated with other junction proteins, such as Tsp2A and Coracle, to form the septate junction. RNAi-conducted genetic assays and mutant clonal analyses by knockout mutant alleles of *Ssk* and *mesh* further revealed that Ssk and Mesh restricted the activity of the transcription coactivator Yki, which governs the production of the cytokine Upd3 along the EB-EC differentiation lineage in adult midgut. Loss of Ssk or Mesh activated Yki to elevate the *upd3* expression and thereby to induce the robust ISC proliferation non-autonomously. Although the total number of EBs in midgut is much fewer than that of ECs, surprisingly, knockdown *Ssk* or *mesh* in EBs resulted in a comparable *upd3* upregulation and ISC proliferation as knockdown their expression in ECs. Leaky midgut caused by knockdown of *Ssk* or *mesh* in ECs activated the stress-responding mechanisms to repair the damaged intestinal epithelium, and was eventually associated with death of animals. The reduction of Ssk and Mesh in EBs displayed much milder gut leakage and lower lethality

further confirmed that Ssk and Mesh in the two distinct cell types had their own roles in governing ISC proliferation.

# CHAPTER I

## INTRODUCTION

Nutrients are vital for survival and health. The digestive system breaks down food into the chemical components for the body to absorb the necessary carbohydrates, fat, and proteins. The luminal side of the digestive tract is covered with a thin layer of epithelial cells for absorption and tissue homeostasis. These epithelial cells in the digestive tract are exposed to the risks of chronic inflammation since they encounter continuous irritation via daily ingestion of food and pathogens. The intestine is the primary site of nutrient absorption in the digestive system. With the physical segmentation and enzymatic activity, the intestine coordinates nearby accessory organs to digest ingested foods and absorb their breakdown products completely.

Colorectal cancer (CRC) is the most prevalent cancer type in the digestive tract. Excluding skin cancer, CRC in the United States is the third most common cancer diagnosed in males and in females. CRC is also the second leading cause of cancer-related death in both genders, and the expected death of CRC is about 51,000 in 2019 (https://seer.cancer.gov). Most of the CRC-related death is due to the metastasis of the liver (Fleming et al., 2012; Neo et al., 2010). The cost of the treatment is a heavy burden for individuals. Depending on the health insurance plan, the average spending from patients ranges from 5,000 to 10,000 in the first year. According to the report from the American society of cancer, the total care cost per CRC patients was more than 120,000 in 2016, an expenditure that continues to increase (Mariotto et al., 2011). Although the lifetime risk to develop the CRC in males is slightly higher, the death rate has been decreasing in both genders for decades due to multiple likely reasons. Cancer screening allows early detection of cancers. For CRC, the incorporation of the colonoscopy

screening significantly improves the accuracy of diagnosis. The colonoscopy detects and removes the polyps much earlier before they develop into cancer, effectively preventing the tumorigenesis.

Anyone can develop CRC. Many factors are associated with the disease progress. Some factors are modifiable, such as diet, obesity, tobacco, and alcohol consumption. However, modification of these factors is not sufficient to avoid CRC. Those non-modifiable factors from the familial history of polyps or CRC, genetic predisposition, ethnic backgrounds, and inflammatory bowel disease have much higher effects on the development of CRC (Simon, 2016). Most colorectal tumors grow slowly and take multiple steps. Polyps are benign but precancerous tissues that aggregate cells with abnormal growth. The dividing cells in the polyps accumulate sufficient genetic mutations such as $APC^{-/-}$, by which they invade the bowel wall and eventually metastasis to distant sites. On average, it takes several years to complete the development from the initiated polyps to CRC (Huels and Sansom, 2015).

Understanding the mechanisms that mediate tissue homeostasis is a potential way to block CRC development. The daily shedding of intestinal epithelial cells results in the turnover of mature cells in the whole epithelial layer in every 4-5 days. Also, physiological reactions, such as peristalsis, need the involvement of endocrines. Therefore, the resident intestinal stem cells (ISCs) divide and differentiate to fulfill those demands and maintain the tissue integrity as well as the health. How to control the ISCs division and the subsequent differentiation is critical to prevent abnormal tissue growth. Studies have shown that Wnt/β-catenin signaling is essential for intestinal homeostasis. Apc deletion in ISCs induces the formation of adenoma. Clinical reports also reveal more than >90%

of CRC patients has the aberrant activation of Wnt/β-catenin signaling (Clevers, 2006). There are also reports indicating the crosstalk between the Wnt/β-catenin signaling and the Hippo pathway, which is an evolutionally conserved signaling in organ size control (Azzolin et al., 2014; Heallen et al., 2011; Imajo et al., 2012). Together, their mutual interaction and regulation govern the ISC behaviors to support intestinal tissue homeostasis.

## The Hippo pathway

### 1. The core kinases of the Hippo signaling pathway and their conservation.

Uncontrolled cell proliferation is the primary impression of cancers. The dysregulation of the Hippo pathway is common in various human cancers, and YAP/TAZ has been identified as a hallmark of cancers (Sasaki et al., 2007; Yu et al., 2015; Zhou et al., 2009). Systematic profiling of 9125 tumor samples showed an extensive dysregulation of the Hippo pathway components in human cancer types, including colorectal cancer (Kosaka et al., 2007). Since the Hippo pathway integrates versatile interior and exterior cues, understanding this sophisticated pathway not only helps us to elucidate the manipulation from embryonic development till the adult tissue homeostasis, but sheds light on the potential targets for the design of cancer drugs.

#### (1) The constituents and the identified regulation of the Hippo pathway in *Drosophila*.

The structure and regulation of the core kinase cascade

Initiating from the genetic screening in *Drosophila*, the Hippo pathway has been known as an evolutionally conserved mechanism across animal phyla (Sebe-Pedros et al., 2012). It participates in diverse physiological functions, such as the lineage specification in early embryogenesis, cell fate specification, tissue-resident stem cell maintenance, and the tissue regeneration while encountering impairment. This pathway is first identified in *Drosophila,* which controls the organ size by arresting cell proliferation and driving apoptosis (Harvey et al., 2003; Huang et al., 2005; Justice et al., 1995; Lai et al., 2005; Tapon et al., 2002; Wu et al., 2003; Zhang et al., 2008b). Genetic mosaic screening based on overgrowth of homozygous mutant clones identifies the first four

tumor suppressors *warts* (*wt*s), *hippo* (*hpo*), *salvador* (*s*av), and *mob as tumor suppressor* (*mats*) (Jia et al., 2003; Justice et al., 1995; Kango-Singh et al., 2002; Lai et al., 2005; Pantalacci et al., 2003; Tapon et al., 2002; Udan et al., 2003; Wu et al., 2003; Xu et al., 1995), which constitute the core kinase cascade. Later on, the identification of the transcription co-activator Yorkie (*yki*) and its DNA-binding partner Scalloped (sd) links the kinase cascade and the downstream transcriptional regulations to coordinate cell proliferation and cell death (Chen, 1992; Wu et al., 2008).

A series of phosphorylation at Serine/Threonine residues is required for the core kinase cascade. Hpo-Sav complex phosphorylates and activates the Wts-Mats complex. Activated Wts-Mats complex further phosphorylates and inactivates Yki to turn off the downstream gene expression (Dong et al., 2007; Huang et al., 2005). Hpo acquires its activity by the phosphorylation within its kinase domain. Tao-1, the upstream ste-20 family kinase, directly phosphorylates the Thr195 (Boggiano et al., 2011; Poon et al., 2011). Besides Tao-1 kinase, Hpo activation requires proper dimerization by its Sav-RASSF-Hippo (SARAH) domain at the C-terminus. The C-terminal dimerization of Hpo leads to the subsequent dimerization at the N-terminus, which is critical for the following inter-subunit trans-autophosphorylation to acquire Hpo kinase activity (Deng et al., 2013; Jin et al., 2012). Sav and RASSF are another two SARAH domain-containing proteins that modulate the dimerization and the following autoactivation. Sav dimerizes with Hpo by their respective SARAH domains and stabilizes the Hpo homodimer (Aerne et al., 2015; Jin et al., 2012). The Hpo-Sav heterotetramer increase the kinase activity of Hpo by trans-autophosphorylation within the Hpo T-loop (Bae et al., 2017). Moreover, the

heterotetramer stabilizes Sav since Hpo antagonizes the E3 ligase Herc4-mediated ubiquitination and degradation (Aerne et al., 2015).

In contrast to Sav, *Drosophila* RASSF (dRASSF) negatively regulates the Hippo pathway. dRASSF competes with Sav for binding to Hpo by its C-terminal SARAH domain. The Hpo-dRASSF complex raises the stability of dRASSF and restricts Hpo activity. Therefore, Sav and dRASSF modulate the activity of Hpo kinase in the opposite manner (Gokhale and Pfleger, 2019; Polesello et al., 2006). The non-structural linker between the kinase and C-terminal SARAH domain of Hpo is another site to modulate the Hpo activity. Hpo autophosphorylates multiple sites within the linker after the Thr195 is phosphorylated. Some phospho-residues become the docking site for Mats recruitment to promote Wts phosphorylation (Ni et al., 2015). Conversely, some phosphorylated residues are for the negative feedback to restrict Hpo activity. Proteomic and RNAi screening identify the *Drosophila* STRIPAK (dSTRIPAK) PP2A phosphatase complex that binds to the linker region of Hpo by its Slamp subunit and dephosphorylates the T195 to inactivate Hpo. (Formstecher et al., 2005; Guruharsha et al., 2011). Therefore, Hpo activity is fine-tuned by multiple built-in mechanisms. (Ribeiro et al., 2010; Zheng et al., 2017).

The effector kinase Wts takes sequential phosphorylation before inactivating Yki. Hpo phosphorylates Thr1077 within the C-terminal hydrophobic motif of Wts followed by autophosphorylation at Ser907 in the activation motif of Wts kinase domain (Chan et al., 2005). To enhance the phosphorylation, Sav behaves as an adaptor downstream to Hpo, interacting with the PPxY-motif of Wts by its WW-domain (Tapon et al., 2002). Sav also has been proposed to act upstream to Hpo by recruiting Hpo toward the plasma membrane to phosphorylate Wts (Su et al., 2017; Yin et al., 2013). The other adaptor

protein within the kinase cascade is Mats (Hergovich, 2011; Ho et al., 2010). Mats physically associates with Wts to facilitate Wts-mediated phosphorylation of Yki (Lai et al., 2005). The Thr431 and the Mats-binding hydrophobic motif in the non-structural linker of Hpo are the docking sites for Mats (Ni et al., 2015). Mats binds to Hpo and enhances the kinase cascade by shortening the spatial distance between Hpo and Wts. Endogenous Mats is detected at the plasma membrane, where it recruits Wts and increases the kinase activity of Wts (Hergovich et al., 2006; Ho et al., 2010). Whether being the substrate of Hpo enhances the interaction between Mats and Wts is no entirely clear. Some studies suggest that Hpo phosphorylates Thr12 and Thr35 of Mats, enabling Mats to interact with the auto-inhibitory region of Wts and promote Wts activation (Wei et al., 2007), whereas other proposes Mats conducts the conformational transition of Wts before Hpo-mediated phosphorylation (Vrabioiu and Struhl, 2015).

The requirement of Hpo for Wts activation is context-dependent. Whether Hpo is the primary Wts regulator varies according to distinct cell types and upstream inputs. Hpo-independent activation of Wts/LATS is first revealed in the MST1/2 null mouse embryonic fibroblast that had unperturbed phosphorylation of LATS1/2 and YAP regardless of cell density (Zhou et al., 2009). Additional reports also show that YAP phosphorylation induced by F-actin depolymerization is MST1/2-independent (Yu et al., 2012a; Zhao et al., 2012). Recently, the identification of the MAP4K family kinases, which act in parallel to *Drosophila* Hpo and mammalian LATS1/2, solves the puzzle (Li et al., 2014a; Meng et al., 2015; Zheng et al., 2015). In *Drosophila*, Misshapen (Msn, ortholog of mammalian MAP4K4/6/7) and Happyhour (Hppy, ortholog of mammalian MAP4K1/2/3/5) function redundantly in response to the F-actin cytoskeleton disruption, cell density, and contact

inhibition. They directly phosphorylate the Thr1077 of Wts hydrophobic motif to activate Wts (Li et al., 2014a; Li et al., 2018; Ma et al., 2019; Zheng et al., 2015).

The regulation of Yki and its DNA-binding partner Sd

The Hippo pathway effector Yki is the vital link between the upstream Wts and the downstream gene expression related to cell cycle and death. Overexpressed Yki recapitulates the phenotypes in tissue outgrowth and compromises apoptosis that are caused by the *hpo, wts*, or *sav* mutant (Huang et al., 2005). Wts-mediated phosphorylation at S168 of Yki (S127 of YAP) induces the interaction with 14-3-3 that restricts Yki in the cytoplasm (Dong et al., 2007). Since it has no DNA-binding motif, Yki interacts with the Sd transcriptional factor to regulate gene transcription (Goulev et al., 2008; Wu et al., 2008; Zhang et al., 2008b). Genome-wide chromatin occupancy studies reveal a substantial overlap of the DNA-binding sites between the mammalian homolog of Yki and Sd, supporting the idea that Sd is the necessary DNA-binding partner of Yki (Zanconato et al., 2015; Zhao et al., 2008). Upon the association with Sd, Yki recruits multiple chromatin-remodeling complexes, such as the Trr H3K4 methyltransferase and SWI/SNF complex, to facilitate gene expression (Oh et al., 2014; Qing et al., 2014; Zhu et al., 2015). Conversely, Sd also represses gene expression. Tgi, the Tondu domain-containing transcriptional corepressor, is identified as the default corepressor. Tgi antagonizes Yki-mediated transcription by competing for the same binding site of Sd. In the absence of Yki, Sd engages Tgi to display its default repression. The presence of Yki replaces Tgi and converts Sd into the transcriptional activator (Guo et al., 2013; Koontz et al., 2013). Therefore, Sd performs another layer to modulate the downstream gene expression appropriately.

**Figure A. The activation mechanisms in the Hippo kinase cascade.**

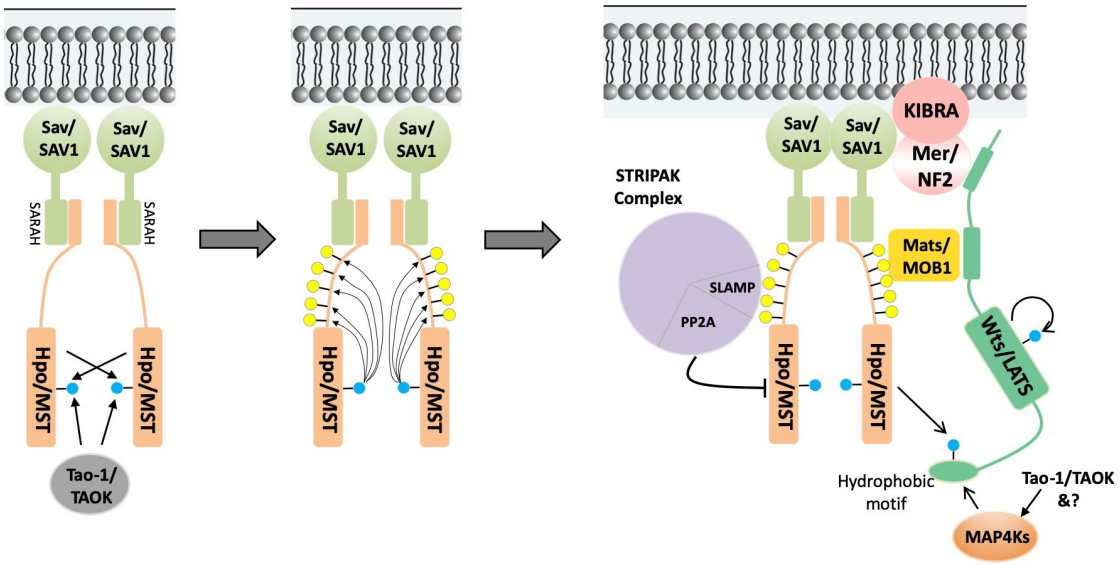


*Ref. Zheng & Pan (2019)*

**Figure B. Multiple signals are integrated to regulate the Hippo pathway.**

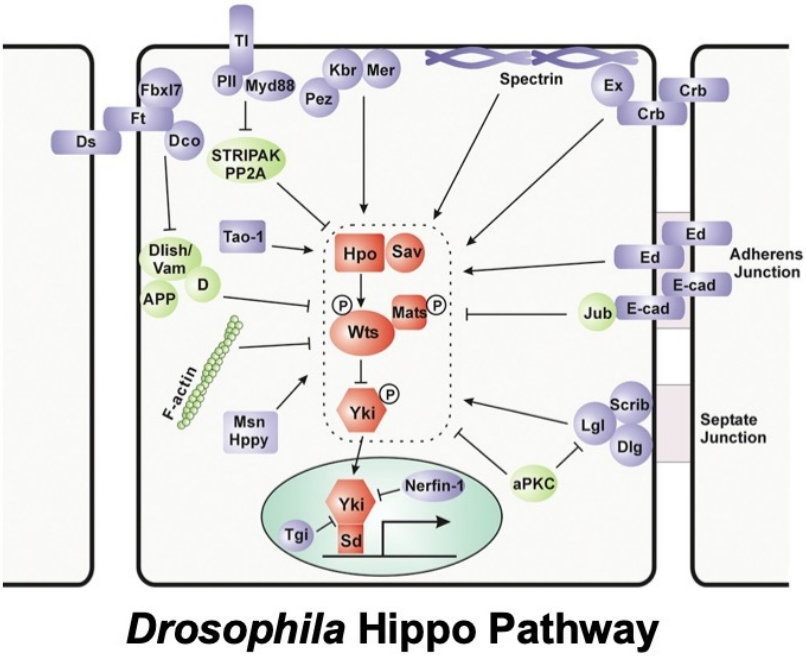


***Drosophila* Hippo Pathway**

*Zheng & Pan (2019)*

**(2) The composition and the modulation of the Hippo signaling pathway are conserved in mammalian, but not identical.**

Mammalian kinase cascade MST1/2-LATS1/2 regulation

After identifying the core components of the Hippo pathway in *Drosophila*, the counterparts of the kinase cascade are soon discovered in the mammalian system. They guard cell proliferation and apoptosis to maintain the appropriate organ size during development, and prevent tumorigenesis in adulthood (Li et al., 2019; Lu et al., 2010; Misra and Irvine, 2018; Zhang and Zhou, 2019). Hence, the Hippo pathway is highly conserved from invertebrates to mammals. The kinase cascade requires multiple layers of phosphorylation to gain the activity (Chan et al., 2005; Zhang et al., 2008a). Ste20-like kinase1/2 (MST1/2; mammalian homolog of Hpo) and the large tumor suppressor 1/2 (LATS1/2; homolog of Wts) consist the core of the mammalian Hippo pathway. MST1/2 phosphorylates the hydrophobic motif of LATS1/2, leading to a series of intermolecular phosphorylation to activate LATS1/2. The physiological output of the MST1/2-LATS1/2 cascade restricts the activity of two transcriptional coactivators, Yes-associated protein and transcriptional coactivator with PDZ-binding motif (YAP/TAZ, the homolog of Yki) (Misra and Irvine, 2018; Moya and Halder, 2019).

Upon activation by extracellular signals, the threonine residues within the activation loop of MST1/2 (Thr183 for MST1 and Thr180 for MST2) are phosphorylated to initiate MST1/2 activity. Upstream TAO kinase phosphorylates the activation loop of MST1/2 and activates MST1/2 (Boggiano et al., 2011; Pflanz et al., 2015; Poon et al., 2011). The scaffold proteins SAV1 (homolog of SAV) assists the homodimerization of MST1/2, which helps MST1/2 gain the activity (Glantschnig et al., 2002). MST1/2 partners with SAV1

through their respective C-terminal SARAH domain and increases the stability of SAV1. The heterodimerization also leads to the phosphorylation of SAV1 to support the subsequent LATS1/2 activation (Callus et al., 2006). Two SAV1-MST1/2 heterodimers are associated together to form one heterotetramer, in which MST1/2 undergoes trans-autophosphorylation (Bae et al., 2017). Besides the allosteric activation, SAV1 maintains MST1/2 kinase activity by antagonizing the PP2A phosphatase STRIPAK. The linker between the kinase domain and the C-terminal SARAH domain of MST1/2 is another region to regulate the kinase activity (Bae et al., 2017). Activated MST1/2 autophosphorylates several threonine and methionine residues of is non-structural linker to create the docking sites. The adaptor SLMAP binds to the phosphorylated linker and recruits STRIPAK to execute PP2A-mediated dephosphorylation. SAV1 protects the MST1/2 activation loop from dephosphorylation by binding to the STRIPAK-PP2A catalytic core (Bae et al., 2017). The phosphorylated linker of MST1/2 is the docking site for MOB1 (homolog of Mats) as well. After Mst1/2-mediated phosphorylation, MOB1 undergoes conformational activation and associates with LATS1/2 to assist MST1/2 in the recruitment and phosphorylation at the hydrophobic motif of LATS1/2 (T1079 for LATS1 and T1041 for LATS2) (Bao et al., 2009; Hergovich et al., 2006; Ni and Luo, 2019; Ni et al., 2015; Praskova et al., 2008). Therefore, the effector kinase LATS1/2 acquires the ability to modulate YAP/TAZ.

Although *Drosophila* RASSF inhibits the binding of Sav to Hpo, mammalian RASSF family proteins display controversial roles (Crose et al., 2014; Guo et al., 2007; Hwang et al., 2007; Ikeda et al., 2009; Liao et al., 2016; Oh et al., 2006; Song et al., 2012). The interaction with membrane-anchored Ras converts the SARAH domain of RASSF1A and

RASSF5 toward open status and makes them more accessible to MST1/2, enhancing MST1/2 autophosphorylation and LATS1/2 activation (Guo et al., 2007; Hwang et al., 2007; Liao et al., 2016; Oh et al., 2006). Several reports reveal the tumor-suppressing roles of RASSF proteins. Delayed mitosis and defective cytokinesis-induced multinucleate aneuploid are cancer hallmarks which are frequently observed in Rassf1a-deficiency mouse embryo fibroblast (Guo et al., 2007). RASSF3 suppresses tumor growth by protecting p53 from ubiquitination although the details need further investigation (Kudo et al., 2012). However, not all RASSF family members are tumor suppressors. FOXO1-elevated RASSF4 has been reported to promote an aggressive skeletal muscle sarcoma by suppressing MST1 activity (Crose et al., 2014), and RASSF6 inhibits MST2 in mammalian HEK293T cells (Ikeda et al., 2009). As for RASSF2, it regulates osteoblast for appropriate bone modeling by inhibiting NF-κB signaling (Song et al., 2012).

MST1/2-independent activation of LATS1/2 is conserved in mammals (Meng et al., 2015; Plouffe et al., 2016). Unaltered LATS1/2 activity and YAP phosphorylation are discovered in the MST1/2 null mice, suggesting other mechanisms activate LATS1/2 in parallel to MST1/2 (Zhou et al., 2009). MAP4K kinases family, as well as TAO kinase, directly phosphorylate LATS1/2 at the hydrophobic motif, leading to LATS1/2 activation. Noteworthily, the deletion of MST1/2, MAP4K, or TAO kinases alone only partially relieves the YAP/TAZ inhibition in mammalian cells (Meng et al., 2015). Combined ablation of all three kinases dramatically reduces YAP/TAZ phosphorylation in response to LATS1/2-activating signals such as serum deprivation and F-actin disassembly, indicating their redundant roles upstream to LATS1/2. In adult *Drosophila* midgut, the MAP4K4 homolog Msn in the enteroblasts and the Ste-20 kinase Hpo in enterocytes cooperatively restrict

the production of Upd3 cytokine to regulate ISC proliferation. Hence, the relative dominance of MST1/2, MAP4K, and TAO kinases in mammal highly depends on the cell types and input signals.

YAP/TAZ/TEAD regulation

The Hippo pathway inactivates YAP and TAZ by cytoplasmic retention and ubiquitin-dependent degradation (Luo, 2010; Zhao et al., 2007). LATS1/2 phosphorylates YAP/TAZ (Residues S127 of YAP1 and S89 of TAZ) to generate 14-3-3-binding sites. Association with 14-3-3 retains YAP/TAZ in the cytoplasm (Garcia and Castano, 1991; Zhao et al., 2007). The LATS1/2-induced phosphorylation further primes the subsequent casein kinase 1 (CK1)-mediated phosphorylation of YAP/TAZ and recruits the SCF E3 ubiquitin ligase, eventually leading to the ubiquitination and degradation of YAP/TAZ (Kodaka and Hata, 2015; Liu et al., 2010; Zhao et al., 2010).

YAP and TAZ are transcription coactivators without DNA-binding motifs. Although other DNA-binding partners for YAP/TAZ have been identified, TEAD family (TEAD1-4) transcription factors are the principal DNA-binding partners that convert the upstream signals to various gene expression of cell growth and apoptosis (Lin et al., 2017). The TEAD binding-defective YAP fails to induce transcription of YAP target genes, recapitulating the YAP knockout mice (Zhao et al., 2008). The deletion of TEAD results in the cytoplasmic retention of YAP/TAZ even when they are not phosphorylated (Stein et al., 2015; Zanconato et al., 2015). Moreover, chromatin occupancy experiments revealed TEAD as the mandatory DNA-binding partner of YAP-mediated growth control. The chromatin binding peaks of YAP/TAZ significantly overlap with TEAD binding sites in oncogenic growth (Stein et al., 2015; Zanconato et al., 2015). VGLL4 negatively regulates

YAP/TAZ transcription activity. Different from its *Drosophila* ortholog Vg that has one Vg domain in the N-terminus, VGLL4 contains two Vg domains in the C-terminus. VGLL4 directly competes with YAP for binding to TEAD and functions as a default transcription repressor. Consistently, the VGLL4-mimicking peptide compromises gastric cancer caused by hyperactivated YAP, supporting the antagonistic effect of VGLL4. Several chromatin-remodeling complexes associate with YAP/TAZ and control gene expression under different contexts, including the bromodomain-containing protein4 (BRD4), Trr-homolog methyltransferase NcoA6, and SWI/SNF (Chang et al., 2018; Fujisawa et al., 1987; Oh et al., 2014; Zanconato et al., 2018), suggesting the accessibility of target genes is another parameter to influence YAP/TAZ-mediated transcription.

**Figure C. The Hippo pathway coordinates multiple signals to regulate the activity of YAP/TAZ.**

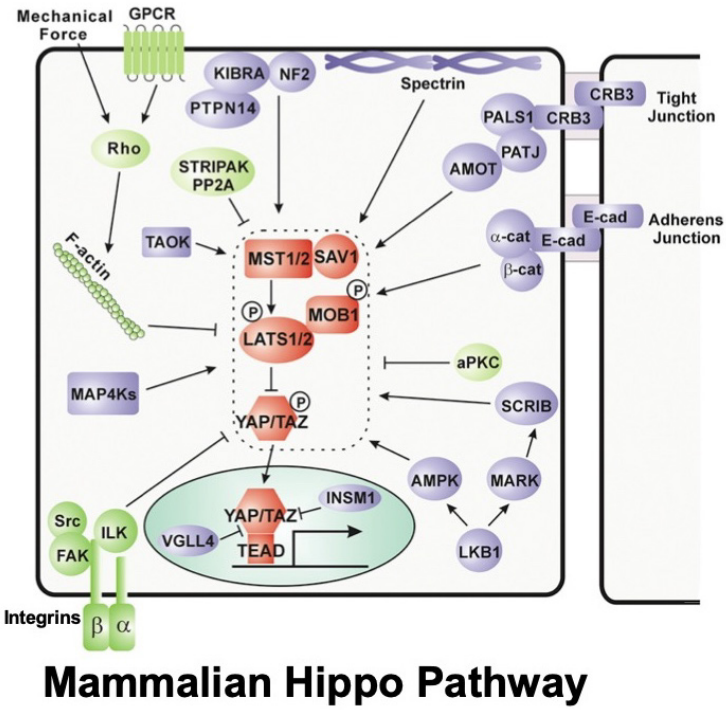


*Zheng & Pan (2019)*

## 2. Versatile upstream signals to regulate the Hippo signaling pathway.

Studies in the past decades have shown that Yki/YAP/TAZ are the primary effectors of the Hippo pathway, which employs kinase-mediated phosphorylation to induce cytoplasmic retention and degradation of Yki/YAP/TAZ in response to diverse biological demands (Misra and Irvine, 2018). These intrinsic and extrinsic signals function through peripheral components to modulate the phosphorylation of the kinase cascade. Recent genome-wide chromatin immunoprecipitation and expression profiling analysis also confirm genes that are targets of the Hippo pathway and regulate cell proliferation and death are enriched in both *Drosophila* and mammals (Galli et al., 2015; Stein et al., 2015; Zanconato et al., 2015; Zhao et al., 2008). One class of these target genes encodes negative regulators upstream to the kinase cascade and Yki/YAP/TAZ, while another class participates in cell migration, organization of extracellular matrix, and assembly of F-actin cytoskeleton. Unlike other classic pathways that mostly rely on specific ligand-receptor pairing, the Hippo pathway is linked to a broad spectrum of both intrinsic and extrinsic upstream signals, such as cell polarity, cell-cell contact, mechanical force, and metabolism.

### (1) Cell polarity

The apicobasal polarity is established by the asymmetric distribution of the cellular components and maintained through a conserved network among protein complexes. The functional interaction between membrane-associated protein complexes divides the plasma membrane into the apical and basolateral domains. The shape of the epithelial cells depends on the polarity. Loss of the polarity and tissue architecture highly correlate with the potential metastasis. Many identified upstream regulators of the Hippo pathway

are components of tight junctions, adherens junctions, and apicobasal polarity complexes. Therefore, disruption of the cell junction or apicobasal polarity triggers cell outgrowth and is a hallmark of the cancerous epithelial tumors. CRB complex (CRB/PATJ/PALS1), PAR complex (PAR3/PAR6/aPKC), and Scribble complex (SCRIB/DLG/LGL) are responsible for the epithelial polarity and proliferation control. The upstream regulators of the Hippo pathway that interact with Crb further provide additional aspects to connect polarity and growth control.

Merlin/NF2, Ex, Kibra

Merlin (Mer) and Expanded (Ex) are the first two upstream regulators genetically linked to the Hippo kinase cascade in *Drosophila* and act together to regulate cell proliferation and differentiation (Hamaratoglu et al., 2006; McCartney et al., 2000). Being members of the FERM (4.1, Ezrin, Radxin, and Moesin) family proteins, which crosslink actin with the plasma membrane, Mer and Ex act as the linker to recruit other components to the plasma membrane (Sato and Sekido, 2018). Inactivation of both Mer and Ex results in the comparable overgrowth caused by *hpo* mutant. Kibra is subsequently identified to physically interact with Mer and Ex, forming a complex at the apical domain of epithelial cells (Genevet et al., 2010; Yu et al., 2010). Kibra interacts with phospholipids by its C2 domain and targets partner proteins to the cell membrane (Kremerskothen et al., 2003). Indeed, further studies support the importance of the plasma membrane for Hippo signaling activation. Mats is activated at the plasma membrane (Ho et al., 2010). Tethering MST1 and Msn to the plasma membrane by myristoylation constitutively activates their kinase activity (Brooks, 1975; Kaneko et al., 2011; Kline et al., 2018). Mechanistically, Mer and Ex physically associate with Hpo-Sav complex and Kibra

directly binds to Wts, suggesting that Mer/Ex/Kibra complex cooperatively recruits the components of the Hippo kinase cascade toward the apical domain where kinases acquire their activity (Genevet et al., 2010; Yu et al., 2010).

The regulation of the Mer/Ex/Kibra complex on the Hippo pathway is mostly conserved in mammals (Cockburn et al., 2013; Petrilli and Fernandez-Valle, 2016; Verma et al., 2019). FRMD6, the ortholog of Ex, is an upstream component of the Hippo pathway to suppress the progression of hepatocellular carcinoma (Guan et al., 2019). Association of mammalian KIBRA with aPKC/Par3 inactivates the Hippo pathway and promotes the metastasis of prostate cancer (Zhou et al., 2017). NF2, the homolog of Mer, is identified by the development of neurofibromatosis type 2. Extensive studies of NF2 from a variety of tissues also present its role in tumor suppression (Petrilli and Fernandez-Valle, 2016). Overexpression of NF2 in mammalian cells results in LATS1/2 activation and YAP inhibition (Yin et al., 2013). Conditionally deletion of NF2 in mouse liver induces hepatocellular carcinoma and cholangiocarcinoma (Benhamouche et al., 2010; Zhang et al., 2010). NF2 patients and mice with conditional NF2 knockout in lens epithelium frequently have ocular abnormalities such as cataracts derived from hyperplasia in the eyes. Conversely, heterozygous deletion of YAP and TAZ largely suppresses the hyperplastic phenotype in the liver and eyes (Moon et al., 2018; Zhang et al., 2010).

Crb/Std/Patj

The transmembrane protein Crumbs (Crb) is an apical domain determinant that is important to organize epithelial polarity and the configuration of adherens junction in *Drosophila* (Tepass, 1996; Wodarz et al., 1995). Loss of Crb causes proliferation, whereas overexpression of Crb also leads to overgrowth in both *Drosophila* and

mammals (Chen et al., 2010). Two motifs in its C' terminal intracellular tail make Crb as an interface between epithelial polarity and growth. The PDZ-binding motif unites with Patj and Stardust (Std) to form the Crb complex, which antagonizes the activity of the basolateral Scrib complex. The juxtamembrane FERM-binding motif of Crb affects the apical distribution and the abundance of Ex, and allows Crb to be the peripheral regulator of the Hippo pathway (Chen et al., 2010; Grzeschik et al., 2010; Ling et al., 2010; Robinson et al., 2010).

Three mammalian Crb homologs have been identified. CRB1 predominantly functions during eye development and is related to a group of degenerative diseases of the retina, such as retinitis pigmentosa (Bujakowska et al., 2012). CRB2 is associated with cystic kidney disease in addition to retina-relevant syndromes. As for CRB3, it is found widely expressed in epithelial cells and predominantly localized to the apical and subapical domain (Lemmers et al., 2004; Li et al., 2015a). CRB3 knockout mice have defects in epithelial morphogenesis and die shortly after birth because of the disorganized cytoskeleton and defective junctions (Whiteman et al., 2014). The expression level of murine CRB3 negatively corelates with carcinogenesis and migration in epithelial cells (Karp et al., 2008; Mao et al., 2017; Varelas et al., 2010b). Loss of CRB3 favors the expression of vimentin and reduces the E-cadherin, two features of the epithelial mesenchymal transition. These studies suggest that CRB3 can suppress the invasion and metastasis. Recent reports also show that CRB3 inhibits tumor growth by either working with angiomotin (AMOT)-like protein to promote the Hippo pathway (Varelas et al., 2010b) or recruiting KIBRA and FRMD6 to regulate contact inhibition through the Hippo pathway (Mao et al., 2017). Together, these studies not only demonstrate the

conserved role of CRB3 in the maintenance of epithelial polarity and tumor progression, but greatly help in the therapeutic design for cancer.

Par3/Par6/aPKC

Par complex, which consists of Par3, Par6, and atypical protein kinase C (aPKC), is another apical-localized complex for epithelial polarity. The Crb and Par complex cooperatively antagonize the expansion of the Scrib-mediated basolateral domain (Martin-Belmonte and Perez-Moreno, 2011). Similar to the Crb complex, Par complex modulates the Hippo pathway to control cell growth and apoptosis. Constitutively active aPKC mislocalizes Hpo and RASSF and activates the target genes of the Hippo pathway. aPKC also acts in concert with Jun N-terminal kinase (JNK) to increase Yki activity during the wing development and when adult midgut encounters damages, suggesting a cell type- and context-dependent manner (Sun and Irvine, 2011; Xu et al., 2019). Clinical studies consistently indicate that increased aPKC expression tightly correlates with higher pathological stage and poor patient survival in lung adenocarcinoma (Kim et al., 2019). Likewise, abnormal expression of Par3 works with the Hippo pathway to trigger tumor formation. Low cell density leads to the translocation of PAR3. Cytoplasmic PAR3 recruits the phosphatase PP1A to dephosphorylate LATS1 and promote YAP activity in mammalian cells (Sun and Irvine, 2011). Consistently, loss of CRB3 attenuates the Hippo pathway and results in the prostatic tumorigenesis and neoplasia (Zhou et al., 2019). Interestingly, elevated PAR3 segregates KIBRA from NF2/FRMD6 and forms the PAR3/aPKC/KIBRA. This PAR3-mediated restrain of KIBRA also inactivates the Hippo pathway and accelerates the metastasis of prostate cancer (Zhou et al., 2017). Together,

Mammalian cells have similar polarity machinery of the Par complex to regulate the Hippo pathway.

Scrib/Dlg/Lgl

Another indispensable group of proteins to establish epithelial polarity is also identified in *Drosophila*. Scribble (Scrib), Disc large (Dlg), and Lethal giant larva (Lgl) locate beneath the adherens junctions in epithelial cells (Macara, 2004) and form another complex. aPKC-mediated exclusion of Lgl from the apical domain and the association between Crb and Par complexes allow the specification of the apical domain. Scribble complex, in turn, antagonizes the activity of the apical Crb and aPKC complexes to defines the basolateral domain. Mutations in either one disassemble the adherens junctions and lead to the spreading of apical marker toward the basolateral domain, resulting in disorganized overgrowth of epithelial tissues (Bilder, 2004; Grzeschik et al., 2007; Macara, 2004).

Proper localization of Scrib complex components is required for Hippo pathway activity in both *Drosophila* and mammalian. Homozygous mutant of *scrib*, *dlg*, or *lgl* shows elevated Yki activity and its target genes expression, which lead to massive overgrowth and tumors in *Drosophila* imaginal discs (Chen et al., 2012a; Grzeschik et al., 2010; Yang et al., 2015). Downregulated expression of these components has been reported in epithelium-relevant disease (Daulat et al., 2019). Decreased expression of SCRIB is found in polycystic kidney disease, and overexpressed SCRIB reduces the cyst formation by mediating YAP phosphorylation and nuclear shuttling (Xu et al., 2018). SCRIB concurrently modulates the Hippo and MAPK/ERK to repress the expression of YAP1, c-Myc, and cyclin D1 in liver. Therefore, SCRIB deficiency enhances liver tumor growth

(Kapil et al., 2017). The depletion of DLG5 decreases the phosphorylation of MST1/2, LATS1/2, and MOB1. Mutant DLG5 and mislocalized SCRIB synergistically compromise the Hippo pathway and increase the nuclear YAP ratio, thus enhancing the epithelial-mesenchymal transition and deteriorating the breast cancer malignancy (Liu et al., 2017).

Loss of Lgl increases cell proliferation with very limited disrupted polarity, indicating Lgl adopts another manner to manage cell proliferation. Hpo is no longer restricted near the plasma membrane and disperses into the cytoplasm in *lgl* mutant clones. Cytoplasmic Hpo interacts with RASSF, which replaces Sav binding and reduces Hpo kinase activity (Grzeschik et al., 2010).

Altogether, apicobasal polarity-mediated Hippo signaling for cell growth is evolutionary conserved. Besides the regulation of the Hippo pathway, recent proteomic studies reveal the negative role of SCRIB in modulating the Wnt/ β-catenin signaling in colorectal cancer, suggesting the apicobasal polarity complexes act through a distinct molecular pathway to regulate cell growth and physiological health.

**Figure D. The components of cell junctions are conserved.**

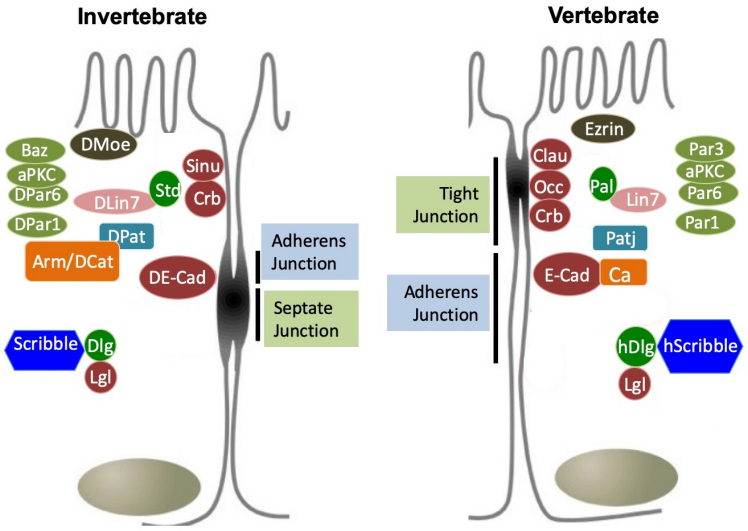


*Janssens & Chavrier (2004)*
*Ashida et al (2012)*

**(2) Cell-cell contact: Cytoskeleton and mechanotransduction**

Organ growth coordinates lots of actions to adapt to physical requirements and extracellular mechanical cues. Tissue architecture responds to the demands to restricts cell growth or exit quiescence. Cell-cell contact at high cell density induces inhibitory signals that are adjusted mainly by the Hippo pathway (Gumbiner and Kim, 2014). In cultured mammalian cells, LATS kinase is activated in high density to represses YAP/TAZ activity. During embryo development, cell-cell contact is critical to fine-tuning YAP/TAZ-mediated transcription (Nishioka et al., 2009). Increased tight junctions and adherens junctions in confluent cells lead to the activation of LATS and YAP/TAZ inactivation. Since attachment to the extracellular matrix (ECM) is essential for cell survival and growth, ECM stiffness also influences cell spreading. Altered cell geometry and cytoskeleton tension regulate the subcellular localization of YAP/TAZ and influence its activity (Aragona et al., 2013).

Junction proteins are required for the cell-cell contact inhibition. E-cadherin (E-cad), a component of adherens junctions, is reported to perform contact inhibition in the cultured mammalian cells along NF-2/KIBRA-LATS axis (Kim et al., 2011). Another adherens junction component α-catenin also restricts Yki/YAP activity. In mammals, α-catenin restricts YAP either through direct binding or inhibiting integrin-mediated activation of SRC tyrosine kinase (Li et al., 2016; Schlegelmilch et al., 2011). *Drosophila* α-catenin recruits LIM domain-containing protein Jub to adherens junction, where Jub inhibits Wts, to promote wing growth (Rauskolb et al., 2014). Besides the cadherin-catenin complex, Echinoid (Ed), an immunoglobulin domain-containing adhesion molecule, also functions as a tumor suppressor upstream to Hpo-Wts kinase cascade.

Different from the cadherin-catenin complex that acts through Mer/Kibra, Ed physically interacts and stabilizes Sav at adherens junction (Yue et al., 2012).

Besides the aforementioned cadherin-mediated adherens junctions, tight junctions and focal adhesions are another two types of machinery implicated in mammalian Hippo pathway. Multiple Hippo pathway components have been found at the tight junctions and they suppress tumorigenesis (Zhao et al., 2011; Zhou et al., 2018). Focal adhesion connects cells and their substrate via transmembrane protein integrins. Hyperactive YAP/TAZ caused by Integrin-linked kinase (ILK)-mediated suppression of NF2 has been identified in breast, prostate, and colon cancer. Furthermore, ErbB2 receptor tyrosine kinase activates YAP/TAZ in the presence of ILK to initiate mammary tumors (Serrano et al., 2013). When cells attach on fibronectin, focal adhesion kinase (FAK) acts through Src-PI3K to inhibit LATS and activate YAP (Kim and Gumbiner, 2015). The shear force also uses integrins to modulates YAP activity. JNK-induced inflammation accelerates the plaque deposition and deteriorates atherosclerosis. Unidirectional shear force, such as blood flow, guides integrin to interact with G-protein Gα13. Integrin-Gα13 together inhibits RhoA and compromises YAP-TAZ-induced proinflammatory gene expression (Wang et al., 2016).

Besides binding to integrins, contractile actomyosin also modulates RhoA to communicate with the Hippo signaling in fly and mammal. Myosin II is a non-muscle myosin responsible for the tension within the actin cytoskeleton. Rho-associated protein kinase (ROCK) phosphorylates the light chain of Myosin II and increases the contractility (Riento and Ridley, 2003). In *Drosoph*ila wing discs, increased ROCK activity results in high cytoskeletal tension and brings Jub to associate with α-catenin at the adherens

junction where Jub antagonizes Wts (Rauskolb et al., 2014). RhoA also elevates YAP activity and the expression of c-Myc to initiate polycystic kidney through RhoA-induced abnormal high cytoskeletal tension (Cai et al., 2018). A recent study shows cell spreading adopts the small GTPase RAP2 to activate LATS1/2 through RhoA inhibition and MAP4K4/6/7 activation, suggesting ECM stiffness executes RhoA-dependent and -independent mechanism simultaneously to inhibits YAP/TAZ (Meng et al., 2018).

Spectrin regulates Yki/YAP activity by antagonizing the cytoskeletal tension (Deng et al., 2015; Fletcher et al., 2015). Spectrin is an actin crosslinking protein at the cytoskeleton-membrane interface. Spectrin-defective cells exhibit significantly high cytoskeletal tension, suggesting spectrin modulates non-muscle Myosin II to control cortical actomyosin and regulates Yki/YAP activity. Human spectrin regulates the subcellular localization of YAP in response to density in human Caco-2 adenocarcinoma colon cells (Fletcher et al., 2015). Mutation of the β-spectrin perturbs the basal actin filament network and upregulates Yki activity to disrupt the oocyte polarity (Wong et al., 2015). α- and β-heavy spectrin (α/βH) form the dimer and localize to the epithelial domain of the imaginal discs. The β-heavy spectrin binds to Ex and promotes the clustering of Crb-Mer-Ex-Kibra complex to antagonize Yki. However, the basolateral α/β spectrin, rather than the apical α/βH spectrin, is critical to restrict Yki activity in the *Drosophila* intestinal epithelium and ovarian follicle epithelium (Fletcher et al., 2015). Collectively, these studies show the varied dependency of spectrin in distinct tissues and subcellular compartments.

**(3) Metabolites**

First reported in glucose starvation, energy deficits skew the AMP:ATP ratio and activates the energy sensor AMP-activated protein kinase (AMPK) to restore energy homeostasis. To retain YAP in the cytoplasm, AMPK phosphorylates AMOTL1 at S793 to activate LATS1/2. Meanwhile, AMPK directly phosphorylates YAP at multiple serine residues to disrupt YAP-TEAD binding (DeRan et al., 2014; Mo et al., 2015; Wang et al., 2015). In *Drosophila*, nutrient-sensing liver kinase B1(LKB1)-AMPK cascade functions independently of Hpo-Wts to regulate Yki activity during the development of the central brain and ventral nerve core (Gailite et al., 2015). The accessibility of nutrients also affects Yki activity. The gluconeogenesis-regulating kinases salt-induced kinase 2 and 3 phosphorylates Sav at Ser413 to promote Yki target gene expression (Wehr et al., 2013). Noticeably, mTOR positively regulates YAP activity through inhibiting autophagy in perivascular epithelioid cell tumors (Santinon et al., 2016). In fly, Tor inhibition by nutrient deprivation keeps Yki away from the promoter of its target genes (Parker and Struhl, 2015). Therefore, Yki/YAP serves as a nexus that coordinates nutrient availability with the genetic program to sustain tissue growth and tumor progression.

**(4) GPCR is responsible for soluble factors and hormone-mediated Hippo signaling.**

Diffusible hormones and growth factors can act through the Hippo pathway to participate the cell proliferation and tissue homeostasis. Once ligands pair to their corresponding receptors, associated G-protein coupled receptors deliver either activation or inhibition signals depending on the subunit constituents of the coupled heterotrimeric G protein (Mo et al., 2012; Yu et al., 2013; Yu et al., 2012a). Lysophosphatidic acid (LPA) and sphingosine 1-phosphate (S1P) are the first two discovered diffusive hormone

molecules. They activate and stabilize YAP/TAZ by acting through their cognate GPCR (Miller et al., 2012; Yu et al., 2012a). Gα12/13- and Gαq/11-coupled GPCR lead to the activation of the Rho GTPase, which triggers actin polymerization to attenuate LATS1/2 (Yu et al., 2012a). Activation of YAP/TAZ caused by Gα12/13- coupled thrombin GPCR has been reported in human glioblastoma (Mo et al., 2012; Yu et al., 2016). Epinephrine performs its physiological function via Gαs-coupled GPCR. Upon stimulation of Gαs-coupled GPCR, protein kinase A (PKA)-mediated inhibition of the Rho GTPase increases LATS1/2 activity, supporting the idea that exercise-induced epinephrine reduces the risks of breast cancer development (Dethlefsen et al., 2017; Gabriel et al., 2016).

## 3. The crosstalk between the Hippo signaling and other pathways to regulate ISCs behavior.

### (1) Mammalian intestine

The intestine is responsible for food uptake, digestion, nutrition absorption, and defecation. Recent reports show that GI cancers are one of the major causes of mortality worldwide. Colorectal cancer (CRC) has been recognized as the top 3 commonly diagnosed cancer, and the fourth leading cause of cancer death worldwide (Bray et al., 2018; Hirata et al., 2019). CRC is more prevalent in Western countries than in Asian countries due to lifestyle, diet variations, and inheritance factors (Deng, 2017). The small intestine is the primary site of nutrient absorption and endocrine secretion and is essential for the human immune response. The small intestine comprises two connected structures: the projected finger-like villi and the crypts, which derive from invaginated epithelium around the villi. Since being the front line to encounter environmental challenges via food

intake, daily shedding of intestinal epithelial cells drives their continuous renewal every 4-5 days. All regenerated epithelial cells are from Lgr5$^{+}$-intestinal stem cells (ISCs), which reside at the base of crypts. To maintain the integrity of intestinal inner lining, ISCs give rise to transit-amplifying cells that further differentiate and migrate up along the crypt-villus axis (Crosnier et al., 2006). Crypt-localized Paneth cells and villus-located Goblet cells together secrete mucin and antimicrobial substance that form a protective coat on the external epithelial surface. Enterocytes, the largest population in the intestine, are along the villus and participate in active transepithelial absorption of nutrients from the lumen. Enteroendocrine cells also locate in the villus and assist in digestion by regulating the secretion of hormones.

**Figure E. The structure and the cell lineages of the mammalian intestine.**

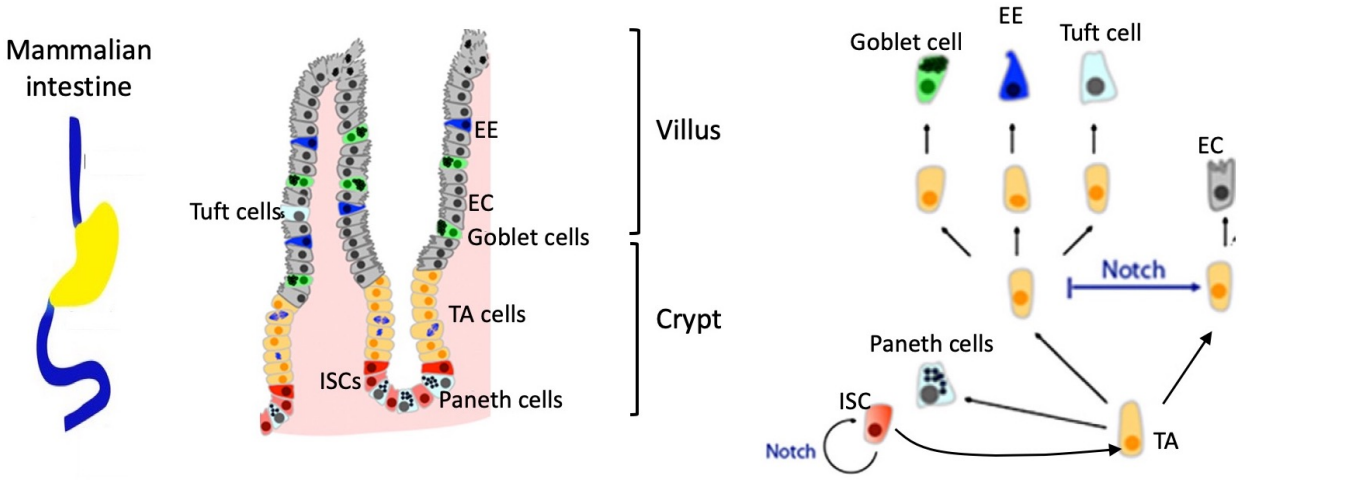


*Perdigoto et al (2013)*

Multiple signaling pathways such as Wnt, Notch, Hedgehog, and EGFR have linked to the Hippo pathway and cooperatively regulate ISCs proliferation under different context. Among them, the crosstalk between the Wnt signaling and the Hippo pathway has been studied most extensively. Both Hippo and Wnt signaling pathways are essential to maintain tissue homeostasis and organ size through managing cell proliferation, differentiation, and apoptosis-mediated cell death (Fevr et al., 2007; Hong et al., 2016; Segditsas and Tomlinson, 2006). Adenomatous polyposis coli (APC), casein kinase Iα (CKIα), and Glycogen syn-thase kinase 3β (GSK3β) form a cytoplasmic destructive complex. In the absence of Wnt ligands, this complex phosphorylates and retains β-catenin in the cytoplasm where proteasome mediates the degradation of β-catenin (Pinto et al., 2003). When canonical Wnt ligands bind to the transmembrane receptors Frizzled and Lrp, β-catenin translocates into the nucleus to interact with LEF/TCF transcription factors and activate target genes (Guezguez et al., 2014; Miyoshi, 2017). The development and regeneration of the intestinal epithelium require the well-controlled canonical Wnt signaling, which participates in ISC proliferation, fate determination, and survival (Fevr et al., 2007). Insufficient Wnt/ β-catenin leads to ISCs loss and tissue degeneration.

Dysfunction of the destructive complex as well as constitutive activation of β-catenin leads to aberrant Wnt signaling, which in turn stimulates ISC proliferation and the development of polyposis and colon cancer. The most prominent mutation in colon cancer is the *Apc* gene (Krausova and Korinek, 2014; Souris et al., 2019). Not relying on β-catenin, Wnt-planar cell polarity, Wnt-$Ca2^{+}$, and Wnt-PKC pathways are categorized in non-canonical Wnt signaling (Chien et al., 2009; Luna-Ulloa et al., 2011). The

transmembrane receptor Frizzled either functions alone or cooperatively with tyrosine-protein kinase receptor ROR2 for Wnt ligands binding. Upon ligands binding, non-canonical Wnt signaling, acting through small GTPase Rho and Rac or transiently promoting the intracellular $Ca2^{+}$ reservoir, contributes to certain developmental processes such as planar cell polarity or cytoskeleton remodeling (Semenov et al., 2007). Knockout Wnt5a or ROR2 presents similar developmental defects and perinatal lethality (Li et al., 2002; Schwabe et al., 2004; Tai et al., 2009; Yamaguchi et al., 1999) and compromised polarity (Nishita et al., 2010). Notably, Wnt dysfunction leads to the development of over 80% of human colorectal carcinomas (White et al., 2012).

With recently emerging evidence, the Hippo pathway and Wnt signaling present overlapping functions in mammalian gastrointestinal tumorigenesis, although controversial opinions exist. YAP overexpression or MST1/2 deletion leads to increased β-catenin transcription activity and downstream target genes (Camargo et al., 2007; Chiurillo, 2015; Li et al., 2019; Zhou et al., 2011). Cytoplasmic YAP1/TAZ represses β-catenin activity by limiting Dishevelled, a positive regulator of Wnt signaling (Barry et al., 2013; Imajo et al., 2012; Varelas et al., 2010a). YAP1 also can cooperate with the destructive complex to phosphorylate β-catenin and retain it in the cytoplasm. The crosstalk is bidirectional. Overexpressed YAP caused by loss of functional APC is often observed in colon cancer. APC can directly interact with SAV and LATS to restrict YAP activity without β-catenin involvement (Cai et al., 2015). When canonical Wnt ligand Wnt3a binds to Frizzled/Lrp receptor, both β-catenin and YAP1/TAZ translocate to nuclear and gain their transcription activity, suggesting that YAP could be a potential downstream target of the Wnt signaling (Park and Jeong, 2015). Consistently, knockdown

β-catenin in colon cancer cells reduced YAP mRNA and protein levels (Konsavage et al., 2012). Wnt3a stabilize TAZ by protects TAZ from binding to 14-3-3 protein (Byun et al., 2014). Additionally, non-canonical Wnt signaling promotes YAP/TAZ activity as well. The binding of Wnt5a to Frizzled/ROR2 receptors leads to the Gα12/13-mediated activation of GPCR, which activates YAP1/TAZ by Rho GTPase-mediated inhibition of LATS1/2 (Park et al., 2015).

### *(2) Drosophila* midgut

Adult stem cells are critical for maintaining tissue homeostasis throughout lifespan. The balance between stem cell proliferation, self-renewal and differentiation of progenies has to be well controlled. Imbalance among these processes may lead to tumorigenesis or tissue degeneration. With comparable epithelial features as the mammalian intestine, the adult *Drosophila* midgut is a powerful genetic tool to dissect the mechanisms that govern the intestinal stem cell (ISC)-mediated homeostasis under various context. The *Drosophila* adult midgut consists of a simple monolayer epithelium surrounded by visceral muscle, nerve, and the trachea (Miguel-Aliaga et al., 2018). Approximately a thousand ISCs are evenly distributed throughout the adult *Drosophila* midgut epithelium. These ISCs are localized at the basal side of the epithelium, underneath a monolayer of enterocytes (ECs), which are the major cell type lining the midgut. An ISC undergoes asymmetric division to generate a renewed ISC and another daughter cell, which can differentiate along the enteroblast (EB)-EC lineage or along the enteroendocrine (preEE-EE) lineage in response to diverse signals (Guo and Ohlstein, 2015; Micchelli and Perrimon, 2006; Micchelli et al., 2011; Ohlstein and Spradling, 2007).

**Figure F. The *Drosophila* midgut.**

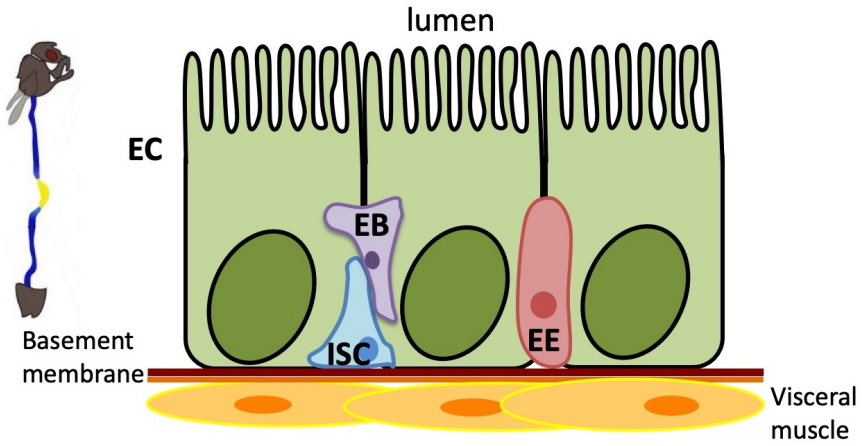


Basal activities of multiple conserved signaling are required to coordinate the ISC proliferation for the intestinal tissue homeostasis. Escargot plays a pivotal role in maintaining the stem cell pool and blocking premature differentiation (Korzelius et al., 2014; Loza-Coll et al., 2014). Delta/Notch pathway modulates the asymmetric division that preserves the ISC pools and generate functional differentiated cells. Canonical Wnt signaling from circular viscera muscles and bone morphogenetic protein (BMP) signaling from ECs antagonize Notch activation to promotes ISC self-renewal (Lin et al., 2008; Tian and Jiang, 2014). Hedgehog (Hh) signaling is negatively mediated by Debra in ISC to restrict its proliferation in a minimal requirement level (Li et al., 2014b). Additionally, Hippo signaling is required in the precursors to restrain ISC proliferation (Ren et al., 2010). Aging has been known a factor that disrupts the balance between JNK signaling and Delta/Notch pathway induces ISC mid-differentiation (Biteau et al., 2008). The intestine epithelium is constantly exposed to lumen for nutrient absorption and serves as the front line to encounter pathogen and toxics along with food ingestion. Dietary infection stresses out the EC. Damaged EC as well as the surrounding visceral muscle secrete the IL6-like

cytokine, EGFR ligands, and BMP ligand to drive ISC proliferation and accelerate differentiation for tissue repair. Epithelial impairment also triggers the expression of Wg in undifferentiated EB that stimulates ISC proliferation along c-Myc axis (Cordero et al., 2012).

**Figure G. Epithelial niche and conserved signaling regulate ISC division and cell fate to control homeostasis.**

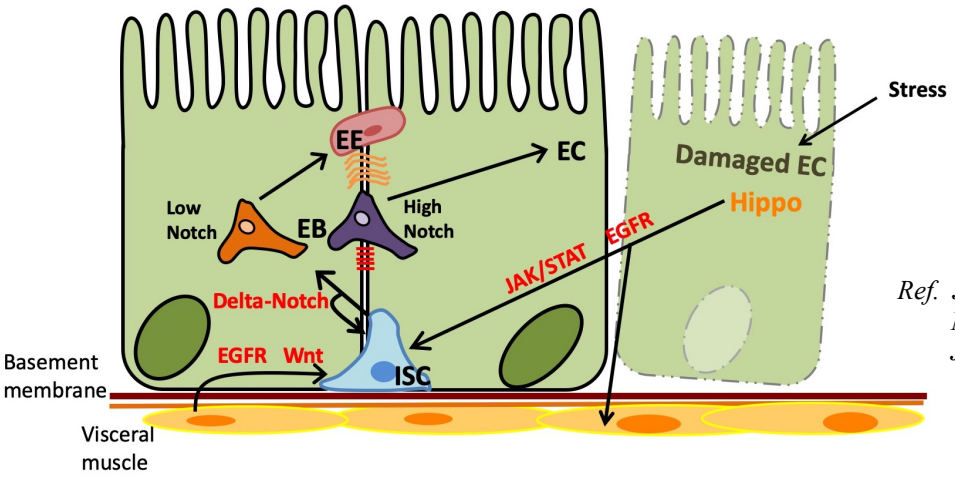


*Ref. Jiang & Edgar (2011)*
*Navascues et. al (2012)*
*Jiang et al (2016)*

The Hippo signaling is a conserved signaling pathway to control tissue growth and organ size during development (Pan, 2010; Zhang et al., 2009). In adult *Drosophila* midgut, Hippo signaling is known to restrains the ISC proliferation. A variety of biological inputs converge in the effector Yki and then turn into various signals to maintain the tissue homeostasis (Karpowicz et al., 2010; Staley and Irvine, 2010). Although Yki has no effect on homeostatic ISC renewal`, it is required to execute damaged-induced tissue regeneration since knockdown yki in ISC completely blocks damage-induced proliferation. Bacterial infection or bleomycin feeding damages the intestinal epithelium. The Hippo signaling cooperates with JAK/STAT and EGFR pathway`, responding to the injured intestinal epithelium. Yki in ECs conducts the secretion of the cytokine Upd3 and EGFR ligands to simulate ISC proliferation. Increased JNK signaling in injured ECs also activates Yki to release cytokine and EGFR ligands. However`, Yki inactivation in ECs only partially suppress infection- or bleomycin-triggered proliferation`, suggesting the existing of other regulators (Ren et al., 2010; Shaw et al., 2010). The identification of Misshapen (Msn) partially fills out the missing part (Li et al., 2014a). Biochemical assay shows that Msn physically interacts with Wts and phosphorylates Wts. Genetic studies further reveal that Msn acts specifically in EBs to inhibit Yki activity and the production of Upd3, whereas ECs rely on Hpo.

Disrupted cell junction is a feature of dying ECs. In adult midgut, reduced expression of smooth septate junction proteins induces robust ISC proliferation due to Yki activation. To maintain the midgut homeostasis, smooth septate junctions adopt both Hpo-dependent and -independent manner. Tsp2A-mediated endocytosis of aPKC leads to the activation of Hpo in EC (Xu et al., 2019). In contrast, Yki directly interacts with Ssk and

Mesh and is restrained in the membrane compartment regardless of Hpo or Wts activity (Chapter II).

## 3. Cell Junction

The epithelium is a continuous sheet of tightly associated cells that cover the external surface of the tissue. As a necessary component of metazoa, epithelium forms barriers to create and maintain biological compartments in the organism. Contacts between adjacent cells are made up of tight junctions (TJs), adherens junctions (AJs), and desmosomes. With their unique cellular functions and delicate collaboration, cell junctions gather cells together to regulate critical processes for tissue homeostasis, including tissue barrier, cell proliferation, and cell migration.

### 1. Vertebrate epithelia contain Tight Junctions, Adherens Junctions, and Desmosome.

#### (1) Tight Junction

Tight junctions (TJs) are in the apical domains of the lateral membrane and encircle the epithelial cells to connect adjacent cells. Therefore, TJs regulates the paracellular diffusion of ions and solutes (Pummi et al., 2004). TJs create the fence and gate barrier. The fence segregates the apicolateral and basolateral membrane proteins, while the gate regulates the paracellular pathway (Zihni et al., 2016). TJs can be sub-categorized into the integral and cytoplasmic proteins. Occludin and claudin are tetra-spanning membrane proteins with N- and C-termini residing in the cytoplasm, and zonular occludens (ZO proteins) are the cytoplasmic adaptor protein. They are the three best-characterized components in tight junctions, and the interaction with the cytoskeleton is crucial for the organization and integrity of the junctions in the vertebrate epithelium (Runkle and Mu, 2013; Van Itallie et al., 2017).

Occludin

Occludin, the first identified transmembrane protein of the tight junctions, consists of four transmembrane motifs with both N'- and C'- terminal cytoplasmic domains. (Ando-Akatsuka et al., 1996; Furuse et al., 1993; Rao, 2009). Two extracellular loops and one short intracellular loop participate in the barrier formation and the paracellular permeability (Fanning et al., 2012). Although the protein structure of occludin is similar to claudin, they do not exhibit any sequence similarities. The extracellular loops confer adhesiveness to seal adjacent cells and stabilize the whole structure of TJs (Medina et al., 2000; Van Itallie and Anderson, 1997). The synthetic homologous peptide against the second extracellular loop leads to the formation of multilayered unpolarized cell clusters and a significant reduction of the TJ-localized occludin. Phosphorylation at cytoplasmic C'-terminal tail is critical for occludin to accumulate at the TJs and form the paracellular barriers (Furuse, 2010). PKC, CK2, and non-receptor tyrosine kinases c-Yes phosphorylates distinct serine, threonine, and tyrosine residues depending on various demands (Andreeva et al., 2001; Chen et al., 2002b; Raleigh et al., 2011; Sakakibara et al., 1997). Moreover, mechanical force changes cells shape and leads to the reorganization of the F-actin cytoskeleton (Ishiyama et al., 2018). To respond to the mechanical force-induced deformation, Occludin indirectly interacts with F-actin by associating with the TJs plaque proteins ZO-1, ZO-2, and ZO-3 (Furuse, 2010).

Although overexpressed occludin integrates into the TJs successfully, altered transepithelial electric resistance and paracellular flux indicate the weaker adhesiveness, suggesting its supportive role in TJs assembly (Balda et al., 1996; Realini et al., 1999). Consistently, Occludin-deficient epithelial cells have no overtly morphological

abnormalities (Saitou et al., 2000). Reduced occludin impairs wound healing ability when epithelial cells encounter mechanical stress (Volksdorf et al., 2017). Many chronic inflammation-related diseases also highly correlate with the compromised occludin expression, including colorectal cancer (Chelakkot et al., 2017; Wang et al., 2013).

Claudin

After the identification of occludin, the viable occludin-deficient mice and the formation of TJs in occludin-deficient stem cells lead to the discovery of another tetra-transmembrane protein in TJs (Saitou et al., 2000). Claudins polymerize linearly and form the tight junction strands in the apical part of the cell membrane, where strands adhere to each other in either homophilic or heterophilic fashion (Günzel and Yu, 2013). Varied mixing ratio moderates the permeability of the transepithelial barriers in TJs. Hence, Claudins play a crucial role in the formation of the paracellular barrier to control the distribution of various solutes (Furuse et al., 1998a; Suzuki et al., 2014; Umeda et al., 2006). Twenty-seven claudin subtypes have been identified in mammals. They share basic structure with some differences in their extracellular regions, accounting for their varying roles in growth control in addition to the well-known cell junction (Furuse et al., 1998b; Mineta et al., 2011; Tamura and Tsukita, 2014; Tsukita et al., 2019).

Abnormal claudin expression leads to a variety of disease conditions. Impaired formation of the paracellular barrier in the claudin knockout mice demonstrates the roles in preventing water balance, inflammation, tumorigenesis (Bao et al., 2019; Plissonnier et al., 2017; Tamura and Tsukita, 2014; Tanaka et al., 2015). Dehydration and the leakage of sweat glands caused by loss of claudin-1 and -3 induce atopic dermatitis (Tokumasu et al., 2016; Yamaga et al., 2018). Insufficient claudin-3, 7, and 18 compromise the

paracellular barrier along the digestive tract, and have been associated with gastrointestinal cancers. Claudin-18 deficiency is known to accelerate the progression of gastric cancer (Tanaka et al., 2015). The depletion of claudin-7 initiates the colon inflammation due to the increased sensitivity to bacterial products. Claudin-3 knockout mice have leaky colonic epithelium and are highly potential to develop invasive adenocarcinoma. Excessive IL-6 cytokine and hyperactive Wnt/β-catenin cooperatively worsen the malignancy and promote colon cancer. Consistently, reduced claudin-3 expression highly correlates with poor survival in colorectal cancer patients (Ahmad et al., 2017).

The cytoplasmic scaffold proteins that connect claudin and the actin cytoskeleton is required for claudin to participate in cellular events. The C-terminal cytoplasmic region of claudin interacts with the PDZ domain of ZO protein to regulate epithelial growth and morphology (Spadaro et al., 2017). Conformational change of ZO-1 caused by actomyosin contractility recruits the transcriptional factor Dbp1 to tight junctions, where ZO-1 and claudin together sequester Dbp1 in the cytoplasm. Therefore, Dbp1-mediated gene expression and proliferation are suppressed. YAP activation is widespread in human tumors and is essential for cancer initiation and progression. Deficiency of claudin-18 results in the YAP nuclear accumulation, which induces the abnormal overgrowth of alveolar cells, and the formation of lung adenocarcinoma (Zhou et al., 2018). Collectively, Claudins integrate the paracellular barrier and signaling function of TJs in different contexts to establish tissue homeostasis.

Zona occludens (ZO)

The cytoplasmic plaque of the TJs serves as an interface to convey extracellular cues inward the cytoplasm (Zihni et al., 2016). The cytoplasmic plaque contains lots of adaptor proteins with several motifs for protein interaction to create an intricate network (Van Itallie and Anderson, 2014; Zihni et al., 2016). The membrane-associated guanylate kinase (MAGUK) family proteins Zona occludens (ZOs) are prevalent in the cytoplasmic plaque and consist of ZO-1, ZO-2, and ZO-3 that regulate epithelial cell proliferation in response to the cell density (Balda et al., 2003; Haskins et al., 1998; Jesaitis and Goodenough, 1994). The conserved domain structure in the N'-terminal half, comprising three PDZ domains and an SH3 domain followed by a guanylate kinase homology (GUK) domain, associates with the transmembrane TJs proteins, whereas the C'-terminal part with varying length contacts the actin cytoskeleton (Van Itallie et al., 2013).

PDZ domains-mediated heterodimerization of ZO proteins is essential for the membrane recruitment to the TJs. ZO proteins associate with junctional proteins and help the polymerization of claudin to form TJ strands, suggesting their role in TJ assembly (Fanning and Anderson, 2009; Gumbiner et al., 1991; Haskins et al., 1998; Rodgers et al., 2013; Umeda et al., 2006). Knockdown ZO-1 in mammalian MDCK cells results in the impaired TJ localization of occludin and claudin. Consequently, this improper TJ assembly leads to the expansion of apical actomyosin array as well as the increased epithelial permeability (Rodgers et al., 2013). GUK domains guide ZO-1 to bind the occludin (Schmidt et al., 2004). Other studies further reveal the SH3 domain blocks the gene expression of cell cycle by associating with the Y-box transcription factor ZONAB (Balda and Matter, 2000; Tsapara et al., 2006). Varied length and diameter of the

microvillus result in irregular apical surface is found in the intestinal epithelium of the ZO-1 KO mice. This abnormal morphology suggests the essential roles of ZO proteins to reorganize the F-actin cytoskeleton (Odenwald et al., 2018). In addition to tissue morphology, ZO proteins regulate cell growth by restrain YAP in the cytoplasm. ZO-2 directly binds to YAP via the first PDZ domain. Knockdown ZO-2 in sparse mammary and kidney epithelial cells abrogates the nuclear localization of YAP (Bence et al., 2012; Spadaro et al., 2014), indicating ZO proteins as mechanotransducers that connect TJ to F-actin and intracellular signaling molecules (Fanning et al., 2012; Karaman and Halder, 2018). Altogether, each motif has its characters and functions cooperatively to maintain junctional integrity and regulate proliferation in a context-dependent manner.

**Figure H. Schematic representation of the basic structural components of tight junctions and adherens junctions.**

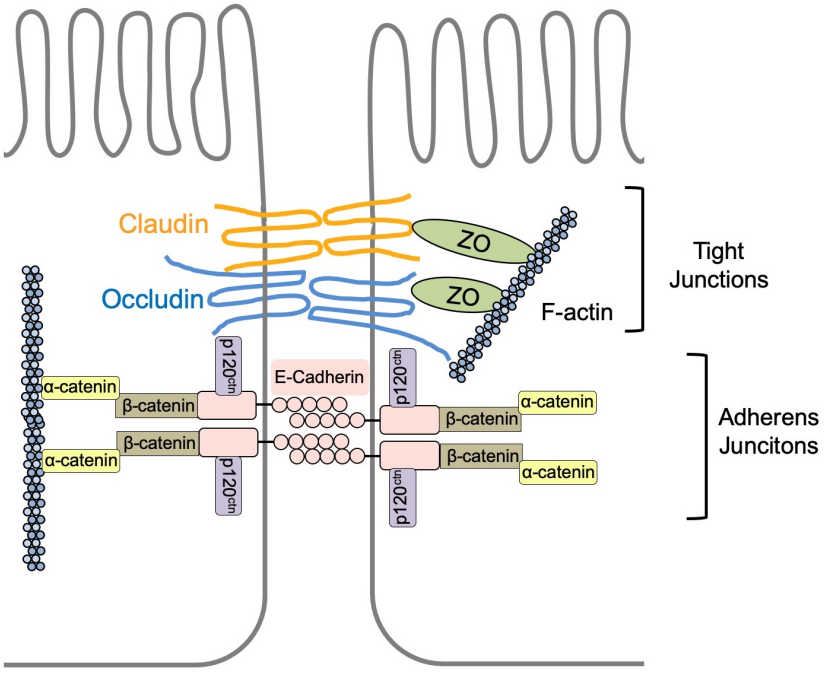

**(2) Adherens Junctions (AJs)**

The epithelium is the most prevalent tissue architecture which covers the organ and body surface. Continuous epithelial cells form a sheet to delineate the interior space from the exterior environment. Epithelial cells undergo multiple rounds of changes in their cell shape, cell-cell interaction, and cell numbers during the development to fit different demands. In mammals, adherens junctions (AJs) connect epithelial cells beneath the apical TJs and is a prerequisite for TJs formation (Watabe et al., 1994). Together with TJs, AJs strengthen the cohesiveness between adjacent cells, critical for epithelial integrity and physiological maintenance (Samiei et al., 2019; Shigetomi and Ikenouchi, 2019).

The core of AJs is E-cadherin, which form the adhesive homodimer in trans by the N'-terminal extracellular domain (Samiei et al., 2019; Takeichi, 2014). E-cadherin-, α-catenin and nectin-afadin complexes immediately develop into the spot-like AJs in the presence of $Ca^{2+}$. These newly-formed spot-like AJs then fuse and form a continuous belt-like structure (Vasioukhin et al., 2000; Yonemura et al., 1995). In addition to the apical E-cadherin band, mature epithelial sheets also exhibit a belt-like circumferential actin ring that is oriented parallel to the AJs plane. The stability of AJs relies on anchoring E-cadherin to the underlying circumferential actin ring (Zhang et al., 2005). The cytoplasmic part of E-cadherin interacts with p120 catenin and β-catenin, which associate with α-catenin, to form the E-cadherin-catenin complex at cell-cell boundaries (Laguna, 1984; Watabe et al., 1994). Whether α-catenin directly interacts with F-actin remains debatable for many years. Recent crystal structure studies reveal the actin-binding protein vinculin binds to the modulatory domain of α -catenin, thereby connecting the E-cadherin-catenin

complex to the underlying F-actin (Choi et al., 2012; Ishiyama et al., 2013; Peng et al., 2010; Rangarajan and Izard, 2012).

How to maintain the structure and integrity of AJs is complicated. $Ca^{2+}$ is required for the rigidity of E-cadherin and initiates the formation of AJs (Gumbiner et al., 1988; Ivanov et al., 2004; McMahon, 2000). Cultured cells fail to establish the cell adhesion and turn into a rounded shape when $Ca^{2+}$ is absent (Watabe et al., 1994). The abundance of cytosolic p120 catenin prevents the clathrin-dependent endocytosis of E-cadherin (Harris, 2012a; Xiao et al., 2007). The polymerization of actin filaments is crucial to stabilize AJs. The activity of the Rho family of small GTPase, including RhoA, Rac, Cdc42, is a spatial and temporal switch to control actin polymerization throughout the development of the perijunctional actin ring (Priya et al., 2015). Moreover, RhoA-involved turnover of F-actin has been linked to cell growth control and tumor invasion, suggesting a tumor suppressor role of AJs (Meng et al., 2018; Qiao et al., 2017).

**(3) Desmosome**

Desmosome is an intercellular junction that connects the intermediate filament to the cell surface. The primary role of the desmosome in the cell junction is to resist mechanical stress. Therefore, it is prominent in the tissues that are subject to strong mechanical force such as myocardium and stratified squamous epithelial (Broussard et al., 2015). Besides serving as a node where protein components cluster and mediate cell adhesion, desmosome also engages in the organization of cytoskeleton, intracellular signaling, and developmental patterning to maintain physiological homeostasis (Kottke et al., 2006).

Desmosome consists of desmosomal cadherins, armadillo proteins, and plakin family of cytolinkers. It is appreciated by the highly electro-dense plasma membrane domain that associates with the intermediate filaments network (Garrod et al., 2002b). The spatial organization of the desmosome includes the intercellular space with tight cell-cell adhesion and the cytoplasmic plaque that transmits the adhesive interaction inwardly to the intermediate filaments (McGrath et al., 1999; Zhurinsky et al., 2000). $Ca^{2+}$ is required for desmosome assembly and the post-translational modifications such as phosphorylation and proteolysis, which in turn stabilize the structure (Yin and Green, 2004).

**Figure I. Schematic representation of the structural components of Desmosome.**

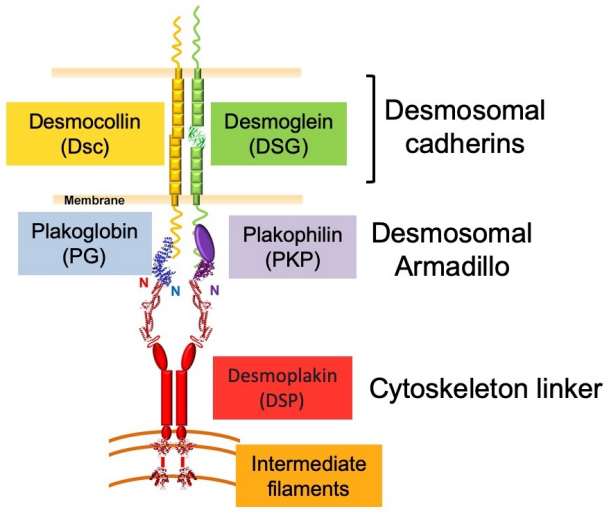


*Al-Jassar et al (2013)*

(1) Desmosomal cadherins

Transmembrane proteins desmoglein (Dsg) and desmocollin (Dsc) are desmosomal cadherins, and couple the adjacent cells by trans-interaction (Cheng and Koch, 2004; Garrod et al., 2002a). Intracellularly, desmosomal cadherins interact with the armadillo

proteins plakophilin (PKP) and plakoglobin (PG) to link the linker desmoplakin (DSP), which anchors the intermediate filaments in the desmosomal plaque of epithelial cells (Bornslaeger et al., 1996; McGrath et al., 1999; Nekrasova and Green, 2013).

Mutations of Dsg disrupt the normal differentiation of skin and hair follicle cells, leading to defective hair growth and human epidermal diseases (Kato et al., 2015; Kljuic et al., 2003; Rickman et al., 1999). Fewer desmosomes and abnormal keratinization are found in monilethrix, a hair shaft characterized by beaded hair with periodic changes in hair thickness. Dsg4 mutation is associated with Monilethrix. Frameshift-induced premature DSG4 loses its affinity to the adaptor plakoglobin and accumulates in the endoplasmic reticulum where DSG4 is degraded by proteasome. Therefore, fewer desmosomes and abnormal keratinization are found in monilethrix (Kato et al., 2015). Depleting the unique region within the C-terminal tail of Dsg1 abrogates the binding to the scaffolding protein Erbin, activates Ras-Raf pathway, and obstructs the differentiation of keratinocytes (Hammers and Stanley, 2013; Harmon et al., 2013). Dimerization and blocked internalization of Dsg2 lead to strong adhesion in the epithelial junctions (Chen et al., 2012b). Dsg2 knockout results in mice lethality at the early embryonic stage (Eshkind et al., 2002). The interrupted dimerization and accelerated internalization caused by either mutation in the unique C-terminal region of Dsg2 or other mutations affecting the post-translational modification are highly corelated with cardiomyopathy (Chen et al., 2012b; Gehmlich et al., 2010; Gehmlich et al., 2012). DSG3 functions as an oncogene to facilitate the growth of head neck cancer by activating the TCF/LEF transcription activity (Chen et al., 2013). Anti-sera from patients with autoimmune skin disease pemphigus vulgaris (PV) phosphorylates DGS3. Phosphorylated DSG3 then

dissociates from the underlying adaptor plakoglobin and activates PKC activity by transiently increased $Ca^{2+}$ concentration (Brown et al., 2014; Gliem et al., 2010). Consistently, abnormal epidermal morphogenesis in mice with misexpressed human DSG3 also highly correlates with the alteration of β-catenin-mediated LEF/TCF activity. Similar to the-cadherin of AJs, the transmembrane-desmosomal cadherins incorporate intracellular signaling to modulate cell fate in addition to forming the cell junction.

(2) Desmosomal armadillo

Desmosomal armadillo includes plakophilin (PKP) and plakoglobin (PG) that integrate the desmosomal cadherins and the cytoskeleton linker desmoplakin (DSP) to interact with intermediate filaments and enhance the adhesion (Moccia et al., 2019).

Plakophilin

Plakophilin (PKP) is a vertebrate-specific desmosomal armadillo protein of $p120^{CTN}$-related family and have diverse roles in biology and clinical pathology (Leick et al., 2019). PKP1, 2, and 3 are the isoforms exhibit tissue- and differentiation-dependent patterns (Hatzfeld, 2007; Hatzfeld et al., 2014). PKP1 expression is high in the suprabasal layers of the desmosome complex and stratified epithelial. PKP2 and 3 are detected in most simple and stratified epithelia, except for the cardiomyocytes where the expression of PKP2 is exclusive. Being the scaffolds, PKPs interact with both transmembrane desmosomal cadherins and DSP in variable extent to promote desmosome assembly, maturation, and anchorage to the intermediate filament cytoskeleton (Hatzfeld et al., 2014).

Redistribution of DSP is found in both $PKP1^{-/-}$ patient and conditional PKP3 knockout mice with reduced epithelial stability but not lethal. In contrast, knockout PKP2, the only

PKP existing in cardiomyocytes, leads to embryonic lethality due to heart failure (Grossmann et al., 2004). PKP1 and PKP2 are also present in the nucleus, but the function is not clear yet. Although PKPs are categorized in desmosomes, they associate with AJs protein under certain circumstances. PKP2 can form a mixed junction in cardiomyocytes (Pieperhoff et al., 2008). PKP2 also associate with β-catenin to upregulate the endogenous β-catenin/TCF ability that is abolished by ectopic E-cadherin expression (Chen et al., 2002a). Moreover, E-cadherin and plakoglobin are required for PKP3 recruitment to cell borders where PKP3 initiates the desmosome assembly.

Plakoglobin

Plakoglobin (PG) is another armadillo family protein in desmosome to enhance adhesion. Similar to PKP, the subcellular localization of PG is in the nucleus as well as the cytoplasmic desmosome, and PG participates in the regulation of β-catenin/Wnt signaling (Aktary and Pasdar, 2012; Lam et al., 2012).

PG is essential for normal skin physiology. Conditional knockout PG in mouse epidermal keratinocytes results in the epidermal cornification, epidermal thickening, and exacerbate inflammation (Li et al., 2012). Besides the disturbed structure of desmosome and AJs, loss of PG induces the accumulation of β-catenin at the cell-cell junction. As a compensational effect, accumulated β-catenin activates the expression of desmosomal cadherins by the LEF transcription factor and EDA/NF-kB signaling (Li et al., 2012; Li et al., 2011; Tokonzaba et al., 2013). Reduced PG in human keratinocytes activates p38 MAPK to disconnect the cell adhesion and collapses the keratin network (Spindler et al., 2014).

PG knockout mice die between E10.5 and birth because of severe cardiac and skin defects (Bierkamp et al., 1996). In humans, PG is associated with skin and heart disease and some types of cancer. The first reported desmosome-associated cardiocutaneous syndrome is from PG mutations (Asimaki et al., 2007). Although two human mutations don't show heart defects, they have fragile skin, diffuse palmoplantar keratoderma, and wooly hair (Cabral et al., 2010). Another nonsense mutation of PG leads to undetectable PG in the skin and fragile congenital skin, but the patients have no apparent cardiac dysfunction (Pigors et al., 2011). Since PG is critical for the tissues subject to strong mechanical stress such as heart and skin, the discrepancy probably is attributed to the level and timing of genetic deletion of PG. Both PG and β-catenin are cadherin-binding proteins. Simultaneous ablation of PG and β-catenin in the mouse leads to much more extensive collapse of cell junctions, including connexin43-mediated gap junction, and sudden cardiac death (Swope et al., 2012), suggesting the indispensable requirement of armadillo family protein.

Desmoplakin (DSP)

Plakin family organizes the intermediate filaments cytoskeleton and anchor the network to the cell membrane (Subramanian et al., 2003). Although the plakin family has several members, desmoplakin (DSP) is an indispensable desmosomal component that links the transmembrane desmosomal cadherin complex to the intermediate filament cytoskeleton, which provides tensile strength (Määttä et al., 2001). DSP-null mouse embryos die at E6.5 indicates, indicating the importance of DSP (Gallicano et al., 1998). Tissue-specific conditional knockouts later exhibit the requirement for DSP in vascular development, epidermal integrity, and cardiac function (Gallicano et al., 2001; Lyon et al.,

2014; Vasioukhin et al., 2001b; Yang et al., 2006). A wide range of DSP mutations in humans is highlighted by severe skin or cardiac defects (Thomason et al., 2010). Patients with autosomal dominant mutations in the gene encoding DSP have abnormal keratoderma and cardiomyopathy (Getsios et al., 2004). Systematic deletion of DSP or mutation in the IF-binding C-terminus leads to an inherited blistering disease due to the failed desmosome assembly (Hobbs et al., 2010). Missense mutation leads to Carvajal/Naxos syndrome, featured by cardiomyopathy, abnormal thickening of the palm skin, and wooly hair (Keller et al., 2012). However, the underlying mechanism to initiating the phenotypes remains unclear.

Desmosome assembly is important for the formation of other cell junctions. Reduced expression of DSP in the adult epidermis is associated with the reduced number of AJ, suggesting the establishment of desmosome can influence the AJs maturation. Several studies further indicate that failed desmosome assembly results in aberrant gap junctions. Incomplete formation of the gap junction causes deleterious dysfunction of the heart and epidermis, such as arrhythmogenic cardiomyopathy (ACM), an inherited disorder that frequently results in deadly arrhythmias (Cohen Barak et al., 2019; Kam et al., 2018; Schinner et al., 2019). DSP interacts with the microtubule-associated proteins EB1 to modulate microtubular dynamics and delivers connexin43 toward the plasma membrane (Patel et al., 2014a; Patel et al., 2014b). Loss of DSP triggers activation of ERK1/2-MAPK and phosphorylation of connexin43 to initiate clathrin-mediated internalization, followed by lysosomal degradation, to impair gap junction (Kam et al., 2018). Moreover, improper electrical coupling problems caused by inadequate connexin are found in DSP-related cardiomyopathies (Asimaki et al., 2009; Gomes et al., 2012).

Collectively, the components of desmosomes not only perform the adhesiveness to strengthen the connection of epithelial cells but incorporate different intracellular signaling to regulate cell fate decision during epidermal development and cancer progression.

## 2. The cell junctions of the invertebrates exhibit comparable functions, but with fewer similarities of the molecular composition and spatial arrangement.

*Drosophila melanogaster* is a powerful tool to dissect the molecular mechanisms that establish and maintain the epithelial polarity. Many vital polarity regulators are studied in the fly before or in parallel with their evolutionally conserved counterparts in other organisms. Despite the similarity, these conserved regulators of epithelial polarity have distinct roles in a tissue-dependent manner.

The cytoarchitecture of cell junctions in most *Drosophila* epithelia includes the adherens junctions (AJs) and septate junctions (SJs), but desmosome or desmosomal proteins have not been identified in fly's epithelia. The AJs of *Drosophila* epithelium is very similar to the mammalian AJs in the structural features, the molecular composition, and the adhesive function (Harris, 2012b). The tight junctions of mammals and the septate junctions of most invertebrates are the places to establish the paracellular barriers (Schulte et al., 2003). Although TJs and SJs exhibit their differences in ultrastructure, spatial arrangement, and molecular composition, they share certain similarities that enable them to perform polarity and effective permeability control. For example, Crb, as well as the Par complex, is the regulator to maintain the shape and polarity of *Drosophila* epithelial. The claudin family proteins Megatrachea, sinuous, and Kune-Kune present in the SJs of *Drosophila* epithelia for the barrier integrity (Behr et al., 2003;

Nelson et al., 2010). Moreover, both TJs and SJs are composed of cytosolic strands with varying amounts in a tissue-dependent manner. The cytosolic multi-stranded composition appears to be necessary to block the paracellular flow of substances effectively (Müller, 2018).

SJs are characterized by the ladder-like array of the septa, which span 15-20 nm intermembrane space of adjacent cells (Yanagihashi et al., 2012). *Drosophila* contains two types of SJs: pleated SJs and smooth SJs. Although both SJs are organized in ladder-like septa, the zigzag and smooth lines along the cell membrane in tracer-infiltrated specimens are pleated SJs and smooth SJs, respectively (Yanagihashi et al., 2012). The origins of pleated and smooth SJs are different. Pleated SJs are found in ectodermal epithelia such as epidermis, hindgut, and tracheae. In contrast, smooth SJs are in the midgut epithelial developed from endoderm (Tepass and Hartenstein, 1994a). Snakeskin (Ssk), Mesh, and Tetraspanin 2A (Tsp2A) are three identified smooth SJs-specific proteins (Izumi et al., 2016; Izumi et al., 2012; Yanagihashi et al., 2012). In addition to the well-known barrier function, they incorporate intracellular signaling to regulate the resident ISCs proliferation in response to the environmental demands (Chapter II & (Izumi et al., 2019; Xu et al., 2019).

The spatial arrangement of these junctional proteins in earlier studies from *Drosophila* embryo and exhibits the opposite orientation between the vertebrates and *Drosophila*. SJs locate in the apical region immediately below the AJs along the lateral cell surface of adjacent cells while the TJs is apical to the AJ in mammals (Tepass, 2003). However, a recent report shows the *Drosophila* midgut is more like vertebrate epithelia that form occluding junctions above the AJs and need integrin adhesion complex for its integrity

(Chen et al., 2018a). Conventionally, apical-localized Crb and Par complex and basolateral-localized Scrib complex mutually antagonize to define the apical-basal polarity and decide the AJs position in most *Drosophila* epithelia. In the adult midgut, these complexes have no effects on the ECs polarity. Instead, ECs polarization in the adult midgut, as well as mammalian epithelium, requires the cues from basal integrin-mediated adhesion (Lee and Streuli, 2014). Talin, encoded by *Drosophila rhea*, mediates the integrin adhesive machinery to establish the EC polarity followed by proper sSJs assembly (Lee and Streuli, 2014). Mutation analysis of Mesh and Tsp2A further reveals the requirement of proper sSJs formation for newly-born EC to integrate into the midgut epithelium (Chen et al., 2018a).

What drives the difference existed exclusively in adult midgut? One explanation is the different origination. The midgut epithelium is from endoderm, while other epithelia are derived from ectoderm that originates from the blastoderm. Failed assembly of precursor AJs leads to the lack of basolateral polarity in blastoderm and converts the blastoderm epithelium into a mesenchymal cell mass during gastrulation (Müller and Wieschaus, 1996). In contrast, two embryonic endoderm precursors, the anterior and the posterior midgut primordia, undergo an epithelial-mesenchymal transition (EMT), migrate, and then take a mesenchymal-epithelial transition to regain the epithelial features. The anterior and the posterior midgut join together, forming a continuous tube in the late embryo (Campbell et al., 2011; Devenport and Brown, 2004; Tepass and Hartenstein, 1994b). Along with the development, midgut epithelium does not express polarity genes, such as *crb*, to establish a junctional complex and form apical AJs (Goldberg and Yates, 1990; Tepass and Hartenstein, 1994a).

The adult midgut progenitors (AMPs) are the beginning to build the adult midgut. AMPs initially appearing in the embryonic midgut epithelium among a small number of diploid cells are set aside from the midgut primordia. The AMPs form clusters where AMPs continuously proliferate in late larval and pupal stages and then generate the adult midgut epithelium during metamorphosis. Some AMPs that remain attached to the basolateral domain of the adult midgut epithelium turn into intestinal stem cells (ISCs), which support the homeostasis of adult midguts (Jiang and Edgar, 2011; Micchelli and Perrimon, 2006; Micchelli et al., 2011; Ohlstein and Spradling, 2007).

In addition to the endogenous mechanisms, the interface that cells contact with ECM may be another parameter to influence the epithelial polarity when ISCs undergo differentiation in adult midgut. ECM has been known as a crucial factor in mammals to regulate the epithelial polarity and morphogenesis through the integrin-mediated interaction (Manninen, 2015). Moreover, studies of the suspended multicellular cyst demonstrate that cell-cell or cell-substratum contact orient the polarity in the suspended multicellular cyst. In suspension culture, MDCK cells form a multicellular cyst, consisting of polarized epithelia in which apical domains encounter the growth medium and basolateral membranes face toward the central lumen. When the cysts are placed in a collagen gel, rapid disassembly and redistribution of the membrane domains by endocytosis and endosomal trafficking reverse the polarity without cell dissociation (Wang et al., 1990a, b). The deposition of laminin A is vital to drive MET during mammalian kidney development (Klein et al., 1988). Hence, basal cues seem superior to the signals from the apical domains for polarity establishment in the epithelial cells derived from mesenchymal cells or stem cells (Kim et al., 2017). Since adult midgut is originated from

endoderm, ISCs might keep the MET characteristics of midgut primordia to respond to the environment demands after AMPs undergo metamorphosis. Whether the polarity can be established in AMPs during metamorphosis and is inherited by adult midgut ECs needs more efforts to elucidate it.

### 3. The pathways and mechanisms that cell junctions use to regulate cell growth.

Aberrant polarity and epithelial disorganization are features of cancer development. Components that establish the cell polarity are found along the cell junctions. Therefore, it is not surprising that loss of cell polarity triggers abnormal cell proliferation (Schimizzi et al., 2016). Additionally, contact inhibition and altered tension caused by loss of cell junctions also influence cell growth, suggesting mechanotransduction is another independent mechanism involved in growth control (Balda et al., 2003; Betanzos et al., 2004; Brückner and Janshoff, 2018; Huerta et al., 2007; Yu et al., 2012b).

ZO proteins link TJs transmembrane proteins to the actin cytoskeleton and are implicated in regulating cell proliferation and differentiation by interacting with transcription regulators and signaling pathways (Domínguez-Calderón et al., 2016; González-Mariscal et al., 2014; González-Mariscal et al., 2008; Huerta et al., 2007). In mouse embryonic stem cells, ZO-1 regulates the c-Myc expression to mediate the proliferation and antagonize differentiation (Xu et al., 2012). The Y-box containing transcription factor, ZONAB (ZO-1-associated nucleic acid-binding protein) binds to the promoter of the proto-oncogene ErbB-2 and several cell cycle regulators (Balda and Matter, 2000). ZONAB has been found in the nucleus and associates with the TJs. ZONAB interacts with CDK4 and their nuclear accumulation is required for cell

proliferation. Enhanced expression of ZO-1 sequesters ZONAB in the cytoplasm and reduces the nuclear accumulation of CDK4 as well as the cyclin D1 expression. The mRNA and protein of the DNA replication factor PCNA are diminished as well. Therefore, ZO-1/ZONAB can modulate the progression of the cell cycle and DNA replication to influence cell growth (Balda et al., 2003; Maga and Hubscher, 2003; Sourisseau et al., 2006).

ZO-2 influences cell growth by regulating transcription in parallel to ZO-1/ZONAB axis. ZO-2 has been reported to interact with Jun, Fos, and C/EBP and dampens the transcription activity of AP-1 site-mediated promoters (Betanzos et al., 2004). ZO-2 also associates with SAF-B, a regulator of transcriptome assembly, to slow the rate of cell proliferation (Dobrzycka et al., 2006; Townson et al., 2000; Traweger et al., 2003). A variety of stimuli initiate cancer development with upregulated cyclin D1 (Albanese et al., 1995; Quelle et al., 1993; Watanabe et al., 1996). The promoter of cyclin D1 harbors a typical E-box. ZO-2 interacts with c-Myc at the E-box, followed by HDAC1 recruitment, to inhibit the transcription of cyclin D1 (Huerta et al., 2007). Moreover, ZO-2 engages in YAP-mediated cell hypertrophy. Knockdown ZO-2 leads to the nuclear translocation of YAP, which in turn activates the Akt/mTOR pathway to increase protein synthesis (Domínguez-Calderón et al., 2016). Independent of contact inhibition, ZO-2 stimulates LATS-dependent phosphorylation of YAP and relocates YAP from nucleus to cytoplasm in confluence culture (Liu et al., 2018). Collectively, ZO-2 modulates the transcription activity or direct the spatial distribution of the transcription factors to regulate cell growth.

AJs-mediated cell-cell adhesion is mainly dependent on anchoring the transmembrane E-cadherin molecules to the underlying actin filaments. p120 catenin

directly stabilizes and retains E-cadherin at the cell surface by suppressing the endocytosis of E-cadherin (Ishiyama and Ikura, 2012; Nanes et al., 2012; Xiao et al., 2003). β-Catenin binds to the cytoplasmic tail of E-cadherin and is essential for the formation of AJs in epithelial cells. α-catenin links E-cadherin/β-catenin to actin filaments (Pokutta et al., 2014; Stockinger et al., 2001). *In trans* homophilic binding of the transmembrane E-cadherin leads to cell contact-mediated inhibition through modulating several growth inhibitory signals such as the Hippo pathway, RTK, and FAK-Src-PI3K kinase signaling (Gumbiner and Kim, 2014; Kim et al., 2011). Dysfunction of E-cadherin has been linked to epithelial-related cancer. p120 catenin inhibits NF-kB pathway to restrict epithelial hyperproliferation. Abrogated p120 catenin accompanied with altered Rho GTPase activity leads to activation of NF-kB without obvious defective barrier function and intercellular adhesion (Perez-Moreno et al., 2006; Xie et al., 2018). Besides its essential roles in cadherin-mediated adhesion, β-catenin involves in canonical Wnt signaling to regulate proliferation in a variety of epithelia-composed tissues, including the intestine (Sebio et al., 2014).

Different from the abovementioned three components, α-catenin is more like a mechanosensor that undergoes dynamic conformational change in response to altered cytoskeleton tension and thus adjusts the linkage between E-cadherin and actin filaments. (Leerberg et al., 2014; Thomas et al., 2013; Yonemura et al., 2010). The deletion of α-catenin in the developing CNS leads to the expanded cerebral cortex because of the abnormal activation of the Hedgehog signaling, which increases the proliferation and suppresses apoptosis in the neural progenitors (Lien et al., 2006). Whereas, the neuronal differentiation in the α-catenin-null mice is not affected. In epidermal keratinocytes, α-

catenin inactivates Ras-MAPK-Erk 1/2 pathway to mediate skin development. Ablation of α-catenin in keratinocytes results in mildly disrupted apicobasal polarity, decreased desmosomes and TJs, and enlarged intercellular space. Moreover, large multinucleated keratinocytes and hyperproliferation cause the perturbation of epidermis, resembling squamous cell carcinoma (Vasioukhin et al., 2001a). These studies suggest α-catenin modulates distinct signaling to control cell growth and survival depending on the cellular context.

Nuclear translocation of YAP is found in the hyperproliferative α-catenin-null epidermis. However, YAP activity in the epidermis is not governed by the canonical core kinase cascade. Instead, α-catenin forms a tripartite complex with YAP and 14-3-3 and cooperates with PP2A phosphatase to control the phosphorylation and activity of YAP (Schlegelmilch et al., 2011). Interestingly, knockdown other AJs components such as E-cadherin does not affect the activity and subcellular localization of YAP, indicating YAP activation is not managed by AJs-mediated cell adhesion. Actin-remodeling is a parameter to regulate YAP activity (Dasgupta and McCollum, 2019; Kim et al., 2016; Liu et al., 2016b; Morikawa et al., 2015). Although both α-catenin and AMOT associate with actin, the detailed mechanism remains elusive

## CHAPTER II

# The Ssk-Mesh Complex of Smooth Septate Junction Restricts Yorkie to Regulate Intestinal Homeostasis in *Drosophila*

**Author contributions**

Hsi-Ju Chen and Y. Tony Ip conceived the project and designed the experiments; Hsi-Ju Chen, Qi Li and Niraj K. Nirala carried out the experiments; Hsi-Ju Chen and Y. Tony Ip wrote the manuscript and all authors amended the manuscript.


**ABSTRACT**

Tight junctions in mammals and septate junctions in insects are essential for epithelial tissue integrity. We show here that in the Drosophila intestine, smooth septate junction proteins not only provide a barrier function but also serve as a signaling complex to regulate tissue growth. During an RNAi screen for genes that regulate intestinal stem cell division, we found that loss of two smooth septate junction components, Snakeskin and Mesh, caused a hyperproliferation phenotype in the adult midgut. By examining epitope-tagged endogenous Snakeskin and Mesh, we demonstrate that the two proteins are present in cytoplasm of differentiating enteroblasts and in cytoplasm and septate junctions of mature enterocytes. In enteroblasts and enterocytes, loss of Snakeskin and Mesh causes Yorkie-dependent expression of the JAK-STAT pathway ligand Upd3, which in turn promotes proliferation of intestinal stem cells. Snakeskin and Mesh form a complex with each other, with other septate junction proteins and with Yorkie. Therefore, the Snakeskin-Mesh complex has both barrier and signaling function to maintain stem cell-mediated tissue homeostasis.

## Introduction

The balance between self-renewal of stem cells and differentiation of progeny cells has to be maintained precisely, or otherwise may lead to tumor growth or tissue degeneration (Clevers et al., 2014; Qin and Zhang, 2017). The adult *Drosophila* midgut has comparable epithelial features and functions as the mammalian intestine, thus the midgut is a highly useful genetic model system to dissect intestinal stem cell (ISC)-mediated homeostasis (Herrera and Bach, 2019; Micchelli and Perrimon, 2006; Ohlstein and Spradling, 2006; Zwick et al., 2019).

Approximately a thousand ISCs are evenly distributed throughout the adult Drosophila midgut epithelium (Micchelli and Perrimon, 2006; Ohlstein and Spradling, 2006). An ISC undergoes asymmetric division to generate a renewed ISC and another daughter cell called enteroblast (EB) or pre-enteroendocrine cell (pre-EE), which can differentiate to become an enterocyte (EC) for absorption or EE for hormone production, respectively (Fig. 1A) (Chen et al., 2018b; Ohlstein and Spradling, 2007; Zeng and Hou, 2015). The Delta-Notch pathway modulates the ISC asymmetric division, while many other conserved pathways including Insulin, JAK-STAT, BMP and Wnt are employed to control ISC division and subsequent differentiation along the two lineages (Amcheslavsky et al., 2009; Biteau and Jasper, 2011; Chen et al., 2018b; Cordero et al., 2012; Guo and Ohlstein, 2015; Jiang et al., 2009; Ohlstein and Spradling, 2007; Tian and Jiang, 2014; Xu et al., 2011; Zeng and Hou, 2015).

We and others recently show that the Ste20 kinases Misshapen (Msn) and Happyhour (Hppy) functions similarly as Hippo (Hpo) to regulate the Warts-Yorkie (Wts-Yki) axis (Karpowicz et al., 2010; Li et al., 2014a; Li et al., 2018; Li et al., 2015b; Meng et

al., 2015; Ren et al., 2010; Shaw et al., 2010; Staley and Irvine, 2010; Zheng et al., 2015). In adult *Drosophila* midguts, Msn is expressed rather specifically in ISCs/EBs (Li et al., 2018), and loss of function of Msn in EBs leads to activation of Yki and Unpaired3 (Upd3) to promote ISC division and tissue growth. The physiological function of Msn in EBs is modulated by ingested solid food particles that change the mechanical stretching of the midgut epithelium (Li et al., 2018). Hpo has a possible parallel mechanosensing function in ECs to regulate ISC division during epithelial damage (Karpowicz et al., 2010; Li et al., 2014a; Li et al., 2015b; Meng et al., 2015; Ren et al., 2010; Shaw et al., 2010; Staley and Irvine, 2010; Zheng et al., 2015). Adherens junction proteins have been linked to mechanosensing and regulation of Yki (Boggiano and Fehon, 2012; Misra and Irvine, 2018). How various upstream components including junction proteins regulate the above mentioned conserved signaling pathways to modulate intestinal tissue homeostasis is still largely unknown (Ma et al., 2019; Meng et al., 2018; Misra and Irvine, 2018; Poon et al., 2018; Yu and Pan, 2018).

The intestinal epithelium is an inside-out layer that separates the internal tissue from the outside environment, therefore have tight junctions that serve as epithelial barrier (Clark and Walker, 2018; Garcia-Hernandez et al., 2017; Harden et al., 2016; Vancamelbeke and Vermeire, 2017). Insects have the equivalent septate junctions, and in endoderm-derived tissues such as the midgut are called smooth septate junction, while in ectoderm-derived tissues such as imaginal discs are called pleated septate junction (Furuse and Izumi, 2017). Recent reports have identified conserved components of smooth septate junctions in silkworm and Drosophila, including two transmembrane proteins called Snakeskin (Ssk) and Mesh (Izumi et al., 2012; Yanagihashi et al., 2012).

Ssk and Mesh represent a novel complex of smooth septate junctions in developing insect intestines (Furuse and Izumi, 2017; Izumi et al., 2012; Yanagihashi et al., 2012). More recent reports have also implicated their functions in adult midgut homeostasis (Izumi et al., 2019; Salazar et al., 2018). Here we illustrate the genetic and molecular functions of Ssk and Mesh in EBs and ECs of adult Drosophila midguts, involving direct regulation of Yki to modulate the expression of Upd3 and thereby ISC division and intestinal homeostasis.

## Result

### Loss of smooth septate junction proteins in EBs leads to ISC proliferation

Differentiating EBs have been shown to produce multiple growth factors that regulate ISC proliferation (Doupe et al., 2018; Izumi et al., 2012; Li et al., 2014a; Li et al., 2018; Yanagihashi et al., 2012). Therefore, we used the Su(H)Gbe promoter-Gal4, UAS-GFP; tubulin-Gal80$^{ts}$ (abbreviated as Su(H)$^{ts}$>GFP) temperature-sensitive strain as the driver and marker for RNA interference (RNAi) screens in EBs (Fig. 1A). We used 452 UAS-based transgenic double-stranded RNA strains to target 262 genes including many that encode cell adhesion and membrane associated proteins (Table 1).

The knockdown of *msn* and *Tao* produced highly increased number of GFP$^+$ cells by initial visual inspection during our screen and served as controls (Fig.1B, C) (Li et al., 2014a; Li et al., 2018). While knockdown of adherens junction, Hippo signaling and other pathways occasionally gave mild increase of GFP$^+$ cells (Table 1), knockdown of many septate junction components led to a more noticeable increase (Fig. 1B). The three most consistent results were RNAi against Ssk, mesh, and Fasciclin3 (Fas3). Quantification of mitotic cell in midguts that mostly represent dividing ISCs by antibody staining for phosphorylated-histone3 (p-H3) (Amcheslavsky et al., 2009; Micchelli and Perrimon, 2006; Ohlstein and Spradling, 2006) showed that multiple Ssk, mesh or Fas3 RNAi lines all induced midgut proliferation to a high level (Fig. 1C), consistent with increased number of GFP$^+$ precursor cells (Fig. 1D-F).

Fig. 1

A

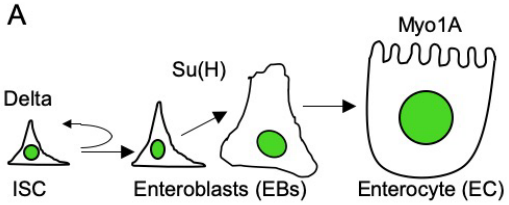


B

| RNAi stock | Gene number | Gene name | Su(H)> Midgut proliferation | Functional description |
|---|---|---|---|---|
| 101517 | CG16973 | misshapen | ++++ | Ste20 kinase |
| B28791 | CG16973 | misshapen | ++ | Ste20 kinase |
| 17432 | CG14217 | Tao | +++ | Ste20 kinase |
| 107645 | CG14217 | Tao | +++ | Ste20 kinase |
| 9788 | CG11949 | coracle | + | septate junction |
| 108749 | CG11949 | coracle | ++ | septate junction |
| 42229 | CG5803 | Fascilin 3 | +++ | cell adhesion |
| 100642 | CG5803 | Fascilin 3 | +++ | cell adhesion |
| 100765 | CG33967 | kibra | +++ | hippo signaling |
| 106507 | CG33967 | kibra | ++ | hippo signaling |
| 3962 | CG1298 | kune-kune | + | Claudin, septate junction |
| 108224 | CG1298 | kune-kune | + | Claudin, septate junction |
| 6867 | CG31004 | mesh | +++ | smooth septate junction |
| 10829 | CG31004 | mesh | +++ | smooth septate junction |
| 37917 | CG10701 | Moesin | + | cytoskeleton binding |
| 110654 | CG10701 | Moesin | ++ | cytoskeleton binding |
| 1800 | CG4322 | moody | + | GPCR, septate junction |
| 109601 | CG4322 | moody | ++ | GPCR septate junction |
| 40399 | CG6831 | rhea | +++ | talin, integrin signaling |
| 40400 | CG6831 | rhea | ++ | talin, integrin signaling |
| 10906 | CG6981 | Snakeskin | ++++ | smooth septate junction |
| 105193 | CG6981 | Snakeskin | ++++ | smooth septate junction |
| 24157 | CG9326 | varicose | + | septate junction |
| 104548 | CG9326 | varicose | ++ | septate junction |

Fig. 1

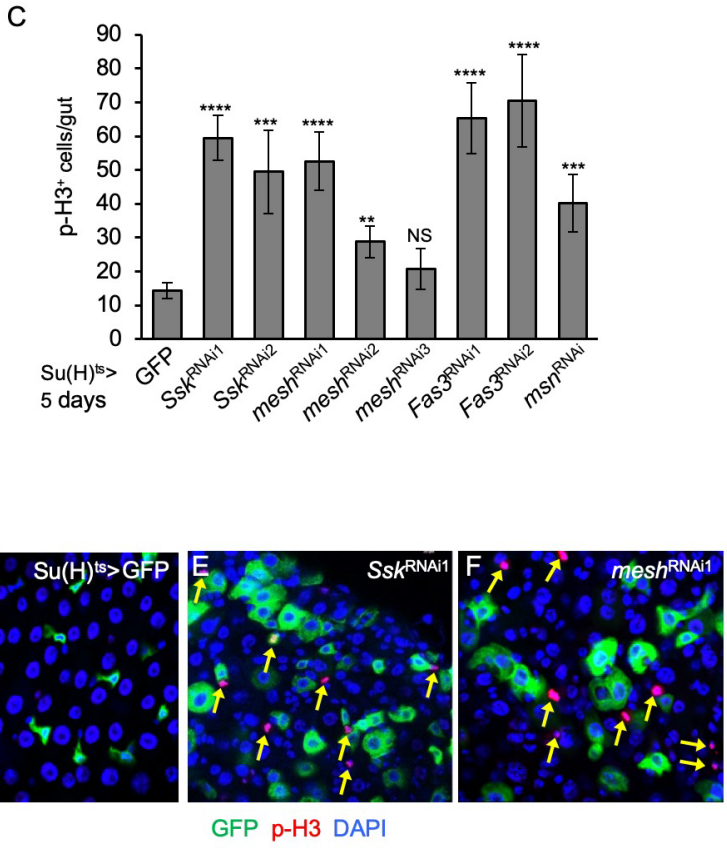
C
p-H3+ cells/gut
90
80
70
60
50
40
30
20
10
0
****
***
****
**
NS
****
****
***
Su(H)ts>
5 days
GFP
SskRNAi1
SskRNAi2
meshRNAi1
meshRNAi2
meshRNAi3
Fas3RNAi1
Fas3RNAi2
msnRNAi
D
Su(H)ts>GFP
E
SskRNAi1
F
meshRNAi1
GFP p-H3 DAPI

**Figure 1. Loss of smooth septate junction proteins in EBs leads to ISC proliferation.**

(A) An illustration of ISC asymmetric division and enteroblast (EB)-enterocyte (EC) differentiation lineage in the adult *Drosophila* midgut. Delta is an ISC marker, Su(H) is expressed in EBs, and Myo1A is expressed in ECs.

(B) A list of genes that when knockdown by Su(H)Gal4 driven RNAi exhibited increased number of $GFP^+$ cells. The degree of proliferation is based on visual examination of GFP in dissected midguts, and by comparing to the results of the previously known regulator Msn. The full list of RNAi lines screened is in Table 1.

(C) A graph showing the average number of p-$H3^+$ cells per whole midgut after crossing with the $Su(H)^{ts}$Gal4 driver, and temperature shifted to 29°C for 5 days to inactivate the $Gal80^{ts}$ repressor to allow Gal4 dependent expression of UAS-dsRNA from the indicated transgenic lines. The control is UAS-GFP, which is also included in all the RNAi experiments.

(D) A confocal image showing surface view of a midgut from a control fly with the $Su(H)^{ts}$Gal4 driver and UAS-GFP transgenes.

(E) Image of a midgut from a similar cross with an additional UAS-*Ssk* RNAi transgene.

(F) Image of a midgut from a similar cross with an additional UAS-*mesh* RNAi transgene.

For all images in this figure, green is GFP, blue is DAPI for DNA, arrows indicate some of the p-H3 staining in red, scale bars represent 20 μm. For all graphs, error bars are standard error of the means (SE), and *P* values are represented as **< 0.01, ***< 0.001, ****<0.0001. NS is no significance.

We used the CRISPR/Cas9 gene engineering to generate insertion-deletions in Ssk or stop codons in mesh (Fig. 2A, B). These CRISPR-generated Ssk and mesh mutants were homozygous lethal, similar to the other mutant combinations previously reported (Izumi et al., 2012; Yanagihashi et al., 2012). In order to study their functions in adult midguts, we used the Mosaic Analysis with Repressible Cell Marker (MARCM) technique (Lee and Luo, 2001). The *Ssk* and *mesh* mutations were generated on FRT80B or FRT82B parental chromosomes, which allow the generation of homozygous mutant clones marked with GFP, in otherwise heterozygous animals (Fig. 2C-F). $Ssk^{1}$ and $Ssk^{4-3}$, which contain insertion-deletions in the first and second exons of *Ssk*, respectively, as well as $mesh^{1}$ were used (Fig. 2A, B). Ten days after initial pulses of heat shock-induced FLP-dependent mitotic recombination, the flies were used for quantification of the MARCM clone size as the number of $GFP^{+}$ cells in a cluster. The results show that both *Ssk* and *mesh* mutants had significant albeit modest increase of clone size when compared to those in parental strains, suggesting an increased ISC proliferation (Fig. 2G, H). More importantly, we observed that the increase of p-$H3^{+}$ cells was more obvious when more mutant cells were present, and the majority of p- $H3^{+}$ cells were located outside the $GFP^{+}$ mutant clones (Fig. 2I, J). These results indicate that *Ssk* and *mesh* loss of function mutant clones increase not only their own proliferation but also the proliferation of surrounding wild-type ISCs, thus can act through an ISC-non-autonomous mechanism. The quantification of $Delta^{+}$ ISCs, $Prospero^{+}$ EEs, and p-$H3^{+}$ mitotic cells within the clones Fig. 3A-G) revealed that there was no significant increase of other cell types. The results together suggest that after loss of Ssk or Mesh there is increased proliferation of ISCs

and subsequent accumulation of GFP$^{+}$ EBs and ECs, but not change of cell fate, therefore a midgut hyperplasia phenotype.

Fig. 2

A

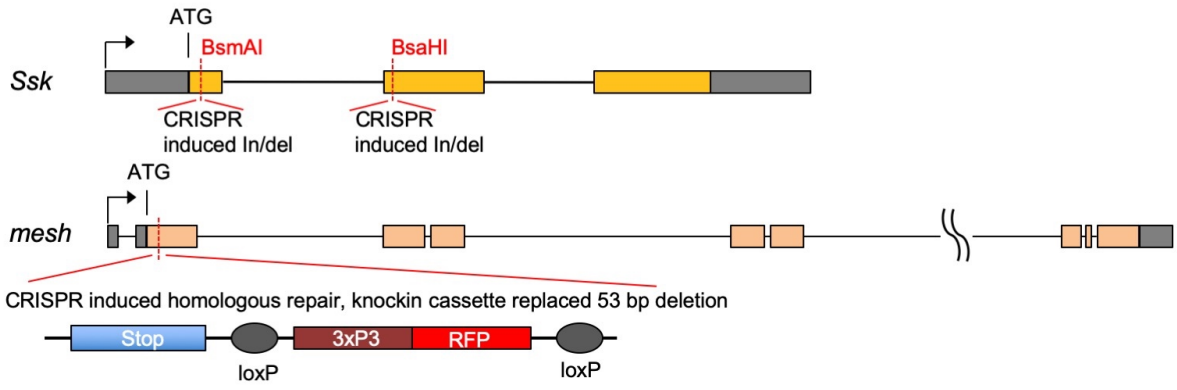


B

| | modification through CRISPR | 1st Premature Stop codon |
|---|---|---|
| FRT80B, Ssk$^{1}$/TM3, Sb | +8 (exon1) | 10$^{th}$a.a., fram-shifted |
| FRT80B, Ssk$^{2}$/TM3, Sb | -1 (exon1) | 7$^{th}$a.a., fram-shifted |
| FRT80B, Ssk$^{3-1}$/TM3, Sb | +1 (exon1) | 82$^{th}$a.a., fram-shifted |
| FRT80B, Ssk$^{3-2}$/TM3, Sb | +1 (exon1) | |
| FRT80B, Ssk$^{4-1}$/TM3, Sb | -1 (exon2) | 64$^{th}$a.a., fram-shifted |
| FRT80B, Ssk$^{4-2}$/TM3, Sb | -1 (exon2) | |
| FRT80B, Ssk$^{4-3}$/TM3, Sb | -1 (exon2) | |
| FRT80B, Ssk$^{5-1}$/TM3, Sb | -7 (exon2) | 62$^{th}$a.a., fram-shifted |
| FRT80B, Ssk$^{5-2}$/TM3, Sb | -7 (exon2) | |
| FRT80B, Ssk$^{6}$/TM3, Sb | -3 (exon2) | Gly58 in-frame deletion |

| | modification through CRISPR | 1st Premature Stop codon |
|---|---|---|
| FRT82B, mesh$^{1}$/TM3, Sb | Insert STOP codon in 1$^{s}$t exon | 124$^{th}$ a.a |

**Figure 2. Ssk and mesh loss of function mutant clones increase proliferation majorly through an ISC-non-autonomous mechanism.**

(A). Cartoons illustrated the strategies to generate *Ssk* and *mesh* mutant fly. For *Ssk*, two guide RNAs target the two restriction sites located on two exons as indicated were injected to induce CRISPR-dependent insertion/deletion (indel). Individual F1 flies were crossed to balancers and each line was used for genomic DNA isolation and PCR, followed by restriction digestion to identify possible mutants. The individual mutant lines were confirmed by PCR and sequencing. For *mesh*, the indicated homologous template was used together with the guide RNA, to induce the placement of a STOP codon and deletion immediately downstream of the first ATG of mesh.

(B) List of *Ssk* and *mesh* mutant alleles generated by CRISPR, and their mutations and predicted stop codons.

Fig. 2

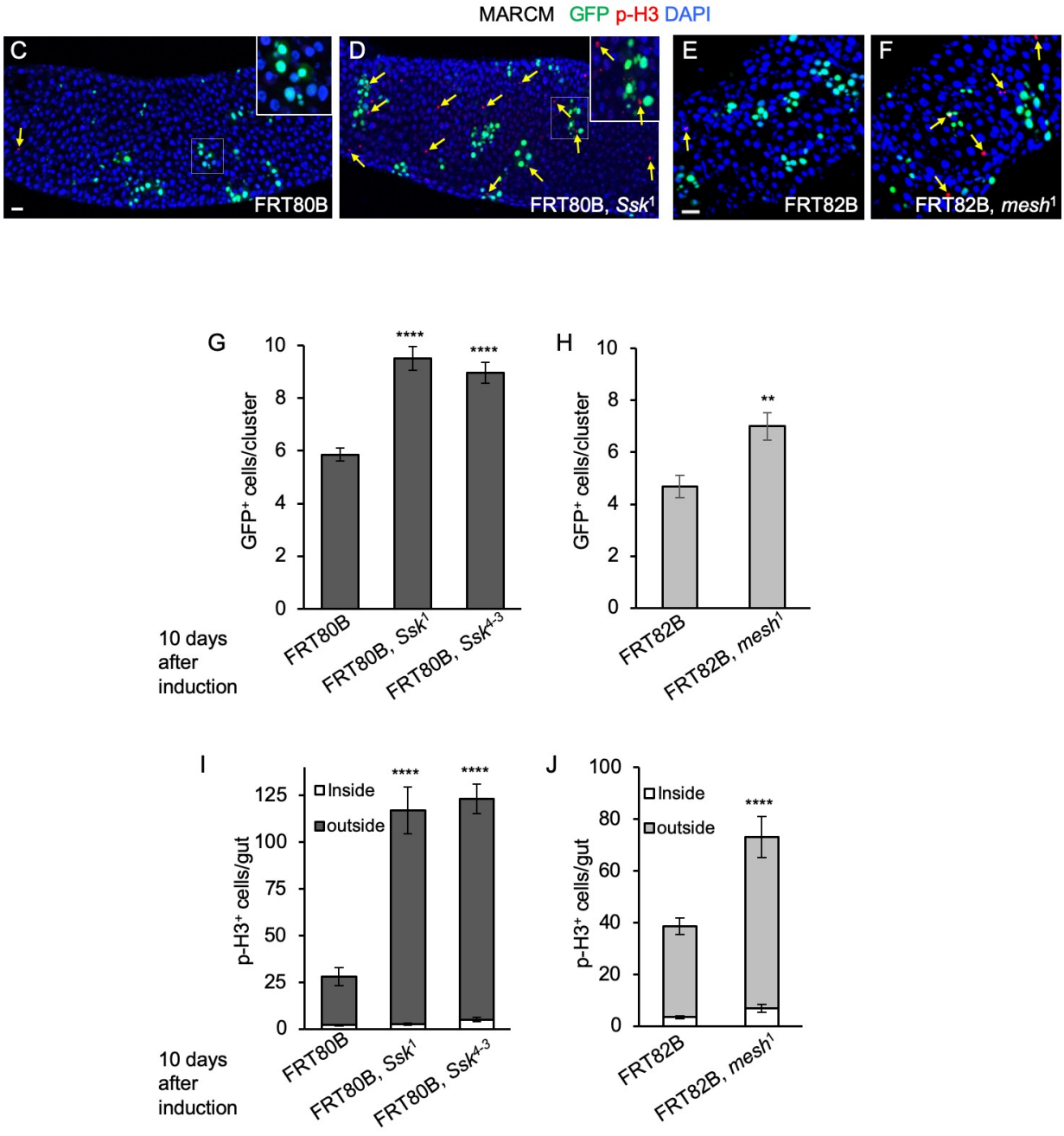
MARCM GFP p-H3 DAPI
C
FRT80B
D
FRT80B, Ssk1
E
FRT82B
F
FRT82B, mesh1
G
GFP+ cells/cluster
10 days after induction
FRT80B
FRT80B, Ssk1
FRT80B, Ssk4-3
H
GFP+ cells/cluster
FRT82B
FRT82B, mesh1
I
p-H3+ cells/gut
Inside
outside
10 days after induction
FRT80B
FRT80B, Ssk1
FRT80B, Ssk4-3
J
p-H3+ cells/gut
Inside
outside
FRT82B
FRT82B, mesh1

**Figure 2. Ssk and mesh loss of function mutant clones increase proliferation majorly through an ISC-non-autonomous mechanism.**

(C) Image of a MARCM experiment using control FRT80 flies, and the gut was also stained for p-H3, shown in red. The arrow indicates a p-H3$^+$ mitotic cell. A representative clone with GFP is shown in the enlarged image.

(D) Image of a similar MARCM experiment using the *Ssk*$^1$ mutant flies. Arrows indicate p-H3$^+$ cells, some of them are inside the clones but many are outside the clones. The enlarged image shows an example of both.

(E) Image of a similar MARCM experiment using control FRT82B flies

(F) Image of a similar MARCM experiment using the *mesh*$^1$ mutant flies.

(K) Quantification of the parental *FRT80* alleles and the two different *Ssk* mutant used for MARCM, and individual clone size is the number of GFP$^+$ cells in a cluster. More than 30 clones were counted in each experiment and the average is plotted as shown. (L) Similar MARCM experiments using the *mesh*$^1$ mutant and the parental *FRT82B* alleles.

(M) Quantification of mitotic cells by p-H3 staining in MARCM guts. Those p-H3$^+$ cells that also had GFP were counted as inside the MARCM clones (white portion). Those p-H3$^+$ cells that had no GFP were counted as outside the MARCM clones (grey portion). (N) Similar MARCM experiments using the *mesh*$^1$ mutant and the parental *FRT82B* alleles to quantify p-H3$^+$ cells that are inside or outside the clones.

Fig. 3

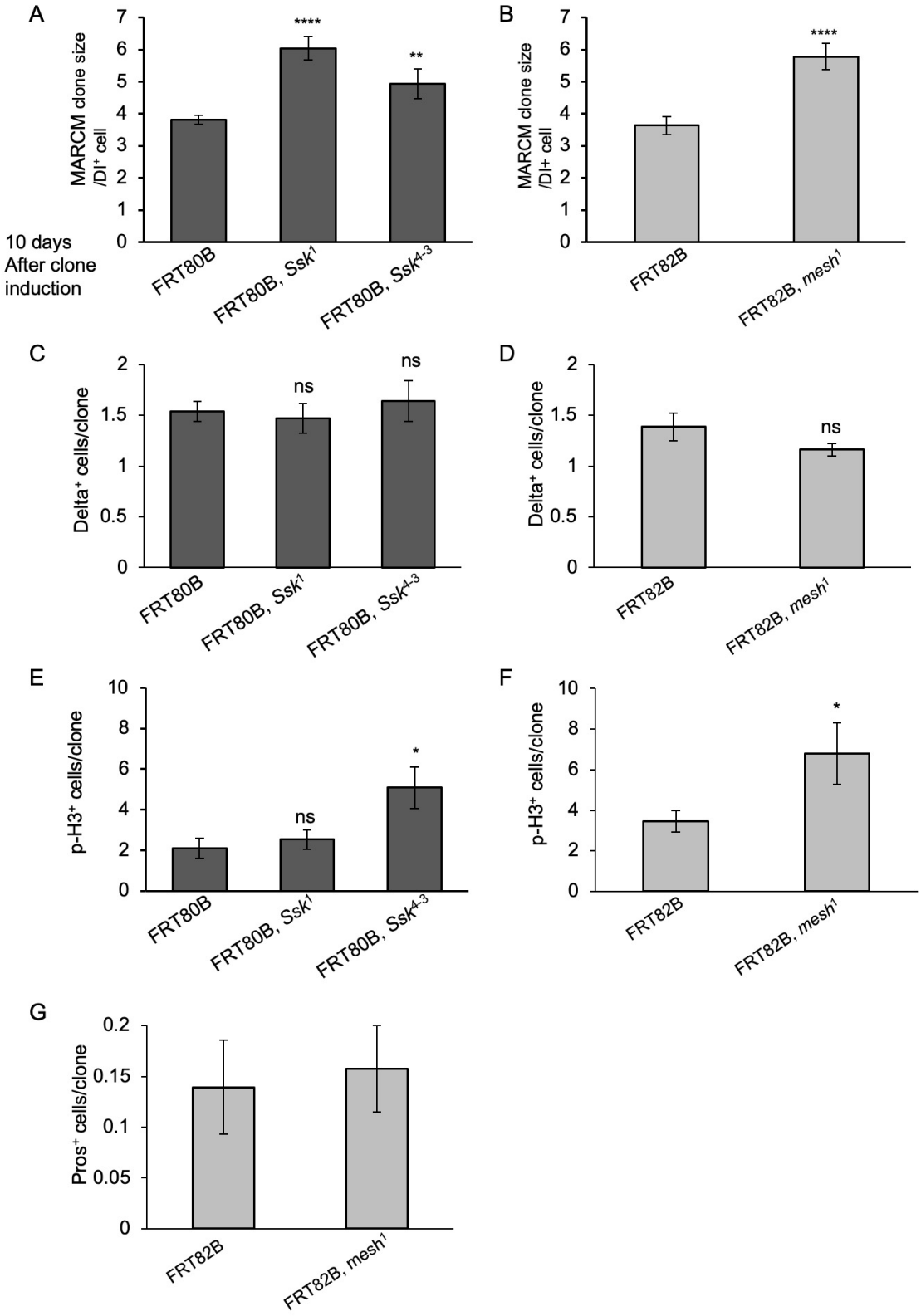
A
MARCM clone size /DI+ cell
10 days After clone induction
FRT80B
FRT80B, Ssk1
FRT80B, Ssk4-3
****
**
B
MARCM clone size /DI+ cell
FRT82B
FRT82B, mesh1
****
C
Delta+ cells/clone
ns
ns
D
Delta+ cells/clone
ns
E
p-H3+ cells/clone
ns
*
F
p-H3+ cells/clone
*
G
Pros+ cells/clone

**Figure 3. *Ssk* and *mesh* mutant neither skew the asymmetric division nor affect the differentiation of ISCs.**

(A-B) Quantification of MARCM clone size relative to Delta$^+$ cell staining. Individual clone size was defined as the number of GFP$^+$ cells divided by the number of Delta$^+$ ISCs in a cluster. More than 30 clones were counted in each experiment. FRT80B and FRT82B were the control for *Ssk* and *mes*h mutants, respectively. The MARCM clone size of *Ssk* and *me*sh mutant was increased with statistical significance.

(C-D) Quantification of the number of Delta$^+$ cells in *Ssk* or *mesh* mutant MARCM clones, that is co-localization with GFP$^+$ cell clusters. There was no change in average number, suggesting loss of *Ssk* or *mesh* did not change the ISC asymmetric division.

(E-F) Quantification of p-H3$^+$ cells within GFP$^+$ *Ssk* or *mesh* mutant MARCM clones.

(G) Quantification of Prospero (Pros) staining as EE marker in mutant clones. The average number of Pros$^+$ cells per *mesh* MARCM clone had no significant change.

**Yorkie and Upd3 mediate the growth after loss of Ssk or Mesh**

Because loss of *Ssk* or *mesh* in EBs leads to an ISC-non-autonomous mechanism to increase midgut proliferation, a prediction is that loss of *Ssk* or *mesh* causes the secretion of a growth factor that can increase ISC proliferation. We evaluated the expression of multiple ligands that are known to be important for adult midgut homeostasis, by reverse transcription quantitative PCR (RT-qPCR) of total RNA isolated from midguts where *Ssk* RNAi or *mesh* RNAi was induced by the Su(H)$^{ts}$> driver. The result revealed that the expression of *upd3*, which encodes a ligand of the JAK-STAT pathway, was robustly increased in terms of fold change (FIg. 4A, B).

A functional test of the requirement of Upd3 was performed by double knockdown experiments by using the Su(H)$^{ts}$> driver and two independent *upd3* RNAi constructs. The mitotic cell numbers were significantly reduced after *upd3* double knockdown (Fig. 4C, D). Confocal imaging (Fig. 4E-I) also revealed that in the double RNAi samples, the Su(H)$^{ts}$>driven GFP$^{+}$ cell number and organization resembled that of wild type guts. It is noteworthy that the suppression of mitotic counts in the *mesh;upd3* double RNAi experiments were only approximately 50% (Fig. 4D), suggesting that loss of *mesh* may also activate other factors, such as Vein, Keren and Spitz of the EGF pathway that showed modest fold increases of RNA expression (Fig. 4A, B), or some other factors not examined.

Fig. 4

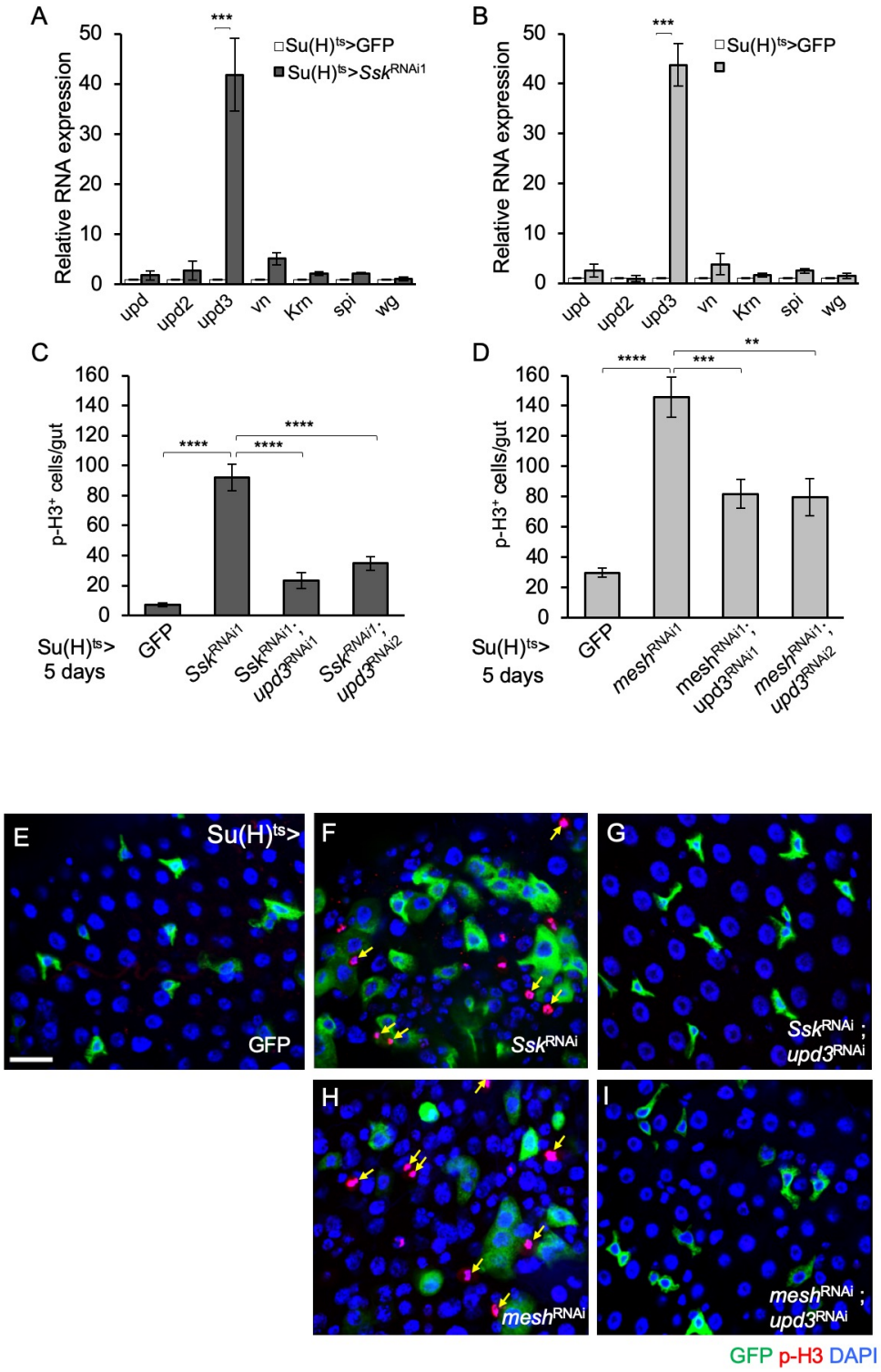
A
B
Relative RNA expression
Su(H)ts>GFP
Su(H)ts>SskRNAi1
upd
upd2
upd3
vn
Krn
spi
wg
C
D
p-H3+ cells/gut
Su(H)ts>
5 days
GFP
SskRNAi1
SskRNAi1; upd3RNAi1
SskRNAi1; upd3RNAi2
meshRNAi1
meshRNAi1; upd3RNAi1
meshRNAi1; upd3RNAi2
E
F
G
H
I
Su(H)ts>
GFP
SskRNAi
SskRNAi; upd3RNAi
meshRNAi
meshRNAi; upd3RNAi
GFP p-H3 DAPI

**Figure 4. Upd3 is secreted out to mediate the growth after loss of Ssk or Mesh.**

(A) Quantification of RNA expression of the indicated genes by qPCR of total RNA isolated from guts of control (GFP) or *Ssk* RNAi flies driven by the Su(H)$^{ts}$-Gal4. Parallel PCR reactions using the *rp49* primers were used as the reference and the expression of each gene was normalized to that of *rp49* and set as 1 in control samples (white bars). The expression level of each gene in the *Ssk* RNAi fly guts was normalized to that of *rp49* and then calculated as fold change compared to that in control.

(B) Similar qPCR quantification of the genes and showing the relative expression in *mesh* RNAi flies comparing to the control.

(C) The graph shows the average mitotic counts in midguts of flies with the indicated control GFP, and *Ssk* plus *upd3* RNAi lines, driven by the Su(H)$^{ts}$-Gal4.

(D) Similar experiment showing the mitotic counts of control, and *mesh* plus *upd3* RNAi lines.

(E) A representative confocal image showing surface view of a midgut from control flies of the genotype Su(H)$^{ts}$>GFP.

(F) A confocal image showing surface view of a midgut from Su(H)$^{ts}$>GFP,*Ssk*$^{RNAi}$ flies. The arrows indicate some of the nuclear p-H3$^{+}$ cells in red. More GFP$^{+}$ cells also illustrate increased proliferation in the midgut.

(G) A confocal image showing surface view of a midgut from Su(H)$^{ts}$>*Ssk*$^{RNAi}$,*upd3*$^{RNAi}$ flies.

(H) A confocal image showing surface view of a midgut from Su(H)$^{ts}$>*mesh*$^{RNAi}$ flies.

(I) A confocal image showing surface view of a midgut from Su(H)$^{ts}$>*mesh*$^{RNAi}$,*upd3*$^{RNAi}$ flies.

Previous reports demonstrate that the expression of *upd3* in the adult midgut can be regulated by multiple pathways, including the Wts-Yki pathway (Houtz et al., 2017; Li et al., 2014a; Li et al., 2018). The kinase Wts phosphorylates and inhibits Yki. When this phosphorylation is reduced, Yki is released and acts as a transcriptional coactivator to increase the expression of target genes. Therefore, we tested the requirement of Yki by using Su(H)$^{ts}$> to drive the expression of two different *yki* RNAi strains in EBs. The inclusion of *yki* RNAi highly reduced the expression of *upd3* RNA (Fig. 5A, B). The suppression of mitotic counts after the inclusion of *yki* RNAi was very similar to that by *upd3* RNAi, such that there is almost complete suppression in the *Ssk* RNAi background but only 50% in the *mesh* RNAi background (compare Fig. 5C, D with Fig. 4C, D). Addition of a control UAS-mCherry did not provide such suppression (Fig. 5E). Therefore, in EBs, Yki is primarily responsible for the expression of Upd3 after loss of Ssk or Mesh, while Upd3 and possibly other factors in turn promote ISC division.

Fig. 5

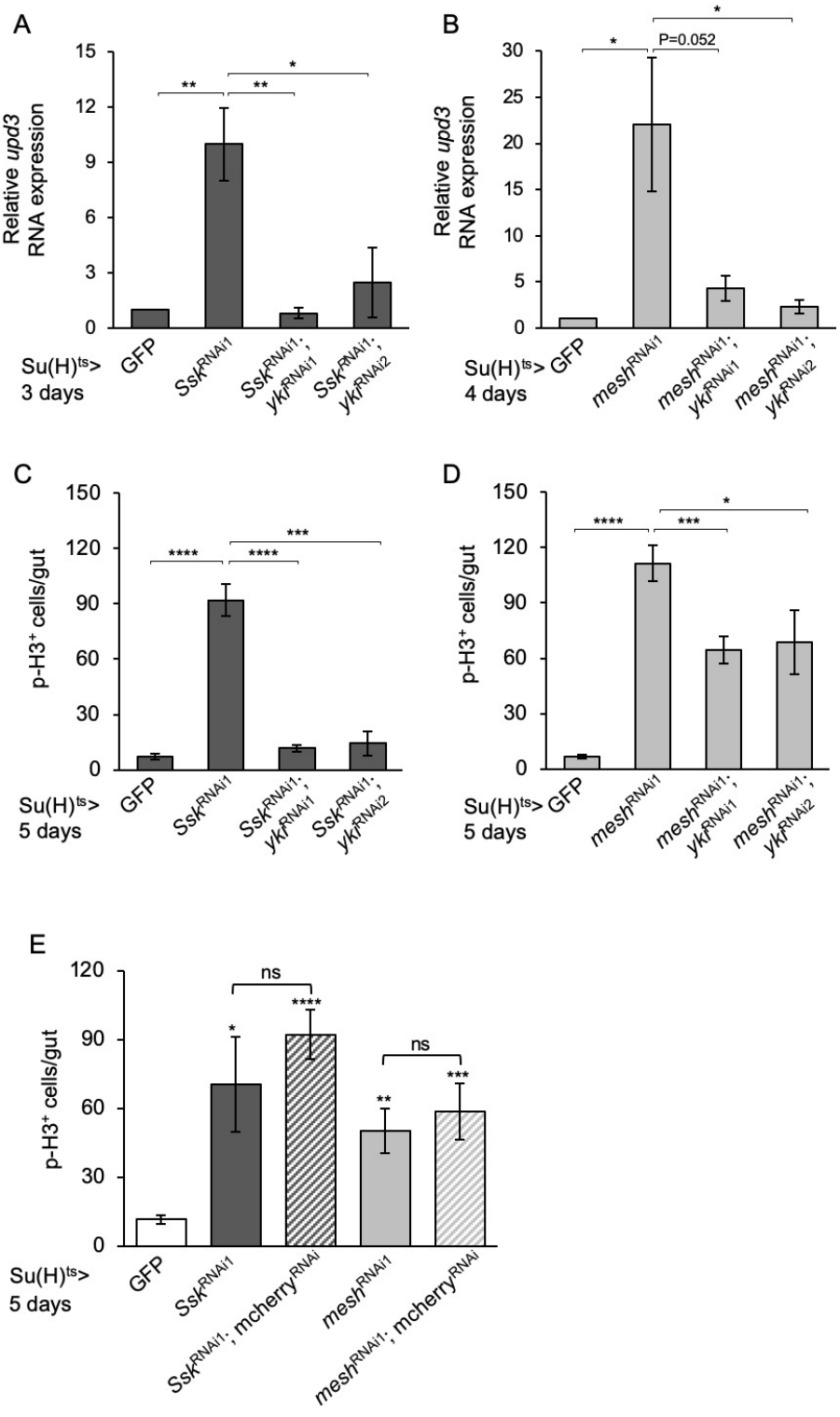
A
Relative upd3 RNA expression
15
12
9
6
3
0
**
**
*
Su(H)ts> 3 days
GFP
SskRNAi1
SskRNAi1; ykiRNAi1
SskRNAi1; ykiRNAi2
B
Relative upd3 RNA expression
30
25
20
15
10
5
0
*
P=0.052
*
Su(H)ts> 4 days
GFP
meshRNAi1
meshRNAi1; ykiRNAi1
meshRNAi1; ykiRNAi2
C
p-H3+ cells/gut
150
120
90
60
30
0
****
****
***
Su(H)ts> 5 days
GFP
SskRNAi1
SskRNAi1; ykiRNAi1
SskRNAi1; ykiRNAi2
D
p-H3+ cells/gut
150
120
90
60
30
0
****
***
*
Su(H)ts> 5 days
GFP
meshRNAi1
meshRNAi1; ykiRNAi1
meshRNAi1; ykiRNAi2
E
p-H3+ cells/gut
120
90
60
30
0
ns
****
*
ns
**
***
Su(H)ts> 5 days
GFP
SskRNAi1
SskRNAi1; mcherryRNAi
meshRNAi1
meshRNAi1; mcherryRNAi

**Figure 5. Yki regulates the Upd3 expression to control the growth after loss of Ssk or Mesh**

(A) Quantification of *upd3* RNA expression in adult midguts of the indicated control, *Ssk* and *yki* RNAi lines. Each qPCR was compared to that of *rp49* as internal control and set as 1 in the control GFP sample. Other samples were plotted as fold change compared to the control. The 29°C incubation was for 3 days.

(B) Quantification of *upd3* RNA expression in adult midguts of the indicated control, *mesh* and *yki* RNAi lines. The 29 °C incubation was for 4 days.

(C) Mitotic counts in adult midguts of the indicated control, *Ssk* and *yki* RNAi lines after 5 days of incubation at 29°C driven by the $Su(H)^{ts}$Gal4. The dissected guts were staining for p-H3 and counted throughout the whole midgut. The average number is plotted.

(D) Mitotic counts in adult midguts of the indicated control, *mesh* and *yki* RNAi lines.

(E) Mitotic counts of midguts from flies that contained the $Su(H)^{ts}$> driven RNAi in single or double as indicated. The addition of a control UAS-mCherry RNAi construct was not sufficient to cause significant suppression of the proliferation induced by loss of Ssk or Mesh.

**Ssk and Mesh expression and function are initiated in EBs to produce Upd3 for ISC proliferation**

EBs are differentiating precursor cells that will mature to become ECs, which as shown below have septate junctions to form the epithelial barrier. The strong midgut proliferation phenotypes induced by using the EB driver suggest that either Ssk and Mesh have a function within EBs or the RNAi effects sustain long enough to affect the function later in ECs. To assess these possibilities, we generated alleles that express as Ssk-Streptavidin Binding Peptide ($Ssk^{ki\text{-}SBP}$) and Mesh-V5 ($Mesh^{ki\text{-}V5}$) (Fig. 6A) endogenous tagged proteins, with the tags at the C-termini/cytoplasmic domains. High levels of SBP and V5 staining were observed in ECs, likely representing apical-lateral smooth septate junctions (also see sections below). Nonetheless, we also detected some cytoplasmic punctate staining in EBs (Fig. 6B, C, arrow). Phalloidin stains for actin bundles in apical brush borders of mature ECs (Fig. 6D-G) and Myo1A>GFP (Fig. 6H-K) labels mature ECs; these two EC marker staining were distinct from those smaller EBs that had low but detectable cytoplasmic SBP and V5 (Fig. 6D-K, arrow). On the other hand, direct labeling of EBs by the Su(H)-promoter-LacZ reporter illustrated the presence of SBP staining in these EBs (Fig. 6L, M).

As shown above, $Su(H)^{ts}$> driven *Ssk* or *mesh* RNAi caused an increased proliferation and accumulation of $GFP^+$ cells of various sizes (e.g. see Fig. 1E, F, 4J, L). Among those $GFP^+$ cells, we could find some that were of medium size, not yet fully integrated with ECs, but had low levels of Phalloidin staining (Fig. 6O, arrow). Moreover, most of these Su(H)>GFP marked cells of varying sizes still expressed the EB marker Headcase (Hdc) (Fig. 7A-C) (Resende et al., 2017). Therefore, loss of Ssk or Mesh within

EBs promotes ISC proliferation to generate more EBs that will continue the differentiation into ECs. This is consistent with the increased expression of Upd3, which can activate the JAK-STAT pathway to promote ISC proliferation and subsequent differentiation, as previously reported (Jiang et al., 2009; Xu et al., 2011; Zhou et al., 2013). In contrast, the *Ssk* or *mesh* RNAi within ISCs by the Delta-Gal4 driver even for prolonged period did not show an increased proliferation phenotype (Fig. 8). To ascertain that the JAK-STAT pathway ligand Upd3 is produced within EBs, we crossed a 4 kb *upd3* promoter-driven lacZ reporter to the *Ssk* or *mesh* mutants and performed MARCM (Li et al., 2014a; Zhou et al., 2013). The MARCM results showed that 76.6 % of the *Ssk* mutant GFP+ clones (n=141) versus 21.2% of the FRT80 control clones (n=146) also contained β-galactosidase staining (Fig 9A). Similarly, 83.5% of *mesh* mutant clones (n=94) versus 21.1% of the FRT82B control clones (n=57) had β-galactosidase and GFP co-staining (Fig 9B). These results demonstrate that the *upd3* reporter is expressed largely within the mutant cells. Confocal imaging revealed that the β-galactosidase staining in *Ssk* or *mesh* mutant clones was not obvious in ISCs and early EBs (small cells), but became detectable in EBs of medium sizes (arrow in Fig 9D, F). Further staining showed that these medium-sized upd3-LacZ expressing cells also expressed the EB marker Hdc (Fig 9G). Together, we conclude that loss of Ssk or Mesh function is sufficient to initiate the expression of Upd3 within EBs.

Fig. 6

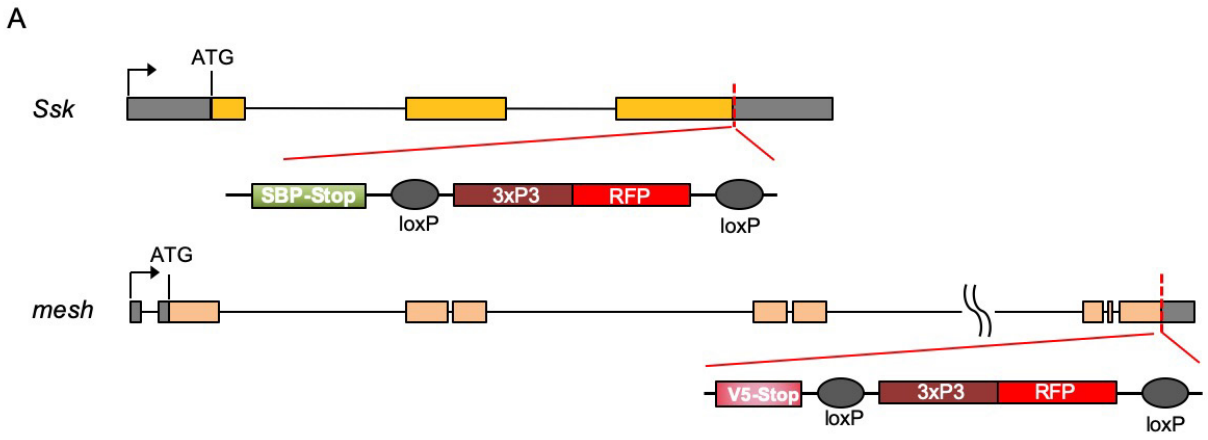
A
ATG
Ssk
SBP-Stop
loxP
3xP3
RFP
loxP
ATG
mesh
V5-Stop
loxP
3xP3
RFP
loxP

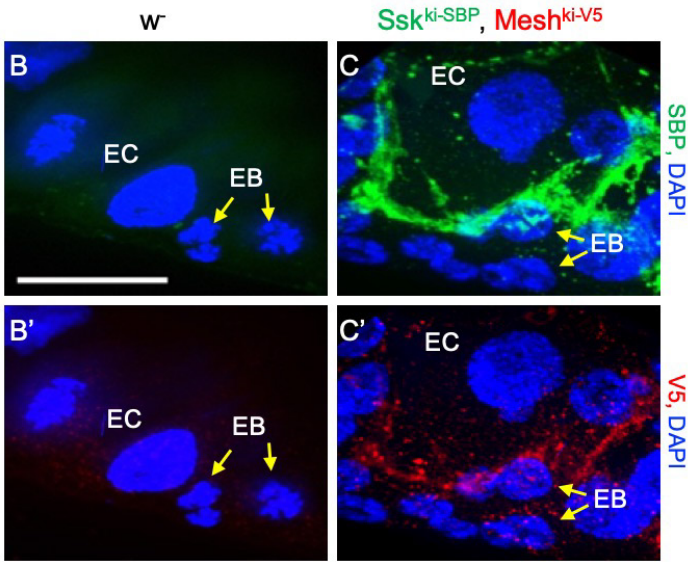
w-
Sskki-SBP, Meshki-V5
B
EC
EB
C
EC
EB
SBP, DAPI
B'
EC
EB
C'
EC
EB
V5, DAPI

**Figure 6. Ssk and Mesh expression and function are initiated in EBs**

(A) CRISPR-induced homologous repair to generate knockin $Ssk^{ki\text{-}SBP}$ and $mesh^{ki\text{-}V5}$ tagged alleles. We used 1 guide RNA and a dsDNA plasmid donor. By design, the homologous replacement would result in tag-stop, followed by floxed 3XP3 promoter-driven RFP, to substitute the stop codon of interested genes. The 3XP3-RFP marker that facilitated the genetic screening would be flipped out by Cre recombinase and left a short linker sequence between tag-stop codon and 3'UTR.

(B) Control staining for SBP and V5 around a cell nest using the parental $w^-$ fly gut. The arrows indicate EBs based on the size.

(C) Confocal images of staining for SBP and V5 using guts from flies with both the knockin alleles crossed together. High level staining appears in circumference of the EC, and low-level punctate staining is also present in EBs, indicated by arrows. The images in panels A and B are single optical sections of 0.2 μm each.

Fig. 6

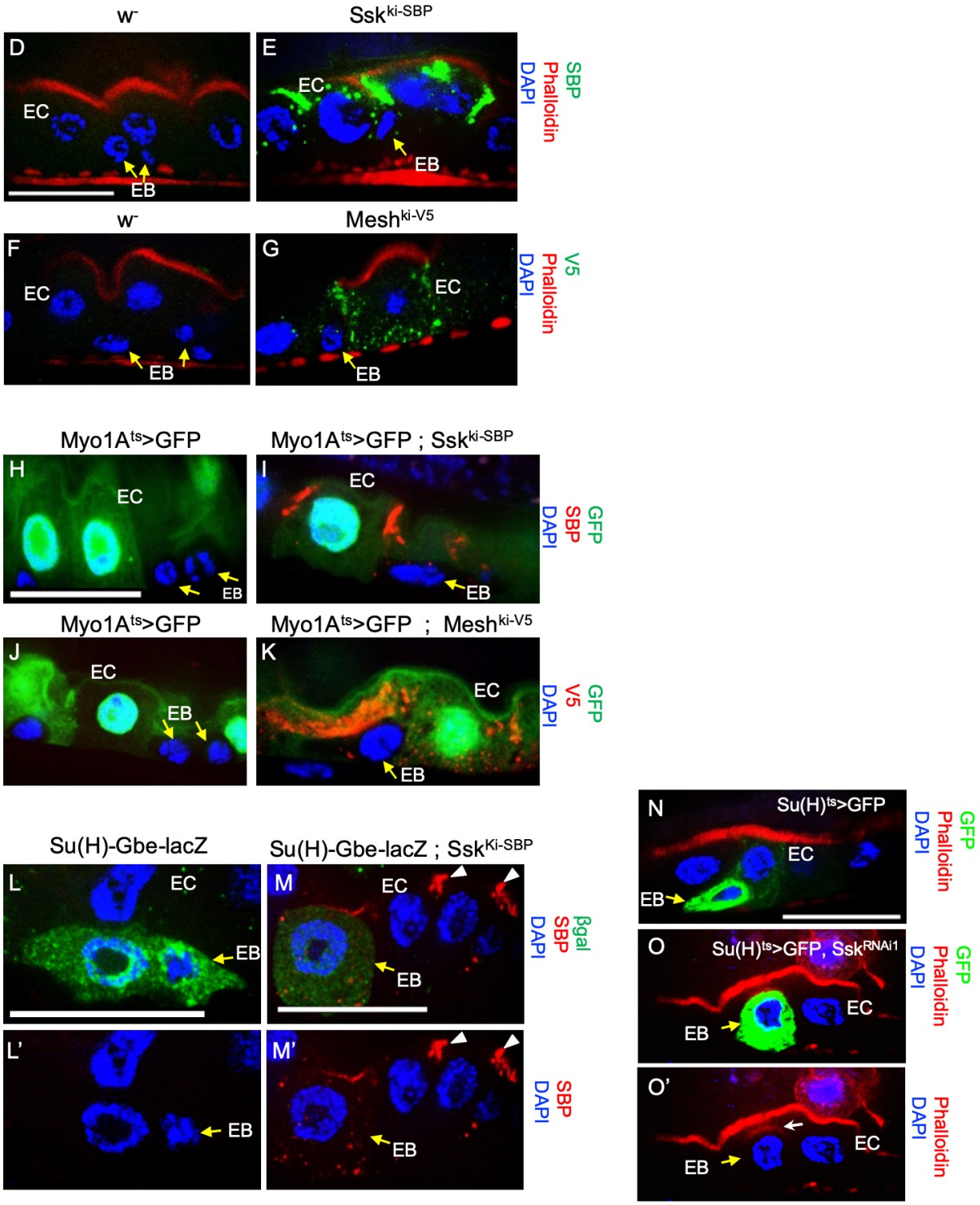
w-
Sskki-SBP
D
E
EC
EB
SBP
Phalloidin
DAPI
w-
Meshki-V5
F
G
V5
Phalloidin
DAPI
Myo1Ats>GFP
Myo1Ats>GFP ; Sskki-SBP
H
I
GFP
SBP
DAPI
Myo1Ats>GFP
Myo1Ats>GFP ; Meshki-V5
J
K
GFP
V5
DAPI
Su(H)-Gbe-lacZ
Su(H)-Gbe-lacZ ; SskKi-SBP
L
M
βgal
SBP
DAPI
L'
M'
SBP
DAPI
N
Su(H)ts>GFP
GFP
Phalloidin
DAPI
O
Su(H)ts>GFP, SskRNAi1
GFP
Phalloidin
DAPI
O'
Phalloidin
DAPI

**Figure 6. Ssk and Mesh expression and function are initiated in EBs.**

(D) Confocal image of longitudinal cross-section of $w^-$ control midgut, showing double Phalloidin staining in red for F-actin and SBP staining in green. The brush border of ECs at the apical side and the smooth muscle at the basal side had high levels of Phalloidin staining. The EBs are indicated by arrows and did not show red or green staining.

(E) Similar double staining using the $Ssk^{ki\text{-}SBP}$ flies. The EB indicated by an arrow showed cytoplasmic punctate SBP staining, but not Phalloidin staining. The more apically located large ECs were labelled strongly with Phalloidin as well as strong SBP staining at junctions and cytoplasmic punctate.

(F) Similar $w^-$ control midgut double stained with Phalloidin in red and V5 in green.

(G) Similar $Mesh^{ki\text{-}V5}$ midgut double stained with Phalloidin in red and V5 in green. The smaller EB indicated by an arrow also showed cytoplasmic punctate V5 staining.

(H) Confocal image of control $Myo1A^{ts}$>GFP midgut, with GFP expressed only in ECs. Costaining with SBP did not show any signal in EBs, indicated by arrows.

(I) Similar staining shows SBP cytoplasmic punctate in an EB of $Ssk^{ki\text{-}SBP}$ that had no GFP, indicated by an arrow.

(J) Similar V5 staining showing no signal in EBs indicated by arrows of control

(K) Similar V5 staining showing cytoplasmic punctate in an EB from $Mesh^{ki\text{-}V5}$, which is not labelled with GFP.

(L, M) Images of midgut cells from flies carrying the transgene Su(H)-Gbe-lacZ that is used to label EBs. When EBs continue to differentiate and become bigger, Su(H)-Gbe-lacZ levels become lower (compare the EBs in L and M). Immunostaining showed that punctate SBP staining from $Ssk^{ki\text{-}SBP}$ is detectable in cytoplasm of late EBs (arrows in

panel M). Along with EC maturation, Ssk accumulates and localizes at the apical-lateral region of ECs to form the smooth septate junction (arrowheads in panel M).

(N) Confocal image of a gut from control Su(H)$^{ts}$>GFP strain. The arrow indicates an EB that had strong GFP expression and no Phalloidin.

(O, O') Confocal image of a gut from *Ssk* RNAi flies. The arrow indicates an EB of medium size that had both GFP signal and weak apical Phalloidin staining (white arrow), suggesting that it was an EB continuing with its differentiating.

Fig. 7

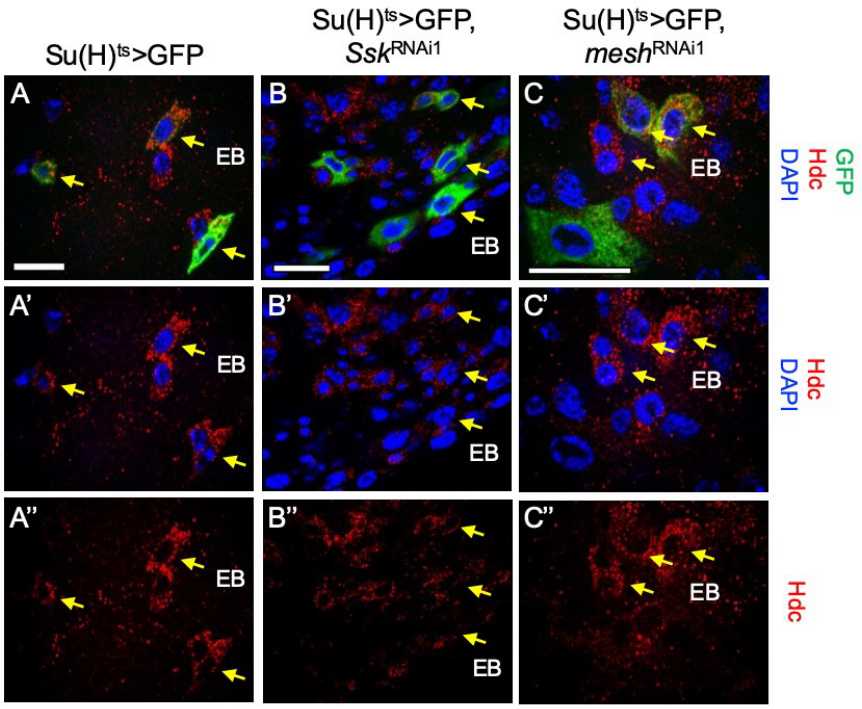


**Figure 7. Loss of Ssk or Mesh within EBs does not affect the differentiation into ECs.**

(A-C) Confocal images showing GFP marked EBs driven by Su(H)$^{ts}$-Gal4. The inclusion of *Ssk* or *mesh* RNAi constructs still allowed differentiation of these EBs, as demonstrated by the presence of more GFP$^{+}$ cells, with some of them have medium sizes and still retained GFP and the Hdc staining as another EB marker.

Fig. 8

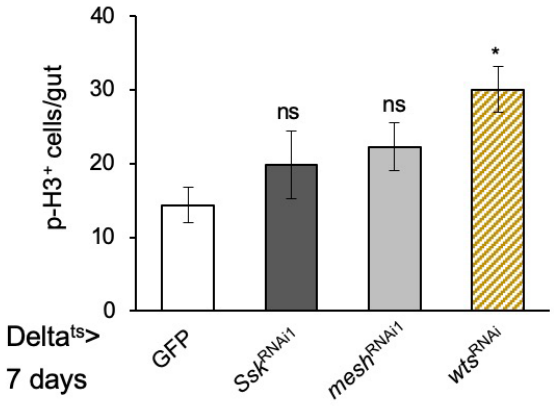


**Figure 8. Loss of Ssk or Mesh within ISCs did not show an increased proliferation phenotype.**

The plot shows the mitotic cell counts in midguts, from flies containing Ssk or mesh RNAi driven by Delta$^{ts}$-Gal4. No significant increase of proliferation was observed. A warts RNAi line was included as a comparison, in which proliferation was increased mildly but significantly.

Fig. 9

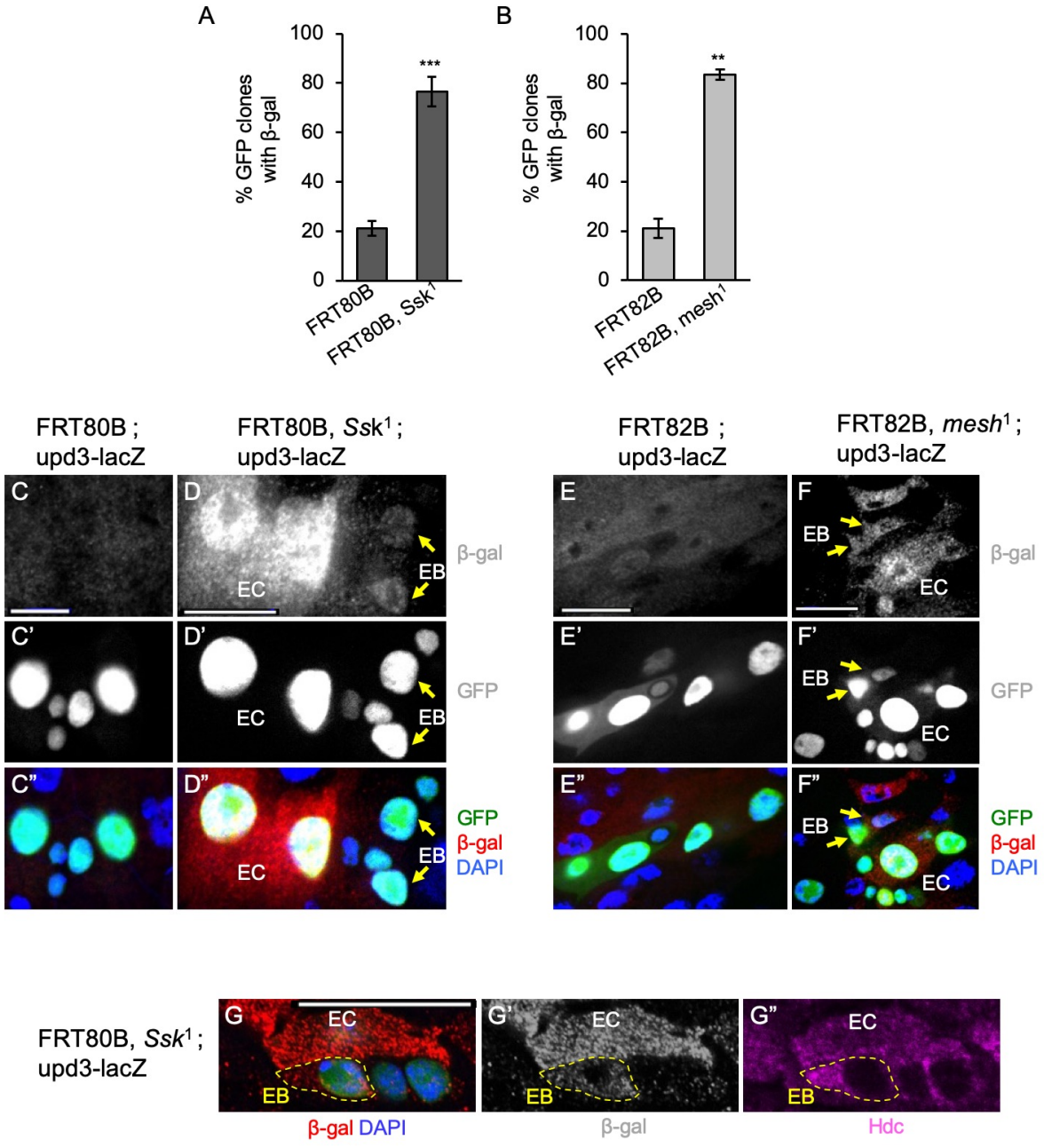
A
% GFP clones with β-gal
100
80
60
40
20
0
***
FRT80B
FRT80B, Ssk1
B
% GFP clones with β-gal
100
80
60
40
20
0
**
FRT82B
FRT82B, mesh1
FRT80B ; upd3-lacZ
FRT80B, Ssk1 ; upd3-lacZ
FRT82B ; upd3-lacZ
FRT82B, mesh1 ; upd3-lacZ
C
D
E
F
EB
EC
β-gal
C'
D'
E'
F'
GFP
C"
D"
E"
F"
GFP
β-gal
DAPI
FRT80B, Ssk1 ; upd3-lacZ
G
G'
G"
EC
EB
β-gal DAPI
β-gal
Hdc

**Figure 9. Loss of Ssk or Mesh function initiates the expression of Upd3 within EBs.**

(A) Quantification of GFP$^+$ MARCM clones stained for β-galactosidase expressed from the 4kb *upd3* promoter-lacZ reporter. MARCM clones were induced in control FRT80B or *Ssk*$^1$ mutant flies, both crossed with the lacZ reporter. After recovery for 10 days, guts were dissected and stained for β-galactosidase. An individual GFP$^+$ MARCM clone that contained at least one β-galactosidase$^+$ cell regardless of cell type was counted as double positive. More than 50 GFP$^+$ clones were counted, and the percent that also contained β-galactosidase is as shown.

(B) Similar quantification of GFP$^+$ MARCM clones that also stained positive for β-galactosidase expressed from the 4kb *upd3* promoter-lacZ reporter. MARCM clones were induced in control FRT82B or *mesh*$^1$ mutant flies.

(C, C', C") A high magnification confocal image showing a GFP$^+$ MARCM clone from FRT80B control flies that also contained the *upd3*-promoter-LacZ reporter. The staining is shown in white in panels C and C'. The staining is shown as green for GFP and red for β-galactosidase in panel C''.

(D) A similar confocal image showing a GFP$^+$ MARCM clone from *Ssk*$^1$ mutant flies. The arrows indicate EBs with detectable levels of β-galactosidase protein staining, expressing *upd3*. Note that ECs had higher levels of β-galactosidase.

(E) A confocal image showing a GFP$^+$ MARCM clone from FRT82B control flies that also contained the *upd3*-promoter-LacZ reporter.

(F) A similar confocal image showing a GFP$^+$ MARCM clone from *mesh*$^1$ mutant flies. The arrows indicate EBs with detectable levels of β-galactosidase, expressing *upd3*.

(G, G', G") Confocal images of a MARCM mutant clone form *Ssk*$^1$ mutant flies that also

contained the *upd3*-promoter-LacZ reporter. The gut was double stained for Hdc, which is expressed in EB cytoplasm. The dotted lines delineate the Ssk mutant EB with detectable levels of β-galactosidase and also Hdc staining, indicating that it was a differentiating EB expressing *upd3*.

**Ssk and Mesh also have functions in ECs to regulate Yorkie-Upd3 and thereby ISC proliferation**

Because septate junctions in guts are mainly associated with mature ECs, we examined whether *Ssk* and *mesh* are similarly required in ECs to regulate ISC proliferation, by using the Myo1A-Gal4, UAS-GFP; tubulin-Gal80$^{ts}$ (Myo1A$^{ts}$>) driver. Multiple RNAi lines of *Ssk* and *mesh* caused highly increased mitotic counts (Fig 10A). In comparison, a *Coracle* (*Cora*) RNAi line only caused a moderate increase of proliferation, while a *Fas3* RNAi line did not result in an increase, suggesting that Ssk and Mesh are key components in ECs for non-autonomous regulation of ISC proliferation. There was also more small GFP-cells around the Myo1A$^{ts}$>GFP labeled big ECs (Fig 10B-D), illustrating that there was accumulation of precursor cells as a result of increased ISC division.

The knockdown of *Ssk* or *mesh* by RNAi in ECs resulted in highly increased expression of *upd3* (Fig. 10E, F). The fold increase was even higher than that from the knockdown of *Ssk* or *mesh* in EBs (compare to Fig. 4A, B). This is probably due to the fact ECs are the major cell type in the midgut epithelium. The Myo1A$^{ts}$> driven *upd3* RNAi suppressed significantly although not completely (40-50%) the ISC proliferation induced by *Ssk* or *mesh* RNAi (Fig. 10G, H).

Fig. 10

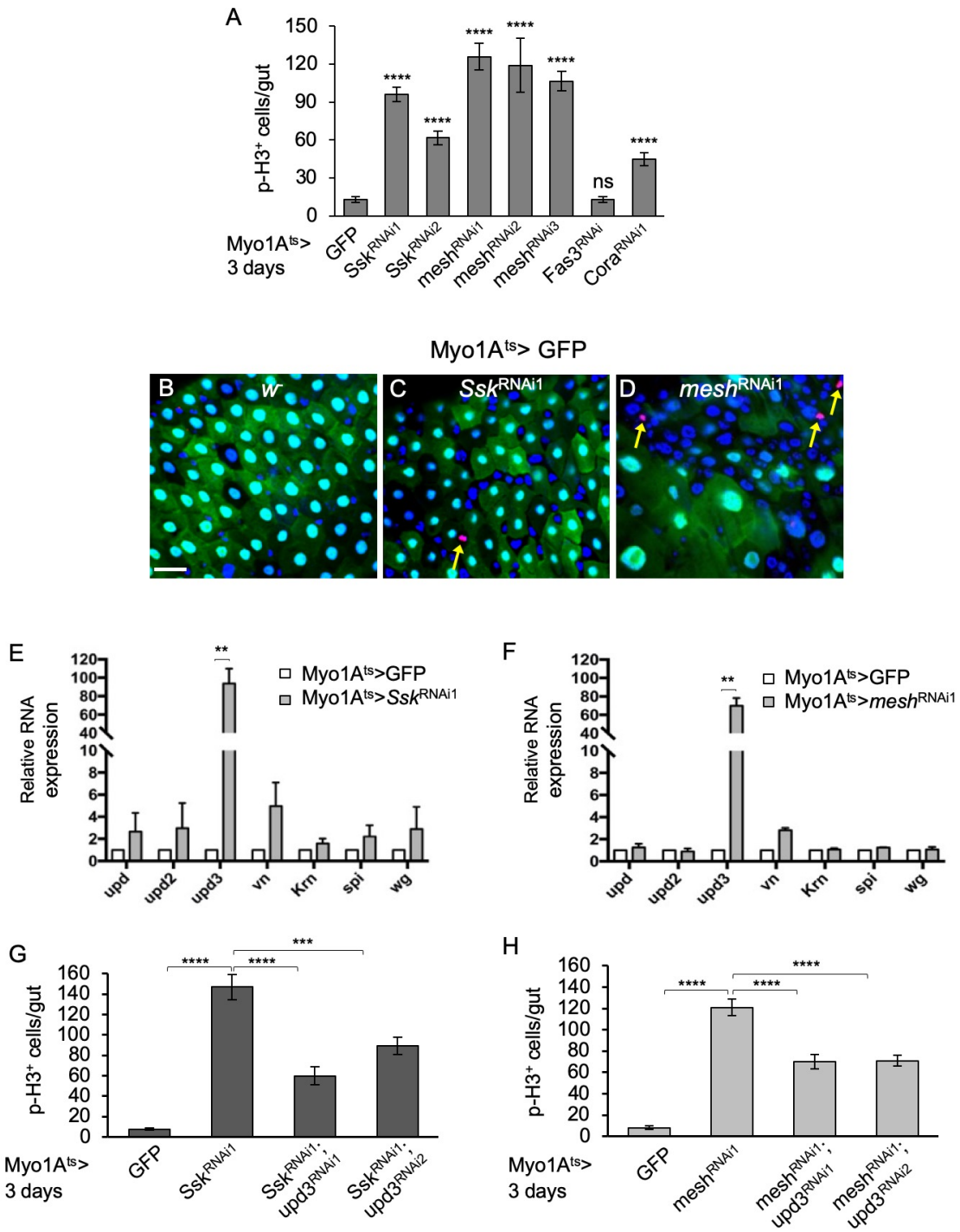
A
p-H3+ cells/gut
150
120
90
60
30
0
****
****
****
****
****
ns
****
Myo1A^ts> 3 days
GFP
Ssk^RNAi1
Ssk^RNAi2
mesh^RNAi1
mesh^RNAi2
mesh^RNAi3
Fas3^RNAi
Cora^RNAi1
Myo1A^ts> GFP
B w-
C Ssk^RNAi1
D mesh^RNAi1
E
Relative RNA expression
**
Myo1A^ts>GFP
Myo1A^ts>Ssk^RNAi1
upd
upd2
upd3
vn
Krn
spi
wg
F
Relative RNA expression
**
Myo1A^ts>GFP
Myo1A^ts>mesh^RNAi1
upd
upd2
upd3
vn
Krn
spi
wg
G
p-H3+ cells/gut
****
****
***
Myo1A^ts> 3 days
GFP
Ssk^RNAi1
Ssk^RNAi1; upd3^RNAi1
Ssk^RNAi1; upd3^RNAi2
H
p-H3+ cells/gut
****
****
****
Myo1A^ts> 3 days
GFP
mesh^RNAi1
mesh^RNAi1; upd3^RNAi1
mesh^RNAi1; upd3^RNAi2

**Figure 10. Ssk and Mesh also have functions in ECs to regulate Upd3 expression and thereby ISC proliferation.**

(A) The graph shows the average number of p-H3$^{+}$ cells per whole midgut from adult flies after crossing with the various indicated RNAi lines with the Myo1A$^{ts}$> driver, and the temperature shift was for 3 days.

(B) Confocal Image of a midgut from a control flies crossed with the Myo1A$^{ts}$> UAS-GFP. All ECs cells are GFP$^{+}$, and other cells are GFP$^{-}$.

(C) Confocal Image of a midgut from a similar cross with an additional UAS-*Ssk*$^{RNAi}$ transgene. The arrow indicates a p-H3$^{+}$ staining.

(D) Confocal Image of a midgut from a similar cross with an additional UAS-*mesh*$^{RNAi}$ transgene. The arrows indicate p-H3$^{+}$ staining.

(E) Quantification of RNA expression by qPCR of the indicated genes from gut samples with the Myo1A$^{ts}$> driver crossed with control or *Ssk*$^{RNAi}$. The temperature shift was for 3 days.

(F) Similar quantification of RNA expression as in panel E, except using the *mesh*$^{RNAi}$.

(G) Quantification of p-H3$^{+}$ cells from whole guts of flies after crossing the Myo1A$^{ts}$> with the indicated single or double *Ssk* and *upd3* RNAi lines. The temperature shift was for 3 days.

(H) Similar quantification of p-H3$^{+}$ cells, except using the *mesh*$^{RNAi}$.

We performed similar suppression experiments in ECs by using the *yki* RNAi. However, if the temperature shift to induce RNAi was carried out for 3 days similar to other experiments described above, the mitotic counts remained high in the double RNAi samples (Fig. 11A, B). Therefore, we assayed shorter time points. Temperature shift for 1 day was not sufficient to induce a significant increase of proliferation (Fig. 11G). After temperature shift for 2 days, there were sufficient increase of both *upd3* expression and mitotic counts. Importantly, the inclusion of *yki* RNAi after 2 days of induction caused significant suppression of the *upd3* expression and mitotic counts (Fig. 11C-F). Addition of a control UAS-mCherry did not provide such suppression (Fig. 11H). These results together indicate that, in ECs, Yki is an important regulator of Upd3 production and ISC proliferation at the early phase of reducing Ssk or Mesh expression. Prolonged knockdown of *Ssk* or *mesh* in ECs likely caused a substantial loss of septate junctions, followed by lethality (see Fig. 15), and therefore might mobilize additional stress response pathways. However, we did not detect an involvement of the JNK pathway (Fig. 12A-D) or a substantial cell death (Fig. 12E-H) after 2-3 days of knockdown of *Ssk* or *mesh* in ECs, suggesting an involvement of other pathways.

Fig. 11

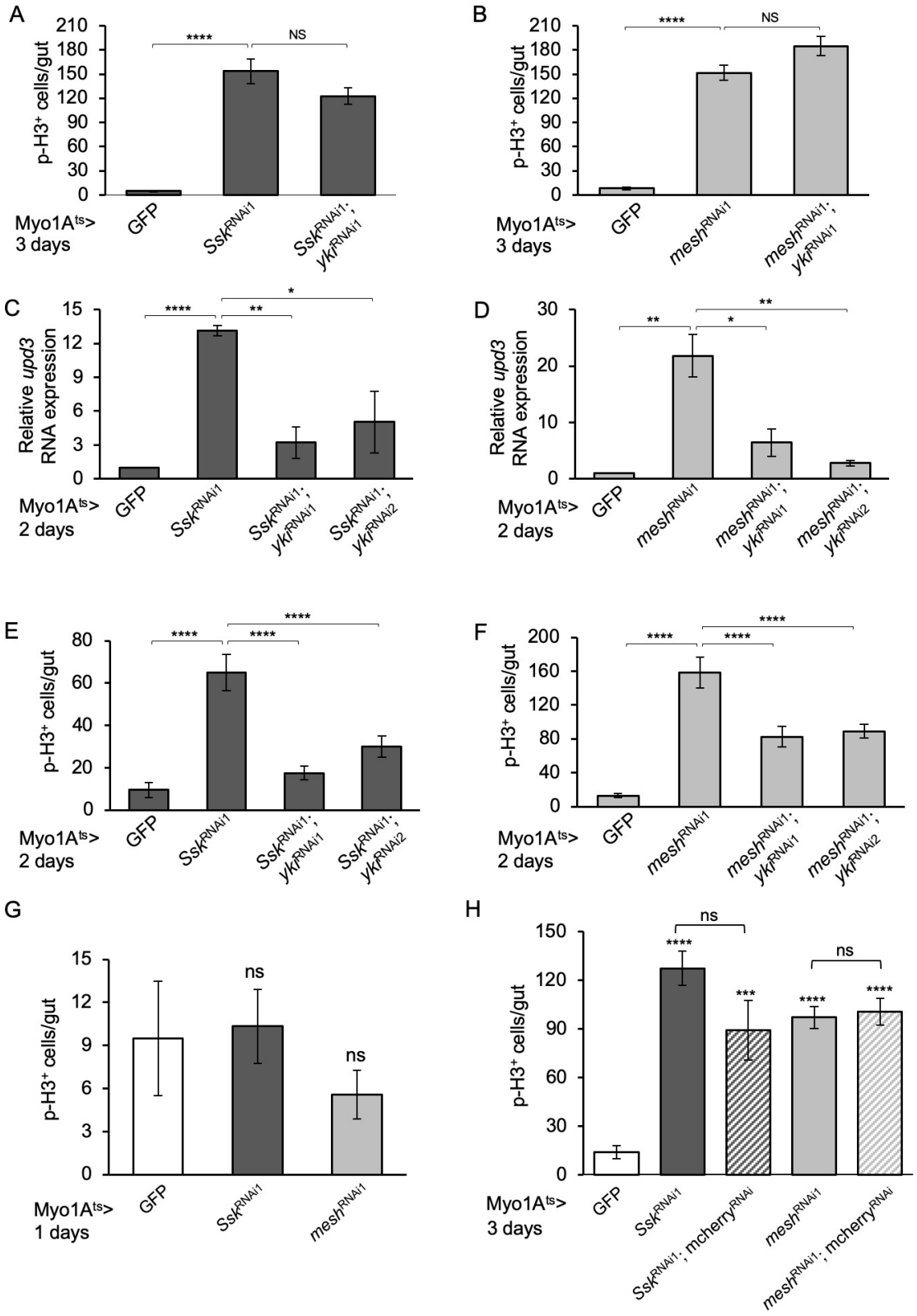
A
p-H3+ cells/gut
210
180
150
120
90
60
30
0
****
NS
Myo1A^ts>
3 days
GFP
Ssk^RNAi1
Ssk^RNAi1; ykiRNAi1
B
p-H3+ cells/gut
****
NS
Myo1A^ts>
3 days
GFP
mesh^RNAi1
mesh^RNAi1; ykiRNAi1
C
Relative upd3 RNA expression
15
12
9
6
3
0
****
**
*
Myo1A^ts>
2 days
GFP
Ssk^RNAi1
Ssk^RNAi1; ykiRNAi1
Ssk^RNAi1; ykiRNAi2
D
Relative upd3 RNA expression
30
20
10
0
**
*
**
Myo1A^ts>
2 days
GFP
mesh^RNAi1
mesh^RNAi1; ykiRNAi1
mesh^RNAi1; ykiRNAi2
E
p-H3+ cells/gut
80
60
40
20
0
****
****
****
Myo1A^ts>
2 days
GFP
Ssk^RNAi1
Ssk^RNAi1; ykiRNAi1
Ssk^RNAi1; ykiRNAi2
F
p-H3+ cells/gut
200
160
120
80
40
0
****
****
****
Myo1A^ts>
2 days
GFP
mesh^RNAi1
mesh^RNAi1; ykiRNAi1
mesh^RNAi1; ykiRNAi2
G
p-H3+ cells/gut
15
12
9
6
3
0
ns
ns
Myo1A^ts>
1 days
GFP
Ssk^RNAi1
mesh^RNAi1
H
p-H3+ cells/gut
150
120
90
60
30
0
ns
ns
****
***
****
****
Myo1A^ts>
3 days
GFP
Ssk^RNAi1
Ssk^RNAi1; mcherry^RNAi
mesh^RNAi1
mesh^RNAi1; mcherry^RNAi

**Figure 11. Yki is responsible to regulate Upd3 expression and thereby ISC proliferation at the early phase of loss of Ssk and Mesh.**

(A, B) Mitotic counts of midguts from flies that contained the Myo1A$^{ts}$> driven RNAi in single or double as indicated. The days of 29 $^{o}$C temperature shift to induce RNAi in adult flies for panels A and B were 3 days. The inclusion of *yk*i RNAi did not suppress the mitotic count induced by *Ssk* (A) or *mesh* (B) RNAi after 3 days of temperature shift.

(C) Quantification of *upd3* RNA expression by qPCR. Whole guts were obtained from flies after crossing the Myo1A$^{ts}$> with the indicated RNAi lines. Note that the temperature shift was shorter, for 2 days.

(D) Similar quantification of *upd3* RNA expression, except using the *mesh*$^{RNAi}$.

(E) Quantification of p-H3$^{+}$ cells from whole guts of flies after crossing the Myo1A$^{ts}$> with the indicated RNAi lines. Note that the temperature shift was for 2 days.

(F) Similar quantification of p-H3$^{+}$ cells, except using the *mesh*$^{RNAi}$.

(G) Mitotic counts of midguts from flies that contained the Myo1A$^{ts}$> driven RNAi. Temperature shift for 1 day was not sufficient to induce a significant increase of proliferation.

(H) Mitotic counts of midguts from flies that contained the Myo1A$^{ts}$> driven RNAi in single or double as indicated. The addition of a control UAS-mCherry RNAi construct was not sufficient to cause significant suppression of the proliferation induced by loss of Ssk or Mesh.

Fig. 12

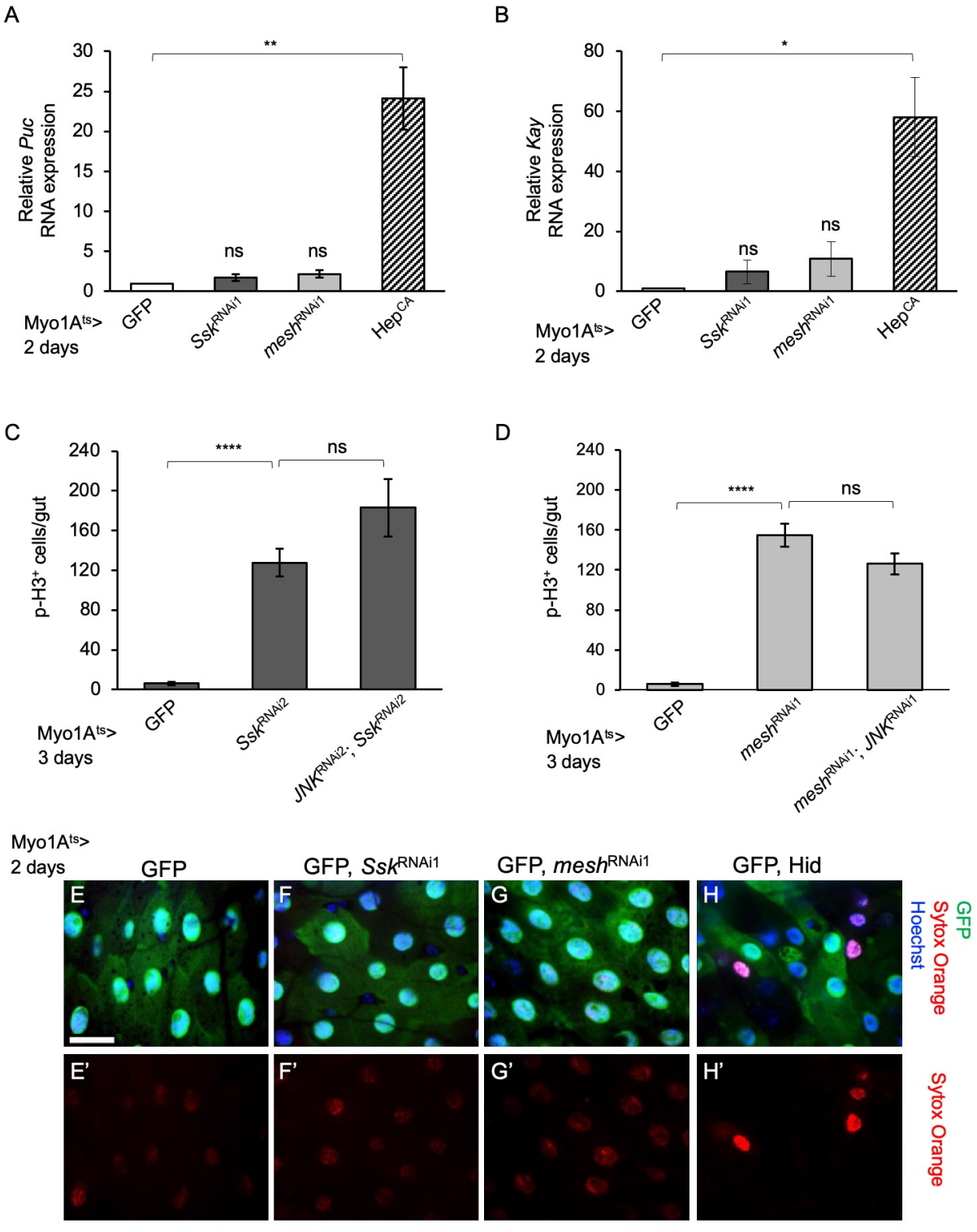
A
Relative Puc RNA expression
30
25
20
15
10
5
0
**
ns
ns
Myo1A^ts>
2 days
GFP
Ssk^RNAi1
mesh^RNAi1
Hep^CA
B
Relative Kay RNA expression
80
60
40
20
0
*
ns
ns
Myo1A^ts>
2 days
GFP
Ssk^RNAi1
mesh^RNAi1
Hep^CA
C
p-H3+ cells/gut
240
200
160
120
80
40
0
****
ns
Myo1A^ts>
3 days
GFP
Ssk^RNAi2
JNK^RNAi2; Ssk^RNAi2
D
p-H3+ cells/gut
240
200
160
120
80
40
0
****
ns
Myo1A^ts>
3 days
GFP
mesh^RNAi1
mesh^RNAi1; JNK^RNAi1
Myo1A^ts>
2 days
GFP
GFP, Ssk^RNAi1
GFP, mesh^RNAi1
GFP, Hid
E
F
G
H
E'
F'
G'
H'
GFP
Sytox Orange
Hoechst
Sytox Orange

**Figure 12. Knockdown of Ssk or Mesh in ECs does not activate the JNK pathway or induce apoptosis.**

(A-B) Quantification of RNA expression by qPCR, of JNK downstream target genes Puckered and Kayak in adult midguts of flies containing the indicated *Ssk*$^{RNAi}$ , *mesh*$^{RNAi}$, or the constitutively active Hemipterous (Hep$^{CA}$) that activates JNK as a positive control. Each qPCR was compared to that of *rp49* as internal control and set as 1 in the control GFP sample. Other samples were plotted as fold change compared to the control. The 29$^{o}$C incubation was for 2 days.

(C-D) Mitotic counts based on the number of p-H3$^{+}$ cell per whole midgut. The guts were from flies of single or double RNAi of Ssk or mesh, together with JNK, driven by the EC driver Myo1A$^{ts}$>. The 29$^{o}$C incubation for inducing RNAi was for 3 days. The addition of JNK RNAi did not suppress the ISC proliferation.

(E-H) Confocal images showing Sytox Orange staining for nucleic acid in cells with 1017 compromised membranes as a cell death indicator (Akagi et al., 2018). Guts were from flies containing the EC driver Myo1A$^{ts}$> and the *Ssk*$^{RNAi}$ , *mesh*$^{RNAi}$ , or a Hid cDNA construct as a positive control. The 29$^{o}$C incubation was for 2 days. Knockdown of Ssk or mesh in ECs did not increase the staining when compared to the GFP control, but Hid overexpression increased the staining.

**The Ssk-Mesh complex are required for the co-localization with other junction proteins in ECs.**

We used the knockin alleles of Ssk and Mesh to perform a series of experiments to investigate whether these two components are critical for septate junction formation in ECs. Confocal imaging showed that both endogenous fusion proteins $Ssk^{ki\text{-}SBP}$ and $Mesh^{ki\text{-}V5}$ formed a ring around the membrane of ECs, as well as some cytoplasmic punctate staining especially for Mesh (Fig. 13A). Longitudinal cross-section view of this staining revealed that the two proteins were colocalized to apical-lateral positions, suggesting that they serve to connect neighboring ECs as expected for septate junctions (Fig. 13B, arrowheads). Moreover, the two proteins can be co-immunoprecipitated from adult gut extracts, suggesting that they are part of the same protein complex (Fig. 13C). The localization of Ssk and Mesh at the junctions are dependent on each other, because RNAi caused dispersion of immunofluorescent signals from the junctions (Fig. 13D-G). The protein composition of smooth septate junction is not entirely known, but previous reports illustrate that Ssk, Mesh and Tsp2A are likely components of smooth septate junctions in developing Drosophila embryos and larvae (Izumi et al., 2016; Izumi et al., 2012; Yanagihashi et al., 2012). Recent reports also implicate these three proteins in adult midgut homeostasis (Izumi et al., 2019; Salazar et al., 2018; Xu et al., 2019). Therefore, we used our knockin alleles to further examine the relationship with Tsp2A, and the results showed that the junction localization of Ssk and Mesh were dependent on Tsp2A (Fig. 13H-K). We extended our analysis to Cora and Fas3, which are known to associate with septate junctions in other epithelial tissues (Boggiano and Fehon, 2012) and are involved in adult midgut proliferation to varying degrees (see Fig.1B, 1C, 10A).

The staining of Cora and Fas3 matched that of Mesh at the junctions of ECs (Fig. 14A, B). Moreover, their localization was largely disrupted after *Ssk* or *mesh* RNAi (Fig. 14C-H). Together, we have established that Ssk and Mesh are localized to and critical for the formation of smooth septate junctions in ECs of adult midgut epithelium.

Fig. 13

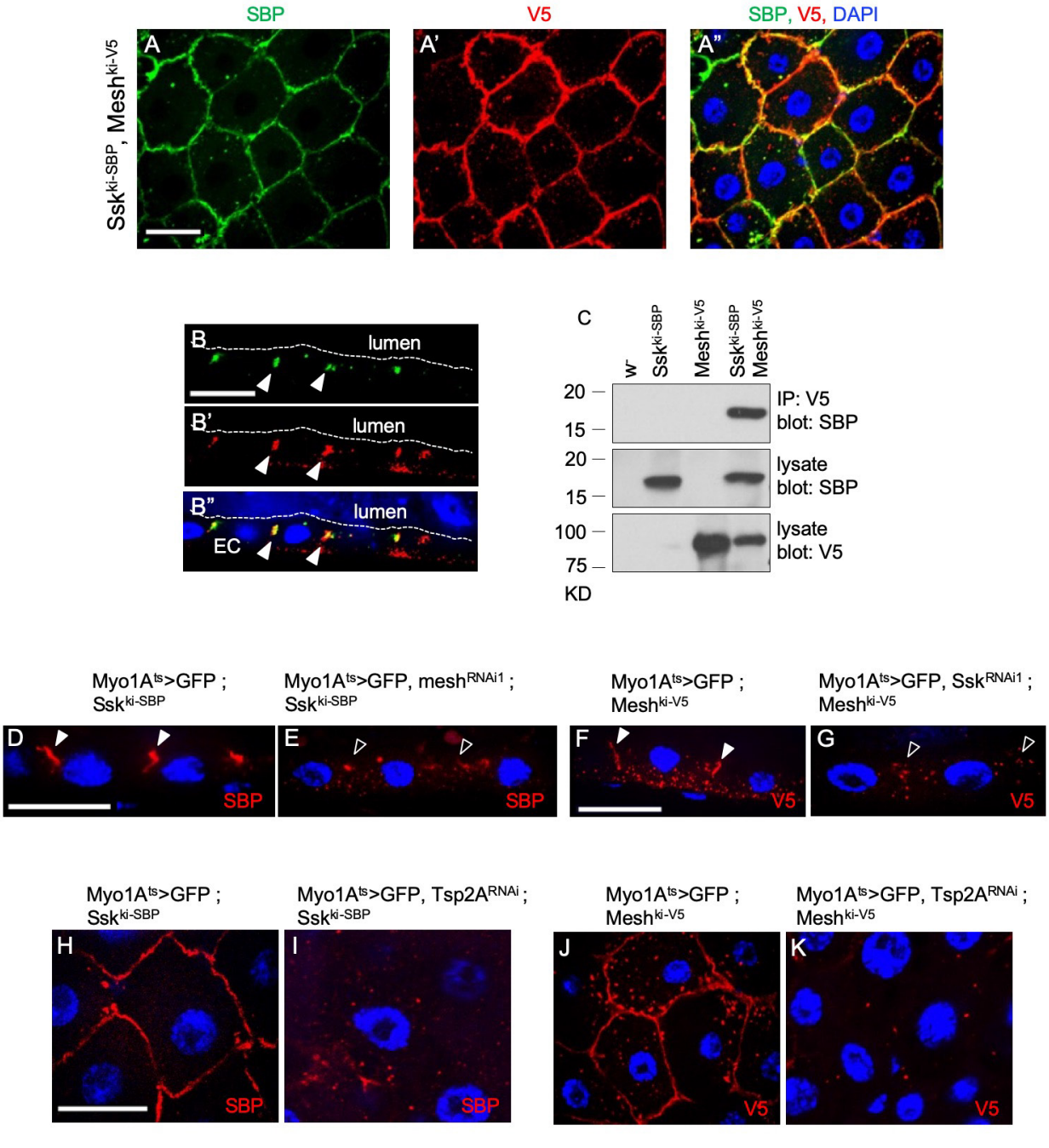
SBP
V5
SBP, V5, DAPI
Ssk^ki-SBP, Mesh^ki-V5
A
A'
A"
B
lumen
B'
lumen
B"
lumen
EC
C
w-
Ssk^ki-SBP
Mesh^ki-V5
Ssk^ki-SBP
Mesh^ki-V5
20
15
20
15
100
75
KD
IP: V5
blot: SBP
lysate
blot: SBP
lysate
blot: V5
Myo1A^ts>GFP ;
Ssk^ki-SBP
Myo1A^ts>GFP, mesh^RNAi1 ;
Ssk^ki-SBP
Myo1A^ts>GFP ;
Mesh^ki-V5
Myo1A^ts>GFP, Ssk^RNAi1 ;
Mesh^ki-V5
D
SBP
E
SBP
F
V5
G
V5
Myo1A^ts>GFP ;
Ssk^ki-SBP
Myo1A^ts>GFP, Tsp2A^RNAi ;
Ssk^ki-SBP
Myo1A^ts>GFP ;
Mesh^ki-V5
Myo1A^ts>GFP, Tsp2A^RNAi ;
Mesh^ki-V5
H
SBP
I
SBP
J
V5
K
V5

**Figure 13. Ssk and Mesh are localized to and critical for the formation of smooth septate junctions in ECs of adult midgut epithelium**

(A, A', A'') Confocal images of surface view of an adult midgut from flies harboring both $Ssk^{ki-SBP}$ and $Mesh^{ki-V5}$. Co-immunostaining was using antibodies for SBP shown in green in panel A, and for V5 shown in red in panel A'. The double color together with DAPI is shown in A''. The focal plan of the images was around the apical side of ECs, where the smooth septate junctions are expected to locate. Some punctate are also observed in the cytosol of ECs.

(B, B', B'') Confocal images of longitudinal cross-section view of a midgut from flies harboring $Ssk^{ki-SBP}$ and $Mesh^{ki-V5}$. The SBP and V5 staining co-localized at presumed septate junctions indicated by the arrowheads near the apical side of ECs. The white dash line indicates the apical border of the epithelium adjacent to the gut lumen.

(C) Western blots showing co-immunoprecipitation of the $Ssk^{ki-SBP}$ and $Mesh^{ki-V5}$ proteins, using extracts prepared from the $w^-$ control, single knockin, and double knockin fly guts. The extracts were used for V5 immunoprecipitation and then SBP Western blots, or for Western blots directly in the two lower panels as indicated.

(D) Confocal image of longitudinal cross-section view of SBP staining of gut from control flies crossing the $Ssk^{ki-SBP}$ with the $Myo1A^{ts}$>GFP. The staining is tightly localized to the EC junctions indicated by arrowheads.

(E) Similar SBP staining except the flies also included the $mesh^{RNAi}$ construct, which caused disruption of staining at the junctions (open arrowheads).

(F) Similar V5 staining in control guts.

(G) Similar V5 staining in guts that also included $Ssk^{RNAi}$.

(H) Confocal image of surface view of SBP staining in control gut.

(I) Similar SBP staining except the flies also included the *Tsp2A*$^{RNAi}$ construct.

(J) Similar V5 staining in control guts.

(K) Similar V5 staining except the flies also included the *Tsp2A*$^{RNAi}$ construct.

Fig. 14

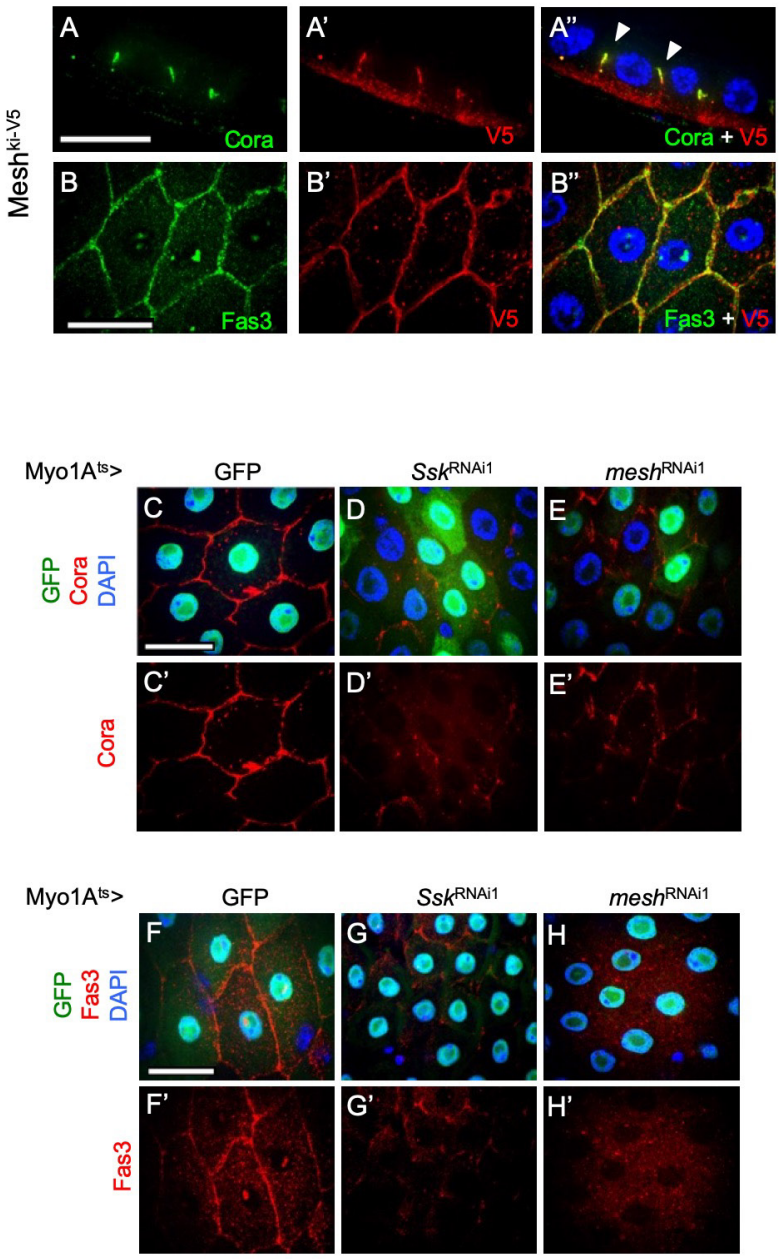
Mesh^ki-V5
A
A'
A''
Cora
V5
Cora + V5
B
B'
B''
Fas3
V5
Fas3 + V5
Myo1A^ts>
GFP
Ssk^RNAi1
mesh^RNAi1
C
D
E
GFP
Cora
DAPI
C'
D'
E'
Cora
Myo1A^ts>
GFP
Ssk^RNAi1
mesh^RNAi1
F
G
H
GFP
Fas3
DAPI
F'
G'
H'
Fas3

**Figure 14. The Ssk-Mesh complex are required for the co-localization with other junction proteins in ECs.**

(A, A', A'') Confocal image of longitudinal cross-section view of gut from the $Mesh^{ki\text{-}V5}$ fly strain stained for V5 and Cora. The arrowheads in A'' indicate colocalization at the apical junctions of the two proteins.

(B, B', B'') Confocal image of surface view of similar gut stained for V5 and Fas3. The confocal section is 0.2 μm and the two proteins had almost identical pattern around the cell membrane.

(C, C') Confocal image of surface view of control gut expressing $Myo1A^{ts}$>GFP and stained for Cora.

(D, D') Similar image showing Cora from membrane junction was dispersed after $Ssk^{RNAi}$.

(E, E') Similar image showing Cora staining was dispersed after $mesh^{RNAi}$.

(F, F') Confocal image of control gut expressing $Myo1A^{ts}$>GFP and stained for Fas3.

(G, G') Similar image showing Fas3 from membrane junction was dispersed after $Ssk^{RNAi}$.

(H, H') Similar image showing Fas3 staining was dispersed after $mesh^{RNAi}$.

**Loss of Ssk and Mesh in EBs and ECs lead to different degrees of gut leakiness and animal viability**

Septate junctions provide the barrier function of the intestinal epithelium and loss of barrier function often leads to compromised epithelial integrity, cell stress and reduced animal viability (Furuse and Izumi, 2017; Garcia-Hernandez et al., 2017; Harden et al., 2016; Rera et al., 2012; Resnik-Docampo et al., 2018; Vancamelbeke and Vermeire, 2017). Because we have found that Ssk and Mesh have functions in both EBs and ECs to regulate the Yki-Upd3 axis for midgut homeostasis, we examined how these two cell types contribute to gut barrier function and whole animal viability. Previous reports showed that leaky guts could lead to the accumulation of a blue dye in the body cavity after the dye was fed to flies, termed as Smurf assay (Rera et al., 2012). By this assay, we found that after 3 days of *Ssk* or *mesh* RNAi when driven by the EB driver led to less that 3% of the flies exhibited the Smurf phenotype (Fig. 15A). The number of dead flies was also limited and closely correlated with the Smurf phenotype (Fig. 15B). Meanwhile, the same experiment using the EC driver caused approximately 10% of flies with Smurf phenotype after 3 days, and that increased sharply afterward (Fig. 15C). The lethality was closely correlated with the profile of Smurf assay (Fig. 15D). These results are consistent with the idea that Ssk and Mesh have essential barrier function in ECs, where the disruption of this complex leads to loss of tissue integrity and soon followed with lethality. Meanwhile, the loss of Ssk and Mesh in EBs has only minor effects on leakiness and viability. Considering the strong ISC proliferation phenotype after loss of Ssk and Mesh in EBs, we speculate that the cytoplasmic localization of Ssk and Mesh

in these precursor cells is sufficient to regulate other signaling components for intestinal homeostasis.

Fig. 15

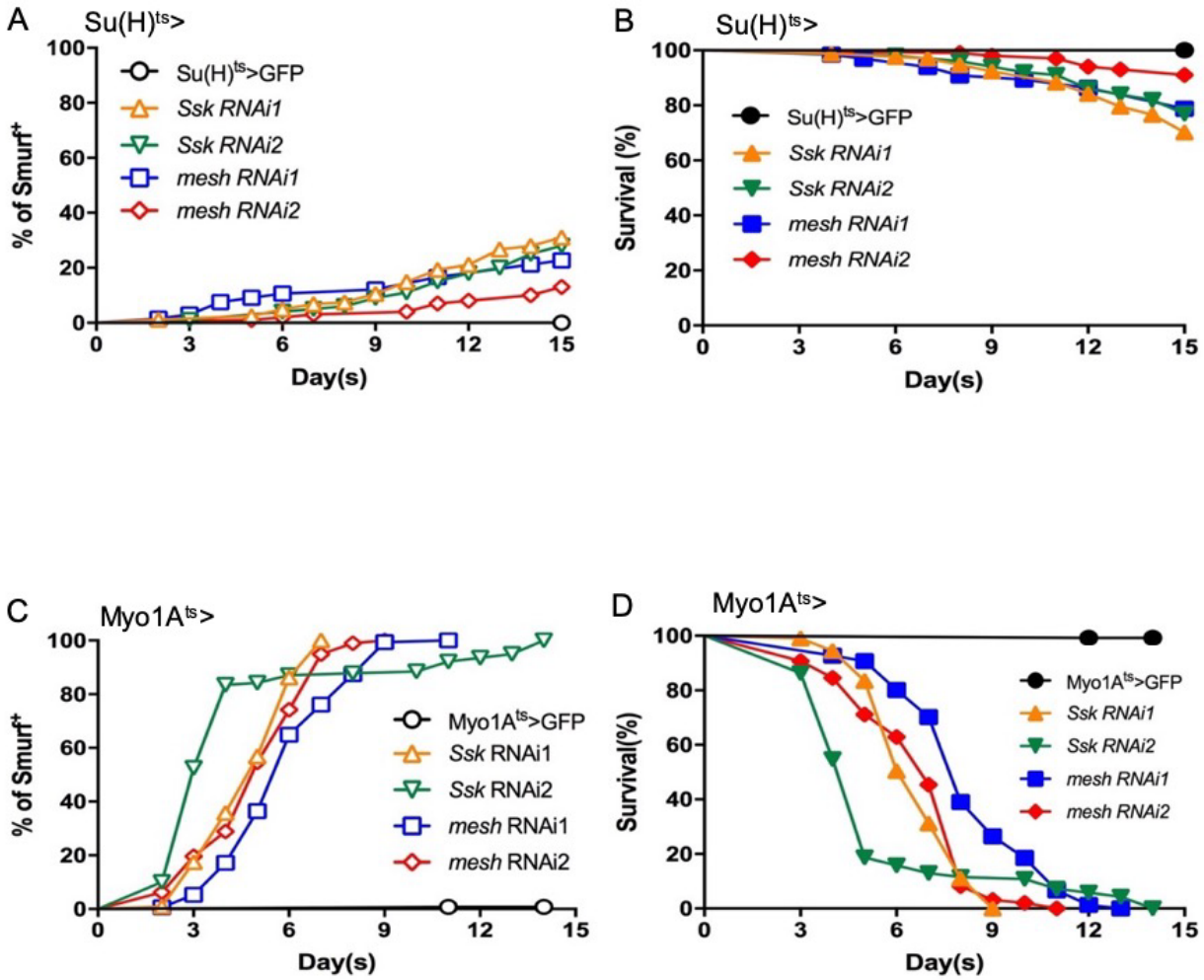
A
Su(H)ts>
% of Smurf+
Su(H)ts>GFP
Ssk RNAi1
Ssk RNAi2
mesh RNAi1
mesh RNAi2
Day(s)
B
Su(H)ts>
Survival (%)
Su(H)ts>GFP
Ssk RNAi1
Ssk RNAi2
mesh RNAi1
mesh RNAi2
Day(s)
C
Myo1Ats>
% of Smurf+
Myo1Ats>GFP
Ssk RNAi1
Ssk RNAi2
mesh RNAi1
mesh RNAi2
Day(s)
D
Myo1Ats>
Survival(%)
Myo1Ats>GFP
Ssk RNAi1
Ssk RNAi2
mesh RNAi1
mesh RNAi2
Day(s)

**Figure 15. Loss of Ssk and Mesh in EBs and ECs lead to different degrees of gut leakiness and animal viability.**

(A) Quantification of Smurf flies after feeding with food dye to flies with the indicated genotypes. Standard fly medium was mixed with blue dye. Newly eclosed flies were aged for 3 days on standard medium under room temperature and 50 flies were placed on dyed medium at 29$^{o}$C . The flies were counted every day. The cumulative percent of Smurf$^{+}$ flies after each day is plotted as shown. The plot is an average of 3 independent experiments for each genotype.

(B) Quantification of viable flies with the indicated genotypes. 50 flies were placed in regulate food vials. The food vials were changed and survived flies counted every day. The cumulative percent of flies still alive after each day is plotted as shown. The plot is an average of 3 independent experiments for each genotype.

(C) Similar quantification of Smurf flies, using the Myo1A$^{ts}$-Gal4 driver

(D) Similar quantification of viable flies, using the Myo1A$^{ts}$-Gal4 driver.

**Ssk and Mesh form a complex with and restrict the activity of Yki**

In both EBs and ECs, the function of Yki is required to mediate the expression of Upd3, which in turn promotes ISC proliferation. Therefore, we investigated how the Ssk-Mesh complex regulated Yki activity. At least two upstream Sterile20 kinases, Msn and Hpo, can phosphorylate and activate Wts, which in turn phoshorylates and inhibits Yki (Li et al., 2014a; Li et al., 2018; Ma et al., 2019; Misra and Irvine, 2018). On phos-tag gels, highly phosphorylated Yki exhibited slower mobility and accumulated at the top of the gel. The faster moving Yki proteins have lower phosphorylation (Fig. 16A, B, arrow). *Ssk* or *mesh* RNAi caused reduced Yki phosphorylation, albeit at lower levels compared to that caused by *wts* RNAi (Fig. 16A, B). One explanation is that Wts is a central kinase that receives many different upstream signals to regulate Yki, while the Ssk-Mesh complex may only represent one of the many upstream events and therefore only partially reduced Yki phosphorylation.

In the adult midgut, Msn is expressed and functions in EBs, while Hpo functions in ECs, to regulate Yki and subsequently ISC proliferation (Li et al., 2014a; Li et al., 2018). One mechanism that regulates Hpo and Msn activities is through phosphorylation of a conserved T194/T187 residue in their kinase domains (Li et al., 2018). We examined the phosphorylation of this activation site on transgenic constructs of Msn and Hpo after *Ssk* or *mesh* RNAi. However, we did not observe any consistent change of this phosphorylation (Fig. 17A, B). Therefore, we speculated that Ssk and Mesh might interact with a downstream component. Co-IP experiments performed in transfected S2 cells showed that Yki could form a complex with Ssk, and in an independent experiment also with Mesh (Fig. 16C, D). We further tested the co-transfection of Ssk and Mesh together

with Yki in S2 cells but we did not observe a further increase of the co-IP signal. The cultured S2 cells probably do not form septate junctions, but the transfection results nonetheless demonstrate that Ssk or Mesh when over-expressed in cells can binds directly or indirectly to Yki.

Fig. 16

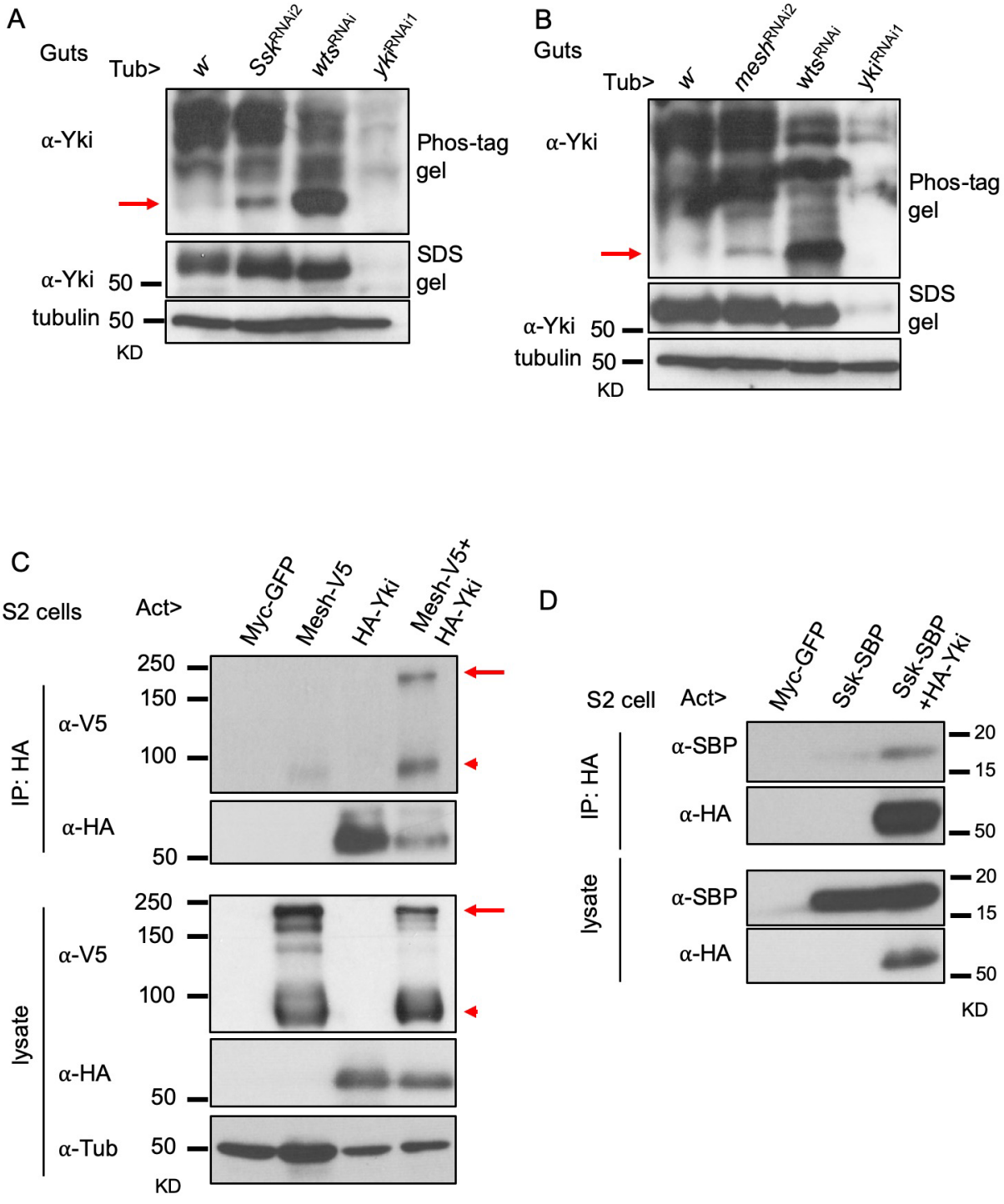
A
Guts
Tub>
w
Ssk^RNAi2
wts^RNAi
yki^RNAi1
α-Yki
Phos-tag gel
α-Yki
50
SDS gel
tubulin
50
KD
B
Guts
Tub>
w
mesh^RNAi2
wts^RNAi
yki^RNAi1
α-Yki
Phos-tag gel
α-Yki
50
SDS gel
tubulin
50
KD
C
S2 cells
Act>
Myc-GFP
Mesh-V5
HA-Yki
Mesh-V5+ HA-Yki
IP: HA
α-V5
250
150
100
α-HA
50
lysate
α-V5
250
150
100
α-HA
50
α-Tub
50
KD
D
S2 cell
Act>
Myc-GFP
Ssk-SBP
Ssk-SBP +HA-Yki
IP: HA
α-SBP
20
15
α-HA
50
lysate
α-SBP
20
15
α-HA
50
KD

**Figure 16. Ssk and Mesh form a complex with and restrict the activity of Yki.**

(A) Western blots using an antibody for endogenous Yki. Guts were dissected from flies with the tubulinGal4 ubiquitous driver and the indicated RNAi lines. Extracts were prepared and resolved on a Phos-tag gel for the upper panel, or regular SDS gel for the middle and lower panels. An Yki antibody was used for the upper and middle blots, and a tubulin antibody was used for the lower blot. The red arrow in the upper panel indicates the Yki protein that had the highest mobility, representing the lowest phosphorylation.

(B) A similar Phos-tag gel for Yki, except that mesh RNAi flies were used.

(C) Co-immunoprecipitation of Mesh and Yki in transfected S2 cells using the tagged protein expression constructs as indicated. The UAS expression constructs were co-transfected with ActinGal4 as the driver. The resulting extracts were used for immunoprecipitation by HA antibody, and blotted for V5 or HA. The lysates were also used for blots as expression control in lower panels. The red arrows indicate the expected size of full-length Mesh protein. The red arrowheads indicate the expected size of a truncate Mesh due to a protease cleavage site, as previously described (Izumi et al., 2012).

(D) A similar co-immunoprecipitation of Ssk and Yki in transfected S2 cells.

Fig. 17

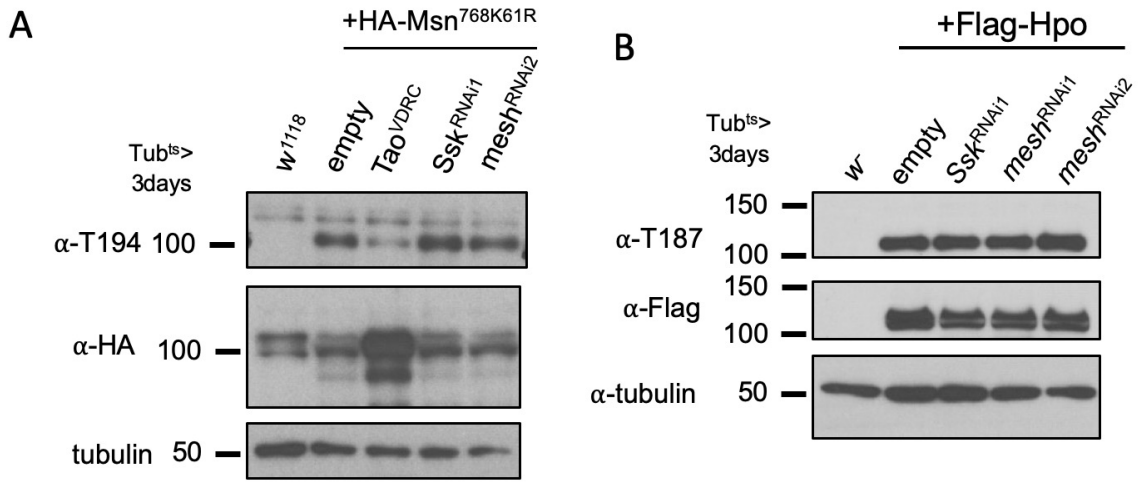


**Figure 17. Phosphorylation of Msn and Hpo was not affected after knockdown of Ssk or mesh.**

(A) Western blots using an antibody recognizes the phosphorylated threonine residue T194 of Msn, to evaluate whether Ssk and Mesh act through Ste20 kinases upstream of Yki. 10 midguts from each genotype as indicated were lysed in SDS sample buffer and boiled for 10minutes at 100$^{o}$C. Proteins were subjected to SDS-PAGE, followed by Western blotting by the rabbit anti-pT194. The flies contained the transgenic UAS-HA Msn768$^{K61R}$, which contained the first 768 a.a. with K to R mutation at a.a. 61 of Msn, as the target for phosphorylation (Li et al., 2018).

(B) Similar Western blot using the same antibody that recognizes phosphorylated T187 of Hpo. The flies contained the transgenic UAS-Flag-Hpo full length as the target for phosphorylation.

Fig. 18

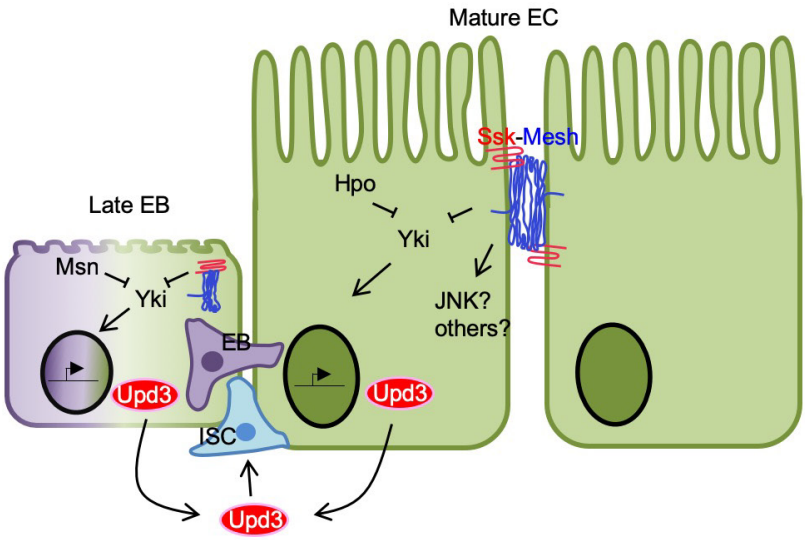


**Figure 18. Ssk and Mesh restrict Yki activity to mediate Upd3 expression and thereby ISC proliferation along EB-EC differentiation.**

A model illustrating the function of smooth septate junction proteins, Ssk and Mesh, in adult *Drosophila* midgut EBs and ECs. The expression of Ssk and Mesh are initiated in differentiating EBs and gradually incorporated into the smooth septate junction at the apical lateral side of mature ECs. In addition to their barrier function, Ssk and Mesh also form a complex with Yki, in the cytoplasm or at membrane. This may spatially facilitate Yki phosphorylation and inhibition by upstream kinases Wts, Msn or Hpo, or may restrict the mobilization of Yki, thereby provides a negative regulation of Yki. Change of septate junction-Yki interaction by mechanical stretching or by tissue damage may allow Yki to become more active to increase Upd3 expression and cause a change of midgut homeostasis.

## DISCUSSION

We have used knockin and knockout alleles of Ssk and Mesh to demonstrate their functions in both EBs and ECs to regulate ISC proliferation. Their functions in both cell types are to restrict the transcription factor Yki, which when active can stimulate the expression of Upd3 for the JAK-STAT pathway to promote midgut growth (Fig. 18). Ssk and Mesh have low but detectable expression in cytoplasm of EBs, while that in ECs are mainly in septate junctions but also some cytoplasmic localization. Multiple lines of evidence suggest that the Ssk and Mesh expression in EBs is of functional importance. First, the EB driver Su(H)> has expression in fewer cells when compared to the Myo1A> driver but still can cause comparable Upd3 expression and proliferation phenotypes. Second, mutant *Ssk* and *mesh* MARCM clones have detectable *upd3-promoter-LacZ* reporter expression in late EBs, in addition to that in mature ECs. Third, the Su(H)> *Ssk* or *mesh* RNAi had very minor Smurf and lethality phenotype, suggesting that the EB RNAi effects do not linger into mature ECs, but yet can cause strong proliferation phenotype.

When EBs continue to mature into ECs, most of the Ssk and Mesh proteins are incorporated into septate junctions, together with other proteins such as Tsp2A, Fas3 and Cora. Loss of function of septate junction proteins in ECs lead to drastic outcomes including leaky gut, lethality and stress response pathways including Yki and Upd3. Recent reports have expanded the Hpo/Mst pathway to include Msn and Hppy, as well as their mammalian homologues MAP4K1-7 (Li et al., 2014a; Li et al., 2015b; Meng et al., 2015; Poon et al., 2018; Zheng et al., 2015). Many membrane-associated proteins such as cadherin-like protein FAT, adherens junction protein a-Catenin and tight junction protein Angiomotin are involved in the Hpo/Mst pathway by regulating upstream

components (Dai et al., 2013; Fletcher et al., 2018; Han et al., 2018; Mana-Capelli and McCollum, 2018; Mana-Capelli et al., 2014; Meng et al., 2018; Su et al., 2017; Yu and Pan, 2018; Zhao et al., 2011). Our results presented in this report, however, suggest that smooth septate junctions may act as a signaling platform by directly binding to Yki. Ssk and Mesh are expressed much higher in guts than in other tissues. That may be the reason why previous protein interaction screens conducted in S2 cells had not identified the Yki complex with Ssk or Mesh (Kwon et al., 2013; Yu and Pan, 2018). A recent report shows that another smooth septate junction component Tsp2A regulates midgut homeostasis through aPKC-Hpo pathway, possibly involving endosomal trafficking (Xu et al., 2019). We also observed that Ssk and Mesh had detectable expression in cytoplasmic punctate (see Fig. 6B-O, 13, and 14), rather similar to that shown for Tsp2A (Xu et al., 2019). However, Tsp2A can act in the whole ISC-EB-EC lineage (Xu et al., 2019), while we did not observe a function of Ssk and Mesh in early EBs. Therefore, it is possible that Mesh, Ssk and Tsp2A can form a complex and are components of the smooth septate junction but each may also have independent functions.

Disruption of paracellular junctions in adult midgut leads to epithelial disorganization along the digestive track (Resnik-Docampo et al., 2018). Loss of tissue integrity initiates damage/stress signals that may also activate other pathways, such as the loss of tricellular junction protein Gliotactin leads to activation of the JNK pathway in EC to stimulate ISC proliferation (Resnik-Docampo et al., 2017). Prolonged RNAi of *Ssk* and *mesh* especially in ECs lead to leaky guts and lethality, consistent with loss of septate junction integrity. The depletion of Yki alone after longer RNAi of *Ssk* or *mesh* in ECs, however, is not sufficient to suppress all the phenotypes, suggesting that such stress may

stimulate multiple downstream response pathways. However, we show that the JNK pathway is not active and cell death is not extensive after loss of Ssk or Mesh. Gut leakage may drive inflammation and trigger systematic immune response contributed by hemocytes, which in turn trigger ISC division indirectly (Chakrabarti et al., 2016). Further investigation will provide a more complete picture of how different pathways are involved.

## MATERIALS AND METHODS

### *Drosophila* stocks and genetics

The strains $w^{1118}$ and UAS-mCD8GFP in the $w^{1118}$ background were used as wild-type stocks to cross with various Gal4 for control experiments. The transgenic RNAi fly stocks for the screening of potential regulators that are involved in adult midgut homeostasis were obtained from VDRC or Bloomington (TRiP) stock center. The transgenic RNAi fly stocks used for experiments described in this report for targeting the specific genes include: *Ssk* (VDRC105193 as RNAi1, VDRC11906 as RNAi2), *mesh* (VDRC108297 as RNAi1, VDRC6867 as RNAi2), *upd3* (TRiP28575 as RNAi1, TRiP32859 as RNAi2), *yki* (TRiP31965 as RNAi1, UAS-Yki-RNAi-N as RNAi2). The driver lines esg-Gal4, Su(H)Gal4, and Myo1AGal4 were as described (Jiang et al., 2009; Micchelli and Perrimon, 2006; Ohlstein and Spradling, 2006; Zeng et al., 2010). The Su(H)Gal4 line on the 2nd chromosome was used for all experiments. For RNAi experiments, the final cross and progeny were maintained at room temperature and shifted to 29°C for 2-5 days for Myo1AGal4 and Su(H)Gal4 as specified in the figures. The 4 kb *upd3* promoter-lacZ (*upd3-lacZ*) fly was a kind gift from Hervé Agaisse (Zhou et al., 2013).

### Generation of Ssk and mesh mutant and knockin tag alleles

CRISPR/Cas9-mediated genome editing by non-homologous end joining (NHEJ) using two nearby guide RNAs was applied to generate the Ssk mutants. To construct the guide RNA (gRNA) expression vectors for Ssk exon 1 and exon 2, complementary oligonucleotides of the target sequences with 4-bp overhangs on both ends (exon1: 5'-cttcGAATAGAGCGTACAGTCTCCA-3' and 5'-aaacTGGAGACTGTAGGCTCTATTC;

exon2: 5'-cttcGAATCCAACCATGACGCCTG-3' and 5'-aaacCAGGCGTCATGGTTGGATTC-3') were annealed to generate a double-strand DNA, and cloned into the guide RNA expression plasmid pDCC6, digested by BbsI (Thermo Scientific), followed by transformation, colony PCR selection and sequencing (Gokcezade et al., 2014). gRNA expression plasmids accompanied with Cas9 expression plasmid were injected into the *FRT80B* host. Surviving F0 flies were individually crossed with $w^{1118}$ to examine their fertility. Individual F1 flies from each cross was mated to the balancer stock *w⁻; Sp/Cyo; TM2a/TM3*. After eclosion of the F2 adults, individual flies were used for genomic DNA isolation, restriction enzyme digestion as indicated in Supp Fig. 2A, and finally confirmed by sequencing. A total of 6 different indel alleles were obtained (Fig. 2B). All indel alleles generated reading frame shift and created premature stop codon except for *FRT80B,* $Ssk^6$, in which one glycine residue in exon2 was in-frame deleted.

The mesh mutant was generated by CRISPR/Cas9-mediated genome editing by homology-dependent repair (HDR) using 1 guide RNA and a dsDNA plasmid donor. By design, the homologous replacement would result in a 53-nucleotide fragment deletion, 124 to 176 nucleotides downstream from ATG, and be replaced by the knock-in stop cassette with 3 frames stop codons, followed by floxed 3XP3 promoter-driven RFP. The 3XP3-RFP marker that facilitated the genetic screening would be flipped out by mating *with* $y^1$ $w^{67c23}$ *P{Crey}1b; D*/TM3,* $Sb^1$ (Bloomington stock #851). This mutant was generated on the FRT82B chromosome. Similar CRISPR/Cas9-mediated genome editing by HDR strategies were used to generate the Ssk-SBP and Mesh-V5 knock in tag alleles

(Fig. 6A). All these Ssk and mesh mutant and knockin tag designs and injections were contracted to and conducted by WellGenetics (Taipei, Taiwan).

**MARCM clonal analysis**

Mutant clones in adult midguts were generated by mitotic recombination using Mosaic Analysis with a Repressible Cell Marker (MARCM) (Lee and Luo, 2001). *y, w, hsFLP, tub-Gal4, UAS-nlsGFP/FM7; FRT80B tubGal80/TM3, Sb*$^{1}$ and *y, w, hsFLP, tub-Gal4, UAS-nlsGFP/FM7; FRT82B tubGal80/TM3* were flippase providing strains and were crossed with CRISPR-generated FRT-*Ssk* and -*mes*h mutants. All crosses were set up and maintained at room temperature. To induce mutant clones, approximately 3-day old flies were heat shocked at 37°C for 50 minutes, performed once each day for 2 consecutive days, and returned to 18°C in between. The flies were then kept at 18°C for one more day and then incubated at room temperature for additional 5-10 days before gut dissection for analysis.

**Immunostaining and fluorescent microscopy**

Female flies were used for gut dissection due to the bigger size. The entire gastrointestinal tracks were pulled out and fixed with 1XPBS plus 4% Formaldehyde (Polysciences) for 2 hours under room temperature, except for Delta staining, for which the fixation time was 40 minutes. The following rinses, washes, and incubations with primary and secondary antibodies were in the 1X PBS containing 0.5% BSA and 0.1% Triton-X100. The following primary antibodies were used: mouse anti-Delta (1:100; DSHB), mouse anti-Pros (1:50; DSHB), mouse anti-Cora (1:50; DSHB), mouse anti-Fas3 (1:50; DSHB), mouse anti- Hdc (1:3; DSHB), mouse anti-beta Galactosidase (1:100, DSHB), rabbit anti-phospho- Histone 3 (1:3000, Abcam), mouse anti-V5 (Invitrogen;

1:2000), mouse anti-SBP (Santa Cruz; 1:1000) and rabbit anti-HA (Cell Signaling Technology; 1:2000). Goat anti-mouse IgG 19 conjugated to Alexa 488, 568 and 633 (Invitrogen) and Goat anti-rabbit IgG conjugated to Alexa 488 and 555 (Invitrogen) were used as the secondary antibodies with 1:2000 dilution. DAPI (Vectorshied, Vector Lab) was used at 1.5 μg/ml. Images were taken by Nikon Spinning Disk confocal microscope and Zeiss LSM 700 confocal microscope. *Real-time PCR* Total RNA was extracted from 10 female guts using TRI Reagent (Sigma-Aldrich) and synthesized cDNA with iScript cDNA synthesis kit (Bio-Rad). qPCR was carried by iTaq Universal SYBR Green Supermix (Bio-Rad) and acquired by iQ5 System (Bio-Rad). The sequences of primers for growth factor detection have been listed in previous reports (Ren et al., 2010). The RT-qPCR was performed in triplicate from each of at least two independent biological samples. The *ribosomal-protein 49* (*rp49*) gene was used as the internal control for normalization of cycle number.

**Smurf assay**

Standard fly medium was mixed with blue dye (FD&C Blue #1, SPS Alfachem) at a concentration of 2.5% (wt/vol). Newly eclosed flies were aged for 3 days on standard medium under room temperature and placed on dyed medium at 29°C. The flies were counted and transfer to new vial every day. A fly was counted as Smurf+ when there was blue color visibly appeared in the abdomen outside of the digestive tract.

**Tissue culture, transfection, and Co-Immunoprecipitation**

*Drosophila* S2 cells were culture in Schneider's medium (Gibco) supplemented with 10% fetal bovine serum (FBS) at room temperature. Plasmids were transfected into S2 cells in 6-well culture plate with Effectene transfection reagent (Qiagen) 3 days prior to

sample collection. Cells were lysed with lysis buffer (500mM Tris-HCl, 150mM NaCl, 1mM EDTA, 1% TritonX-100), plus protease inhibitor and phosphatase inhibitor cocktail (Sigma). Lysates were incubated with mouse anti-HA coated magnetic beads (Thermo Fisher Scientific) at 4°C overnight to precipitate the complex. Beads were washed 5 times using 1.2 ml lysis buffer without inhibitors before heating to dissociate the protein complex from beads. Immunocomplex and S2 cell lysate were separated on SDS-PAGE, transferred to PVDF membrane, and analyzed by Western blotting.

**Phos-tag Gel and Western blot**

To confirm the physical interaction of Ssk and Mesh in adult *Drosophila* midgut, the knockin tag alleles were crossed together and 200 midguts were harvested from each genotype, and *w-* is the control. Fly midguts were mixed with lysis buffer (500mM Tris-HCl, 150mM NaCl, 1mM EDTA, 1% TritonX-100) containing protease and phosphatase inhibitor, homogenized using pestle, and incubated in 4 °C overnight. Mouse anti-V5 antibody (MBL international) was used for immunoprecipitation. The subsequent Western blot was analyzed by rabbit anti-V5 (Sigma; 1:2000) or mouse anti-SBP (Santa Cruz; 1:1000).

To detect Ssk and Mesh-regulated phosphorylation of Yki, 10 female guts were dissected and mixed with 100 µl 2X SDS sample buffer and boiled for 10 minutes at 100°C. Proteins were subjected to SDS-PAGE electrophoresis containing Phos-TagTM (Wako Pure Chemical Industries Ltd.) to separate phosphorylated isoforms of Yki. The proteins on SDS gel were then transferred to PVDF membrane. The membrane was incubated with 5% dry milk (Bio-Rad) for background blocking and subsequently incubated with rabbit anti-Yki (1:500) overnight at 4°C, followed by incubation with horseradish

peroxidase (HRP)-conjugated secondary antibodies, and detected with enhanced chemiluminescence (Thermo Fisher). The Yki antisera were generous gifts from Drs. DJ Pan (UT Southwestern) and Lei Zhang (Shanghai Institutes for Biological Sciences).

**SYTOX orange nucleic acid staining**

Dissected guts were incubated with SYTOX Orange Nucleic Acid Stain (Invitrogen: 1 μM) and Hoechst 33342 (Invitrogen: 10 μg/ml) in pre-cold 1X PBS for 10 minutes at room temperature. Samples were quickly rinsed with 1X PBS twice, then mounted with 1X PBS and immediately analyzed by Nikon Spinning Disk confocal microscope.

# Table 1.

| RNAi stock | Gene number | Gene name | Midgut proliferation | Functional description |
|---|---|---|---|---|
| B29586 | CG3796 | achaete | | bHLH transcription factor |
| 7140 | CG4027 | Actin5c | small flies | cytoskeleton |
| 101438 | CG4027 | Actin5c | small flies | cytoskeleton |
| B42651 | CG4027 | Actin5c | Lethal | cytoskeleton |
| 102480 | CG18290 | Actin87E | wt | cytoskeleton |
| B42652 | CG18290 | Actin87E | wt | cytoskeleton |
| 12174 | CG11062 | Activin-B | wt | TGF-β signaling |
| 108663 | CG11062 | Activin-B | wt | TGF-β signaling |
| 16456 | CG5992 | Adgf-A | ++ | adenosine deaminase |
| 110152 | CG5992 | Adgf-A | wt | adenosine deaminase |
| 25484 | CG5998 | Adgf-B | ++ | adenosine deaminase |
| 100933 | CG5998 | Adgf-B | wt | adenosine deaminase |
| 16639 | CG9621 | Adgf-D | wt | adenosine deaminase |
| 16641 | CG9621 | Adgf-D | wt | adenosine deaminase |
| 51565 | CG10143 | Adgf-E | wt | adenosine deaminase |
| 103063 | CG17484 | Adherens junction protein p120 | wt | adherens junction |
| 26007 | CG7039 | ADP-ribosylation factor related protein 1 | wt | Arfrp1, ARF small GTPase |
| 1326 | CG10001 | Allatostatin A receptor2 | ++ | G protein-coupled receptor |
| 108648 | CG10001 | Allatostatin A receptor2 | wt | G protein-coupled receptor |
| 22290 | CG6193 | Apc2 | wt | wnt signaling |
| 100104 | CG6193 | Apc2 | ++ | wnt signaling |
| 2907 | CG42783 | aPKC | wt | polarity |
| 105624 | CG42783 | aPKC | wt | polarity |
| B34332 | CG42783 | aPKC | wt | polarity |
| B38245 | CG42783 | aPKC | wt | polarity |
| 16826 | CG6741 | arc | wt | PDZ domain |
| 12931 | CG11027 | Arf102F | wt | ADP-ribosylation factor |
| 17826 | CG6025 | Arl1 | wt | ADP-ribosylation factor |
| 7767 | CG11579 | armadillo | lethal | beta catenin, adherens junction |
| 107344 | CG11579 | armadillo | lethal | beta catenin, adherens junction |
| B31895 | CG3258 | asense | wt | bHLH transcription factor |
| B26316 | CG7508 | atonal | wt | bHLH transcription factor |
| B31350 | CG6386 | ballchen | wt | histone kinase |
| 34138 | CG5680 | basket | +++ | JNK, serine/threonine kinase |
| 34139 | CG5680 | basket | +++ | JNK, serine/threonine kinase |
| 104569 | CG5680 | basket | +++ | JNK, serine/threonine kinase |
| B32977 | CG5680 | basket | wt | JNK, serine/threonine kinase |
| 2914 | CG5055 | bazooka | wt | Par3, polarity |
| 2915 | CG5055 | bazooka | wt | Par3, polarity |
| B35002 | CG5055 | bazooka | wt | Par3, polarity |
| B39072 | CG5055 | bazooka | wt | Par3, polarity |
| 109722 | CG1822 | Bifocal | wt | cytoskeleton binding |
| 15974 | CG42230 | big bang | + | septate junction |
| 36111 | CG42230 | big bang | wt | septate junction |
| 101691 | CG42230 | big bang | + | septate junction |
| 34978 | CG5249 | Blimp-1 | wt | zn finger transcription factor |
| 50171 | CG5249 | Blimp-1 | +++ | zn finger transcription factor |
| 108374 | CG5249 | Blimp-1 | wt | zn finger transcription factor |
| 5443 | CG14430 | boudin | wt | septate junction |
| 107102 | CG14430 | boudin | + | septate junction |
| 5730 | CG4608 | branchless | wt | Fibroblast growth factor |
| 101377 | CG4608 | branchless | wt | Fibroblast growth factor |
| 40209 | CG31132 | BRWD3 | wt | Bromodomain, WD40 domain |
| 19679 | CG42281 | bunched | +++ | TSC-22, leucine zipper |
| 19680 | CG42281 | bunched | wt | TSC-22, leucine zipper |
| 18479 | CG14980 | Caffeine, calcium, zinc sensitivity 1 | wt | CcZ1, Rab GTPase exchange factor |
| 100773 | CG10540 | capping protein alpha | +++ | F-actin capping protein, |
| B41685 | CG10540 | capping protein alpha | lethal | F-actin capping protein, |
| 45668 | CG17158 | capping protein beta | ++ | F-actin capping protein |
| B41925 | CG17158 | capping protein beta | wt | F-actin capping protein |
| B50954 | CG17158 | capping protein beta | +++ | F-actin capping protein |
| 21995 | CG33979 | capulet | wt | actin binding protein |
| 101588 | CG33979 | capulet | wt | actin binding protein |
| B33010 | CG33979 | capulet | wt | actin binding protein |
| B6437 | CG10538 | Cd GTPase activation protein-related | wt | CdGAPr, GTPase activation protein |
| B6438 | CG10538 | Cd GTPase activation protein-related | wt | CdGAPr, GTPase activation protein |
| B28021 | CG12530 | Cdc42 | wt | Rho GTPase |
| B35756 | CG12530 | Cdc42 | ++ | Rho GTPase |
| 37521 | CG31811 | Centaurin Gamma 1A | wt | CenG1A, GTPase |
| 5684 | CG5229 | chameau | wt | histone acetyl transferase |
| 35507 | CG11798 | charlatan | wt | zn finger transcription factor |
| 108695 | CG11798 | charlatan | ++ | zn finger transcription factor |
| B26779 | CG11798 | charlatan | wt | zn finger transcription factor |
| 28294 | CG1084 | Contactin | wt | septate junction |
| 40613 | CG1084 | Contactin | + | septate junction |
| 9788 | CG11949 | coracle | + | septate junction |
| 108749 | CG11949 | coracle | ++ | septate junction |
| 39177 | CG6383 | crumbs | ++ | transmembrane, polarity |
| B34999 | CG6383 | crumbs | wt | transmembrane, polarity |
| B38373 | CG6383 | crumbs | wt | transmembrane, polarity |
| 19297 | CG1512 | Cullin 2 | wt | ubiquitin protein ligase |

| | | | | |
|---|---|---|---|---|
| 16331 | CG42616 | Cullin 3 | wt | ubiquitin protein ligase |
| 41838 | CG5363 | Cyclin-dependent kinase 1 | wt | Cdk1, cell cycle |
| 41839 | CG5363 | Cyclin-dependent kinase 1 | lethal | Cdk1, cell cycle |
| 106130 | CG5363 | Cyclin-dependent kinase 1 | wt | Cdk1, cell cycle |
| B32964 | CG17941 | dachsous | wt | Cadherin-like, cell adhesion |
| 109491 | CG3619 | Delta | ++ | Ligand of Notch signaling |
| B28032 | CG3619 | Delta | wt | Ligand of Notch signaling |
| 48495 | CG12029 | dendritic arbor reduction 1 | wt | zn finger transcription factor |
| 101395 | CG12029 | dendritic arbor reduction 1 | wt | zn finger transcription factor |
| 28736 | CG10794 | Diptericin B | wt | humoral immune response |
| 28737 | CG10794 | Diptericin B | wt | humoral immune response |
| 102607 | CG10794 | Diptericin B | ++ | humoral immune response |
| 41134 | CG1725 | discs large 1 | wt | PDZ domain guanylate kinase, polarity |
| 109274 | CG1725 | discs large 1 | + | PDZ domain guanylate kinase, polarity |
| B25780 | CG1725 | discs large 1 | wt | PDZ domain guanylate kinase, polarity |
| B31181 | CG1725 | discs large 1 | wt | PDZ domain guanylate kinase, polarity |
| B31520 | CG1725 | discs large 1 | wt | PDZ domain guanylate kinase, polarity |
| B31521 | CG1725 | discs large 1 | wt | PDZ domain guanylate kinase, polarity |
| 45459 | CG32315 | discs lost | wt | polarity |
| 103709 | CG32315 | discs lost | wt | polarity |
| 10004 | CG2019 | dispatched | ++ | membrane protein, Hedgehog signalling |
| 100537 | CG6794 | Dorsal-related immunity factor | wt | NF-kappaB transcription factor |
| 107064 | CG3727 | dreadlocks | wt | NCK, SH2 SH3 adaptor |
| 28053 | CG7507 | Dynein heavy chain 64C | wt | microtubule motor |
| 28054 | CG7507 | Dynein heavy chain 64C | wt | microtubule motor |
| 937 | CG12676 | echinoid | wt | cell adhesion, hippo signaling |
| 938 | CG12676 | echinoid | wt | cell adhesion, hippo signaling |
| 3087 | CG12676 | echinoid | + | cell adhesion, hippo signaling |
| 104279 | CG12676 | echinoid | + | cell adhesion, hippo signaling |
| 45252 | CG12919 | eiger | wt | TNF, apoptosis |
| 45253 | CG12919 | eiger | wt | TNF, apoptosis |
| 108814 | CG12919 | eiger | wt | TNF, apoptosis |
| 37526 | CG11290 | enoki mushroom | wt | MYST family histone acetyltransferase |
| B28703 | CG4114 | expanded | wt | cell adhesion, hippo signaling |
| B34968 | CG4114 | expanded | wt | cell adhesion, hippo signaling |
| 42229 | CG5803 | Fascilin 3 | +++ | Ig domain cell adhesion |
| 100642 | CG5803 | Fascilin 3 | +++ | Ig domain cell adhesion |
| 9396 | CG3352 | fat | + | Cadherin-like, hippo signaling |
| 108863 | CG3352 | fat | + | Cadherin-like, hippo signaling |
| B34970 | CG3352 | fat | wt | Cadherin-like, hippo signaling |
| 36053 | CG8874 | FER tyrosine kinase | + | F-BAR domain, actin bundling |
| 36054 | CG8874 | FER tyrosine kinase | ++ | F-BAR domain, actin bundling |
| 107266 | CG8874 | FER tyrosine kinase | + | F-BAR domain, actin bundling |
| 2964 | CG2096 | flapwing | ++ | Protein phosphatase 1b at 9C, myosin phosphatase |
| 29622 | CG2096 | flapwing | wt | Protein phosphatase 1b at 9C, myosin phosphatase |
| 17957 | CG10023 | Focal adhesion kinase | + | FERM domain, integrin signaling |
| 108608 | CG10023 | Focal adhesion kinase | wt | FERM domain, integrin signaling |
| B31311 | CG17697 | frizzled | wt | receptor Wnt signaling |
| B31312 | CG9739 | frizzled 2 | wt | receptor Wnt signaling |
| B31390 | CG9739 | frizzled 2 | wt | receptor Wnt signaling |
| 30214 | CG16785 | frizzled 3 | ++ | receptor Wnt signaling |
| 30215 | CG16785 | frizzled 3 | wt | receptor Wnt signaling |
| 26220 | CG3532 | GCC185 | wt | GRIP and coiled-coil domain |
| 21786 | CG4107 | Gcn5 acetyltransferase | ++ | Pcaf, histone acetyltransferase |
| 3270 | CG3002 | Golgi-localized, γ-adaptin ear | wt | Gga, clathrin adaptor |
| | | containing, ARF binding protein | wt | |
| 13687 | CG6964 | Grunge | wt | transcriptional repressor, histone deacetylase |
| B31568 | CG5155 | gudu | wt | Armadillo repeat-containing protein |
| 20144 | CG12085 | half pint | + | pUF68, poly(U) RNA binding |
| 109796 | CG12085 | half pint | wt | pUF68, poly(U) RNA binding |
| B25951 | CG12085 | half pint | wt | pUF68, poly(U) RNA binding |
| 25742 | CG31320 | HEATR2 | wt | Armadillo-like helical |
| 15486 | CG11734 | HECT and RLD domain containing protein 2 | wt | HERC2, ubiquitin protein ligase |
| 1402 | CG4637 | hedgehog | wt | Hh signaling pathway ligand |
| 43255 | CG4637 | hedgehog | wt | Hedgehog signalling |
| 109454 | CG4637 | hedgehog | wt | Hh signaling pathway ligand |
| B31344 | CG17950 | High mobility group protein D | wt | HmgD, DNA binding chromatin organization |
| B26219 | CG17921 | High mobility group protein Z | wt | HmgZ, DNA binding chromatin organization |
| 33459 | CG2051 | Histone acetyltransferase 1 | wt | H4 histone acetyltransferase |
| 30600 | CG7471 | Histone deacetylase 1 | ++ | HDAC1, histone deacetylase |
| 46929 | CG7471 | Histone deacetylase 1 | ++ | HDAC1, histone deacetylase |
| 20814 | CG2128 | Histone deacetylase 3 | wt | HDAC3, histone deacetylase |
| 20522 | CG1770 | Histone deacetylase 4 | wt | HDAC4, histone deacetylase |
| 108831 | CG6170 | Histone deacetylase 6 | ++ | HDAC2/6, histone deacetylase |
| B28966 | CG5499 | Histone H2A variant | wt | H2Av, H2AvD, H2AX, DNA damage |
| B33916 | CG5834 | Hsp70Bbb | wt | Heat shock protein 70 family, chaperone |
| 12414 | CG4472 | Imaginal disc growth factor 1 | ++ | Glycoside hydrolase, chitinase |
| 12416 | CG4472 | Imaginal disc growth factor 1 | wt | Glycoside hydrolase, chitinase |
| 12422 | CG4559 | Imaginal disc growth factor 3 | + | Glycoside hydrolase, chitinase |
| 12423 | CG4559 | Imaginal disc growth factor 3 | + | Glycoside hydrolase, chitinase |
| 14624 | CG1780 | Imaginal disc growth factor 4 | wt | Glycoside hydrolase, chitinase |
| 104968 | CG1780 | Imaginal disc growth factor 4 | wt | Glycoside hydrolase, chitinase |
| 16795 | CG5154 | Imaginal disc growth factor 5 | wt | Glycoside hydrolase, chitinase |

| | | | | |
|---|---|---|---|---|
| 100977 | CG5154 | Imaginal disc growth factor 5 | wt | Glycoside hydrolase, chitinase |
| 18845 | CG10850 | imaginal discs arrested | wt | ubiquitin protein ligase, mitotic regulation |
| 5198 | CG14173 | Insulin-like peptide 1 | wt | insulin receptor signaling |
| 102158 | CG8167 | Insulin-like peptide 2 | wt | insulin receptor signaling |
| 9199 | CG14167 | Insulin-like peptide 3 | wt | insulin receptor signaling |
| 9201 | CG14167 | Insulin-like peptide 3 | wt | insulin receptor signaling |
| 106512 | CG14167 | Insulin-like peptide 3 | wt | insulin receptor signaling |
| 12890 | CG6736 | Insulin-like peptide 4 | wt | insulin receptor signaling |
| 105516 | CG6736 | Insulin-like peptide 4 | wt | insulin receptor signaling |
| 49519 | CG33273 | Insulin-like peptide 5 | wt | insulin receptor signaling |
| 49520 | CG33273 | Insulin-like peptide 5 | wt | insulin receptor signaling |
| 105004 | CG33273 | Insulin-like peptide 5 | wt | insulin receptor signaling |
| 45218 | CG14049 | Insulin-like peptide 6 | wt | insulin receptor signaling |
| 102465 | CG14049 | Insulin-like peptide 6 | wt | insulin receptor signaling |
| 49128 | CG13317 | Insulin-like peptide 7 | wt | insulin receptor signaling |
| 105024 | CG13317 | Insulin-like peptide 7 | wt | insulin receptor signaling |
| 992 | CG18402 | Insulin-like receptor | wt | receptor tyrosine kinase, insulin signaling |
| 12610 | CG4029 | jumeau | wt | Fork head domain, transcription factor |
| 21700 | CG3654 | Jumonji, AT rich interactive domain 2 | ++ | Jarid2, ARID DNA-binding domain |
| 36103 | CG9423 | karyopherin α3 | wt | Armadillo repeat, protein transporter, myosin binding |
| 100765 | CG33967 | kibra | +++ | WW domain, hippo signaling |
| 106507 | CG33967 | kibra | ++ | WW domain, hippo signaling |
| B28836 | CG33967 | kibra | ++ | WW domain, hippo signaling |
| B28750 | CG5175 | kugelkern | wt | nucleus organization |
| 3962 | CG1298 | kune-kune | + | Claudin superfamily, septate junction |
| 108224 | CG1298 | kune-kune | + | Claudin superfamily, septate junction |
| 35524 | CG12369 | Lachesin | + | Ig domain, adhesion |
| 107450 | CG12369 | Lachesin | wt | Ig domain, adhesion |
| 26597 | CG4674 | Leash | wt | arrestin domain, hippo signaling |
| 21928 | CG4713 | lethal (2) giant discs 1 | wt | C2 domain, cellular component organization |
| 51249 | CG2671 | lethal (2) giant larvae | + | WD40-repeat, polarity |
| 109604 | CG2671 | lethal (2) giant larvae | + | WD40-repeat, polarity |
| B31089 | CG2671 | lethal (2) giant larvae | wt | WD40-repeat, polarity |
| B31517 | CG2671 | lethal (2) giant larvae | wt | WD40-repeat, polarity |
| 12703 | CG3839 | lethal of scute | wt | bHLH, transcription factor |
| 47122 | CG3839 | lethal of scute | wt | bHLH, transcription factor |
| B27058 | CG3839 | lethal of scute | wt | bHLH, transcription factor |
| 35949 | CG8532 | liquid facets | + | ENTH domain, ubiquitin interacting |
| 25707 | CG42250 | liquid facets-Related | wt | Epsin related, Telomere maintenance |
| 6216 | CG8440 | Lissencephaly-1 | wt | WD40-repeat, dyenin binding |
| 106777 | CG8440 | Lissencephaly-1 | + | WD40-repeat, dyenin binding |
| 9248 | CG5248 | locomotion defects | wt | GTPase activator |
| 31402 | CG11033 | Lysine-specific demethylase 2 | wt | Kdm2, histone demethylase |
| 32652 | CG15835 | Lysine-specific demethylase 4A | wt | Kdm4A, histone demethylase |
| 34316 | CG5121 | Mediator complex subunit 28 | wt | MED28, Pol II transcription cofactor |
| 7161 | CG14228 | Merlin | + | FERM domain, hippo signaling |
| B28007 | CG14228 | Merlin | wt | FERM domain, hippo signaling |
| B34985 | CG14228 | Merlin | wt | FERM domain, hippo signaling |
| 6867 | CG31004 | mesh | +++ | Ig domain, smooth septate junction |
| 10829 | CG31004 | mesh | +++ | Ig domain, smooth septate junction |
| 40940 | CG31004 | mesh | +++ | Ig domain, smooth septate junction |
| B27495 | CG6936 | methuselah | wt | G-protein coupled receptor |
| 35171 | CG7109 | microtubule star | wt | PP2A, serine/threonine phosphatase |
| 41924 | CG7109 | microtubule star | wt | PP2A, serine/threonine phosphatase |
| B28622 | CG5588 | Mig-2-like | wt | Rac family GTPase |
| B35754 | CG5588 | Mig-2-like | wt | Rac family GTPase |
| 27526 | CG5841 | mind bomb 1 | wt | RING finger, ubiquitin protein ligase |
| 101517 | CG16973 | misshapen | ++++ | Ste20 kinase |
| B28791 | CG16973 | misshapen | ++ | Ste20 kinase |
| 27346 | CG1098 | MLF1-adaptor molecule | ++ | Madm, kinase domain, cell growth |
| 27347 | CG1098 | MLF1-adaptor molecule | wt | Madm, kinase domain, cell growth |
| 101758 | CG1098 | MLF1-adaptor molecule | wt | Madm, kinase domain, cell growth |
| 37917 | CG10701 | Moesin | + | FERM domain, cytoskeleton binding |
| 110654 | CG10701 | Moesin | ++ | FERM domain, cytoskeleton binding |
| 1800 | CG4322 | moody | + | G-protein coupled receptor, septate junction |
| 109601 | CG4322 | moody | ++ | G-protein coupled receptor, septate junction |
| 12635 | CG12399 | Mothers against dpp | wt | MAD, transcription factor BMP signaling |
| 46044 | CG18582 | mushroom bodies tiny | wt | PAK family Ste20 kinase |
| 109880 | CG18582 | mushroom bodies tiny | wt | PAK family Ste20 kinase |
| 2947 | CG10798 | Myc | ++ | bHLH transcription factor |
| 2948 | CG10798 | Myc | ++ | bHLH transcription factor |
| B25784 | CG10798 | Myc | wt | bHLH transcription factor |
| 13121 | CG7555 | Nedd4 | wt | ubiquitin protein ligase |
| 31728 | CG15319 | nejire | wt | CBP, transcription co-activator |
| 46524 | CG9258 | nervana 1 | wt | Na+ K+ ATPase |
| 103702 | CG9258 | nervana 1 | wt | Na+ K+ ATPase |
| 2660 | CG9261 | nervana 2 | + | Na+ K+ ATPase |
| 4306 | CG7050 | Neurexin1 | + | EGF-like domain, neuron adhesion |
| 36328 | CG7050 | Neurexin1 | + | EGF-like domain, neuron adhesion |
| 27202 | CG1634 | Neuroglian | ++ | Ig domain, neuron adhesion |
| 107991 | CG1634 | Neuroglian | + | Ig domain, neuron adhesion |
| 15992 | CG10254 | no assigned name | wt | ubiquitin protein ligase |
| 31609 | CG11983 | no assigned name | wt | tricogen cell |

| | | | | |
|---|---|---|---|---|
| 17052 | CG12204 | no assigned name | wt | unknown |
| 17025 | CG13481 | no assigned name | wt | RING finger, ubiquitin protein ligase |
| 13550 | CG13654 | no assigned name | wt | EGF-like domain |
| 38807 | CG14696 | no assigned name | wt | Arrestin-like domain |
| 5868 | CG3061 | no assigned name | ++ | dnaJ domain |
| 25636 | CG3099 | no assigned name | wt | HECT domain, ubiquitin protein ligase |
| 33754 | CG31064 | no assigned name | wt | FYVE zinc finger, Rab GTPase binding |
| 25784 | CG3165 | no assigned name | ++ | Ribonuclease H-like domain |
| 34599 | CG3356 | no assigned name | wt | HECT domain, ubiquitin protein ligase |
| 34601 | CG3356 | no assigned name | wt | HECT domain, ubiquitin protein ligase |
| 39178 | CG43255 | no assigned name | wt | unkonwn |
| 22326 | CG6966 | no assigned name | ++ | Ankyrin repeat |
| 18817 | CG6974 | no assigned name | + | Astacin-like metallopeptidase domain |
| 29147 | CG6980 | no assigned name | wt | Tetratricopeptide-like helical domain |
| 38230 | CG7058 | no assigned name | wt | SKP1/BTB/POZ domain |
| B31586 | CG8173 | no assigned name | wt | serine/threonine-protein kinase |
| 25033 | CG8176 | no assigned name | wt | F-BAR domain, phospholipid binding |
| 35408 | CG8202 | no assigned name | ++ | UPF0505 family |
| 23735 | CG9286 | no assigned name | wt | BCP1 family, kinase regulator |
| 26066 | CG3983 | Nucleostemin 1 | wt | YlqF/YawG family GTPase |
| 29443 | CG31519 | Odorant receptor 82a | + | multi-transmembrane chemoreceptor |
| 19732 | CG5884 | par-6 | wt | PDZ domain, polarity |
| 108560 | CG5884 | par-6 | wt | PDZ domain, polarity |
| B35000 | CG5884 | par-6 | wt | PDZ domain, polarity |
| B39010 | CG5884 | par-6 | wt | PDZ domain, polarity |
| 9049 | CG2022 | pasang lhamu | wt | Mpv17/PMP22, hypoxia |
| 31620 | CG12021 | patj | wt | PDZ domain, polarity |
| 101877 | CG12021 | patj | wt | PDZ domain, polarity |
| B26282 | CG12021 | Patj | wt | PDZ domain, polarity |
| B35747 | CG12021 | Patj | wt | PDZ domain, polarity |
| 25853 | CG31794 | Paxillin | ++ | integrin signaling adaptor |
| 107789 | CG31794 | Paxillin | + | integrin signaling adaptor |
| 6173 | CG7103 | PDGF- and VEGF-related factor 1 | wt | Pvf1, cystine-knot cytokine |
| 6175 | CG7103 | PDGF- and VEGF-related factor 1 | + | Pvf1, cystine-knot cytokine |
| 46875 | CG7103 | PDGF- and VEGF-related factor 1 | wt | Pvf1, cystine-knot cytokine |
| 102699 | CG7103 | PDGF- and VEGF-related factor 1 | wt | Pvf1, cystine-knot cytokine |
| 7628 | CG13780 | PDGF- and VEGF-related factor 2 | wt | Pvf1, cystine-knot cytokine |
| 15500 | CG34378 | PDGF- and VEGF-related factor 3 | wt | Pvf1, cystine-knot cytokine |
| 50224 | CG34378 | PDGF- and VEGF-related factor 3 | wt | Pvf1, cystine-knot cytokine |
| B27692 | CG1685 | penguin | wt | Armadillo repeats, RNA binding |
| 28892 | CG8315 | Peroxin 11 | wt | Peroxisomal biogenesis factor 11 |
| B42926 | CG17743 | pleiohomeotic | wt | zn finger transciption factor, polycomb recruiter |
| 38863 | CG43140 | polychaetoid | wt | multiple domain, cell adhesion protein binding |
| 104159 | CG43140 | polychaetoid | + | multiple domain, cell adhesion protein binding |
| 29057 | CG9156 | Protein phosphatase 1 at 13C | ++ | serine/threonine phosphatase |
| 29058 | CG9156 | Protein phosphatase 1 at 13C | wt | serine/threonine phosphatase |
| 35024 | CG5650 | Protein phosphatase 1 at 87B | wt | serine/threonine phosphatase |
| 27673 | CG6593 | Protein phosphatase 1α at 96A | wt | serine/threonine phosphatase |
| 49671 | CG17291 | Protein phosphatase 2A at 29B | wt | serine/threonine-protein phosphatase |
| 49672 | CG17291 | Protein phosphatase 2A at 29B | wt | serine/threonine-protein phosphatase |
| 848 | CG7904 | punt | wt | TGF-β type II receptor |
| 22198 | CG5771 | Rab11 | ++ | GTPase, protein traffiking |
| 108382 | CG5771 | Rab11 | wt | GTPase, protein traffiking |
| 24672 | CG4921 | Rab4 | ++ | GTPase, protein traffiking |
| B28985 | CG2248 | Rac1 | wt | Rho family GTPase |
| B34910 | CG2248 | Rac1 | wt | Rho family GTPase |
| 23639 | CG8865 | Ral guanine nucleotide dissociation stimulator-lik | wt | Rgl, Ras GEF |
| 33437 | CG1956 | Rap1 GTPase | ++ | Ras family GTPase |
| 110757 | CG1956 | Rap1 GTPase | ++ | Ras family GTPase |
| 40399 | CG6831 | rhea | +++ | talin, integrin signaling adaptor |
| 40400 | CG6831 | rhea | ++ | talin, integrin signaling adaptor |
| B31178 | CG8606 | Rho guanine nucleotide exchange factor 4 | wt | Rho GEF4 |
| B22727 | CG8416 | Rho1 | wt | GTPase, cytoskeleton organization |
| B32383 | CG8416 | Rho1 | wt | GTPase, cytoskeleton organization |
| B28672 | CG4125 | roughest | wt | Ig domain transmembrane protein, PDZ binding |
| 1258 | CG5811 | RYamide receptor | + | G protein coupled receptor, neuropeptide binding |
| 46446 | CG33193 | salvador | + | scaffolding protein, hippo signaling |
| 101323 | CG33193 | salvador | + | scaffolding protein, hippo signaling |
| B32965 | CG33193 | salvador | wt | scaffolding protein, hippo signaling |
| 7480 | CG10849 | Sc2 | wt | oxidoreductase |
| 27430 | CG43398 | scribbled | wt | scaffolding protein, polarity |
| 45556 | CG43398 | scribbled | + | scaffolding protein, polarity |
| 100363 | CG43398 | scribbled | + | scaffolding protein, polarity |
| B29552 | CG43398 | scribbled | + | scaffolding protein, polarity |
| B26206 | CG3827 | scute | wt | bHLH transcription factor |
| 34191 | CG7073 | Secretion-associated Ras-related 1 | wt | Sar1, ARF/SAR type GTPase |
| 50367 | CG6773 | Secretory 13 | wt | WD40 repeat, COPII-coated vesicle budding |
| 24552 | CG1250 | Secretory 23 | wt | ADF-H/Gelsolin-like domain, COPII-coated vesicle budding |
| 27082 | CG3722 | shotgun | wt | E-cadherin, adherens junction |
| 103962 | CG3722 | shotgun | + | E-cadherin, adherens junction |
| 22497 | CG6521 | Signal transducing adaptor molecule | wt | Stam, ENTH/VHS domain, ubiquitin binding |
| 50384 | CG4250 | Simple-1 | + | small integral membrane protein lysosome endosome |
| 101949 | CG4250 | Simple-1 | + | small integral membrane protein lysosome endosome |

| | | | | |
|---|---|---|---|---|
| 25604 | CG43325 | Simple-10 | wt | small integral membrane protein lysosome endosome |
| 107540 | CG43325 | Simple-10 | wt | small integral membrane protein lysosome endosome |
| 102266 | CG30269 | Simple-11 | wt | small integral membrane protein lysosome endosome |
| 10302 | CG30273 | Simple-12 | wt | small integral membrane protein lysosome endosome |
| 108754 | CG32280 | Simple-13 | + | small integral membrane protein lysosome endosome |
| 24566 | CG12645 | Simple-2 | wt | small integral membrane protein lysosome endosome |
| 102499 | CG12645 | Simple-2 | wt | small integral membrane protein lysosome endosome |
| B28318 | CG12645 | Simple-2 | + | small integral membrane protein lysosome endosome |
| 31856 | CG12684 | Simple-3 | + | small integral membrane protein lysosome endosome |
| 28434 | CG13510 | Simple-4 | + | small integral membrane protein lysosome endosome |
| 103009 | CG13510 | Simple-4 | + | small integral membrane protein lysosome endosome |
| 8840 | CG13511 | Simple-5 | ++ | small integral membrane protein lysosome endosome |
| 6644 | CG13559 | Simple-6 | + | small integral membrane protein lysosome endosome |
| 102577 | CG13559 | Simple-6 | + | small integral membrane protein lysosome endosome |
| 25080 | CG15708 | Simple-7 | wt | small integral membrane protein lysosome endosome |
| 25081 | CG15708 | Simple-7 | wt | small integral membrane protein lysosome endosome |
| 106423 | CG15708 | Simple-7 | + | small integral membrane protein lysosome endosome |
| 35645 | CG30196 | Simple-9 | ++ | small integral membrane protein lysosome endosome |
| 107506 | CG30196 | Simple-9 | + | small integral membrane protein lysosome endosome |
| 9012 | CG10624 | sinuous | wt | Claudin superfamily, septate junction |
| 44928 | CG10624 | sinuous | + | Claudin superfamily, septate junction |
| 23201 | CG5216 | Sirtuin 1 | wt | Sirt1, Sir2, histone deacetylase |
| 24049 | CG9506 | slow as molasses | wt | membrane organization |
| 24050 | CG9506 | slow as molasses | wt | membrane organization |
| 6232 | CG3956 | snail | wt | zn finger transciption factor |
| 50003 | CG3956 | snail | wt | zn finger transciption factor |
| 10906 | CG6981 | Snakeskin | ++++ | Ssk, smooth septate junction |
| 105193 | CG6981 | Snakeskin | ++++ | Ssk, smooth septate junction |
| 3920 | CG10334 | spitz | wt | EGF receptor ligand |
| 3922 | CG10334 | spitz | ++ | EGF receptor ligand |
| 103817 | CG10334 | spitz | wt | EGF receptor ligand |
| 29844 | CG32717 | stardust | wt | membrane-associated guanylate kinase (MAGUK), polarity |
| 100685 | CG32717 | stardust | wt | membrane-associated guanylate kinase (MAGUK), polarity |
| 34124 | CG5203 | STIP1 homology and U-box containing protein 1 | wt | STUB1, ubiquitin protein ligase |
| 37220 | CG9153 | SUMO-related HECT domain and RCC | wt | Sherpa, ubiquitin protein ligase |
| 37221 | CG9153 | repeat protein for Toll pathway activation | wt | Sherpa, ubiquitin protein ligase |
| 18610 | CG10392 | super sex combs | wt | acetylglucosaminyl transferase |
| 21814 | CG4244 | Suppressor of deltex | wt | WW domain, ubiquitin protein ligase |
| 30605 | CG12210 | Synaptobrevin | + | SNAP receptor, vesicle transport |
| 5413 | CG5081 | Syntaxin 7 | wt | SNARE, endocytosis |
| 17432 | CG14217 | Tao | +++ | Ste20 kinase |
| 107645 | CG14217 | Tao | +++ | Ste20 kinase |
| B31226 | CG14217 | Tao | + | Ste20 kinase |
| B34881 | CG14217 | Tao | ++ | Ste20 kinase |
| TOR RNAi | CG5092 | Target of rapamycin | wt | Tor, serine/threonine kinase |
| 24072 | CG9615 | tex | wt | WD40 repeat |
| 30985 | CG3024 | Torsin | wt | ATPase, regulation of lipid storage |
| 23944 | CG9712 | Tumor susceptibility gene 101 | wt | TSG101, ESCRT-I complex, endosomal sorting |
| 110599 | CG4254 | twinstar | wt | cofilin, actin binding |
| B33670 | CG4254 | twinstar | wt | cofilin, actin binding |
| 27467 | CG5604 | Ubiquitin fusion-degradation 4-like | wt | Ankyrin repeat, ubiquitinase |
| 31744 | CG12359 | Ulp1 | wt | SUMO deconjugation |
| 14664 | CG5988 | unpaired 2 | wt | ligand JAK/STAT signaling |
| B33949 | CG5988 | unpaired 2 | wt | ligand JAK/STAT signaling |
| B33988 | CG5988 | unpaired 2 | wt | ligand JAK/STAT signaling |
| 27136 | CG33542 | unpaired 3 | wt | ligand JAK/STAT signaling |
| 106869 | CG33542 | unpaired 3 | wt | ligand JAK/STAT signaling |
| B28575 | CG33542 | unpaired 3 | wt | ligand JAK/STAT signaling |
| B32859 | CG33542 | unpaired 3 | wt | ligand JAK/STAT signaling |
| 24869 | CG14542 | Vacuolar protein sorting 2 | wt | Vps2, ESCRT-III complex, endosomal trafficking |
| 38821 | CG14750 | Vacuolar protein sorting 25 | wt | Vps25, ESCRT-II complex, endosomal trafficking |
| 18396 | CG14804 | Vacuolar protein sorting 26 | wt | Vps26, endosome to Golgi retromer |
| 26625 | CG4764 | Vacuolar protein sorting 29 | wt | Vps29, endosome to Golgi retromer |
| 24157 | CG9326 | varicose | + | Guanylate kinase-like domain, septate junction |
| 104548 | CG9326 | varicose | ++ | Guanylate kinase-like domain, septate junction |
| 22082 | CG5344 | whacked | wt | Rab GAP |
| 13352 | CG4889 | wingless | wt | ligand Wnt/Wg signaling |
| B31249 | CG4889 | wingless | wt | ligand Wnt/Wg signaling |
| B31310 | CG4889 | wingless | wt | ligand Wnt/Wg signaling |
| B32994 | CG4889 | wingless | wt | ligand Wnt/Wg signaling |
| B33902 | CG4889 | wingless | wt | ligand Wnt/Wg signaling |
| B31989 | CG4971 | Wnt10 | wt | Wnt family, unknown function |
| 38077 | CG1916 | Wnt2 | wt | Wnt family, muscle, trachea, axon |
| 38079 | CG1916 | Wnt2 | + | Wnt family, muscle, trachea, axon |
| 104338 | CG1916 | Wnt2 | wt | Wnt family, muscle, trachea, axon |
| 29441 | CG1916 | Wnt2 | wt | Wnt family, muscle, trachea, axon |
| 38010 | CG4698 | Wnt4 | + | Wnt family, hemocyte, neuron, gonad |
| 104671 | CG4698 | Wnt4 | wt | Wnt family, hemocyte, neuron, gonad |
| 29442 | CG4698 | Wnt4 | wt | Wnt family, hemocyte, neuron, gonad |
| 30863 | CG6407 | Wnt5 | wt | Wnt family, salivary gland, axon, muscle |
| 32257 | CG6407 | Wnt5 | wt | Wnt family, salivary gland, axon, muscle |
| 101621 | CG6407 | Wnt5 | wt | Wnt family, salivary gland, axon, muscle |
| B28534 | CG6407 | Wnt5 | wt | Wnt family, salivary gland, axon, muscle |

| | | | | |
|---|---|---|---|---|
| B34644 | CG6407 | Wnt5 | wt | Wnt family, salivary gland, axon, muscle |
| B30493 | CG4969 | Wnt6 | wt | Wnt family, wing, head, eye size |
| 15146 | CG8458 | WntD | wt | Wnt inhibitor of Dorsal, ventral furrow, bacterial response |
| 107727 | CG8458 | WntD | wt | Wnt inhibitor of Dorsal, ventral furrow, bacterial response |
| B28947 | CG8458 | WntD | wt | Wnt inhibitor of Dorsal, ventral furrow, bacterial response |
| 2802 | CG7870 | wollknaeuel | + | glycosyltransferase 2 family, septate junction |
| 108621 | CG7870 | wollknaeuel | + | glycosyltransferase 2 family, septate junction |
| 6248 | CG4158 | worniu | wt | zn finger transciption factor, neural development |
| 105362 | CG4158 | worniu | wt | zn finger transciption factor, neural development |
| 31965 | CG4005 | yorkie | wt | transcriptional co-activator, hippo signaling |
| 34067 | CG4005 | yorkie | wt | transcriptional co-activator, hippo signaling |
| 20123 | CG17947 | α-Catenin | wt | adherens junction |
| 107298 | CG17947 | α-Catenin | wt | adherens junction |
| 25387 | CG1977 | α-Spectrin | wt | membrane skeleton |
| 110417 | CG1977 | α-Spectrin | ++ | membrane skeleton |
| B7078 | CG3936 | {N.dsRNA.P}14E | wt | Notch domain |
| B8548 | CG5671 | {Pten.dsRNA.Exel}1 | wt | Dual specificity phosphatase |
| B6443 | CG34389 | {cv-c-dsRNA}4.1 | wt | Rho GAP |
| B6425 | CG8948 | {Graf-dsRNA}4 | wt | Rho GAP |
| B6426 | CG8948 | {Graf-dsRNA}5.1 | wt | Rho GAP |
| B6439 | CG13345 | {RacGAP50C-dsRNA}1 | wt | Rho GAP |
| B6447 | CG1976 | {RhoGAP100F-dsRNA}3 | wt | Rho GAP |
| B6446 | CG1976 | {RhoGAP100F-dsRNA}6 | wt | Rho GAP |
| B6427 | CG4937 | {RhoGAP15B-dsRNA}1 | wt | Rho GAP |
| B6432 | CG7122 | {RhoGAP16F-dsRNA}3 | wt | Rho GAP |
| B6431 | CG7122 | {RhoGAP16F-dsRNA}6 | wt | Rho GAP |
| B6434 | CG42274 | {RhoGAP18B-dsRNA}3 | wt | Rho GAP |
| B6433 | CG42274 | {RhoGAP18B-dsRNA}5 | wt | Rho GAP |
| B6435 | CG1412 | {RhoGAP19D-dsRNA}2 | wt | Rho GAP |
| B6436 | CG1412 | {RhoGAP19D-dsRNA}3 | wt | Rho GAP |
| B6421 | CG40494 | {RhoGAP1A-dsRNA}2 | wt | Rho GAP |
| B6422 | CG40494 | {RhoGAP1A-dsRNA}3 | + | Rho GAP |
| B6440 | CG6477 | {RhoGAP54D-dsRNA}5 | wt | Rho GAP |
| B6424 | CG3208 | {RhoGAP5A-dsRNA}2.1 | wt | Rho GAP |
| B6442 | CG6811 | {RhoGAP68F-dsRNA}4 | wt | Rho GAP |
| B6444 | CG4755 | {RhoGAP92B-dsRNA}2 | wt | Rho GAP |
| B6686 | CG3421 | {RhoGAP93B-dsRNA}3 | wt | Rho GAP |
| B6430 | CG32555 | {RhoGAPp190.GAP-dsRNA} | wt | Rho GAP |
| B6429 | CG32555 | {RhoGAPp190.N-dsRNA} | wt | Rho GAP |

**Acknowledgements**

We thank the Bloomington Drosophila Stock Center for TRiP lines and stocks. Transgenic RNAi fly stocks were also obtained from the Vienna Drosophila Resource Center (VDRC). Monoclonal antibodies listed as DSHB were obtained from the Developmental Studies Hybridoma Bank, created by the NICHD of the NIH and maintained at The University of Iowa, Department of Biology, Iowa City, IA 52242. We thank Steven Hou, Jin Jiang, Huaqi Jiang, Hervé Agaisse, DJ Pan, Lei Zhang, Norbert Perrimon, and Andreas Bergmann for Drosophila stocks and reagents. This work is supported by NIH grants DK083450 and GM107457. YTI is a member of the UMass DERC (DK32520), and a member of the UMass Center for Clinical and Translational Science (UL1TR000161). YTI was a member of the Guangdong Innovative Research Team Program (No. 201001Y0104789252) and a member of the Science and Technology Program of Guangzhou (No. 201704030044).

# CHAPTER III

# DISCUSION

The work presented in this thesis points out another role of the smooth septate junctions in *Drosophila* midgut besides their well-known paracellular barrier function. Ssk and Mesh, two major smooth septate junction proteins, regulate Yki activity to control the production of growth factor Upd3, therefore governing ISC proliferation. Ssk and Mesh physically interact with Yki and the modulation of Yki activity is probably independent of the upstream kinases, suggesting that Ssk and Mesh might create a platform where membrane-recruited kinases, such as Wts, phosphorylates and inactivates Yki in the smooth septate junctions. In the following sections, I'll discuss some relevant issues and other possible experiments to elaborate this project and further implication.

## 1. What lies between septate junction proteins and the effector Yki to govern the production of Upd3?

Loss of Ssk or Mesh activates Yki to elevate the secretion of Upd3 from EBs and ECs. Yki mediates the target gene expression, and its activity is negatively correlated with its phosphorylated extent. Recent studies have identified Msn and Hppy, the homologs of mammalian MAP4K1-7, act in parallel with the canonical ste-20 kinases Hpo/MST to regulate the activity of Yki/YAP/TAZ (Li et al., 2014a; Li et al., 2018; Meng et al., 2015; Zheng et al., 2015). ECs comprise 90% of the total cell population in the adult midgut and encounter various irritants via ingestion. Hpo is probably an important responder in ECs to mediate the stress signal stimulation of expression of growth factors or cytokines that stimulate ISC proliferation and speed up the differentiation to repair the damaged intestinal epithelium (Jiang et al., 2011; Jiang et al., 2009). Msn, instead of Hpo, functions

exclusively in EBs along the Wts-Yki axis to regulate the production of Upd3 and ISC proliferation (Li et al., 2014a; Li et al., 2018). Phosphorylation of the threonine residue 194 in the kinase domain of Msn is required to activate the kinase activity. However, the T194 residue of Msn and equivalent residue in Hpo remains unphosphorylated when Ssk or Mesh are knockdown, suggesting Msn and Hpo might not be the kinase to restrict Yki activity. Although Hppy phosphorylates Yki in the ectoderm-derived wing discs (Zheng et al., 2015), whether Hppy is the upstream kinase of Yki in adult midgut is unknown. Knock down of Hppy in midgut did not show an overproliferation phenotype.

Wts directly phosphorylates Yki and is the converging point of various upstream inputs (Li et al., 2014a; Li et al., 2018; Zheng et al., 2015). The T1077 in the hydrophobic motif of Wts is the kinase activity indicator and is recognized by a phospho-specific antibody p-Wts. However, we were not able to obtain positive signal using this antibody in the midgut samples. In addition to the constituent cells, adult midgut contains a variety of substances in the lumen, including food, digestive enzymes, protective chitinous peritrophic matrix, and commensal microbiota. These substances may increase background noise that can't be removed completely and may block the detection of p-Wts is when applying to the midgut samples.

Apical membrane recruitment of the upstream kinase promotes the phosphorylation of Wts/LATS (Hergovich et al., 2005; Hergovich et al., 2006; Yu et al., 2010; Yue et al., 2012). Spatial organization of Wts at the plasma membrane positively regulates the Yki phosphorylation regardless of the intrinsic Hpo activity (Yin et al., 2013), suggesting the apical-localized Ssk and Mesh perhaps create a compartment for Wts. Further studies are required to investigate if Wts physically interacts with Ssk and Mesh in the midgut.

Immunoprecipitation followed by mass spectrometry can identify what membrane components interact with Wts. Alternatively, it is worthy to examine if reducing Ssk and Mesh will lead to compromised phosphorylation at the T1077 of Wts *in vitro*, although S2 cells cannot fully represent the midgut

Continual renewal of the membrane is a requirement to maintain epithelial integrity. Proper endocytosis protects the epithelia from dysplasia (D'Agostino et al., 2019; Nie et al., 2019). Endocytosis controls the turnover as well as the abundance of the transmembrane proteins and membrane-associated components. Most internalized membrane proteins undergo dynamic recycling and then return to the plasma membrane, while some are delivered to the late endosomes and ultimately degraded in the lysosomes (Maxfield and McGraw, 2004). A recent report shows that another smooth septate junction component Tsp2A incorporates endocytosis to regulate ISC proliferation through the aPKC-Hpo axis (Xu et al., 2019). Consistently, our tag-knockin alleles show that endogenous Ssk and Mesh present detectable punctate in the cytoplasm besides their apical junction localization. However, single-cell RNA-seq reveals that Tsp2A expression is detectable throughout the ISC-EB-EC lineage, whereas Ssk and Mesh initiate their function to regulate the production of Upd3 in the late EBs. Therefore, Ssk, Mesh, and Tsp2A may adopt distinct mechanisms to regulate ISC proliferation even though they form a complex to construct the smooth septate junction in adult midgut ECs.

**2. Not just glue, the smooth septate junctions serve as a signaling transduction center.**

Cell-cell junctions seal adjacent cells and block leakage to maintain the epithelial integrity and tissue homeostasis. Besides the glue function, many components that are

involved in the cell adhesion work together to define the epithelial polarity (Garcia et al., 2018). Emerging evidence shows that cell-cell junctions indirectly regulate cell proliferation by sequestering transcription factors at the plasma membrane (Balda et al., 2003; Cochella and Green, 2004; Kavanagh et al., 2006; Oka et al., 2010; Spadaro et al., 2014; Thomas et al., 2018). In mammalian tight junctions, cytoplasmic ZO-1 restricts the nuclear translocation of ZONAB that regulates the transcription of CDK4 and cyclin D1 (Balda et al., 2003; Kavanagh et al., 2006). ZO-2 retains YAP in the cytoplasm to turn off the downstream transcription as well (Oka et al., 2010; Spadaro et al., 2014; Thomas et al., 2018). β-catenin, which comprises the adherens junction, is a transcription factor downstream to the Wnt signaling in regulating cell proliferation and is well-known to accelerate the progression of colon cancer (Cochella and Green, 2004; Vogelstein et al., 2013).

Many cell junction proteins, such as the apical-localized Crb and Par complex, cadherin-like Fat, tight junction-associated AMOT, and the adherens junction α-Catenin, are involved in the Hippo pathway (Chen et al., 2010; Grzeschik et al., 2010; Mana-Capelli and McCollum, 2018; Mana-Capelli et al., 2014; Matakatsu and Blair, 2012; Rauskolb et al., 2014; Robinson et al., 2010; Sarpal et al., 2019). Co-immunoprecipitation results of this project show a direct binding of Yki to Ssk and Mesh. Our preliminary mass spectrometry results also indicate a direct interaction between endogenous Yki and Mesh. Thus, this study suggests that the smooth septate junction may function as a signaling platform where Yki is restricted. Ssk and Mesh have almost exclusive expression in the adult midgut than in other tissues. The substantially low expression in other tissues may be the reason why earlier mass spectrometry-based protein interaction screening that

overexpressed Yki as the bait in cultured S2 cells does not reveal the Yki-Ssk-Mesh complex (Kwon et al., 2013).

### 3. Two are not enough. Bicellular and tricellular junctions cooperatively strength the structure and integrity of the epithelia.

Epithelial sheets cover the surfaces of many tissue and organs in multicellular organisms and create specialized compartments for the regulation of fluid and solutes. Cells rearrange and pack themselves two-dimensionally to build up the epithelial sheets. The immunostaining and the Smurf assay presented in Chapter II demonstrate that epithelial cells are polarized and form apical cell junctions to seal neighboring cells. In addition to the bicellular junction that connects two adjacent cells, the tricellular junction is present at the point where three cells meet. Tricellular junctions, as well as bicellular junctions, are seals to control permeability. The intercellular space among the three cells is connected by regularly spaced, vertically stacked triangular diaphragms (Higashi and Miller, 2017). Tricellular junctions consist of tricellular AJs (tAJs) and tricellular SJs (tSJs) in invertebrates. Not surprisingly, components of tricellular junctions also exhibit critical biological roles in cell division orientation, regulation of cell proliferation, and ionic barrier formation.

The adherens junctions (AJs) are geometrically superior to the septate junctions (SJs) in invertebrates (Baldi et al., 2011). tAJs are thought to be the points encountering high tension at the vertices. Sidekick (Sdk) is the only identified component of tAJs and acts to resolve cell rearrangement. Sdk is detected at the tricellular corner much earlier than other tSJ proteins, suggesting the formation of tAJs is before that of tSJs (Letizia et al., 2019; Uechi and Kuranaga, 2019). Bicellular AJs are involved in the initiation and the

following maintenance of tAJs. E-cadherin is required for the localization of Sdk since depletion of E-cadherin disrupts the localization of Sdk to tAJs. Canoe (Cno), the *Drosophila* Afadin homolog at the bicellular AJs takes over the maintenance of the tAJs. Although Cno is not necessary for the initial localization of Sdk, loss of Cno reduces the enrichment of Sdk at tAJs in late embryo and wing disc development.

Gliotactin (Gli), Anakonda (Aka), and M6 are three identified components of the tSJs in *Drosophila*. Gli, a cholinesterase-like transmembrane protein, is first noticed by its necessary to form the glial-based blood-nerve barrier and maintain neurons functions (Auld et al., 1995). Additionally, loss of Gli in the adult midgut exhibits aging-related phenotypes, including the ISC proliferation and mis-differentiated ECs (Resnik-Docampo et al., 2017). With the unusual tripartite repeat structure in its extracellular domain, Aka supports the formation of tricellular junctions by self-assembly. Additionally, the expression of Aka and M6 is necessary for the proper localization of Gli at the tricellular junction (Byri et al., 2015; Dunn et al., 2018). Mutation of Nrx or Cora, the component of bicellular SJs, leads to the widespread distribution of Gli toward the basal domain. Therefore, the existence of the bicellular SJs is required for the vertex-localized tSJ components. Although the formation of the bicellular junctions is not affected by Gli, the maturation is compromised when Gli is mutated. (Schulte et al., 2003).

Similar to *Drosophila*, there are limited tricellular junction components that have been identified in mammalian. Tricellulin (TRIC) is the first categorized molecule of mammalian tTJs. Later, lipolysis-stimulated lipoprotein receptor (LSR) is found that recruits TRIC to the tTJs through the interaction between their cytoplasmic domains (Kurth et al., 2011). Defective TRIC and LSR impair the structure of tTJs and cause the degeneration of

cochlear hair cells in the inner ear, leading to progressive hearing loss (Kamitani et al., 2015; Kim et al., 2015). In addition to their barrier function, tTJs are involved in the progression of a variety of epithelial-related tumors (Kohno et al., 2019; Korompay et al., 2012; Kyuno et al., 2019; Masuda et al., 2010; Reaves et al., 2014; Sartori et al., 2016; Somoracz et al., 2014). Low expression of both TRIC and LSR is highly correlated with the malignancy and is an indicator of poor prognosis (Key, 2007; Reaves et al., 2014; Somoracz et al., 2014). Suppressed expression of TRIC is related to Snail transcription factor-induced epithelial-mesenchymal-transition in human gastric carcinoma (Masuda et al., 2010). Reintroduced LSR inhibits the epithelial-mesenchymal-transition phenotype and the migration of breast cancer cells (Reaves et al., 2014). These tTJs may act through polarity and Hippo/YAP pathway to modulate the production of growth factor, therefore suppressing abnormal proliferation and the subsequent migration. LSR colocalize with TRIC, AMOT, NF2, and YAP at the tTJS. Analysis of the endometrial carcinoma reveals that LSR misexpresses along the lateral plasma membrane. Knockdown LSR in the endometrial cancer-derived cell line decreases the expression of AMOT and NF2 and leads to the nuclear translocation of YAP1. YAP1 drives the expression of TEAD1 and AREG, a ligand of EGFR, to enhance cell migration and invasion. Consistently, loss of LSR accelerates the tumor progression by elevated AREG in human pancreatic cancer. Although TRIC colocalizes with LSR and is correlated with tumor malignancy and prognosis, the underlying mechanism is not clear yet.

Collectively, mammalian tight junctions and invertebrate septate junctions share conserved features to govern tissue homeostasis. They form the barrier to protect

epithelial integrity and suppress tumor progression by restricting cell proliferation as well as preventing epithelial-mesenchymal-transition.

**4. The roles of septate/tight junction proteins in ISC proliferation and tissue homeostasis.**

Since the primary purpose of cell junctions is to maintain epithelial integrity, epithelial cells initiate a variety of signaling to compensate for the loss when the connections are about to fall apart. ISC proliferation and the leakage of midgut are the most prominent phenotypes when the junctional proteins are gone.

The Smurf assay as shown in chapter II indicates that the impaired epithelial integrity and stem cell proliferation are concomitant. The bicellular SJs proteins Ssk and Mesh in late EBs and ECs sense the initial disconnection and lead to kinase-independent Yki activation. Tsp2A, expressing along the ISC-EC lineage, cooperates with endocytosis to modulate Yki via aPKC-Hpo pathway in parallel (Xu et al., 2019). Meanwhile, depletion of Ssk, Mesh, or Tsp2A in ECs activates the MAP kinases (Izumi et al., 2019). Activated Yki and MAP kinases together mediate the production of cytokine Upd3 and growth factors to stimulate ISC proliferation in response to the impaired epithelial integrity (Jiang et al., 2011; Jiang et al., 2009; Jiang et al., 2016). Also, knockdown Gli in ECs triggers ISC proliferation in young flies as well (Resnik-Docampo et al., 2017). Therefore, the proper expression level of the septate junction proteins is essential for tissue homeostasis.

Although Gli also mediates ISC proliferation, it acts through the JNK signaling instead of the Yki mechanism mentioned above (Resnik-Docampo et al., 2017). One explanation is the different subcategories of the septate junction components. Gli belongs to the tSJs that localize to the tricellular corner, whereas Ssk, Mesh, and Tsp2A are bicellular SJs

that connect lateral cells. Alternatively, the damages caused by the depletion of tSJs are more destructive than that of bicellular SJs. Temperature shift to conduct *Ssk*$^{RNAi}$ or *mesh*$^{RNAi}$ for two days is sufficient to induce ISC proliferation by Yki-mediated production of Upd3 without overt alternation of the midgut morphology. The prolonged knockdown of *Ssk* or *mesh* in EC results in a substantial loss of the septate junction, followed by lethality. Accumulation of delaminated ECs and significant reduction of midgut length indicate the severe midgut destruction. The nearly collapsed midgut probably leads to systematic inflammation, which activates multiple signaling simultaneously to mend the impaired tissue. Hence, reduced JNK activity alone is not sufficient to suppress the robust ISC proliferation caused by extensive depletion of the bicellular SJs components even though the phenotype recapitulates *Gli*$^{RNAi}$.

Many studies have revealed that junctional proteins are involved in regulating Yki/YAP activity. These proteins bind to Yki/YAP at cell junction to block their nuclear translocation and activity (Karaman and Halder, 2018). F-actin filament is essential to stabilize the cell junction by associating with the cytoplasmic adaptor proteins and remodel itself in response to physiological demands such as protrusion and detachment. Many studies implicate the actin cytoskeleton as a regulator of Yki/YAP activity (Alegot et al., 2019; Fernandez et al., 2011; Fletcher et al., 2015; Kim et al., 2013; Richardson, 2011; Yu and Guan, 2013; Zhao et al., 2012). The core kinases of the Hippo pathway are well known that they dominantly control the subcellular localization and activity of Yki/YAP. Several studies have reported that actin influences YAP independently of Wts/LATS (Chan et al., 2011; Driscoll et al., 2015; Elosegui-Artola et al., 2017). Ssk and Mesh may function as the angiomotin (AMOT), which suppresses YAP/TAZ activity by tethering

YAP/TAZ to tight junctions regardless of their phosphorylation status, where AIP4/Itch ubiquitin E3 ligase degrades YAP/TAZ (Chan et al., 2011). Alternatively, the altered cell shape and delamination caused by knockdown Ssk or Mesh in ECs probably stretch the nuclear pore via F-actin remodeling to facilitate Yki nuclear transport. Therefore, the smooth septate junction proteins, Ssk and Mesh, present in Chapter II bypass the canonical Hippo pathway to regulate Yki activity and ISC proliferation in adult midgut.

The mammalian tight junctions are functionally analogous to the invertebrate septate junctions. Disrupted TJ barrier function is frequently found in Inflammatory Bowel Syndrome (IBD), the chronic inflammation of the digestive tract, including ulcerative colitis and Crohn's disease. Chronic inflammation is believed to promote tumorigenesis and is the third risk factor to initiate colorectal cancer in patients suffering from IBD (Itzkowitz and Yio, 2004; Kim and Chang, 2014; Ullman and Itzkowitz, 2011). ZO-1 is tightly associated with IBD. Incomplete formation of TJs due to lack of claudin results in the altered expression level and mislocalization of ZO-1, ultimately leading to the disrupted barrier and intestinal inflammation (Gassler et al., 2001; Poritz et al., 2007).

Besides the barrier function to maintain the tissue homeostasis, TJs sequester specific transcription factors at the plasma membrane to regulate ISCs indirectly. Nuclear translocation of ZONAB is tightly correlated with increased proliferation in the intestinal epithelium of ethanol-fed mice. Consistently, nuclear accumulation of ZONAB is a common feature in adenomas of chronic alcoholics (Pannequin et al., 2007). Moreover, ZONAB, together with symplekin, negatively regulates the differentiation of goblet cells by suppressing the expression of AML1/Runx1 transcription factor (Buchert et al., 2009). YAP is another transcription factor that can be regulated by TJs and involved in the

intestinal homeostasis (Hong et al., 2016; Ma et al., 2019). ZO-2 is required for YAP nuclear import (Spadaro et al., 2014). AMOT at the mammalian tight junction sequesters the nuclear translocation of YAP by binding to YAP directly, therefore regulating YAP activity in response to the cell-cell contact signals (Chan et al., 2011). Alternatively, AMOT interacts with and activates NF2 to stimulate LATS1/2 kinase activity, thus inhibiting YAP activity by LATS-mediated phosphorylation (Hirate and Sasaki, 2014; Li et al., 2015c). In summary, mammalian TJs and insect septate junctions share conserved roles in the formation of paracellular barrier and regulating ISC proliferation to govern the intestine homeostasis.

**5. Ssk and Mesh exhibit conserved functions in the insecta, but their vertebrate counterparts are multifaceted.**

The smooth septate junctions have conserved expression patterns and functions across the Insecta. Larval mosquito regulates the transcript abundance of *Ssk* and *mesh* to adjust the midgut epithelial integrity in response to altered environmental salt levels (Jonusaite et al., 2017). Double-stranded RNA diet feeding against the expression of *dvssj1*, the *Ssk* homolog of the corn rootworm, impairs the barrier function of the midgut and results in larval mortality, suggesting dsRNA targeting smooth septate junctions is a potentially practical approach for corn rootworm control (Hu et al., 2016; Hu et al., 2019). However, Ssk homologs are conserved only within the insecta species.

Although there is no homolog of Ssk identified in the vertebrate, claudins may be the functional analog of Ssk. *Drosophila* Ssk is an integral membrane protein with four transmembrane domains. Protein analysis further reveals that Ssk consists of four hydrophobic transmembrane, two short extracellular loops, the N- and C-terminal

cytoplasmic domains, and a cytoplasmic turn (Günzel and Yu, 2013; Yanagihashi et al., 2012). The overall structure and protein size are comparable to claudins, which is the tetra-transmembrane protein of mammalian tight junction. Indeed, most members of the claudin family are detectable along the digestive tract, and emerging evidence indicates their importance in the intestinal integrity and the progression of colorectal cancer (Lu et al., 2013). Hyperactive Wnt signaling is known as the primary cause of colorectal cancer. It leads to the expression of claudin-1 along the β-Catenin-TCF/LEF axis, suggesting claudin-1 is one of the critical factors involved in colorectal cancer progression (Miwa et al., 2001). Consistently, mRNA and protein levels of the claudin-1 in colorectal cancer tissue are elevated (Huo et al., 2009). Immunostaining further reveals that claudin-1 is weakly detected at the apicolateral membrane of noncancerous epithelial tissue, whereas it is strongly expressesed at the cell-cell boundaries and in the cytoplasm of cancer cells (Miwa et al., 2001). Besides claudin-1, the expression of other members, such as claudin-2, 3, 4, 7, also increases in the colorectal carcinoma (Aung et al., 2006; Darido et al., 2008; Mees et al., 2009), but claudin-8 is downregulated in the adenoma (Galamb et al., 2010). The discrepancy in expression among claudins may function as the potential marker for the diagnosis.

According to the similarity of the extracellular domains, SUSD2 is recognized as the vertebrate homolog of Mesh (Kisaalita and Robinson, 2012). SUSD2 belongs to the type I transmembrane proteins that harbor several functional domains, including somatomedin B, AMOP, von Willebrand factor type D, and sushi domains and is considered as an adhesion molecule. Indeed, expressing SUSD2 in HeLa cells induces the cell aggregation. Meanwhile, expression of SUSD2 inactivates Akt to induces apoptosis and reverses the

tumorigenic phenotype. Therefore, SUSD2 functions as a tumor suppressor (Sugahara et al., 2007a; Sugahara et al., 2007b). Extensive studies from a variety of cancer types derived from endoderm- or mesoderm-originated tissues, such as intestine, lung, renal, liver, and ovary, further corroborates its tumor suppressor role (Cheng et al., 2016; Liu et al., 2016a; Pan et al., 2014; Sheets et al., 2016; Zhang et al., 2017). Reduced SUSD2 in the tumor-derived cancel cell lines interferes with the cell cycle by regulating cyclin D1 and CDK6 to drive overproliferation. Meanwhile, SUSD2 has inverse relationship with mesenchymal proteins, including well-known Twist-1, N-cad, and Snail-1, suggesting SUSD2 has roles in impeding epithelial-mesenchymal-transition, migration, and invasion. In consistent with *in vitro* assays, reduced expression of mRNA and protein of SUSD2 is frequently observed in tumor tissues and highly correlates with advanced clinical stage and poor prognosis.

Conversely, SUSD2 in breast cancer behaves as an enhancer. Elevated expression of SUSD2 is found in pathological breast lesions as well as in lobular and ductal carcinoma. SUSD2 is required for the cancer cell surface expression of Galectin-1, which leads to the apoptosis of Jurkat T cells. Moreover, SUSD2 recruits tumor-associated macrophages to the tumor microenvironment for tumor angiogenesis. With immune evasion and enhanced angiogenesis, SUSD2 in breast cancer promotes the metastasis and worsens the clinical stage (Hultgren et al., 2017; Watson et al., 2013). Different from the tissues mentioned above, human breast comprises parenchyma and underlying stroma. Most prevalent ductal and lobular carcinomas belong to parenchyma, which derives from ectoderm (Javed and Lteif, 2013). The different origination of breast tissue perhaps is the reason why SUSD2 exhibits an opposite role in breast cancer.

## 6. Future direction & prospective application

Septate junction components are known to maintain the epithelial integrity and tissue homeostasis. In this project, we reveal their other roles in regulating ISC proliferation by coupling with Yki-Upd3. Although genetic assays show that Yki acts downstream of Ssk and Mesh to regulate Upd3 expression, reduced upd3 expression alone is not sufficient to completely suppress ISC proliferation. We noticed that the expression of EGFR ligands mildly but significantly increases when *Ssk* or *mesh*.is knockdown, suggesting Upd3 is the major but not the only mechanism to stimulate ISCs proliferation. RNA-seq can be used here to further explore other possibility. After RNA-seq, we can evaluate if the increased p-H3 counts caused by loss of Ssk or Mesh is suppressed when
the expression of both upd3 and the identified targets are knockdown. We also found the extent of ISC proliferation are different between *Ssk* and *mesh*. Whether they function in the same pathway or act in parallel to regulate ISC proliferation, double RNAi knockdown or MARCM mutant clonal analysis of *Ssk* and *mesh* double mutant can distinguish the two possibilities. If the upd3 expression and the quantification of p-H3 have no increase in double RNAi or mutant combination, Ssk and Mesh are in the same pathway and functionally equivalent.

Healthy epithelial cells are physically coupled together by specialized cell junctions that seal the paracellular pathway and maintain cellular cohesion. Environmental stress results in cell death that associates with impaired cell junctions and breakdown of plasma membrane integrity, leading to inflammatory response and subsequent regenerative proliferation. Cell junction proteins comprise cell junctions and cell-cell adhesion, but not all components are directly involved in ISC proliferation (Fig 10A-D). We examine the

expression of JNK effectors and exclude the possibility that ISC proliferation caused by loss of Ssk and Mesh is the death-triggered compensation (Fig.12A, B). Injured plasma membrane is an indicator of cell death and can be evaluated by Sytox Orange dye that stains nucleic acid in cell with compromised membrane. However, the membrane integrity appears to have mild defects (Fig.12E-H). Because Sytox orange dye is not compatible with fixed tissue, the mild expression detected in the nucleic acid perhaps is from the rapid proteolytic degradation of unfixed midgut. TUNEL assay and anti-Dcp1 that directly detect fragmented DNA and effector caspase-1 can be used in fixed tissue and are more suitable for cell death analysis.

Epithelium covers the tissue surface creates a specialized compartment for various physiological demands. How to properly maintain the integrity is vital for health. In this work, the tag-knockin alleles of Ssk and Mesh show the cytoplasmic punctate in addition to the apicolateral expression, suggesting the involvement of the endosomal trafficking. Endosomal trafficking is required for the intestinal epithelium renewal. Dysfunction of internalization or recycling leads to the ISC proliferation and tumorigenesis (D'Agostino et al., 2019; Nie et al., 2019; Xu et al., 2019). Many signaling pathways rely on the binding between ligands and the membrane-anchored receptors to initiate downstream events. Whether Ssk and Mesh and their mammalian counterparts associate with these membrane receptors and bring them to degradation through continuous endosomal trafficking might be another direction to explore how junction proteins are involved in growth signals.

Loss of epithelial barrier increases the permeability and induces inflammation in the gut. Chronic inflammation is the cause to initiate colorectal cancer. Therefore, integral

tight junctions are a critical factor in preventing the inflammation and ameliorate the tumor progression. Treatment of anti-TNF antibodies successfully compromises the inflammation and restores intestinal wellness. Accompanied with oncogenic signals such as Ras, loss of the tight junction proteins accelerates the metastasis and invasion (Dunn et al., 2018). Whether enhancement of the tight junctions in the tissues that are ready to develop into cancer can slow the progression and retain the cancerous tissue *in situ* needs more effort to investigate.

However, strengthened cell junctions might raise another caveat. Aged intestinal epithelial cells have age-onset barrier dysfunction and microbial dysbiosis that activates JNK signaling to induce ISC proliferation. These age-induced phenotypes can be reversed by increased the expression of the junction proteins and suppressing JNK. There is limited understanding about whether the aged epithelial cells with enhanced cell junctions fully restore their functions, including the polarity and the formation of specialized compartments for signaling crosstalk. Also, strengthened cell junctions perhaps prolong the epithelial turnover frequency. It is not clear yet if cells turn on aging-relevant signaling to disturb the overall tissue wellness even though they have young, intact cell junctions. Overall, our study provides insights into the important roles of Ssk and Mesh as part of septate junctions in normal growth and disease progression.

Figure I.

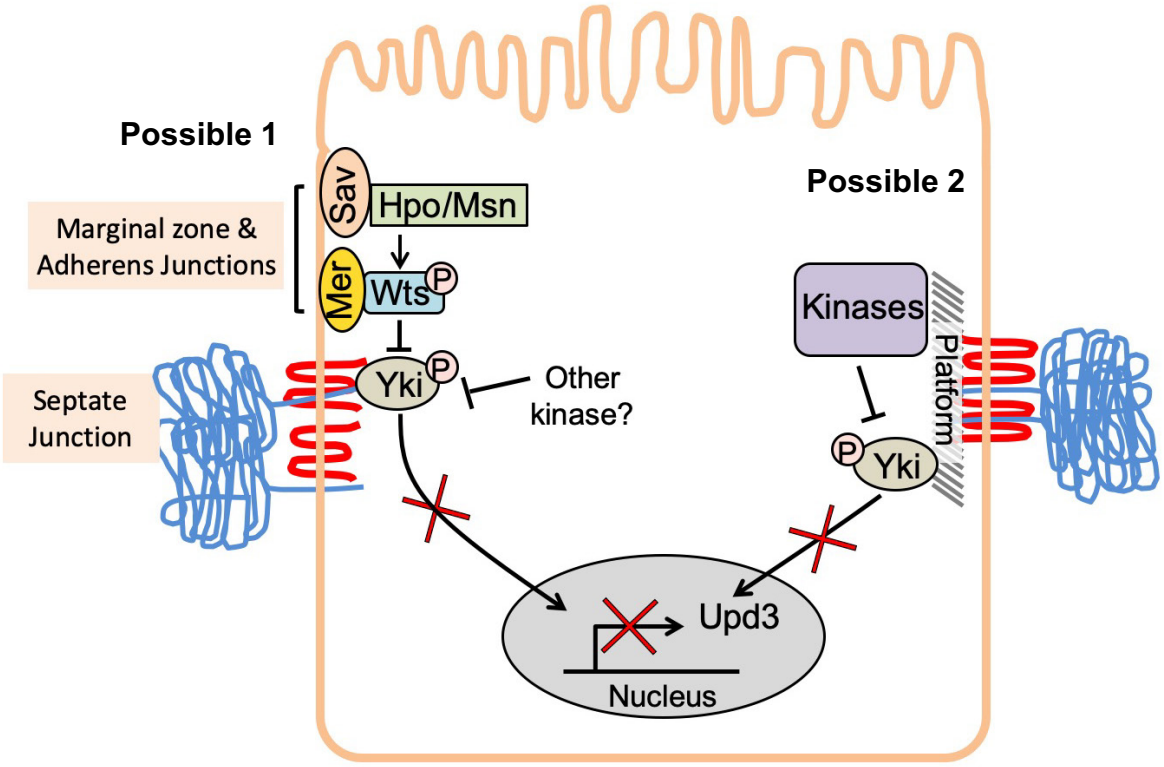


**Model 1.** Ssk-Mesh tethers Yki to the smooth septate junction and shortens the spatial distance to the upstream kinases.

**Model 2.** In addition to the foundation of the septate junctions, Ssk-Mesh establishes the docking platform for kinases and Yki, enhancing the phosphorylation and inactivation of Yki

## REFERENCE

Aerne, B.L., Gailite, I., Sims, D., and Tapon, N. (2015). Hippo Stabilises Its Adaptor Salvador by Antagonising the HECT Ubiquitin Ligase Herc4. PLoS One *10*, e0131113.

Ahmad, R., Kumar, B., Chen, Z., Chen, X., Müller, D., Lele, S.M., Washington, M.K., Batra, S.K., Dhawan, P., and Singh, A.B. (2017). Loss of claudin-3 expression induces IL6/gp130/Stat3 signaling to promote colon cancer malignancy by hyperactivating Wnt/β-catenin signaling. Oncogene *36*, 6592-6604.

Aktary, Z., and Pasdar, M. (2012). Plakoglobin: role in tumorigenesis and metastasis. Int J Cell Biol *2012*, 189521.

Albanese, C., Johnson, J., Watanabe, G., Eklund, N., Vu, D., Arnold, A., and Pestell, R.G. (1995). Transforming p21ras mutants and c-Ets-2 activate the cyclin D1 promoter through distinguishable regions. J Biol Chem *270*, 23589-23597.

Alegot, H., Markosian, C., Rauskolb, C., Yang, J., Kirichenko, E., Wang, Y.C., and Irvine, K.D. (2019). Recruitment of Jub by alpha-catenin promotes Yki activity and Drosophila wing growth. J Cell Sci *132*.

Amcheslavsky, A., Jiang, J., and Ip, Y.T. (2009). Tissue damage-induced intestinal stem cell division in Drosophila. Cell Stem Cell *4*, 49-61.

Ando-Akatsuka, Y., Saitou, M., Hirase, T., Kishi, M., Sakakibara, A., Itoh, M., Yonemura, S., Furuse, M., and Tsukita, S. (1996). Interspecies diversity of the occludin sequence: cDNA cloning of human, mouse, dog, and rat-kangaroo homologues. J Cell Biol *133*, 43-47.

Andreeva, A.Y., Krause, E., Müller, E.C., Blasig, I.E., and Utepbergenov, D.I. (2001). Protein kinase C regulates the phosphorylation and cellular localization of occludin. J Biol Chem *276*, 38480-38486.

Aragona, M., Panciera, T., Manfrin, A., Giulitti, S., Michielin, F., Elvassore, N., Dupont, S., and Piccolo, S. (2013). A mechanical checkpoint controls multicellular growth through YAP/TAZ regulation by actin-processing factors. Cell *154*, 1047-1059.

Asimaki, A., Syrris, P., Ward, D., Guereta, L.G., Saffitz, J.E., and McKenna, W.J. (2009). Unique epidermolytic bullous dermatosis with associated lethal cardiomyopathy related to novel desmoplakin mutations. J Cutan Pathol *36*, 553-559.

Asimaki, A., Syrris, P., Wichter, T., Matthias, P., Saffitz, J.E., and McKenna, W.J. (2007). A novel dominant mutation in plakoglobin causes arrhythmogenic right ventricular cardiomyopathy. Am J Hum Genet *81*, 964-973.

Auld, V.J., Fetter, R.D., Broadie, K., and Goodman, C.S. (1995). Gliotactin, a novel transmembrane protein on peripheral glia, is required to form the blood-nerve barrier in Drosophila. Cell *81*, 757-767.

Aung, P.P., Mitani, Y., Sanada, Y., Nakayama, H., Matsusaki, K., and Yasui, W. (2006). Differential expression of claudin-2 in normal human tissues and gastrointestinal carcinomas. Virchows Arch *448*, 428-434.

Azzolin, L., Panciera, T., Soligo, S., Enzo, E., Bicciato, S., Dupont, S., Bresolin, S., Frasson, C., Basso, G., Guzzardo, V*., et al.* (2014). YAP/TAZ incorporation in the β-catenin destruction complex orchestrates the Wnt response. Cell *158*, 157-170.

Bae, S.J., Ni, L., Osinski, A., Tomchick, D.R., Brautigam, C.A., and Luo, X. (2017). SAV1 promotes Hippo kinase activation through antagonizing the PP2A phosphatase STRIPAK. Elife *6*.

Balda, M.S., Garrett, M.D., and Matter, K. (2003). The ZO-1-associated Y-box factor ZONAB regulates epithelial cell proliferation and cell density. J Cell Biol *160*, 423-432.

Balda, M.S., and Matter, K. (2000). The tight junction protein ZO-1 and an interacting transcription factor regulate ErbB-2 expression. EMBO J *19*, 2024-2033.

Balda, M.S., Whitney, J.A., Flores, C., González, S., Cereijido, M., and Matter, K. (1996). Functional dissociation of paracellular permeability and transepithelial electrical resistance and disruption of the apical-basolateral intramembrane diffusion barrier by expression of a mutant tight junction membrane protein. J Cell Biol *134*, 1031-1049.

Baldi, D., Menini, M., Pera, F., Ravera, G., and Pera, P. (2011). Sinus floor elevation using osteotomes or piezoelectric surgery. Int J Oral Maxillofac Surg *40*, 497-503.

Bao, Y., Sumita, K., Kudo, T., Withanage, K., Nakagawa, K., Ikeda, M., Ohno, K., Wang, Y., and Hata, Y. (2009). Roles of mammalian sterile 20-like kinase 2-dependent phosphorylations of Mps one binder 1B in the activation of nuclear Dbf2-related kinases. Genes Cells *14*, 1369-1381.

Bao, Z., Dai, X., Wang, P., Tao, Y., and Chai, D. (2019). Capsaicin induces cytotoxicity in human osteosarcoma MG63 cells through TRPV1-dependent and -independent pathways. Cell Cycle *18*, 1379-1392.

Barry, E.R., Morikawa, T., Butler, B.L., Shrestha, K., de la Rosa, R., Yan, K.S., Fuchs, C.S., Magness, S.T., Smits, R., Ogino, S.*, et al.* (2013). Restriction of intestinal stem cell expansion and the regenerative response by YAP. Nature *493*, 106-110.

Behr, M., Riedel, D., and Schuh, R. (2003). The claudin-like megatrachea is essential in septate junctions for the epithelial barrier function in Drosophila. Dev Cell *5*, 611-620.

Bence, M., Koller, J., Sasvari-Szekely, M., and Keszler, G. (2012). Transcriptional modulation of monoaminergic neurotransmission genes by the histone deacetylase inhibitor trichostatin A in neuroblastoma cells. J Neural Transm (Vienna) *119*, 17-24.

Benhamouche, S., Curto, M., Saotome, I., Gladden, A.B., Liu, C.H., Giovannini, M., and McClatchey, A.I. (2010). Nf2/Merlin controls progenitor homeostasis and tumorigenesis in the liver. Genes Dev *24*, 1718-1730.

Betanzos, A., Huerta, M., Lopez-Bayghen, E., Azuara, E., Amerena, J., and González-Mariscal, L. (2004). The tight junction protein ZO-2 associates with Jun, Fos and C/EBP transcription factors in epithelial cells. Exp Cell Res *292*, 51-66.

Bierkamp, C., Mclaughlin, K.J., Schwarz, H., Huber, O., and Kemler, R. (1996). Embryonic heart and skin defects in mice lacking plakoglobin. Dev Biol *180*, 780-785.

Bilder, D. (2004). Epithelial polarity and proliferation control: links from the Drosophila neoplastic tumor suppressors. Genes Dev *18*, 1909-1925.

Biteau, B., Hochmuth, C.E., and Jasper, H. (2008). JNK activity in somatic stem cells causes loss of tissue homeostasis in the aging Drosophila gut. Cell Stem Cell *3*, 442-455.

Biteau, B., and Jasper, H. (2011). EGF signaling regulates the proliferation of intestinal stem cells in Drosophila. Development *138*, 1045-1055.

Boggiano, J.C., and Fehon, R.G. (2012). Growth control by committee: intercellular junctions, cell polarity, and the cytoskeleton regulate Hippo signaling. Dev Cell *22*, 695-702.

Boggiano, J.C., Vanderzalm, P.J., and Fehon, R.G. (2011). Tao-1 phosphorylates Hippo/MST kinases to regulate the Hippo-Salvador-Warts tumor suppressor pathway. Dev Cell *21*, 888-895.

Bornslaeger, E.A., Corcoran, C.M., Stappenbeck, T.S., and Green, K.J. (1996). Breaking the connection: displacement of the desmosomal plaque protein desmoplakin from cell-cell interfaces disrupts anchorage of intermediate filament bundles and alters intercellular junction assembly. J Cell Biol *134*, 985-1001.

Bray, F., Ferlay, J., Soerjomataram, I., Siegel, R.L., Torre, L.A., and Jemal, A. (2018). Global cancer statistics 2018: GLOBOCAN estimates of incidence and mortality worldwide for 36 cancers in 185 countries. CA Cancer J Clin *68*, 394-424.

Brooks, D.H. (1975). How to spot mesenteric infarction more quickly. Med Times *103*, 130-134.

Broussard, J.A., Getsios, S., and Green, K.J. (2015). Desmosome regulation and signaling in disease. Cell Tissue Res *360*, 501-512.

Brown, L., Waseem, A., Cruz, I.N., Szary, J., Gunic, E., Mannan, T., Unadkat, M., Yang, M., Valderrama, F., O'Toole, E.A*., et al.* (2014). Desmoglein 3 promotes cancer cell migration and invasion by regulating activator protein 1 and protein kinase C-dependent-Ezrin activation. Oncogene *33*, 2363-2374.

Brückner, B.R., and Janshoff, A. (2018). Importance of integrity of cell-cell junctions for the mechanics of confluent MDCK II cells. Sci Rep *8*, 14117.

Buchert, M., Darido, C., Lagerqvist, E., Sedello, A., Cazevieille, C., Buchholz, F., Bourgaux, J.F., Pannequin, J., Joubert, D., and Hollande, F. (2009). The

symplekin/ZONAB complex inhibits intestinal cell differentiation by the repression of AML1/Runx1. Gastroenterology *137*, 156-164, 164 e151-153.

Bujakowska, K., Audo, I., Mohand-Said, S., Lancelot, M.E., Antonio, A., Germain, A., Leveillard, T., Letexier, M., Saraiva, J.P., Lonjou, C.*, et al.* (2012). CRB1 mutations in inherited retinal dystrophies. Hum Mutat *33*, 306-315.

Byri, S., Misra, T., Syed, Z.A., Batz, T., Shah, J., Boril, L., Glashauser, J., Aegerter-Wilmsen, T., Matzat, T., Moussian, B.*, et al.* (2015). The Triple-Repeat Protein Anakonda Controls Epithelial Tricellular Junction Formation in Drosophila. Dev Cell *33*, 535-548.

Byun, M.R., Hwang, J.H., Kim, A.R., Kim, K.M., Hwang, E.S., Yaffe, M.B., and Hong, J.H. (2014). Canonical Wnt signalling activates TAZ through PP1A during osteogenic differentiation. Cell Death Differ *21*, 854-863.

Cabral, R.M., Liu, L., Hogan, C., Dopping-Hepenstal, P.J., Winik, B.C., Asial, R.A., Dobson, R., Mein, C.A., Baselaga, P.A., Mellerio, J.E.*, et al.* (2010). Homozygous mutations in the 5' region of the JUP gene result in cutaneous disease but normal heart development in children. J Invest Dermatol *130*, 1543-1550.

Cai, J., Maitra, A., Anders, R.A., Taketo, M.M., and Pan, D. (2015). beta-Catenin destruction complex-independent regulation of Hippo-YAP signaling by APC in intestinal tumorigenesis. Genes Dev *29*, 1493-1506.

Cai, J., Song, X., Wang, W., Watnick, T., Pei, Y., Qian, F., and Pan, D. (2018). A RhoA-YAP-c-Myc signaling axis promotes the development of polycystic kidney disease. Genes Dev *32*, 781-793.

Callus, B.A., Verhagen, A.M., and Vaux, D.L. (2006). Association of mammalian sterile twenty kinases, Mst1 and Mst2, with hSalvador via C-terminal coiled-coil domains, leads to its stabilization and phosphorylation. FEBS J *273*, 4264-4276.

Camargo, F.D., Gokhale, S., Johnnidis, J.B., Fu, D., Bell, G.W., Jaenisch, R., and Brummelkamp, T.R. (2007). YAP1 increases organ size and expands undifferentiated progenitor cells. Curr Biol *17*, 2054-2060.

Campbell, K., Whissell, G., Franch-Marro, X., Batlle, E., and Casanova, J. (2011). Specific GATA factors act as conserved inducers of an endodermal-EMT. Dev Cell *21*, 1051-1061.

Chakrabarti, S., Dudzic, J.P., Li, X., Collas, E.J., Boquete, J.P., and Lemaitre, B. (2016). Remote Control of Intestinal Stem Cell Activity by Haemocytes in Drosophila. PLoS Genet *12*, e1006089.

Chan, E.H., Nousiainen, M., Chalamalasetty, R.B., Schafer, A., Nigg, E.A., and Sillje, H.H. (2005). The Ste20-like kinase Mst2 activates the human large tumor suppressor kinase Lats1. Oncogene *24*, 2076-2086.

Chan, S.W., Lim, C.J., Chong, Y.F., Pobbati, A.V., Huang, C., and Hong, W. (2011). Hippo pathway-independent restriction of TAZ and YAP by angiomotin. J Biol Chem *286*, 7018-7026.

Chang, L., Azzolin, L., Di Biagio, D., Zanconato, F., Battilana, G., Lucon Xiccato, R., Aragona, M., Giulitti, S., Panciera, T., Gandin, A.*, et al.* (2018). The SWI/SNF complex is a mechanoregulated inhibitor of YAP and TAZ. Nature *563*, 265-269.

Chelakkot, C., Ghim, J., Rajasekaran, N., Choi, J.S., Kim, J.H., Jang, M.H., Shin, Y.K., Suh, P.G., and Ryu, S.H. (2017). Intestinal Epithelial Cell-Specific Deletion of PLD2 Alleviates DSS-Induced Colitis by Regulating Occludin. Sci Rep *7*, 1573.

Chen, C.L., Gajewski, K.M., Hamaratoglu, F., Bossuyt, W., Sansores-Garcia, L., Tao, C., and Halder, G. (2010). The apical-basal cell polarity determinant Crumbs regulates Hippo signaling in Drosophila. Proc Natl Acad Sci U S A *107*, 15810-15815.

Chen, C.L., Schroeder, M.C., Kango-Singh, M., Tao, C., and Halder, G. (2012a). Tumor suppression by cell competition through regulation of the Hippo pathway. Proc Natl Acad Sci U S A *109*, 484-489.

Chen, J., Nekrasova, O.E., Patel, D.M., Klessner, J.L., Godsel, L.M., Koetsier, J.L., Amargo, E.V., Desai, B.V., and Green, K.J. (2012b). The C-terminal unique region of desmoglein 2 inhibits its internalization via tail-tail interactions. J Cell Biol *199*, 699-711.

Chen, J., Sayadian, A.C., Lowe, N., Lovegrove, H.E., and St Johnston, D. (2018a). An alternative mode of epithelial polarity in the Drosophila midgut. PLoS Biol *16*, e3000041.

Chen, J., Xu, N., Wang, C., Huang, P., Huang, H., Jin, Z., Yu, Z., Cai, T., Jiao, R., and Xi, R. (2018b). Transient Scute activation via a self-stimulatory loop directs enteroendocrine cell pair specification from self-renewing intestinal stem cells. Nat Cell Biol *20*, 152-161.

Chen, W.S. (1992). Late neuropathy in chronic dislocation of the radial head. Report of two cases. Acta Orthop Scand *63*, 343-344.

Chen, X., Bonne, S., Hatzfeld, M., van Roy, F., and Green, K.J. (2002a). Protein binding and functional characterization of plakophilin 2. Evidence for its diverse roles in desmosomes and beta -catenin signaling. J Biol Chem *277*, 10512-10522.

Chen, Y.H., Lu, Q., Goodenough, D.A., and Jeansonne, B. (2002b). Nonreceptor tyrosine kinase c-Yes interacts with occludin during tight junction formation in canine kidney epithelial cells. Mol Biol Cell *13*, 1227-1237.

Chen, Y.J., Lee, L.Y., Chao, Y.K., Chang, J.T., Lu, Y.C., Li, H.F., Chiu, C.C., Li, Y.C., Li, Y.L., Chiou, J.F.*, et al.* (2013). DSG3 facilitates cancer cell growth and invasion through the DSG3-plakoglobin-TCF/LEF-Myc/cyclin D1/MMP signaling pathway. PLoS One *8*, e64088.

Cheng, X., and Koch, P.J. (2004). In vivo function of desmosomes. J Dermatol *31*, 171-187.

Cheng, Y., Wang, X., Wang, P., Li, T., Hu, F., Liu, Q., Yang, F., Wang, J., Xu, T., and Han, W. (2016). SUSD2 is frequently downregulated and functions as a tumor suppressor in RCC and lung cancer. Tumour Biol *37*, 9919-9930.

Chien, A.J., Conrad, W.H., and Moon, R.T. (2009). A Wnt survival guide: from flies to human disease. J Invest Dermatol *129*, 1614-1627.

Chiurillo, M.A. (2015). Role of the Wnt/beta-catenin pathway in gastric cancer: An in-depth literature review. World J Exp Med *5*, 84-102.

Choi, H.J., Pokutta, S., Cadwell, G.W., Bobkov, A.A., Bankston, L.A., Liddington, R.C., and Weis, W.I. (2012). αE-catenin is an autoinhibited molecule that coactivates vinculin. Proc Natl Acad Sci U S A *109*, 8576-8581.

Clark, R.I., and Walker, D.W. (2018). Role of gut microbiota in aging-related health decline: insights from invertebrate models. Cell Mol Life Sci *75*, 93-101.

Clevers, H. (2006). Wnt/beta-catenin signaling in development and disease. Cell *127*, 469-480.

Clevers, H., Loh, K.M., and Nusse, R. (2014). Stem cell signaling. An integral program for tissue renewal and regeneration: Wnt signaling and stem cell control. Science *346*, 1248012.

Cochella, L., and Green, R. (2004). Isolation of antibiotic resistance mutations in the rRNA by using an in vitro selection system. Proc Natl Acad Sci U S A *101*, 3786-3791.

Cockburn, K., Biechele, S., Garner, J., and Rossant, J. (2013). The Hippo pathway member Nf2 is required for inner cell mass specification. Curr Biol *23*, 1195-1201.

Cohen Barak, E., Godsel, L.M., Koetsier, J.L., Hegazy, M., Kushnir-Grinbaum, D., Hammad, H., Danial-Farran, N., Harmon, R., Khayat, M., Bochner, R.*, et al.* (2019). The role of Desmoglein 1 in gap junction turnover revealed through the study of SAM syndrome. J Invest Dermatol.

Cordero, J.B., Stefanatos, R.K., Scopelliti, A., Vidal, M., and Sansom, O.J. (2012). Inducible progenitor-derived Wingless regulates adult midgut regeneration in Drosophila. EMBO J *31*, 3901-3917.

Crose, L.E., Galindo, K.A., Kephart, J.G., Chen, C., Fitamant, J., Bardeesy, N., Bentley, R.C., Galindo, R.L., Chi, J.T., and Linardic, C.M. (2014). Alveolar rhabdomyosarcoma-associated PAX3-FOXO1 promotes tumorigenesis via Hippo pathway suppression. J Clin Invest *124*, 285-296.

Crosnier, C., Stamataki, D., and Lewis, J. (2006). Organizing cell renewal in the intestine: stem cells, signals and combinatorial control. Nat Rev Genet *7*, 349-359.

D'Agostino, L., Nie, Y., Goswami, S., Tong, K., Yu, S., Bandyopadhyay, S., Flores, J., Zhang, X., Balasubramanian, I., Joseph, I.*, et al.* (2019). Recycling Endosomes in Mature Epithelia Restrain Tumorigenic Signaling. Cancer Res *79*, 4099-4112.

Dai, X., She, P., Chi, F., Feng, Y., Liu, H., Jin, D., Zhao, Y., Guo, X., Jiang, D., Guan, K.L.*, et al.* (2013). Phosphorylation of angiomotin by Lats1/2 kinases inhibits F-actin binding, cell migration, and angiogenesis. J Biol Chem *288*, 34041-34051.

Darido, C., Buchert, M., Pannequin, J., Bastide, P., Zalzali, H., Mantamadiotis, T., Bourgaux, J.F., Garambois, V., Jay, P., Blache, P.*, et al.* (2008). Defective claudin-7 regulation by Tcf-4 and Sox-9 disrupts the polarity and increases the tumorigenicity of colorectal cancer cells. Cancer Res *68*, 4258-4268.

Dasgupta, I., and McCollum, D. (2019). Control of cellular responses to mechanical cues through YAP/TAZ regulation. J Biol Chem.

Daulat, A.M., Wagner, M.S., Walton, A., Baudelet, E., Audebert, S., Camoin, L., and Borg, J.P. (2019). The Tumor Suppressor SCRIB is a Negative Modulator of the Wnt/beta-Catenin Signaling Pathway. Proteomics *19*, e1800487.

Deng, H., Wang, W., Yu, J., Zheng, Y., Qing, Y., and Pan, D. (2015). Spectrin regulates Hippo signaling by modulating cortical actomyosin activity. Elife *4*, e06567.

Deng, Y. (2017). Rectal Cancer in Asian vs. Western Countries: Why the Variation in Incidence? Curr Treat Options Oncol *18*, 64.

Deng, Y., Matsui, Y., Zhang, Y., and Lai, Z.C. (2013). Hippo activation through homodimerization and membrane association for growth inhibition and organ size control. Dev Biol *375*, 152-159.

DeRan, M., Yang, J., Shen, C.H., Peters, E.C., Fitamant, J., Chan, P., Hsieh, M., Zhu, S., Asara, J.M., Zheng, B.*, et al.* (2014). Energy stress regulates hippo-YAP signaling involving AMPK-mediated regulation of angiomotin-like 1 protein. Cell Rep *9*, 495-503.

Dethlefsen, C., Hansen, L.S., Lillelund, C., Andersen, C., Gehl, J., Christensen, J.F., Pedersen, B.K., and Hojman, P. (2017). Exercise-Induced Catecholamines Activate the Hippo Tumor Suppressor Pathway to Reduce Risks of Breast Cancer Development. Cancer Res *77*, 4894-4904.

Devenport, D., and Brown, N.H. (2004). Morphogenesis in the absence of integrins: mutation of both Drosophila beta subunits prevents midgut migration. Development *131*, 5405-5415.

Dobrzycka, K.M., Kang, K., Jiang, S., Meyer, R., Rao, P.H., Lee, A.V., and Oesterreich, S. (2006). Disruption of scaffold attachment factor B1 leads to TBX2 up-regulation, lack of p19ARF induction, lack of senescence, and cell immortalization. Cancer Res *66*, 7859-7863.

Domínguez-Calderón, A., Ávila-Flores, A., Ponce, A., López-Bayghen, E., Calderón-Salinas, J.V., Luis Reyes, J., Chávez-Munguía, B., Segovia, J., Angulo, C., Ramírez, L.*, et al.* (2016). ZO-2 silencing induces renal hypertrophy through a cell cycle mechanism and the activation of YAP and the mTOR pathway. Mol Biol Cell *27*, 1581-1595.

Dong, J., Feldmann, G., Huang, J., Wu, S., Zhang, N., Comerford, S.A., Gayyed, M.F., Anders, R.A., Maitra, A., and Pan, D. (2007). Elucidation of a universal size-control mechanism in Drosophila and mammals. Cell *130*, 1120-1133.

Doupe, D.P., Marshall, O.J., Dayton, H., Brand, A.H., and Perrimon, N. (2018). Drosophila intestinal stem and progenitor cells are major sources and regulators of homeostatic niche signals. Proc Natl Acad Sci U S A *115*, 12218-12223.

Driscoll, T.P., Cosgrove, B.D., Heo, S.J., Shurden, Z.E., and Mauck, R.L. (2015). Cytoskeletal to Nuclear Strain Transfer Regulates YAP Signaling in Mesenchymal Stem Cells. Biophys J *108*, 2783-2793.

Dunn, B.S., Rush, L., Lu, J.Y., and Xu, T. (2018). Mutations in the Drosophila tricellular junction protein M6 synergize with Ras(V12) to induce apical cell delamination and invasion. Proc Natl Acad Sci U S A *115*, 8358-8363.

Elosegui-Artola, A., Andreu, I., Beedle, A.E.M., Lezamiz, A., Uroz, M., Kosmalska, A.J., Oria, R., Kechagia, J.Z., Rico-Lastres, P., Le Roux, A.L.*, et al.* (2017). Force Triggers YAP Nuclear Entry by Regulating Transport across Nuclear Pores. Cell *171*, 1397-1410 e1314.

Eshkind, L., Tian, Q., Schmidt, A., Franke, W.W., Windoffer, R., and Leube, R.E. (2002). Loss of desmoglein 2 suggests essential functions for early embryonic development and proliferation of embryonal stem cells. Eur J Cell Biol *81*, 592-598.

Fanning, A.S., and Anderson, J.M. (2009). Zonula occludens-1 and -2 are cytosolic scaffolds that regulate the assembly of cellular junctions. Ann N Y Acad Sci *1165*, 113-120.

Fanning, A.S., Van Itallie, C.M., and Anderson, J.M. (2012). Zonula occludens-1 and -2 regulate apical cell structure and the zonula adherens cytoskeleton in polarized epithelia. Mol Biol Cell *23*, 577-590.

Fernandez, B.G., Gaspar, P., Bras-Pereira, C., Jezowska, B., Rebelo, S.R., and Janody, F. (2011). Actin-Capping Protein and the Hippo pathway regulate F-actin and tissue growth in Drosophila. Development *138*, 2337-2346.

Fevr, T., Robine, S., Louvard, D., and Huelsken, J. (2007). Wnt/beta-catenin is essential for intestinal homeostasis and maintenance of intestinal stem cells. Mol Cell Biol *27*, 7551-7559.

Fleming, M., Ravula, S., Tatishchev, S.F., and Wang, H.L. (2012). Colorectal carcinoma: Pathologic aspects. J Gastrointest Oncol *3*, 153-173.

Fletcher, G.C., Diaz-de-la-Loza, M.D., Borreguero-Munoz, N., Holder, M., Aguilar-Aragon, M., and Thompson, B.J. (2018). Mechanical strain regulates the Hippo pathway in Drosophila. Development *145*.

Fletcher, G.C., Elbediwy, A., Khanal, I., Ribeiro, P.S., Tapon, N., and Thompson, B.J. (2015). The Spectrin cytoskeleton regulates the Hippo signalling pathway. EMBO J *34*, 940-954.

Formstecher, E., Aresta, S., Collura, V., Hamburger, A., Meil, A., Trehin, A., Reverdy, C., Betin, V., Maire, S., Brun, C.*, et al.* (2005). Protein interaction mapping: a Drosophila case study. Genome Res *15*, 376-384.

Fujisawa, R., Kuboki, Y., and Sasaki, S. (1987). Effects of dentin phosphophoryn on precipitation of calcium phosphate in gel in vitro. Calcif Tissue Int *41*, 44-47.

Furuse, M. (2010). Molecular basis of the core structure of tight junctions. Cold Spring Harb Perspect Biol *2*, a002907.

Furuse, M., Fujita, K., Hiiragi, T., Fujimoto, K., and Tsukita, S. (1998a). Claudin-1 and -2: novel integral membrane proteins localizing at tight junctions with no sequence similarity to occludin. J Cell Biol *141*, 1539-1550.

Furuse, M., Hirase, T., Itoh, M., Nagafuchi, A., Yonemura, S., and Tsukita, S. (1993). Occludin: a novel integral membrane protein localizing at tight junctions. J Cell Biol *123*, 1777-1788.

Furuse, M., and Izumi, Y. (2017). Molecular dissection of smooth septate junctions: understanding their roles in arthropod physiology. Ann N Y Acad Sci *1397*, 17-24.

Furuse, M., Sasaki, H., Fujimoto, K., and Tsukita, S. (1998b). A single gene product, claudin-1 or -2, reconstitutes tight junction strands and recruits occludin in fibroblasts. J Cell Biol *143*, 391-401.

Gabriel, B.M., Hamilton, D.L., Tremblay, A.M., and Wackerhage, H. (2016). The Hippo signal transduction network for exercise physiologists. J Appl Physiol (1985) *120*, 1105-1117.

Gailite, I., Aerne, B.L., and Tapon, N. (2015). Differential control of Yorkie activity by LKB1/AMPK and the Hippo/Warts cascade in the central nervous system. Proc Natl Acad Sci U S A *112*, E5169-5178.

Galamb, O., Spisak, S., Sipos, F., Toth, K., Solymosi, N., Wichmann, B., Krenacs, T., Valcz, G., Tulassay, Z., and Molnar, B. (2010). Reversal of gene expression changes in the colorectal normal-adenoma pathway by NS398 selective COX2 inhibitor. Br J Cancer *102*, 765-773.

Galli, G.G., Carrara, M., Yuan, W.C., Valdes-Quezada, C., Gurung, B., Pepe-Mooney, B., Zhang, T., Geeven, G., Gray, N.S., de Laat, W.*, et al.* (2015). YAP Drives Growth by Controlling Transcriptional Pause Release from Dynamic Enhancers. Mol Cell *60*, 328-337.

Gallicano, G.I., Bauer, C., and Fuchs, E. (2001). Rescuing desmoplakin function in extra-embryonic ectoderm reveals the importance of this protein in embryonic heart, neuroepithelium, skin and vasculature. Development *128*, 929-941.

Gallicano, G.I., Kouklis, P., Bauer, C., Yin, M., Vasioukhin, V., Degenstein, L., and Fuchs, E. (1998). Desmoplakin is required early in development for assembly of desmosomes and cytoskeletal linkage. J Cell Biol *143*, 2009-2022.

Garcia, M.A., Nelson, W.J., and Chavez, N. (2018). Cell-Cell Junctions Organize Structural and Signaling Networks. Cold Spring Harb Perspect Biol *10*.

Garcia, P., and Castano, M.A. (1991). [Importance of food-handlers in the transmission of cryptosporidiosis]. Enferm Infecc Microbiol Clin *9*, 583-584.

Garcia-Hernandez, V., Quiros, M., and Nusrat, A. (2017). Intestinal epithelial claudins: expression and regulation in homeostasis and inflammation. Ann N Y Acad Sci *1397*, 66-79.

Garrod, D.R., Merritt, A.J., and Nie, Z. (2002a). Desmosomal adhesion: structural basis, molecular mechanism and regulation (Review). Mol Membr Biol *19*, 81-94.

Garrod, D.R., Merritt, A.J., and Nie, Z. (2002b). Desmosomal cadherins. Curr Opin Cell Biol *14*, 537-545.

Gassler, N., Rohr, C., Schneider, A., Kartenbeck, J., Bach, A., Obermuller, N., Otto, H.F., and Autschbach, F. (2001). Inflammatory bowel disease is associated with changes of enterocytic junctions. Am J Physiol Gastrointest Liver Physiol *281*, G216-228.

Gehmlich, K., Asimaki, A., Cahill, T.J., Ehler, E., Syrris, P., Zachara, E., Re, F., Avella, A., Monserrat, L., Saffitz, J.E.*, et al.* (2010). Novel missense mutations in exon 15 of

desmoglein-2: role of the intracellular cadherin segment in arrhythmogenic right ventricular cardiomyopathy? Heart Rhythm *7*, 1446-1453.

Gehmlich, K., Syrris, P., Reimann, M., Asimaki, A., Ehler, E., Evans, A., Quarta, G., Pantazis, A., Saffitz, J.E., and McKenna, W.J. (2012). Molecular changes in the heart of a severe case of arrhythmogenic right ventricular cardiomyopathy caused by a desmoglein-2 null allele. Cardiovasc Pathol *21*, 275-282.

Genevet, A., Wehr, M.C., Brain, R., Thompson, B.J., and Tapon, N. (2010). Kibra is a regulator of the Salvador/Warts/Hippo signaling network. Dev Cell *18*, 300-308.

Getsios, S., Huen, A.C., and Green, K.J. (2004). Working out the strength and flexibility of desmosomes. Nat Rev Mol Cell Biol *5*, 271-281.

Glantschnig, H., Rodan, G.A., and Reszka, A.A. (2002). Mapping of MST1 kinase sites of phosphorylation. Activation and autophosphorylation. J Biol Chem *277*, 42987-42996.

Gliem, M., Heupel, W.M., Spindler, V., Harms, G.S., and Waschke, J. (2010). Actin reorganization contributes to loss of cell adhesion in pemphigus vulgaris. Am J Physiol Cell Physiol *299*, C606-613.

Gokcezade, J., Sienski, G., and Duchek, P. (2014). Efficient CRISPR/Cas9 plasmids for rapid and versatile genome editing in Drosophila. G3 (Bethesda) *4*, 2279-2282.

Gokhale, R., and Pfleger, C.M. (2019). The Power of Drosophila Genetics: The Discovery of the Hippo Pathway. Methods Mol Biol *1893*, 3-26.

Goldberg, C.C., and Yates, A. (1990). The use of anatomically correct dolls in the evaluation of sexually abused children. Am J Dis Child *144*, 1334-1336.

Gomes, J., Finlay, M., Ahmed, A.K., Ciaccio, E.J., Asimaki, A., Saffitz, J.E., Quarta, G., Nobles, M., Syrris, P., Chaubey, S.*, et al.* (2012). Electrophysiological abnormalities

precede overt structural changes in arrhythmogenic right ventricular cardiomyopathy due to mutations in desmoplakin-A combined murine and human study. Eur Heart J *33*, 1942-1953.

González-Mariscal, L., Domínguez-Calderón, A., Raya-Sandino, A., Ortega-Olvera, J.M., Vargas-Sierra, O., and Martínez-Revollar, G. (2014). Tight junctions and the regulation of gene expression. Semin Cell Dev Biol *36*, 213-223.

González-Mariscal, L., Tapia, R., and Chamorro, D. (2008). Crosstalk of tight junction components with signaling pathways. Biochim Biophys Acta *1778*, 729-756.

Goulev, Y., Fauny, J.D., Gonzalez-Marti, B., Flagiello, D., Silber, J., and Zider, A. (2008). SCALLOPED interacts with YORKIE, the nuclear effector of the hippo tumor-suppressor pathway in Drosophila. Curr Biol *18*, 435-441.

Grossmann, K.S., Grund, C., Huelsken, J., Behrend, M., Erdmann, B., Franke, W.W., and Birchmeier, W. (2004). Requirement of plakophilin 2 for heart morphogenesis and cardiac junction formation. J Cell Biol *167*, 149-160.

Grzeschik, N.A., Amin, N., Secombe, J., Brumby, A.M., and Richardson, H.E. (2007). Abnormalities in cell proliferation and apico-basal cell polarity are separable in Drosophila lgl mutant clones in the developing eye. Dev Biol *311*, 106-123.

Grzeschik, N.A., Parsons, L.M., Allott, M.L., Harvey, K.F., and Richardson, H.E. (2010). Lgl, aPKC, and Crumbs regulate the Salvador/Warts/Hippo pathway through two distinct mechanisms. Curr Biol *20*, 573-581.

Guan, C., Chang, Z., Gu, X., and Liu, R. (2019). MTA2 promotes HCC progression through repressing FRMD6, a key upstream component of hippo signaling pathway. Biochem Biophys Res Commun *515*, 112-118.

Guezguez, A., Pare, F., Benoit, Y.D., Basora, N., and Beaulieu, J.F. (2014). Modulation of stemness in a human normal intestinal epithelial crypt cell line by activation of the WNT signaling pathway. Exp Cell Res *322*, 355-364.

Gumbiner, B., Lowenkopf, T., and Apatira, D. (1991). Identification of a 160-kDa polypeptide that binds to the tight junction protein ZO-1. Proc Natl Acad Sci U S A *88*, 3460-3464.

Gumbiner, B., Stevenson, B., and Grimaldi, A. (1988). The role of the cell adhesion molecule uvomorulin in the formation and maintenance of the epithelial junctional complex. J Cell Biol *107*, 1575-1587.

Gumbiner, B.M., and Kim, N.G. (2014). The Hippo-YAP signaling pathway and contact inhibition of growth. J Cell Sci *127*, 709-717.

Günzel, D., and Yu, A.S. (2013). Claudins and the modulation of tight junction permeability. Physiol Rev *93*, 525-569.

Guo, C., Tommasi, S., Liu, L., Yee, J.K., Dammann, R., and Pfeifer, G.P. (2007). RASSF1A is part of a complex similar to the Drosophila Hippo/Salvador/Lats tumor-suppressor network. Curr Biol *17*, 700-705.

Guo, T., Lu, Y., Li, P., Yin, M.X., Lv, D., Zhang, W., Wang, H., Zhou, Z., Ji, H., Zhao, Y., *et al.* (2013). A novel partner of Scalloped regulates Hippo signaling via antagonizing Scalloped-Yorkie activity. Cell Res *23*, 1201-1214.

Guo, Z., and Ohlstein, B. (2015). Stem cell regulation. Bidirectional Notch signaling regulates Drosophila intestinal stem cell multipotency. Science *350*.

Guruharsha, K.G., Rual, J.F., Zhai, B., Mintseris, J., Vaidya, P., Vaidya, N., Beekman, C., Wong, C., Rhee, D.Y., Cenaj, O.*, et al.* (2011). A protein complex network of Drosophila melanogaster. Cell *147*, 690-703.

Hamaratoglu, F., Willecke, M., Kango-Singh, M., Nolo, R., Hyun, E., Tao, C., Jafar-Nejad, H., and Halder, G. (2006). The tumour-suppressor genes NF2/Merlin and Expanded act through Hippo signalling to regulate cell proliferation and apoptosis. Nat Cell Biol *8*, 27-36.

Hammers, C.M., and Stanley, J.R. (2013). Desmoglein-1, differentiation, and disease. J Clin Invest *123*, 1419-1422.

Han, H., Qi, R., Zhou, J.J., Ta, A.P., Yang, B., Nakaoka, H.J., Seo, G., Guan, K.L., Luo, R., and Wang, W. (2018). Regulation of the Hippo Pathway by Phosphatidic Acid-Mediated Lipid-Protein Interaction. Mol Cell *72*, 328-340 e328.

Harden, N., Wang, S.J., and Krieger, C. (2016). Making the connection - shared molecular machinery and evolutionary links underlie the formation and plasticity of occluding junctions and synapses. J Cell Sci *129*, 3067-3076.

Harmon, R.M., Simpson, C.L., Johnson, J.L., Koetsier, J.L., Dubash, A.D., Najor, N.A., Sarig, O., Sprecher, E., and Green, K.J. (2013). Desmoglein-1/Erbin interaction suppresses ERK activation to support epidermal differentiation. J Clin Invest *123*, 1556-1570.

Harris, T.J. (2012a). Adherens junction assembly and function in the Drosophila embryo. Int Rev Cell Mol Biol *293*, 45-83.

Harris, T.J. (2012b). An introduction to adherens junctions: from molecular mechanisms to tissue development and disease. Subcell Biochem *60*, 1-5.

Harvey, K.F., Pfleger, C.M., and Hariharan, I.K. (2003). The Drosophila Mst ortholog, hippo, restricts growth and cell proliferation and promotes apoptosis. Cell *114*, 457-467.

Haskins, J., Gu, L., Wittchen, E.S., Hibbard, J., and Stevenson, B.R. (1998). ZO-3, a novel member of the MAGUK protein family found at the tight junction, interacts with ZO-1 and occludin. J Cell Biol *141*, 199-208.

Hatzfeld, M. (2007). Plakophilins: Multifunctional proteins or just regulators of desmosomal adhesion? Biochim Biophys Acta *1773*, 69-77.

Hatzfeld, M., Wolf, A., and Keil, R. (2014). Plakophilins in desmosomal adhesion and signaling. Cell Commun Adhes *21*, 25-42.

Heallen, T., Zhang, M., Wang, J., Bonilla-Claudio, M., Klysik, E., Johnson, R.L., and Martin, J.F. (2011). Hippo pathway inhibits Wnt signaling to restrain cardiomyocyte proliferation and heart size. Science *332*, 458-461.

Hergovich, A. (2011). MOB control: reviewing a conserved family of kinase regulators. Cell Signal *23*, 1433-1440.

Hergovich, A., Bichsel, S.J., and Hemmings, B.A. (2005). Human NDR kinases are rapidly activated by MOB proteins through recruitment to the plasma membrane and phosphorylation. Mol Cell Biol *25*, 8259-8272.

Hergovich, A., Schmitz, D., and Hemmings, B.A. (2006). The human tumour suppressor LATS1 is activated by human MOB1 at the membrane. Biochem Biophys Res Commun *345*, 50-58.

Herrera, S.C., and Bach, E.A. (2019). JAK/STAT signaling in stem cells and regeneration: from Drosophila to vertebrates. Development *146*.

Higashi, T., and Miller, A.L. (2017). Tricellular junctions: how to build junctions at the TRICkiest points of epithelial cells. Mol Biol Cell *28*, 2023-2034.

Hirata, A., Hatano, Y., Niwa, M., Hara, A., and Tomita, H. (2019). Heterogeneity of Colon Cancer Stem Cells. Adv Exp Med Biol *1139*, 115-126.

Hirate, Y., and Sasaki, H. (2014). The role of angiomotin phosphorylation in the Hippo pathway during preimplantation mouse development. Tissue Barriers *2*, e28127.

Ho, L.L., Wei, X., Shimizu, T., and Lai, Z.C. (2010). Mob as tumor suppressor is activated at the cell membrane to control tissue growth and organ size in Drosophila. Dev Biol *337*, 274-283.

Hobbs, R.P., Han, S.Y., van der Zwaag, P.A., Bolling, M.C., Jongbloed, J.D., Jonkman, M.F., Getsios, S., Paller, A.S., and Green, K.J. (2010). Insights from a desmoplakin mutation identified in lethal acantholytic epidermolysis bullosa. J Invest Dermatol *130*, 2680-2683.

Hong, A.W., Meng, Z., and Guan, K.L. (2016). The Hippo pathway in intestinal regeneration and disease. Nat Rev Gastroenterol Hepatol *13*, 324-337.

Houtz, P., Bonfini, A., Liu, X., Revah, J., Guillou, A., Poidevin, M., Hens, K., Huang, H.Y., Deplancke, B., Tsai, Y.C.*, et al.* (2017). Hippo, TGF-beta, and Src-MAPK pathways regulate transcription of the upd3 cytokine in Drosophila enterocytes upon bacterial infection. PLoS Genet *13*, e1007091.

Hu, X., Richtman, N.M., Zhao, J.Z., Duncan, K.E., Niu, X., Procyk, L.A., Oneal, M.A., Kernodle, B.M., Steimel, J.P., Crane, V.C.*, et al.* (2016). Discovery of midgut genes for the RNA interference control of corn rootworm. Sci Rep *6*, 30542.

Hu, X., Steimel, J.P., Kapka-Kitzman, D.M., Davis-Vogel, C., Richtman, N.M., Mathis, J.P., Nelson, M.E., Lu, A.L., and Wu, G. (2019). Molecular characterization of the insecticidal activity of double-stranded RNA targeting the smooth septate junction of western corn rootworm (Diabrotica virgifera virgifera). PLoS One *14*, e0210491.

Huang, J., Wu, S., Barrera, J., Matthews, K., and Pan, D. (2005). The Hippo signaling pathway coordinately regulates cell proliferation and apoptosis by inactivating Yorkie, the Drosophila Homolog of YAP. Cell *122*, 421-434.

Huels, D.J., and Sansom, O.J. (2015). Stem vs non-stem cell origin of colorectal cancer. Br J Cancer *113*, 1-5.

Huerta, M., Muñoz, R., Tapia, R., Soto-Reyes, E., Ramírez, L., Recillas-Targa, F., González-Mariscal, L., and López-Bayghen, E. (2007). Cyclin D1 is transcriptionally down-regulated by ZO-2 via an E box and the transcription factor c-Myc. Mol Biol Cell *18*, 4826-4836.

Hultgren, E.M., Patrick, M.E., Evans, R.L., Stoos, C.T., and Egland, K.A. (2017). SUSD2 promotes tumor-associated macrophage recruitment by increasing levels of MCP-1 in breast cancer. PLoS One *12*, e0177089.

Huo, Q., Kinugasa, T., Wang, L., Huang, J., Zhao, J., Shibaguchi, H., Kuroki, M., Tanaka, T., Yamashita, Y., Nabeshima, K.*, et al.* (2009). Claudin-1 protein is a major factor involved in the tumorigenesis of colorectal cancer. Anticancer Res *29*, 851-857.

Hwang, E., Ryu, K.S., Paakkonen, K., Guntert, P., Cheong, H.K., Lim, D.S., Lee, J.O., Jeon, Y.H., and Cheong, C. (2007). Structural insight into dimeric interaction of the SARAH domains from Mst1 and RASSF family proteins in the apoptosis pathway. Proc Natl Acad Sci U S A *104*, 9236-9241.

Ikeda, M., Kawata, A., Nishikawa, M., Tateishi, Y., Yamaguchi, M., Nakagawa, K., Hirabayashi, S., Bao, Y., Hidaka, S., Hirata, Y.*, et al.* (2009). Hippo pathway-dependent and -independent roles of RASSF6. Sci Signal *2*, ra59.

Imajo, M., Miyatake, K., Iimura, A., Miyamoto, A., and Nishida, E. (2012). A molecular mechanism that links Hippo signalling to the inhibition of Wnt/β-catenin signalling. EMBO J *31*, 1109-1122.

Ishiyama, N., and Ikura, M. (2012). The three-dimensional structure of the cadherin-catenin complex. Subcell Biochem *60*, 39-62.

Ishiyama, N., Sarpal, R., Wood, M.N., Barrick, S.K., Nishikawa, T., Hayashi, H., Kobb, A.B., Flozak, A.S., Yemelyanov, A., Fernandez-Gonzalez, R.*, et al.* (2018). Force-dependent allostery of the α-catenin actin-binding domain controls adherens junction dynamics and functions. Nat Commun *9*, 5121.

Ishiyama, N., Tanaka, N., Abe, K., Yang, Y.J., Abbas, Y.M., Umitsu, M., Nagar, B., Bueler, S.A., Rubinstein, J.L., Takeichi, M.*, et al.* (2013). An autoinhibited structure of α-catenin and its implications for vinculin recruitment to adherens junctions. J Biol Chem *288*, 15913-15925.

Itzkowitz, S.H., and Yio, X. (2004). Inflammation and cancer IV. Colorectal cancer in inflammatory bowel disease: the role of inflammation. Am J Physiol Gastrointest Liver Physiol *287*, G7-17.

Ivanov, A.I., Nusrat, A., and Parkos, C.A. (2004). Endocytosis of epithelial apical junctional proteins by a clathrin-mediated pathway into a unique storage compartment. Mol Biol Cell *15*, 176-188.

Izumi, Y., Furuse, K., and Furuse, M. (2019). Septate junctions regulate gut homeostasis through regulation of stem cell proliferation and enterocyte behavior in. J Cell Sci *132*.

Izumi, Y., Motoishi, M., Furuse, K., and Furuse, M. (2016). A tetraspanin regulates septate junction formation in Drosophila midgut. J Cell Sci *129*, 1155-1164.

Izumi, Y., Yanagihashi, Y., and Furuse, M. (2012). A novel protein complex, Mesh-Ssk, is required for septate junction formation in the Drosophila midgut. J Cell Sci *125*, 4923-4933.

Javed, A., and Lteif, A. (2013). Development of the human breast. Semin Plast Surg *27*, 5-12.

Jesaitis, L.A., and Goodenough, D.A. (1994). Molecular characterization and tissue distribution of ZO-2, a tight junction protein homologous to ZO-1 and the Drosophila discs-large tumor suppressor protein. J Cell Biol *124*, 949-961.

Jia, J., Zhang, W., Wang, B., Trinko, R., and Jiang, J. (2003). The Drosophila Ste20 family kinase dMST functions as a tumor suppressor by restricting cell proliferation and promoting apoptosis. Genes Dev *17*, 2514-2519.

Jiang, H., and Edgar, B.A. (2011). Intestinal stem cells in the adult Drosophila midgut. Exp Cell Res *317*, 2780-2788.

Jiang, H., Grenley, M.O., Bravo, M.J., Blumhagen, R.Z., and Edgar, B.A. (2011). EGFR/Ras/MAPK signaling mediates adult midgut epithelial homeostasis and regeneration in Drosophila. Cell Stem Cell *8*, 84-95.

Jiang, H., Patel, P.H., Kohlmaier, A., Grenley, M.O., McEwen, D.G., and Edgar, B.A. (2009). Cytokine/Jak/Stat signaling mediates regeneration and homeostasis in the Drosophila midgut. Cell *137*, 1343-1355.

Jiang, H., Tian, A., and Jiang, J. (2016). Intestinal stem cell response to injury: lessons from Drosophila. Cell Mol Life Sci *73*, 3337-3349.

Jin, Y., Dong, L., Lu, Y., Wu, W., Hao, Q., Zhou, Z., Jiang, J., Zhao, Y., and Zhang, L. (2012). Dimerization and cytoplasmic localization regulate Hippo kinase signaling activity in organ size control. J Biol Chem *287*, 5784-5796.

Jonusaite, S., Donini, A., and Kelly, S.P. (2017). Salinity alters snakeskin and mesh transcript abundance and permeability in midgut and Malpighian tubules of larval mosquito, Aedes aegypti. Comp Biochem Physiol A Mol Integr Physiol *205*, 58-67.

Justice, R.W., Zilian, O., Woods, D.F., Noll, M., and Bryant, P.J. (1995). The Drosophila tumor suppressor gene warts encodes a homolog of human myotonic dystrophy kinase and is required for the control of cell shape and proliferation. Genes Dev *9*, 534-546.

Kam, C.Y., Dubash, A.D., Magistrati, E., Polo, S., Satchell, K.J.F., Sheikh, F., Lampe, P.D., and Green, K.J. (2018). Desmoplakin maintains gap junctions by inhibiting Ras/MAPK and lysosomal degradation of connexin-43. J Cell Biol *217*, 3219-3235.

Kamitani, T., Sakaguchi, H., Tamura, A., Miyashita, T., Yamazaki, Y., Tokumasu, R., Inamoto, R., Matsubara, A., Mori, N., Hisa, Y.*, et al.* (2015). Deletion of Tricellulin Causes Progressive Hearing Loss Associated with Degeneration of Cochlear Hair Cells. Sci Rep *5*, 18402.

Kaneko, S., Chen, X., Lu, P., Yao, X., Wright, T.G., Rajurkar, M., Kariya, K., Mao, J., Ip, Y.T., and Xu, L. (2011). Smad inhibition by the Ste20 kinase Misshapen. Proc Natl Acad Sci U S A *108*, 11127-11132.

Kango-Singh, M., Nolo, R., Tao, C., Verstreken, P., Hiesinger, P.R., Bellen, H.J., and Halder, G. (2002). Shar-pei mediates cell proliferation arrest during imaginal disc growth in Drosophila. Development *129*, 5719-5730.

Kapil, S., Sharma, B.K., Patil, M., Elattar, S., Yuan, J., Hou, S.X., Kolhe, R., and Satyanarayana, A. (2017). The cell polarity protein Scrib functions as a tumor suppressor in liver cancer. Oncotarget *8*, 26515-26531.

Karaman, R., and Halder, G. (2018). Cell Junctions in Hippo Signaling. Cold Spring Harb Perspect Biol *10*.

Karp, C.M., Tan, T.T., Mathew, R., Nelson, D., Mukherjee, C., Degenhardt, K., Karantza-Wadsworth, V., and White, E. (2008). Role of the polarity determinant crumbs in suppressing mammalian epithelial tumor progression. Cancer Res *68*, 4105-4115.

Karpowicz, P., Perez, J., and Perrimon, N. (2010). The Hippo tumor suppressor pathway regulates intestinal stem cell regeneration. Development *137*, 4135-4145.

Kato, M., Shimizu, A., Yokoyama, Y., Kaira, K., Shimomura, Y., Ishida-Yamamoto, A., Kamei, K., Tokunaga, F., and Ishikawa, O. (2015). An autosomal recessive mutation of DSG4 causes monilethrix through the ER stress response. J Invest Dermatol *135*, 1253-1260.

Kavanagh, E., Buchert, M., Tsapara, A., Choquet, A., Balda, M.S., Hollande, F., and Matter, K. (2006). Functional interaction between the ZO-1-interacting transcription

factor ZONAB/DbpA and the RNA processing factor symplekin. J Cell Sci *119*, 5098-5105.

Keller, D.I., Stepowski, D., Balmer, C., Simon, F., Guenthard, J., Bauer, F., Itin, P., David, N., Drouin-Garraud, V., and Fressart, V. (2012). De novo heterozygous desmoplakin mutations leading to Naxos-Carvajal disease. Swiss Med Wkly *142*, w13670.

Key, J.E. (2007). Development of contact lenses and their worldwide use. Eye Contact Lens *33*, 343-345; discussion 362-343.

Kim, E.R., and Chang, D.K. (2014). Colorectal cancer in inflammatory bowel disease: the risk, pathogenesis, prevention and diagnosis. World J Gastroenterol *20*, 9872-9881.

Kim, H.Y., Jackson, T.R., and Davidson, L.A. (2017). On the role of mechanics in driving mesenchymal-to-epithelial transitions. Semin Cell Dev Biol *67*, 113-122.

Kim, K.H., Chung, C., Kim, J.M., Lee, D., Cho, S.Y., Lee, T.H., Cho, H.J., and Yeo, M.K. (2019). Clinical significance of atypical protein kinase C (PKCiota and PKCzeta) and its relationship with yes-associated protein in lung adenocarcinoma. BMC Cancer *19*, 804.

Kim, M., Kim, M., Lee, S., Kuninaka, S., Saya, H., Lee, H., Lee, S., and Lim, D.S. (2013). cAMP/PKA signalling reinforces the LATS-YAP pathway to fully suppress YAP in response to actin cytoskeletal changes. EMBO J *32*, 1543-1555.

Kim, M.H., Kim, J., Hong, H., Lee, S.H., Lee, J.K., Jung, E., and Kim, J. (2016). Actin remodeling confers BRAF inhibitor resistance to melanoma cells through YAP/TAZ activation. EMBO J *35*, 462-478.

Kim, N.G., and Gumbiner, B.M. (2015). Adhesion to fibronectin regulates Hippo signaling via the FAK-Src-PI3K pathway. J Cell Biol *210*, 503-515.

Kim, N.G., Koh, E., Chen, X., and Gumbiner, B.M. (2011). E-cadherin mediates contact inhibition of proliferation through Hippo signaling-pathway components. Proc Natl Acad Sci U S A *108*, 11930-11935.

Kim, N.K., Higashi, T., Lee, K.Y., Kim, A.R., Kitajiri, S., Kim, M.Y., Chang, M.Y., Kim, V., Oh, S.H., Kim, D.*, et al.* (2015). Downsloping high-frequency hearing loss due to inner ear tricellular tight junction disruption by a novel ILDR1 mutation in the Ig-like domain. PLoS One *10*, e0116931.

Kisaalita, N.R., and Robinson, M.E. (2012). Analgesic placebo treatment perceptions: acceptability, efficacy, and knowledge. J Pain *13*, 891-900.

Klein, G., Langegger, M., Timpl, R., and Ekblom, P. (1988). Role of laminin A chain in the development of epithelial cell polarity. Cell *55*, 331-341.

Kline, A., Curry, T., and Lewellyn, L. (2018). The Misshapen kinase regulates the size and stability of the germline ring canals in the Drosophila egg chamber. Dev Biol *440*, 99-112.

Kljuic, A., Bazzi, H., Sundberg, J.P., Martinez-Mir, A., O'Shaughnessy, R., Mahoney, M.G., Levy, M., Montagutelli, X., Ahmad, W., Aita, V.M.*, et al.* (2003). Desmoglein 4 in hair follicle differentiation and epidermal adhesion: evidence from inherited hypotrichosis and acquired pemphigus vulgaris. Cell *113*, 249-260.

Kodaka, M., and Hata, Y. (2015). The mammalian Hippo pathway: regulation and function of YAP1 and TAZ. Cell Mol Life Sci *72*, 285-306.

Kohno, T., Konno, T., and Kojima, T. (2019). Role of Tricellular Tight Junction Protein Lipolysis-Stimulated Lipoprotein Receptor (LSR) in Cancer Cells. Int J Mol Sci *20*.

Konsavage, W.M., Jr., Kyler, S.L., Rennoll, S.A., Jin, G., and Yochum, G.S. (2012). Wnt/beta-catenin signaling regulates Yes-associated protein (YAP) gene expression in colorectal carcinoma cells. J Biol Chem *287*, 11730-11739.

Koontz, L.M., Liu-Chittenden, Y., Yin, F., Zheng, Y., Yu, J., Huang, B., Chen, Q., Wu, S., and Pan, D. (2013). The Hippo effector Yorkie controls normal tissue growth by antagonizing scalloped-mediated default repression. Dev Cell *25*, 388-401.

Korompay, A., Borka, K., Lotz, G., Somoracz, A., Torzsok, P., Erdelyi-Belle, B., Kenessey, I., Baranyai, Z., Zsoldos, F., Kupcsulik, P.*, et al.* (2012). Tricellulin expression in normal and neoplastic human pancreas. Histopathology *60*, E76-86.

Korzelius, J., Naumann, S.K., Loza-Coll, M.A., Chan, J.S., Dutta, D., Oberheim, J., Glasser, C., Southall, T.D., Brand, A.H., Jones, D.L.*, et al.* (2014). Escargot maintains stemness and suppresses differentiation in Drosophila intestinal stem cells. EMBO J *33*, 2967-2982.

Kosaka, Y., Mimori, K., Tanaka, F., Inoue, H., Watanabe, M., and Mori, M. (2007). Clinical significance of the loss of MATS1 mRNA expression in colorectal cancer. Int J Oncol *31*, 333-338.

Kottke, M.D., Delva, E., and Kowalczyk, A.P. (2006). The desmosome: cell science lessons from human diseases. J Cell Sci *119*, 797-806.

Krausova, M., and Korinek, V. (2014). Wnt signaling in adult intestinal stem cells and cancer. Cell Signal *26*, 570-579.

Kremerskothen, J., Plaas, C., Buther, K., Finger, I., Veltel, S., Matanis, T., Liedtke, T., and Barnekow, A. (2003). Characterization of KIBRA, a novel WW domain-containing protein. Biochem Biophys Res Commun *300*, 862-867.

Kudo, T., Ikeda, M., Nishikawa, M., Yang, Z., Ohno, K., Nakagawa, K., and Hata, Y. (2012). The RASSF3 candidate tumor suppressor induces apoptosis and G1-S cell-cycle arrest via p53. Cancer Res *72*, 2901-2911.

Kurth, T., Mohamed, S., Maillard, P., Zhu, Y.C., Chabriat, H., Mazoyer, B., Bousser, M.G., Dufouil, C., and Tzourio, C. (2011). Headache, migraine, and structural brain lesions and function: population based Epidemiology of Vascular Ageing-MRI study. BMJ *342*, c7357.

Kwon, Y., Vinayagam, A., Sun, X., Dephoure, N., Gygi, S.P., Hong, P., and Perrimon, N. (2013). The Hippo signaling pathway interactome. Science *342*, 737-740.

Kyuno, T., Kyuno, D., Kohno, T., Konno, T., Kikuchi, S., Arimoto, C., Yamaguchi, H., Imamura, M., Kimura, Y., Kondoh, M*., et al.* (2019). Tricellular tight junction protein LSR/angulin-1 contributes to the epithelial barrier and malignancy in human pancreatic cancer cell line. Histochem Cell Biol.

Laguna, A. (1984). Alkaloids and Coumarins from the Leaves of Amyris diatripa. Planta Med *50*, 112.

Lai, Z.C., Wei, X., Shimizu, T., Ramos, E., Rohrbaugh, M., Nikolaidis, N., Ho, L.L., and Li, Y. (2005). Control of cell proliferation and apoptosis by mob as tumor suppressor, mats. Cell *120*, 675-685.

Lam, L., Aktary, Z., Bishay, M., Werkman, C., Kuo, C.Y., Heacock, M., Srivastava, N., Mackey, J.R., and Pasdar, M. (2012). Regulation of subcellular distribution and oncogenic potential of nucleophosmin by plakoglobin. Oncogenesis *1*, e4.

Lee, J.L., and Streuli, C.H. (2014). Integrins and epithelial cell polarity. J Cell Sci *127*, 3217-3225.

Lee, T., and Luo, L. (2001). Mosaic analysis with a repressible cell marker (MARCM) for Drosophila neural development. Trends Neurosci *24*, 251-254.

Leerberg, J.M., Gomez, G.A., Verma, S., Moussa, E.J., Wu, S.K., Priya, R., Hoffman, B.D., Grashoff, C., Schwartz, M.A., and Yap, A.S. (2014). Tension-sensitive actin assembly supports contractility at the epithelial zonula adherens. Curr Biol *24*, 1689-1699.

Leick, K.M., Rodriguez, A.B., Melssen, M.M., Benamar, M., Lindsay, R.S., Eki, R., Du, K.P., Parlak, M., Abbas, T., Engelhard, V.H.*, et al.* (2019). The Barrier Molecules Junction Plakoglobin, Filaggrin, and Dystonin Play Roles in Melanoma Growth and Angiogenesis. Ann Surg *270*, 712-722.

Lemmers, C., Michel, D., Lane-Guermonprez, L., Delgrossi, M.H., Medina, E., Arsanto, J.P., and Le Bivic, A. (2004). CRB3 binds directly to Par6 and regulates the morphogenesis of the tight junctions in mammalian epithelial cells. Mol Biol Cell *15*, 1324-1333.

Letizia, A., He, D., Astigarraga, S., Colombelli, J., Hatini, V., Llimargas, M., and Treisman, J.E. (2019). Sidekick Is a Key Component of Tricellular Adherens Junctions that Acts to Resolve Cell Rearrangements. Dev Cell *50*, 313-326 e315.

Li, C., Xiao, J., Hormi, K., Borok, Z., and Minoo, P. (2002). Wnt5a participates in distal lung morphogenesis. Dev Biol *248*, 68-81.

Li, D., Zhang, W., Liu, Y., Haneline, L.S., and Shou, W. (2012). Lack of plakoglobin in epidermis leads to keratoderma. J Biol Chem *287*, 10435-10443.

Li, J., Swope, D., Raess, N., Cheng, L., Muller, E.J., and Radice, G.L. (2011). Cardiac tissue-restricted deletion of plakoglobin results in progressive cardiomyopathy and activation of {beta}-catenin signaling. Mol Cell Biol *31*, 1134-1144.

Li, N., Lu, N., and Xie, C. (2019). The Hippo and Wnt signalling pathways: crosstalk during neoplastic progression in gastrointestinal tissue. FEBS J *286*, 3745-3756.

Li, P., Mao, X., Ren, Y., and Liu, P. (2015a). Epithelial cell polarity determinant CRB3 in cancer development. Int J Biol Sci *11*, 31-37.

Li, P., Silvis, M.R., Honaker, Y., Lien, W.H., Arron, S.T., and Vasioukhin, V. (2016). alphaE-catenin inhibits a Src-YAP1 oncogenic module that couples tyrosine kinases and the effector of Hippo signaling pathway. Genes Dev *30*, 798-811.

Li, Q., Li, S., Mana-Capelli, S., Roth Flach, R.J., Danai, L.V., Amcheslavsky, A., Nie, Y., Kaneko, S., Yao, X., Chen, X.*, et al.* (2014a). The conserved misshapen-warts-Yorkie pathway acts in enteroblasts to regulate intestinal stem cells in Drosophila. Dev Cell *31*, 291-304.

Li, Q., Nirala, N.K., Nie, Y., Chen, H.J., Ostroff, G., Mao, J., Wang, Q., Xu, L., and Ip, Y.T. (2018). Ingestion of Food Particles Regulates the Mechanosensing Misshapen-Yorkie Pathway in Drosophila Intestinal Growth. Dev Cell *45*, 433-449 e436.

Li, S., Cho, Y.S., Yue, T., Ip, Y.T., and Jiang, J. (2015b). Overlapping functions of the MAP4K family kinases Hppy and Msn in Hippo signaling. Cell Discov *1*, 15038.

Li, Y., Zhou, H., Li, F., Chan, S.W., Lin, Z., Wei, Z., Yang, Z., Guo, F., Lim, C.J., Xing, W.*, et al.* (2015c). Angiomotin binding-induced activation of Merlin/NF2 in the Hippo pathway. Cell Res *25*, 801-817.

Li, Z., Guo, Y., Han, L., Zhang, Y., Shi, L., Huang, X., and Lin, X. (2014b). Debra-mediated Ci degradation controls tissue homeostasis in Drosophila adult midgut. Stem Cell Reports *2*, 135-144.

Liao, T.J., Tsai, C.J., Jang, H., Fushman, D., and Nussinov, R. (2016). RASSF5: An MST activator and tumor suppressor in vivo but opposite in vitro. Curr Opin Struct Biol *41*, 217-224.

Lien, W.H., Klezovitch, O., Fernandez, T.E., Delrow, J., and Vasioukhin, V. (2006). alphaE-catenin controls cerebral cortical size by regulating the hedgehog signaling pathway. Science *311*, 1609-1612.

Lin, G., Xu, N., and Xi, R. (2008). Paracrine Wingless signalling controls self-renewal of Drosophila intestinal stem cells. Nature *455*, 1119-1123.

Lin, K.C., Park, H.W., and Guan, K.L. (2017). Regulation of the Hippo Pathway Transcription Factor TEAD. Trends Biochem Sci *42*, 862-872.

Ling, C., Zheng, Y., Yin, F., Yu, J., Huang, J., Hong, Y., Wu, S., and Pan, D. (2010). The apical transmembrane protein Crumbs functions as a tumor suppressor that regulates Hippo signaling by binding to Expanded. Proc Natl Acad Sci U S A *107*, 10532-10537.

Liu, C.Y., Zha, Z.Y., Zhou, X., Zhang, H., Huang, W., Zhao, D., Li, T., Chan, S.W., Lim, C.J., Hong, W.*, et al.* (2010). The hippo tumor pathway promotes TAZ degradation by phosphorylating a phosphodegron and recruiting the SCF{beta}-TrCP E3 ligase. J Biol Chem *285*, 37159-37169.

Liu, J., Li, J., Li, P., Wang, Y., Liang, Z., Jiang, Y., Li, J., Feng, C., Wang, R., Chen, H., *et al.* (2017). Loss of DLG5 promotes breast cancer malignancy by inhibiting the Hippo signaling pathway. Sci Rep *7*, 42125.

Liu, O.X., Lin, L.B., Chew, T., Motegi, F., and Low, B.C. (2018). ZO-2 induces cytoplasmic retention of YAP by promoting a LATS1-ZO-2-YAP complex at tight junctions. bioRxiv, 355081.

Liu, X.R., Cai, C.X., Luo, L.M., Zheng, W.L., Shi, R., Zeng, J., Xu, Y.Q., Wei, M., and Ma, W.L. (2016a). Decreased expression of Sushi Domain Containing 2 correlates to progressive features in patients with hepatocellular carcinoma. Cancer Cell Int *16*, 15.

Liu, Z., Wu, H., Jiang, K., Wang, Y., Zhang, W., Chu, Q., Li, J., Huang, H., Cai, T., Ji, H., *et al.* (2016b). MAPK-Mediated YAP Activation Controls Mechanical-Tension-Induced Pulmonary Alveolar Regeneration. Cell Rep *16*, 1810-1819.

Loza-Coll, M.A., Southall, T.D., Sandall, S.L., Brand, A.H., and Jones, D.L. (2014). Regulation of Drosophila intestinal stem cell maintenance and differentiation by the transcription factor Escargot. EMBO J *33*, 2983-2996.

Lu, L., Li, Y., Kim, S.M., Bossuyt, W., Liu, P., Qiu, Q., Wang, Y., Halder, G., Finegold, M.J., Lee, J.S., *et al.* (2010). Hippo signaling is a potent in vivo growth and tumor suppressor pathway in the mammalian liver. Proc Natl Acad Sci U S A *107*, 1437-1442.

Lu, Z., Ding, L., Lu, Q., and Chen, Y.H. (2013). Claudins in intestines: Distribution and functional significance in health and diseases. Tissue Barriers *1*, e24978.

Luna-Ulloa, L.B., Hernandez-Maqueda, J.G., Castaneda-Patlan, M.C., and Robles-Flores, M. (2011). Protein kinase C in Wnt signaling: implications in cancer initiation and progression. IUBMB Life *63*, 915-921.

Luo, X. (2010). Snapshots of a hybrid transcription factor in the Hippo pathway. Protein Cell *1*, 811-819.

Lyon, R.C., Mezzano, V., Wright, A.T., Pfeiffer, E., Chuang, J., Banares, K., Castaneda, A., Ouyang, K., Cui, L., Contu, R.*, et al.* (2014). Connexin defects underlie arrhythmogenic right ventricular cardiomyopathy in a novel mouse model. Hum Mol Genet *23*, 1134-1150.

Ma, S., Meng, Z., Chen, R., and Guan, K.L. (2019). The Hippo Pathway: Biology and Pathophysiology. Annu Rev Biochem *88*, 577-604.

Määttä, A., DiColandrea, T., Groot, K., and Watt, F.M. (2001). Gene targeting of envoplakin, a cytoskeletal linker protein and precursor of the epidermal cornified envelope. Mol Cell Biol *21*, 7047-7053.

Macara, I.G. (2004). Parsing the polarity code. Nat Rev Mol Cell Biol *5*, 220-231.

Maga, G., and Hubscher, U. (2003). Proliferating cell nuclear antigen (PCNA): a dancer with many partners. J Cell Sci *116*, 3051-3060.

Mana-Capelli, S., and McCollum, D. (2018). Angiomotins stimulate LATS kinase autophosphorylation and act as scaffolds that promote Hippo signaling. J Biol Chem *293*, 18230-18241.

Mana-Capelli, S., Paramasivam, M., Dutta, S., and McCollum, D. (2014). Angiomotins link F-actin architecture to Hippo pathway signaling. Mol Biol Cell *25*, 1676-1685.

Manninen, A. (2015). Epithelial polarity--generating and integrating signals from the ECM with integrins. Exp Cell Res *334*, 337-349.

Mao, X., Li, P., Wang, Y., Liang, Z., Liu, J., Li, J., Jiang, Y., Bao, G., Li, L., Zhu, B.*, et al.* (2017). CRB3 regulates contact inhibition by activating the Hippo pathway in mammary epithelial cells. Cell Death Dis *8*, e2546.

Mariotto, A.B., Yabroff, K.R., Shao, Y., Feuer, E.J., and Brown, M.L. (2011). Projections of the cost of cancer care in the United States: 2010-2020. J Natl Cancer Inst *103*, 117-128.

Martin-Belmonte, F., and Perez-Moreno, M. (2011). Epithelial cell polarity, stem cells and cancer. Nat Rev Cancer *12*, 23-38.

Masuda, R., Semba, S., Mizuuchi, E., Yanagihara, K., and Yokozaki, H. (2010). Negative regulation of the tight junction protein tricellulin by snail-induced epithelial-mesenchymal transition in gastric carcinoma cells. Pathobiology *77*, 106-113.

Matakatsu, H., and Blair, S.S. (2012). Separating planar cell polarity and Hippo pathway activities of the protocadherins Fat and Dachsous. Development *139*, 1498-1508.

Maxfield, F.R., and McGraw, T.E. (2004). Endocytic recycling. Nat Rev Mol Cell Biol *5*, 121-132.

McCartney, B.M., Kulikauskas, R.M., LaJeunesse, D.R., and Fehon, R.G. (2000). The neurofibromatosis-2 homologue, Merlin, and the tumor suppressor expanded function together in Drosophila to regulate cell proliferation and differentiation. Development *127*, 1315-1324.

McGrath, J.A., Hoeger, P.H., Christiano, A.M., McMillan, J.R., Mellerio, J.E., Ashton, G.H., Dopping-Hepenstal, P.J., Lake, B.D., Leigh, I.M., Harper, J.I.*, et al.* (1999). Skin fragility and hypohidrotic ectodermal dysplasia resulting from ablation of plakophilin 1. Br J Dermatol *140*, 297-307.

McMahon, A.P. (2000). More surprises in the Hedgehog signaling pathway. Cell *100*, 185-188.

Medina, R., Rahner, C., Mitic, L.L., Anderson, J.M., and Van Itallie, C.M. (2000). Occludin localization at the tight junction requires the second extracellular loop. J Membr Biol *178*, 235-247.

Mees, S.T., Mennigen, R., Spieker, T., Rijcken, E., Senninger, N., Haier, J., and Bruewer, M. (2009). Expression of tight and adherens junction proteins in ulcerative colitis associated colorectal carcinoma: upregulation of claudin-1, claudin-3, claudin-4, and beta-catenin. Int J Colorectal Dis *24*, 361-368.

Meng, Z., Moroishi, T., Mottier-Pavie, V., Plouffe, S.W., Hansen, C.G., Hong, A.W., Park, H.W., Mo, J.S., Lu, W., Lu, S.*, et al.* (2015). MAP4K family kinases act in parallel to MST1/2 to activate LATS1/2 in the Hippo pathway. Nat Commun *6*, 8357.

Meng, Z., Qiu, Y., Lin, K.C., Kumar, A., Placone, J.K., Fang, C., Wang, K.C., Lu, S., Pan, M., Hong, A.W.*, et al.* (2018). RAP2 mediates mechanoresponses of the Hippo pathway. Nature *560*, 655-660.

Micchelli, C.A., and Perrimon, N. (2006). Evidence that stem cells reside in the adult Drosophila midgut epithelium. Nature *439*, 475-479.

Micchelli, C.A., Sudmeier, L., Perrimon, N., Tang, S., and Beehler-Evans, R. (2011). Identification of adult midgut precursors in Drosophila. Gene Expr Patterns *11*, 12-21.

Miguel-Aliaga, I., Jasper, H., and Lemaitre, B. (2018). Anatomy and Physiology of the Digestive Tract of Drosophila melanogaster. Genetics *210*, 357-396.

Miller, E., Yang, J., DeRan, M., Wu, C., Su, A.I., Bonamy, G.M., Liu, J., Peters, E.C., and Wu, X. (2012). Identification of serum-derived sphingosine-1-phosphate as a small molecule regulator of YAP. Chem Biol *19*, 955-962.

Mineta, K., Yamamoto, Y., Yamazaki, Y., Tanaka, H., Tada, Y., Saito, K., Tamura, A., Igarashi, M., Endo, T., Takeuchi, K.*, et al.* (2011). Predicted expansion of the claudin multigene family. FEBS Lett *585*, 606-612.

Misra, J.R., and Irvine, K.D. (2018). The Hippo Signaling Network and Its Biological Functions. Annu Rev Genet *52*, 65-87.

Miwa, N., Furuse, M., Tsukita, S., Niikawa, N., Nakamura, Y., and Furukawa, Y. (2001). Involvement of claudin-1 in the beta-catenin/Tcf signaling pathway and its frequent upregulation in human colorectal cancers. Oncol Res *12*, 469-476.

Miyoshi, H. (2017). Wnt-expressing cells in the intestines: guides for tissue remodeling. J Biochem *161*, 19-25.

Mo, J.S., Meng, Z., Kim, Y.C., Park, H.W., Hansen, C.G., Kim, S., Lim, D.S., and Guan, K.L. (2015). Cellular energy stress induces AMPK-mediated regulation of YAP and the Hippo pathway. Nat Cell Biol *17*, 500-510.

Mo, J.S., Yu, F.X., Gong, R., Brown, J.H., and Guan, K.L. (2012). Regulation of the Hippo-YAP pathway by protease-activated receptors (PARs). Genes Dev *26*, 2138-2143.

Moccia, F., Lodola, F., Stadiotti, I., Pilato, C.A., Bellin, M., Carugo, S., Pompilio, G., Sommariva, E., and Maione, A.S. (2019). Calcium as a Key Player in Arrhythmogenic Cardiomyopathy: Adhesion Disorder or Intracellular Alteration? Int J Mol Sci *20*.

Moon, K.H., Kim, H.T., Lee, D., Rao, M.B., Levine, E.M., Lim, D.S., and Kim, J.W. (2018). Differential Expression of NF2 in Neuroepithelial Compartments Is Necessary for Mammalian Eye Development. Dev Cell *44*, 13-28 e13.

Morikawa, Y., Zhang, M., Heallen, T., Leach, J., Tao, G., Xiao, Y., Bai, Y., Li, W., Willerson, J.T., and Martin, J.F. (2015). Actin cytoskeletal remodeling with protrusion formation is essential for heart regeneration in Hippo-deficient mice. Sci Signal *8*, ra41.

Moya, I.M., and Halder, G. (2019). Hippo-YAP/TAZ signalling in organ regeneration and regenerative medicine. Nat Rev Mol Cell Biol *20*, 211-226.

Müller, H.A., and Wieschaus, E. (1996). armadillo, bazooka, and stardust are critical for early stages in formation of the zonula adherens and maintenance of the polarized blastoderm epithelium in Drosophila. J Cell Biol *134*, 149-163.

Müller, H.J. (2018). More diversity in epithelial cell polarity: A fruit flies' gut feeling. PLoS Biol *16*, e3000082.

Nanes, B.A., Chiasson-MacKenzie, C., Lowery, A.M., Ishiyama, N., Faundez, V., Ikura, M., Vincent, P.A., and Kowalczyk, A.P. (2012). p120-catenin binding masks an endocytic signal conserved in classical cadherins. J Cell Biol *199*, 365-380.

Nekrasova, O., and Green, K.J. (2013). Desmosome assembly and dynamics. Trends Cell Biol *23*, 537-546.

Nelson, K.S., Furuse, M., and Beitel, G.J. (2010). The Drosophila Claudin Kune-kune is required for septate junction organization and tracheal tube size control. Genetics *185*, 831-839.

Neo, J.H., Ager, E.I., Angus, P.W., Zhu, J., Herath, C.B., and Christophi, C. (2010). Changes in the renin angiotensin system during the development of colorectal cancer liver metastases. BMC Cancer *10*, 134.

Ni, L., and Luo, X. (2019). Structural and Biochemical Analyses of the Core Components of the Hippo Pathway. Methods Mol Biol *1893*, 239-256.

Ni, L., Zheng, Y., Hara, M., Pan, D., and Luo, X. (2015). Structural basis for Mob1-dependent activation of the core Mst-Lats kinase cascade in Hippo signaling. Genes Dev *29*, 1416-1431.

Nie, Y., Yu, S., Li, Q., Nirala, N.K., Amcheslavsky, A., Edwards, Y.J.K., Shum, P.W., Jiang, Z., Wang, W., Zhang, B.*, et al.* (2019). Oncogenic Pathways and Loss of the Rab11 GTPase Synergize To Alter Metabolism in Drosophila. Genetics *212*, 1227-1239.

Nishioka, N., Inoue, K., Adachi, K., Kiyonari, H., Ota, M., Ralston, A., Yabuta, N., Hirahara, S., Stephenson, R.O., Ogonuki, N.*, et al.* (2009). The Hippo signaling pathway components Lats and Yap pattern Tead4 activity to distinguish mouse trophectoderm from inner cell mass. Dev Cell *16*, 398-410.

Nishita, M., Enomoto, M., Yamagata, K., and Minami, Y. (2010). Cell/tissue-tropic functions of Wnt5a signaling in normal and cancer cells. Trends Cell Biol *20*, 346-354.

Odenwald, M.A., Choi, W., Kuo, W.T., Singh, G., Sailer, A., Wang, Y., Shen, L., Fanning, A.S., and Turner, J.R. (2018). The scaffolding protein ZO-1 coordinates actomyosin and epithelial apical specializations. J Biol Chem *293*, 17317-17335.

Oh, H., Slattery, M., Ma, L., White, K.P., Mann, R.S., and Irvine, K.D. (2014). Yorkie promotes transcription by recruiting a histone methyltransferase complex. Cell Rep *8*, 449-459.

Oh, H.J., Lee, K.K., Song, S.J., Jin, M.S., Song, M.S., Lee, J.H., Im, C.R., Lee, J.O., Yonehara, S., and Lim, D.S. (2006). Role of the tumor suppressor RASSF1A in Mst1-mediated apoptosis. Cancer Res *66*, 2562-2569.

Ohlstein, B., and Spradling, A. (2006). The adult Drosophila posterior midgut is maintained by pluripotent stem cells. Nature *439*, 470-474.

Ohlstein, B., and Spradling, A. (2007). Multipotent Drosophila intestinal stem cells specify daughter cell fates by differential notch signaling. Science *315*, 988-992.

Oka, T., Remue, E., Meerschaert, K., Vanloo, B., Boucherie, C., Gfeller, D., Bader, G.D., Sidhu, S.S., Vandekerckhove, J., Gettemans, J.*, et al.* (2010). Functional complexes between YAP2 and ZO-2 are PDZ domain-dependent, and regulate YAP2 nuclear localization and signalling. Biochem J *432*, 461-472.

Pan, D. (2010). The hippo signaling pathway in development and cancer. Dev Cell *19*, 491-505.

Pan, W., Cheng, Y., Zhang, H., Liu, B., Mo, X., Li, T., Li, L., Cheng, X., Zhang, L., Ji, J.*, et al.* (2014). CSBF/C10orf99, a novel potential cytokine, inhibits colon cancer cell growth through inducing G1 arrest. Sci Rep *4*, 6812.

Pannequin, J., Delaunay, N., Darido, C., Maurice, T., Crespy, P., Frohman, M.A., Balda, M.S., Matter, K., Joubert, D., Bourgaux, J.F.*, et al.* (2007). Phosphatidylethanol accumulation promotes intestinal hyperplasia by inducing ZONAB-mediated cell density increase in response to chronic ethanol exposure. Mol Cancer Res *5*, 1147-1157.

Pantalacci, S., Tapon, N., and Leopold, P. (2003). The Salvador partner Hippo promotes apoptosis and cell-cycle exit in Drosophila. Nat Cell Biol *5*, 921-927.

Park, H.W., Kim, Y.C., Yu, B., Moroishi, T., Mo, J.S., Plouffe, S.W., Meng, Z., Lin, K.C., Yu, F.X., Alexander, C.M., *et al.* (2015). Alternative Wnt Signaling Activates YAP/TAZ. Cell *162*, 780-794.

Park, J., and Jeong, S. (2015). Wnt activated beta-catenin and YAP proteins enhance the expression of non-coding RNA component of RNase MRP in colon cancer cells. Oncotarget *6*, 34658-34668.

Parker, J., and Struhl, G. (2015). Scaling the Drosophila Wing: TOR-Dependent Target Gene Access by the Hippo Pathway Transducer Yorkie. PLoS Biol *13*, e1002274.

Patel, D., Zhang, X., and Veenstra, R.D. (2014a). Connexin hemichannel and pannexin channel electrophysiology: how do they differ? FEBS Lett *588*, 1372-1378.

Patel, D.M., Dubash, A.D., Kreitzer, G., and Green, K.J. (2014b). Disease mutations in desmoplakin inhibit Cx43 membrane targeting mediated by desmoplakin-EB1 interactions. J Cell Biol *206*, 779-797.

Peng, X., Cuff, L.E., Lawton, C.D., and DeMali, K.A. (2010). Vinculin regulates cell-surface E-cadherin expression by binding to beta-catenin. J Cell Sci *123*, 567-577.

Perez-Moreno, M., Davis, M.A., Wong, E., Pasolli, H.A., Reynolds, A.B., and Fuchs, E. (2006). p120-catenin mediates inflammatory responses in the skin. Cell *124*, 631-644.

Petrilli, A.M., and Fernandez-Valle, C. (2016). Role of Merlin/NF2 inactivation in tumor biology. Oncogene *35*, 537-548.

Pflanz, R., Voigt, A., Yakulov, T., and Jackle, H. (2015). Drosophila gene tao-1 encodes proteins with and without a Ste20 kinase domain that affect cytoskeletal architecture and cell migration differently. Open Biol *5*, 140161.

Pieperhoff, S., Schumacher, H., and Franke, W.W. (2008). The area composita of adhering junctions connecting heart muscle cells of vertebrates. V. The importance of plakophilin-2 demonstrated by small interference RNA-mediated knockdown in cultured rat cardiomyocytes. Eur J Cell Biol *87*, 399-411.

Pigors, M., Kiritsi, D., Krümpelmann, S., Wagner, N., He, Y., Podda, M., Kohlhase, J., Hausser, I., Bruckner-Tuderman, L., and Has, C. (2011). Lack of plakoglobin leads to lethal congenital epidermolysis bullosa: a novel clinico-genetic entity. Hum Mol Genet *20*, 1811-1819.

Pinto, D., Gregorieff, A., Begthel, H., and Clevers, H. (2003). Canonical Wnt signals are essential for homeostasis of the intestinal epithelium. Genes Dev *17*, 1709-1713.

Plissonnier, M.L., Lahlali, T., Raab, M., Michelet, M., Romero-López, C., Rivoire, M., Strebhardt, K., Durantel, D., Levrero, M., Mehlen, P.*, et al.* (2017). Reciprocal antagonism between the netrin-1 receptor uncoordinated-phenotype-5A (UNC5A) and the hepatitis C virus. Oncogene *36*, 6712-6724.

Plouffe, S.W., Meng, Z., Lin, K.C., Lin, B., Hong, A.W., Chun, J.V., and Guan, K.L. (2016). Characterization of Hippo Pathway Components by Gene Inactivation. Mol Cell *64*, 993-1008.

Pokutta, S., Choi, H.J., Ahlsen, G., Hansen, S.D., and Weis, W.I. (2014). Structural and thermodynamic characterization of cadherin·β-catenin·α-catenin complex formation. J Biol Chem *289*, 13589-13601.

Polesello, C., Huelsmann, S., Brown, N.H., and Tapon, N. (2006). The Drosophila RASSF homolog antagonizes the hippo pathway. Curr Biol *16*, 2459-2465.

Poon, C.L., Lin, J.I., Zhang, X., and Harvey, K.F. (2011). The sterile 20-like kinase Tao-1 controls tissue growth by regulating the Salvador-Warts-Hippo pathway. Dev Cell *21*, 896-906.

Poon, C.L.C., Liu, W., Song, Y., Gomez, M., Kulaberoglu, Y., Zhang, X., Xu, W., Veraksa, A., Hergovich, A., Ghabrial, A.*, et al.* (2018). A Hippo-like Signaling Pathway Controls Tracheal Morphogenesis in Drosophila melanogaster. Dev Cell *47*, 564-575 e565.

Poritz, L.S., Garver, K.I., Green, C., Fitzpatrick, L., Ruggiero, F., and Koltun, W.A. (2007). Loss of the tight junction protein ZO-1 in dextran sulfate sodium induced colitis. J Surg Res *140*, 12-19.

Praskova, M., Xia, F., and Avruch, J. (2008). MOBKL1A/MOBKL1B phosphorylation by MST1 and MST2 inhibits cell proliferation. Curr Biol *18*, 311-321.

Priya, R., Gomez, G.A., Budnar, S., Verma, S., Cox, H.L., Hamilton, N.A., and Yap, A.S. (2015). Feedback regulation through myosin II confers robustness on RhoA signalling at E-cadherin junctions. Nat Cell Biol *17*, 1282-1293.

Pummi, K.P., Heape, A.M., Grénman, R.A., Peltonen, J.T., and Peltonen, S.A. (2004). Tight junction proteins ZO-1, occludin, and claudins in developing and adult human perineurium. J Histochem Cytochem *52*, 1037-1046.

Qiao, Y., Chen, J., Lim, Y.B., Finch-Edmondson, M.L., Seshachalam, V.P., Qin, L., Jiang, T., Low, B.C., Singh, H., Lim, C.T.*, et al.* (2017). YAP Regulates Actin Dynamics through ARHGAP29 and Promotes Metastasis. Cell Rep *19*, 1495-1502.

Qin, Y., and Zhang, C. (2017). The Regulatory Role of IFN-gamma on the Proliferation and Differentiation of Hematopoietic Stem and Progenitor Cells. Stem Cell Rev Rep *13*, 705-712.

Qing, Y., Yin, F., Wang, W., Zheng, Y., Guo, P., Schozer, F., Deng, H., and Pan, D. (2014). The Hippo effector Yorkie activates transcription by interacting with a histone methyltransferase complex through Ncoa6. Elife *3*.

Quelle, D.E., Ashmun, R.A., Shurtleff, S.A., Kato, J.Y., Bar-Sagi, D., Roussel, M.F., and Sherr, C.J. (1993). Overexpression of mouse D-type cyclins accelerates G1 phase in rodent fibroblasts. Genes Dev *7*, 1559-1571.

Raleigh, D.R., Boe, D.M., Yu, D., Weber, C.R., Marchiando, A.M., Bradford, E.M., Wang, Y., Wu, L., Schneeberger, E.E., Shen, L.*, et al.* (2011). Occludin S408 phosphorylation regulates tight junction protein interactions and barrier function. J Cell Biol *193*, 565-582.

Rangarajan, E.S., and Izard, T. (2012). The cytoskeletal protein α-catenin unfurls upon binding to vinculin. J Biol Chem *287*, 18492-18499.

Rao, R. (2009). Occludin phosphorylation in regulation of epithelial tight junctions. Ann N Y Acad Sci *1165*, 62-68.

Rauskolb, C., Sun, S., Sun, G., Pan, Y., and Irvine, K.D. (2014). Cytoskeletal tension inhibits Hippo signaling through an Ajuba-Warts complex. Cell *158*, 143-156.

Realini, L., De Ridder, K., Hirschel, B., and Portaels, F. (1999). Blood and charcoal added to acidified agar media promote the growth of Mycobacterium genavense. Diagn Microbiol Infect Dis *34*, 45-50.

Reaves, D.K., Fagan-Solis, K.D., Dunphy, K., Oliver, S.D., Scott, D.W., and Fleming, J.M. (2014). The role of lipolysis stimulated lipoprotein receptor in breast cancer and directing breast cancer cell behavior. PLoS One *9*, e91747.

Ren, F., Wang, B., Yue, T., Yun, E.Y., Ip, Y.T., and Jiang, J. (2010). Hippo signaling regulates Drosophila intestine stem cell proliferation through multiple pathways. Proc Natl Acad Sci U S A *107*, 21064-21069.

Rera, M., Clark, R.I., and Walker, D.W. (2012). Intestinal barrier dysfunction links metabolic and inflammatory markers of aging to death in Drosophila. Proc Natl Acad Sci U S A *109*, 21528-21533.

Resende, L.P., Truong, M.E., Gomez, A., and Jones, D.L. (2017). Intestinal stem cell ablation reveals differential requirements for survival in response to chemical challenge. Dev Biol *424*, 10-17.

Resnik-Docampo, M., Koehler, C.L., Clark, R.I., Schinaman, J.M., Sauer, V., Wong, D.M., Lewis, S., D'Alterio, C., Walker, D.W., and Jones, D.L. (2017). Tricellular junctions regulate intestinal stem cell behaviour to maintain homeostasis. Nat Cell Biol *19*, 52-59.

Resnik-Docampo, M., Sauer, V., Schinaman, J.M., Clark, R.I., Walker, D.W., and Jones, D.L. (2018). Keeping it tight: The relationship between bacterial dysbiosis, septate junctions, and the intestinal barrier in Drosophila. Fly (Austin) *12*, 34-40.

Ribeiro, P.S., Josue, F., Wepf, A., Wehr, M.C., Rinner, O., Kelly, G., Tapon, N., and Gstaiger, M. (2010). Combined functional genomic and proteomic approaches identify a PP2A complex as a negative regulator of Hippo signaling. Mol Cell *39*, 521-534.

Richardson, H.E. (2011). Actin up for Hippo. EMBO J *30*, 2307-2309.

Rickman, L., Simrak, D., Stevens, H.P., Hunt, D.M., King, I.A., Bryant, S.P., Eady, R.A., Leigh, I.M., Arnemann, J., Magee, A.I.*, et al.* (1999). N-terminal deletion in a desmosomal cadherin causes the autosomal dominant skin disease striate palmoplantar keratoderma. Hum Mol Genet *8*, 971-976.

Riento, K., and Ridley, A.J. (2003). Rocks: multifunctional kinases in cell behaviour. Nat Rev Mol Cell Biol *4*, 446-456.

Robinson, B.S., Huang, J., Hong, Y., and Moberg, K.H. (2010). Crumbs regulates Salvador/Warts/Hippo signaling in Drosophila via the FERM-domain protein Expanded. Curr Biol *20*, 582-590.

Rodgers, L.S., Beam, M.T., Anderson, J.M., and Fanning, A.S. (2013). Epithelial barrier assembly requires coordinated activity of multiple domains of the tight junction protein ZO-1. J Cell Sci *126*, 1565-1575.

Runkle, E.A., and Mu, D. (2013). Tight junction proteins: from barrier to tumorigenesis. Cancer Lett *337*, 41-48.

Saitou, M., Furuse, M., Sasaki, H., Schulzke, J.D., Fromm, M., Takano, H., Noda, T., and Tsukita, S. (2000). Complex phenotype of mice lacking occludin, a component of tight junction strands. Mol Biol Cell *11*, 4131-4142.

Sakakibara, A., Furuse, M., Saitou, M., Ando-Akatsuka, Y., and Tsukita, S. (1997). Possible involvement of phosphorylation of occludin in tight junction formation. J Cell Biol *137*, 1393-1401.

Salazar, A.M., Resnik-Docampo, M., Ulgherait, M., Clark, R.I., Shirasu-Hiza, M., Jones, D.L., and Walker, D.W. (2018). Intestinal Snakeskin Limits Microbial Dysbiosis during Aging and Promotes Longevity. iScience *9*, 229-243.

Samiei, M., Ahmadian, E., Eftekhari, A., Eghbal, M.A., Rezaie, F., and Vinken, M. (2019). Cell junctions and oral health. EXCLI J *18*, 317-330.

Santinon, G., Pocaterra, A., and Dupont, S. (2016). Control of YAP/TAZ Activity by Metabolic and Nutrient-Sensing Pathways. Trends Cell Biol *26*, 289-299.

Sarpal, R., Yan, V., Kazakova, L., Sheppard, L., Yu, J.C., Fernandez-Gonzalez, R., and Tepass, U. (2019). Role of alpha-Catenin and its mechanosensing properties in regulating Hippo/YAP-dependent tissue growth. PLoS Genet *15*, e1008454.

Sartori, M., Loregian, A., Pagni, S., De Rosa, S., Ferrari, F., Zampieri, L., Zancato, M., Palu, G., and Ronco, C. (2016). Kinetics of Linezolid in Continuous Renal Replacement Therapy: An In Vitro Study. Ther Drug Monit *38*, 579-586.

Sasaki, H., Kawano, O., Endo, K., Suzuki, E., Yukiue, H., Kobayashi, Y., Yano, M., and Fujii, Y. (2007). Human MOB1 expression in non-small-cell lung cancer. Clin Lung Cancer *8*, 273-276.

Sato, T., and Sekido, Y. (2018). NF2/Merlin Inactivation and Potential Therapeutic Targets in Mesothelioma. Int J Mol Sci *19*.

Schimizzi, G.V., Maher, M.T., Loza, A.J., and Longmore, G.D. (2016). Disruption of the Cdc42/Par6/aPKC or Dlg/Scrib/Lgl Polarity Complex Promotes Epithelial Proliferation via Overlapping Mechanisms. PLoS One *11*, e0159881.

Schinner, C., Erber, B.M., Yeruva, S., and Waschke, J. (2019). Regulation of cardiac myocyte cohesion and gap junctions via desmosomal adhesion. Acta Physiol (Oxf) *226*, e13242.

Schlegelmilch, K., Mohseni, M., Kirak, O., Pruszak, J., Rodriguez, J.R., Zhou, D., Kreger, B.T., Vasioukhin, V., Avruch, J., Brummelkamp, T.R.*, et al.* (2011). Yap1 acts downstream of alpha-catenin to control epidermal proliferation. Cell *144*, 782-795.

Schmidt, A., Utepbergenov, D.I., Mueller, S.L., Beyermann, M., Schneider-Mergener, J., Krause, G., and Blasig, I.E. (2004). Occludin binds to the SH3-hinge-GuK unit of zonula occludens protein 1: potential mechanism of tight junction regulation. Cell Mol Life Sci *61*, 1354-1365.

Schulte, J., Tepass, U., and Auld, V.J. (2003). Gliotactin, a novel marker of tricellular junctions, is necessary for septate junction development in Drosophila. J Cell Biol *161*, 991-1000.

Schwabe, G.C., Trepczik, B., Suring, K., Brieske, N., Tucker, A.S., Sharpe, P.T., Minami, Y., and Mundlos, S. (2004). Ror2 knockout mouse as a model for the developmental pathology of autosomal recessive Robinow syndrome. Dev Dyn *229*, 400-410.

Sebe-Pedros, A., Zheng, Y., Ruiz-Trillo, I., and Pan, D. (2012). Premetazoan origin of the hippo signaling pathway. Cell Rep *1*, 13-20.

Sebio, A., Kahn, M., and Lenz, H.J. (2014). The potential of targeting Wnt/β-catenin in colon cancer. Expert Opin Ther Targets *18*, 611-615.

Segditsas, S., and Tomlinson, I. (2006). Colorectal cancer and genetic alterations in the Wnt pathway. Oncogene *25*, 7531-7537.

Semenov, M.V., Habas, R., Macdonald, B.T., and He, X. (2007). SnapShot: Noncanonical Wnt Signaling Pathways. Cell *131*, 1378.

Serrano, I., McDonald, P.C., Lock, F., Muller, W.J., and Dedhar, S. (2013). Inactivation of the Hippo tumour suppressor pathway by integrin-linked kinase. Nat Commun *4*, 2976.

Shaw, R.L., Kohlmaier, A., Polesello, C., Veelken, C., Edgar, B.A., and Tapon, N. (2010). The Hippo pathway regulates intestinal stem cell proliferation during Drosophila adult midgut regeneration. Development *137*, 4147-4158.

Sheets, J.N., Iwanicki, M., Liu, J.F., Howitt, B.E., Hirsch, M.S., Gubbels, J.A., Drapkin, R., and Egland, K.A. (2016). SUSD2 expression in high-grade serous ovarian cancer correlates with increased patient survival and defective mesothelial clearance. Oncogenesis *5*, e264.

Shigetomi, K., and Ikenouchi, J. (2019). Cell Adhesion Structures in Epithelial Cells Are Formed in Dynamic and Cooperative Ways. Bioessays *41*, e1800227.

Simon, K. (2016). Colorectal cancer development and advances in screening. Clin Interv Aging *11*, 967-976.

Somoracz, A., Korompay, A., Torzsok, P., Patonai, A., Erdelyi-Belle, B., Lotz, G., Schaff, Z., and Kiss, A. (2014). Tricellulin expression and its prognostic significance in primary liver carcinomas. Pathol Oncol Res *20*, 755-764.

Song, H., Kim, H., Lee, K., Lee, D.H., Kim, T.S., Song, J.Y., Lee, D., Choi, D., Ko, C.Y., Kim, H.S.*, et al.* (2012). Ablation of Rassf2 induces bone defects and subsequent haematopoietic anomalies in mice. EMBO J *31*, 1147-1159.

Souris, J.S., Zhang, H.J., Dougherty, U., Chen, N.T., Waller, J.V., Lo, L.W., Hart, J., Chen, C.T., and Bissonnette, M. (2019). A Novel Mouse Model of Sporadic Colon

Cancer Induced by Combination of Conditional Apc Genes and Chemical Carcinogen in the Absence of Cre Recombinase. Carcinogenesis.

Sourisseau, T., Georgiadis, A., Tsapara, A., Ali, R.R., Pestell, R., Matter, K., and Balda, M.S. (2006). Regulation of PCNA and cyclin D1 expression and epithelial morphogenesis by the ZO-1-regulated transcription factor ZONAB/DbpA. Mol Cell Biol *26*, 2387-2398.

Spadaro, D., Le, S., Laroche, T., Mean, I., Jond, L., Yan, J., and Citi, S. (2017). Tension-Dependent Stretching Activates ZO-1 to Control the Junctional Localization of Its Interactors. Curr Biol *27*, 3783-3795.e3788.

Spadaro, D., Tapia, R., Jond, L., Sudol, M., Fanning, A.S., and Citi, S. (2014). ZO proteins redundantly regulate the transcription factor DbpA/ZONAB. J Biol Chem *289*, 22500-22511.

Spindler, V., Dehner, C., Hübner, S., and Waschke, J. (2014). Plakoglobin but not desmoplakin regulates keratinocyte cohesion via modulation of p38MAPK signaling. J Invest Dermatol *134*, 1655-1664.

Staley, B.K., and Irvine, K.D. (2010). Warts and Yorkie mediate intestinal regeneration by influencing stem cell proliferation. Curr Biol *20*, 1580-1587.

Stein, C., Bardet, A.F., Roma, G., Bergling, S., Clay, I., Ruchti, A., Agarinis, C., Schmelzle, T., Bouwmeester, T., Schubeler, D.*, et al.* (2015). YAP1 Exerts Its Transcriptional Control via TEAD-Mediated Activation of Enhancers. PLoS Genet *11*, e1005465.

Stockinger, A., Eger, A., Wolf, J., Beug, H., and Foisner, R. (2001). E-cadherin regulates cell growth by modulating proliferation-dependent beta-catenin transcriptional activity. J Cell Biol *154*, 1185-1196.

Su, T., Ludwig, M.Z., Xu, J., and Fehon, R.G. (2017). Kibra and Merlin Activate the Hippo Pathway Spatially Distinct from and Independent of Expanded. Dev Cell *40*, 478-490 e473.

Subramanian, A., Prokop, A., Yamamoto, M., Sugimura, K., Uemura, T., Betschinger, J., Knoblich, J.A., and Volk, T. (2003). Shortstop recruits EB1/APC1 and promotes microtubule assembly at the muscle-tendon junction. Curr Biol *13*, 1086-1095.

Sugahara, T., Yamashita, Y., Shinomi, M., Isobe, Y., Yamanoha, B., Iseki, H., Takeda, A., Okazaki, Y., Kawai, K., Suemizu, H.*, et al.* (2007a). von Willebrand factor type D domain mutant of SVS-1/SUSD2, vWD(m), induces apoptosis in HeLa cells. Cancer Sci *98*, 909-915.

Sugahara, T., Yamashita, Y., Shinomi, M., Yamanoha, B., Iseki, H., Takeda, A., Okazaki, Y., Hayashizaki, Y., Kawai, K., Suemizu, H.*, et al.* (2007b). Isolation of a novel mouse gene, mSVS-1/SUSD2, reversing tumorigenic phenotypes of cancer cells in vitro. Cancer Sci *98*, 900-908.

Sun, G., and Irvine, K.D. (2011). Regulation of Hippo signaling by Jun kinase signaling during compensatory cell proliferation and regeneration, and in neoplastic tumors. Dev Biol *350*, 139-151.

Suzuki, H., Nishizawa, T., Tani, K., Yamazaki, Y., Tamura, A., Ishitani, R., Dohmae, N., Tsukita, S., Nureki, O., and Fujiyoshi, Y. (2014). Crystal structure of a claudin provides insight into the architecture of tight junctions. Science *344*, 304-307.

Swope, D., Cheng, L., Gao, E., Li, J., and Radice, G.L. (2012). Loss of cadherin-binding proteins β-catenin and plakoglobin in the heart leads to gap junction remodeling and arrhythmogenesis. Mol Cell Biol *32*, 1056-1067.

Tai, C.C., Sala, F.G., Ford, H.R., Wang, K.S., Li, C., Minoo, P., Grikscheit, T.C., and Bellusci, S. (2009). Wnt5a knock-out mouse as a new model of anorectal malformation. J Surg Res *156*, 278-282.

Takeichi, M. (2014). Dynamic contacts: rearranging adherens junctions to drive epithelial remodelling. Nat Rev Mol Cell Biol *15*, 397-410.

Tamura, A., and Tsukita, S. (2014). Paracellular barrier and channel functions of TJ claudins in organizing biological systems: advances in the field of barriology revealed in knockout mice. Semin Cell Dev Biol *36*, 177-185.

Tanaka, H., Takechi, M., Kiyonari, H., Shioi, G., Tamura, A., and Tsukita, S. (2015). Intestinal deletion of Claudin-7 enhances paracellular organic solute flux and initiates colonic inflammation in mice. Gut *64*, 1529-1538.

Tapon, N., Harvey, K.F., Bell, D.W., Wahrer, D.C., Schiripo, T.A., Haber, D., and Hariharan, I.K. (2002). salvador Promotes both cell cycle exit and apoptosis in Drosophila and is mutated in human cancer cell lines. Cell *110*, 467-478.

Tepass, U. (1996). Crumbs, a component of the apical membrane, is required for zonula adherens formation in primary epithelia of Drosophila. Dev Biol *177*, 217-225.

Tepass, U. (2003). Claudin complexities at the apical junctional complex. Nat Cell Biol *5*, 595-597.

Tepass, U., and Hartenstein, V. (1994a). The development of cellular junctions in the Drosophila embryo. Dev Biol *161*, 563-596.

Tepass, U., and Hartenstein, V. (1994b). Epithelium formation in the Drosophila midgut depends on the interaction of endoderm and mesoderm. Development *120*, 579-590.

Thomas, C., Turner, M., Payne, S., Milligan, C., Brearley, S., Seamark, D., Wang, X., and Blake, S. (2018). Family carers' experiences of coping with the deaths of adults in home settings: A narrative analysis of carers' relevant background worries. Palliat Med *32*, 950-959.

Thomas, W.A., Boscher, C., Chu, Y.S., Cuvelier, D., Martinez-Rico, C., Seddiki, R., Heysch, J., Ladoux, B., Thiery, J.P., Mege, R.M.*, et al.* (2013). α-Catenin and vinculin cooperate to promote high E-cadherin-based adhesion strength. J Biol Chem *288*, 4957-4969.

Thomason, H.A., Scothern, A., McHarg, S., and Garrod, D.R. (2010). Desmosomes: adhesive strength and signalling in health and disease. Biochem J *429*, 419-433.

Tian, A., and Jiang, J. (2014). Intestinal epithelium-derived BMP controls stem cell self-renewal in Drosophila adult midgut. Elife *3*, e01857.

Tokonzaba, E., Chen, J., Cheng, X., Den, Z., Ganeshan, R., Muller, E.J., and Koch, P.J. (2013). Plakoglobin as a regulator of desmocollin gene expression. J Invest Dermatol *133*, 2732-2740.

Tokumasu, R., Yamaga, K., Yamazaki, Y., Murota, H., Suzuki, K., Tamura, A., Bando, K., Furuta, Y., Katayama, I., and Tsukita, S. (2016). Dose-dependent role of claudin-1 in vivo in orchestrating features of atopic dermatitis. Proc Natl Acad Sci U S A *113*, E4061-4068.

Townson, S.M., Sullivan, T., Zhang, Q., Clark, G.M., Osborne, C.K., Lee, A.V., and Oesterreich, S. (2000). HET/SAF-B overexpression causes growth arrest and

multinuclearity and is associated with aneuploidy in human breast cancer. Clin Cancer Res *6*, 3788-3796.

Traweger, A., Fuchs, R., Krizbai, I.A., Weiger, T.M., Bauer, H.C., and Bauer, H. (2003). The tight junction protein ZO-2 localizes to the nucleus and interacts with the heterogeneous nuclear ribonucleoprotein scaffold attachment factor-B. J Biol Chem *278*, 2692-2700.

Tsapara, A., Matter, K., and Balda, M.S. (2006). The heat-shock protein Apg-2 binds to the tight junction protein ZO-1 and regulates transcriptional activity of ZONAB. Mol Biol Cell *17*, 1322-1330.

Tsukita, S., Tanaka, H., and Tamura, A. (2019). The Claudins: From Tight Junctions to Biological Systems. Trends Biochem Sci *44*, 141-152.

Udan, R.S., Kango-Singh, M., Nolo, R., Tao, C., and Halder, G. (2003). Hippo promotes proliferation arrest and apoptosis in the Salvador/Warts pathway. Nat Cell Biol *5*, 914-920.

Uechi, H., and Kuranaga, E. (2019). The Tricellular Junction Protein Sidekick Regulates Vertex Dynamics to Promote Bicellular Junction Extension. Dev Cell *50*, 327-338 e325.

Ullman, T.A., and Itzkowitz, S.H. (2011). Intestinal inflammation and cancer. Gastroenterology *140*, 1807-1816.

Umeda, K., Ikenouchi, J., Katahira-Tayama, S., Furuse, K., Sasaki, H., Nakayama, M., Matsui, T., Tsukita, S., and Furuse, M. (2006). ZO-1 and ZO-2 independently determine where claudins are polymerized in tight-junction strand formation. Cell *126*, 741-754.

Van Itallie, C.M., and Anderson, J.M. (1997). Occludin confers adhesiveness when expressed in fibroblasts. J Cell Sci *110 ( Pt 9)*, 1113-1121.

Van Itallie, C.M., and Anderson, J.M. (2014). Architecture of tight junctions and principles of molecular composition. Semin Cell Dev Biol *36*, 157-165.

Van Itallie, C.M., Aponte, A., Tietgens, A.J., Gucek, M., Fredriksson, K., and Anderson, J.M. (2013). The N and C termini of ZO-1 are surrounded by distinct proteins and functional protein networks. J Biol Chem *288*, 13775-13788.

Van Itallie, C.M., Tietgens, A.J., and Anderson, J.M. (2017). Visualizing the dynamic coupling of claudin strands to the actin cytoskeleton through ZO-1. Mol Biol Cell *28*, 524-534.

Vancamelbeke, M., and Vermeire, S. (2017). The intestinal barrier: a fundamental role in health and disease. Expert Rev Gastroenterol Hepatol *11*, 821-834.

Varelas, X., Miller, B.W., Sopko, R., Song, S., Gregorieff, A., Fellouse, F.A., Sakuma, R., Pawson, T., Hunziker, W., McNeill, H.*, et al.* (2010a). The Hippo pathway regulates Wnt/beta-catenin signaling. Dev Cell *18*, 579-591.

Varelas, X., Samavarchi-Tehrani, P., Narimatsu, M., Weiss, A., Cockburn, K., Larsen, B.G., Rossant, J., and Wrana, J.L. (2010b). The Crumbs complex couples cell density sensing to Hippo-dependent control of the TGF-beta-SMAD pathway. Dev Cell *19*, 831-844.

Vasioukhin, V., Bauer, C., Degenstein, L., Wise, B., and Fuchs, E. (2001a). Hyperproliferation and defects in epithelial polarity upon conditional ablation of alpha-catenin in skin. Cell *104*, 605-617.

Vasioukhin, V., Bauer, C., Yin, M., and Fuchs, E. (2000). Directed actin polymerization is the driving force for epithelial cell-cell adhesion. Cell *100*, 209-219.

Vasioukhin, V., Bowers, E., Bauer, C., Degenstein, L., and Fuchs, E. (2001b). Desmoplakin is essential in epidermal sheet formation. Nat Cell Biol *3*, 1076-1085.

Verma, S., Yeddula, N., Soda, Y., Zhu, Q., Pao, G., Moresco, J., Diedrich, J.K., Hong, A., Plouffe, S., Moroishi, T.*, et al.* (2019). BRCA1/BARD1-dependent ubiquitination of NF2 regulates Hippo-YAP1 signaling. Proc Natl Acad Sci U S A *116*, 7363-7370.

Vogelstein, B., Papadopoulos, N., Velculescu, V.E., Zhou, S., Diaz, L.A., Jr., and Kinzler, K.W. (2013). Cancer genome landscapes. Science *339*, 1546-1558.

Volksdorf, T., Heilmann, J., Eming, S.A., Schawjinski, K., Zorn-Kruppa, M., Ueck, C., Vidal-Y-Sy, S., Windhorst, S., Jücker, M., Moll, I.*, et al.* (2017). Tight Junction Proteins Claudin-1 and Occludin Are Important for Cutaneous Wound Healing. Am J Pathol *187*, 1301-1312.

Vrabioiu, A.M., and Struhl, G. (2015). Fat/Dachsous Signaling Promotes Drosophila Wing Growth by Regulating the Conformational State of the NDR Kinase Warts. Dev Cell *35*, 737-749.

Wang, A.Z., Ojakian, G.K., and Nelson, W.J. (1990a). Steps in the morphogenesis of a polarized epithelium. I. Uncoupling the roles of cell-cell and cell-substratum contact in establishing plasma membrane polarity in multicellular epithelial (MDCK) cysts. J Cell Sci *95 ( Pt 1)*, 137-151.

Wang, A.Z., Ojakian, G.K., and Nelson, W.J. (1990b). Steps in the morphogenesis of a polarized epithelium. II. Disassembly and assembly of plasma membrane domains during reversal of epithelial cell polarity in multicellular epithelial (MDCK) cysts. J Cell Sci *95 ( Pt 1)*, 153-165.

Wang, H., Wang, H.S., Zhou, B.H., Li, C.L., Zhang, F., Wang, X.F., Zhang, G., Bu, X.Z., Cai, S.H., and Du, J. (2013). Epithelial-mesenchymal transition (EMT) induced by TNF-α requires AKT/GSK-3β-mediated stabilization of snail in colorectal cancer. PLoS One *8*, e56664.

Wang, L., Luo, J.Y., Li, B., Tian, X.Y., Chen, L.J., Huang, Y., Liu, J., Deng, D., Lau, C.W., Wan, S.*, et al.* (2016). Integrin-YAP/TAZ-JNK cascade mediates atheroprotective effect of unidirectional shear flow. Nature *540*, 579-582.

Wang, W., Xiao, Z.D., Li, X., Aziz, K.E., Gan, B., Johnson, R.L., and Chen, J. (2015). AMPK modulates Hippo pathway activity to regulate energy homeostasis. Nat Cell Biol *17*, 490-499.

Watabe, M., Nagafuchi, A., Tsukita, S., and Takeichi, M. (1994). Induction of polarized cell-cell association and retardation of growth by activation of the E-cadherin-catenin adhesion system in a dispersed carcinoma line. J Cell Biol *127*, 247-256.

Watanabe, G., Howe, A., Lee, R.J., Albanese, C., Shu, I.W., Karnezis, A.N., Zon, L., Kyriakis, J., Rundell, K., and Pestell, R.G. (1996). Induction of cyclin D1 by simian virus 40 small tumor antigen. Proc Natl Acad Sci U S A *93*, 12861-12866.

Watson, A.P., Evans, R.L., and Egland, K.A. (2013). Multiple functions of sushi domain containing 2 (SUSD2) in breast tumorigenesis. Mol Cancer Res *11*, 74-85.

Wehr, M.C., Holder, M.V., Gailite, I., Saunders, R.E., Maile, T.M., Ciirdaeva, E., Instrell, R., Jiang, M., Howell, M., Rossner, M.J.*, et al.* (2013). Salt-inducible kinases regulate growth through the Hippo signalling pathway in Drosophila. Nat Cell Biol *15*, 61-71.

Wei, X., Shimizu, T., and Lai, Z.C. (2007). Mob as tumor suppressor is activated by Hippo kinase for growth inhibition in Drosophila. EMBO J *26*, 1772-1781.

White, B.D., Chien, A.J., and Dawson, D.W. (2012). Dysregulation of Wnt/beta-catenin signaling in gastrointestinal cancers. Gastroenterology *142*, 219-232.

Whiteman, E.L., Fan, S., Harder, J.L., Walton, K.D., Liu, C.J., Soofi, A., Fogg, V.C., Hershenson, M.B., Dressler, G.R., Deutsch, G.H.*, et al.* (2014). Crumbs3 is essential for proper epithelial development and viability. Mol Cell Biol *34*, 43-56.

Wodarz, A., Hinz, U., Engelbert, M., and Knust, E. (1995). Expression of crumbs confers apical character on plasma membrane domains of ectodermal epithelia of Drosophila. Cell *82*, 67-76.

Wong, K.K., Li, W., An, Y., Duan, Y., Li, Z., Kang, Y., and Yan, Y. (2015). beta-Spectrin regulates the hippo signaling pathway and modulates the basal actin network. J Biol Chem *290*, 6397-6407.

Wu, S., Huang, J., Dong, J., and Pan, D. (2003). hippo encodes a Ste-20 family protein kinase that restricts cell proliferation and promotes apoptosis in conjunction with salvador and warts. Cell *114*, 445-456.

Wu, S., Liu, Y., Zheng, Y., Dong, J., and Pan, D. (2008). The TEAD/TEF family protein Scalloped mediates transcriptional output of the Hippo growth-regulatory pathway. Dev Cell *14*, 388-398.

Xiao, K., Allison, D.F., Buckley, K.M., Kottke, M.D., Vincent, P.A., Faundez, V., and Kowalczyk, A.P. (2003). Cellular levels of p120 catenin function as a set point for cadherin expression levels in microvascular endothelial cells. J Cell Biol *163*, 535-545.

Xiao, K., Oas, R.G., Chiasson, C.M., and Kowalczyk, A.P. (2007). Role of p120-catenin in cadherin trafficking. Biochim Biophys Acta *1773*, 8-16.

Xie, Z., Tang, Y., Man, M.Q., Shrestha, C., and Bikle, D.D. (2018). p120-catenin is required for regulating epidermal proliferation, differentiation, and barrier function. J Cell Physiol *234*, 427-432.

Xu, C., Tang, H.W., Hung, R.J., Hu, Y., Ni, X., Housden, B.E., and Perrimon, N. (2019). The Septate Junction Protein Tsp2A Restricts Intestinal Stem Cell Activity via Endocytic Regulation of aPKC and Hippo Signaling. Cell Rep *26*, 670-688 e676.

Xu, D., Lv, J., He, L., Fu, L., Hu, R., Cao, Y., and Mei, C. (2018). Scribble influences cyst formation in autosomal-dominant polycystic kidney disease by regulating Hippo signaling pathway. FASEB J *32*, 4394-4407.

Xu, J., Lim, S.B., Ng, M.Y., Ali, S.M., Kausalya, J.P., Limviphuvadh, V., Maurer-Stroh, S., and Hunziker, W. (2012). ZO-1 regulates Erk, Smad1/5/8, Smad2, and RhoA activities to modulate self-renewal and differentiation of mouse embryonic stem cells. Stem Cells *30*, 1885-1900.

Xu, N., Wang, S.Q., Tan, D., Gao, Y., Lin, G., and Xi, R. (2011). EGFR, Wingless and JAK/STAT signaling cooperatively maintain Drosophila intestinal stem cells. Dev Biol *354*, 31-43.

Xu, T., Wang, W., Zhang, S., Stewart, R.A., and Yu, W. (1995). Identifying tumor suppressors in genetic mosaics: the Drosophila lats gene encodes a putative protein kinase. Development *121*, 1053-1063.

Yamaga, K., Murota, H., Tamura, A., Miyata, H., Ohmi, M., Kikuta, J., Ishii, M., Tsukita, S., and Katayama, I. (2018). Claudin-3 Loss Causes Leakage of Sweat from the Sweat Gland to Contribute to the Pathogenesis of Atopic Dermatitis. J Invest Dermatol *138*, 1279-1287.

Yamaguchi, T.P., Bradley, A., McMahon, A.P., and Jones, S. (1999). A Wnt5a pathway underlies outgrowth of multiple structures in the vertebrate embryo. Development *126*, 1211-1223.

Yanagihashi, Y., Usui, T., Izumi, Y., Yonemura, S., Sumida, M., Tsukita, S., Uemura, T., and Furuse, M. (2012). Snakeskin, a membrane protein associated with smooth septate junctions, is required for intestinal barrier function in Drosophila. J Cell Sci *125*, 1980-1990.

Yang, C.C., Graves, H.K., Moya, I.M., Tao, C., Hamaratoglu, F., Gladden, A.B., and Halder, G. (2015). Differential regulation of the Hippo pathway by adherens junctions and apical-basal cell polarity modules. Proc Natl Acad Sci U S A *112*, 1785-1790.

Yang, Z., Bowles, N.E., Scherer, S.E., Taylor, M.D., Kearney, D.L., Ge, S., Nadvoretskiy, V.V., DeFreitas, G., Carabello, B., Brandon, L.I.*, et al.* (2006). Desmosomal dysfunction due to mutations in desmoplakin causes arrhythmogenic right ventricular dysplasia/cardiomyopathy. Circ Res *99*, 646-655.

Yin, F., Yu, J., Zheng, Y., Chen, Q., Zhang, N., and Pan, D. (2013). Spatial organization of Hippo signaling at the plasma membrane mediated by the tumor suppressor Merlin/NF2. Cell *154*, 1342-1355.

Yin, T., and Green, K.J. (2004). Regulation of desmosome assembly and adhesion. Semin Cell Dev Biol *15*, 665-677.

Yonemura, S., Itoh, M., Nagafuchi, A., and Tsukita, S. (1995). Cell-to-cell adherens junction formation and actin filament organization: similarities and differences between non-polarized fibroblasts and polarized epithelial cells. J Cell Sci *108 ( Pt 1)*, 127-142.

Yonemura, S., Wada, Y., Watanabe, T., Nagafuchi, A., and Shibata, M. (2010). alpha-Catenin as a tension transducer that induces adherens junction development. Nat Cell Biol *12*, 533-542.

Yu, F.X., and Guan, K.L. (2013). The Hippo pathway: regulators and regulations. Genes Dev *27*, 355-371.

Yu, F.X., Zhang, Y., Park, H.W., Jewell, J.L., Chen, Q., Deng, Y., Pan, D., Taylor, S.S., Lai, Z.C., and Guan, K.L. (2013). Protein kinase A activates the Hippo pathway to modulate cell proliferation and differentiation. Genes Dev *27*, 1223-1232.

Yu, F.X., Zhao, B., and Guan, K.L. (2015). Hippo Pathway in Organ Size Control, Tissue Homeostasis, and Cancer. Cell *163*, 811-828.

Yu, F.X., Zhao, B., Panupinthu, N., Jewell, J.L., Lian, I., Wang, L.H., Zhao, J., Yuan, H., Tumaneng, K., Li, H.*, et al.* (2012a). Regulation of the Hippo-YAP pathway by G-protein-coupled receptor signaling. Cell *150*, 780-791.

Yu, J., and Pan, D. (2018). Validating upstream regulators of Yorkie activity in Hippo signaling through scalloped-based genetic epistasis. Development *145*.

Yu, J., Zheng, Y., Dong, J., Klusza, S., Deng, W.M., and Pan, D. (2010). Kibra functions as a tumor suppressor protein that regulates Hippo signaling in conjunction with Merlin and Expanded. Dev Cell *18*, 288-299.

Yu, O.M., Miyamoto, S., and Brown, J.H. (2016). Myocardin-Related Transcription Factor A and Yes-Associated Protein Exert Dual Control in G Protein-Coupled Receptor- and RhoA-Mediated Transcriptional Regulation and Cell Proliferation. Mol Cell Biol *36*, 39-49.

Yu, S.C., Xiao, H.L., Jiang, X.F., Wang, Q.L., Li, Y., Yang, X.J., Ping, Y.F., Duan, J.J., Jiang, J.Y., Ye, X.Z.*, et al.* (2012b). Connexin 43 reverses malignant phenotypes of glioma stem cells by modulating E-cadherin. Stem Cells *30*, 108-120.

Yue, T., Tian, A., and Jiang, J. (2012). The cell adhesion molecule echinoid functions as a tumor suppressor and upstream regulator of the Hippo signaling pathway. Dev Cell *22*, 255-267.

Zanconato, F., Battilana, G., Forcato, M., Filippi, L., Azzolin, L., Manfrin, A., Quaranta, E., Di Biagio, D., Sigismondo, G., Guzzardo, V.*, et al.* (2018). Transcriptional addiction in cancer cells is mediated by YAP/TAZ through BRD4. Nat Med *24*, 1599-1610.

Zanconato, F., Forcato, M., Battilana, G., Azzolin, L., Quaranta, E., Bodega, B., Rosato, A., Bicciato, S., Cordenonsi, M., and Piccolo, S. (2015). Genome-wide association between YAP/TAZ/TEAD and AP-1 at enhancers drives oncogenic growth. Nat Cell Biol *17*, 1218-1227.

Zeng, X., Chauhan, C., and Hou, S.X. (2010). Characterization of midgut stem cell- and enteroblast-specific Gal4 lines in drosophila. Genesis *48*, 607-611.

Zeng, X., and Hou, S.X. (2015). Enteroendocrine cells are generated from stem cells through a distinct progenitor in the adult Drosophila posterior midgut. Development *142*, 644-653.

Zhang, J., Betson, M., Erasmus, J., Zeikos, K., Bailly, M., Cramer, L.P., and Braga, V.M. (2005). Actin at cell-cell junctions is composed of two dynamic and functional populations. J Cell Sci *118*, 5549-5562.

Zhang, J., Smolen, G.A., and Haber, D.A. (2008a). Negative regulation of YAP by LATS1 underscores evolutionary conservation of the Drosophila Hippo pathway. Cancer Res *68*, 2789-2794.

Zhang, L., Ren, F., Zhang, Q., Chen, Y., Wang, B., and Jiang, J. (2008b). The TEAD/TEF family of transcription factor Scalloped mediates Hippo signaling in organ size control. Dev Cell *14*, 377-387.

Zhang, L., Yue, T., and Jiang, J. (2009). Hippo signaling pathway and organ size control. Fly (Austin) *3*, 68-73.

Zhang, N., Bai, H., David, K.K., Dong, J., Zheng, Y., Cai, J., Giovannini, M., Liu, P., Anders, R.A., and Pan, D. (2010). The Merlin/NF2 tumor suppressor functions through the YAP oncoprotein to regulate tissue homeostasis in mammals. Dev Cell *19*, 27-38.

Zhang, S., Zeng, N., Alowayed, N., Singh, Y., Cheng, A., Lang, F., and Salker, M.S. (2017). Downregulation of endometrial mesenchymal marker SUSD2 causes cell senescence and cell death in endometrial carcinoma cells. PLoS One *12*, e0183681.

Zhang, S., and Zhou, D. (2019). Role of the transcriptional coactivators YAP/TAZ in liver cancer. Curr Opin Cell Biol *61*, 64-71.

Zhao, B., Li, L., Lu, Q., Wang, L.H., Liu, C.Y., Lei, Q., and Guan, K.L. (2011). Angiomotin is a novel Hippo pathway component that inhibits YAP oncoprotein. Genes Dev *25*, 51-63.

Zhao, B., Li, L., Tumaneng, K., Wang, C.Y., and Guan, K.L. (2010). A coordinated phosphorylation by Lats and CK1 regulates YAP stability through SCF(beta-TRCP). Genes Dev *24*, 72-85.

Zhao, B., Li, L., Wang, L., Wang, C.Y., Yu, J., and Guan, K.L. (2012). Cell detachment activates the Hippo pathway via cytoskeleton reorganization to induce anoikis. Genes Dev *26*, 54-68.

Zhao, B., Wei, X., Li, W., Udan, R.S., Yang, Q., Kim, J., Xie, J., Ikenoue, T., Yu, J., Li, L.*, et al.* (2007). Inactivation of YAP oncoprotein by the Hippo pathway is involved in cell contact inhibition and tissue growth control. Genes Dev *21*, 2747-2761.

Zhao, B., Ye, X., Yu, J., Li, L., Li, W., Li, S., Yu, J., Lin, J.D., Wang, C.Y., Chinnaiyan, A.M.*, et al.* (2008). TEAD mediates YAP-dependent gene induction and growth control. Genes Dev *22*, 1962-1971.

Zheng, Y., Liu, B., Wang, L., Lei, H., Pulgar Prieto, K.D., and Pan, D. (2017). Homeostatic Control of Hpo/MST Kinase Activity through Autophosphorylation-Dependent Recruitment of the STRIPAK PP2A Phosphatase Complex. Cell Rep *21*, 3612-3623.

Zheng, Y., Wang, W., Liu, B., Deng, H., Uster, E., and Pan, D. (2015). Identification of Happyhour/MAP4K as Alternative Hpo/Mst-like Kinases in the Hippo Kinase Cascade. Dev Cell *34*, 642-655.

Zhou, B., Flodby, P., Luo, J., Castillo, D.R., Liu, Y., Yu, F.X., McConnell, A., Varghese, B., Li, G., Chimge, N.O.*, et al.* (2018). Claudin-18-mediated YAP activity regulates lung stem and progenitor cell homeostasis and tumorigenesis. J Clin Invest *128*, 970-984.

Zhou, D., Conrad, C., Xia, F., Park, J.S., Payer, B., Yin, Y., Lauwers, G.Y., Thasler, W., Lee, J.T., Avruch, J.*, et al.* (2009). Mst1 and Mst2 maintain hepatocyte quiescence and suppress hepatocellular carcinoma development through inactivation of the Yap1 oncogene. Cancer Cell *16*, 425-438.

Zhou, D., Zhang, Y., Wu, H., Barry, E., Yin, Y., Lawrence, E., Dawson, D., Willis, J.E., Markowitz, S.D., Camargo, F.D.*, et al.* (2011). Mst1 and Mst2 protein kinases restrain intestinal stem cell proliferation and colonic tumorigenesis by inhibition of Yes-associated protein (Yap) overabundance. Proc Natl Acad Sci U S A *108*, E1312-1320.

Zhou, F., Rasmussen, A., Lee, S., and Agaisse, H. (2013). The UPD3 cytokine couples environmental challenge and intestinal stem cell division through modulation of JAK/STAT signaling in the stem cell microenvironment. Dev Biol *373*, 383-393.

Zhou, P.J., Wang, X., An, N., Wei, L., Zhang, L., Huang, X., Zhu, H.H., Fang, Y.X., and Gao, W.Q. (2019). Loss of Par3 promotes prostatic tumorigenesis by enhancing cell growth and changing cell division modes. Oncogene *38*, 2192-2205.

Zhou, P.J., Xue, W., Peng, J., Wang, Y., Wei, L., Yang, Z., Zhu, H.H., Fang, Y.X., and Gao, W.Q. (2017). Elevated expression of Par3 promotes prostate cancer metastasis by forming a Par3/aPKC/KIBRA complex and inactivating the hippo pathway. J Exp Clin Cancer Res *36*, 139.

Zhu, Y., Li, D., Wang, Y., Pei, C., Liu, S., Zhang, L., Yuan, Z., and Zhang, P. (2015). Brahma regulates the Hippo pathway activity through forming complex with Yki-Sd and regulating the transcription of Crumbs. Cell Signal *27*, 606-613.

Zhurinsky, J., Shtutman, M., and Ben-Ze'ev, A. (2000). Plakoglobin and beta-catenin: protein interactions, regulation and biological roles. J Cell Sci *113 ( Pt 18)*, 3127-3139.

Zihni, C., Mills, C., Matter, K., and Balda, M.S. (2016). Tight junctions: from simple barriers to multifunctional molecular gates. Nat Rev Mol Cell Biol *17*, 564-580.

Zwick, R.K., Ohlstein, B., and Klein, O.D. (2019). Intestinal renewal across the animal kingdom: comparing stem cell activity in mouse and Drosophila. Am J Physiol Gastrointest Liver Physiol *316*, G313-G322.